Håvard Slettahjell Skjefstad

Development and assessment of a multi-pipe oil-water bulk separator concept for subsea applications

Thesis for the degree of Philosophiae Doctor

Trondheim, November 2019

Norwegian University of Science and Technology
Faculty of Engineering
Department of Geoscience and Petroleum

NTNU
Norwegian University of
Science and Technology

NTNU
Norwegian University of Science and Technology

Thesis for the degree of Philosophiae Doctor

Faculty of Engineering
Department of Geoscience and Petroleum

ISBN 978-82-326-4208-3 (printed version)
ISBN 978-82-326-4209-0 (electronic version)
ISSN 1503-8181

Doctoral theses at NTNU, 2019:306

Printed by Skipnes Kommunikasjon as

Abstract

Subsea produced water separation has emerged as a viable technology for tackling challenges arising from increased water production rates. Removing produced water at the seabed will free up topside capacity constrained water processing facilities, increase production rates, prolong field lifetimes and secure greener and more energy efficient oil and gas production. However, an important challenge connected to subsea produced water separation is that the cost of constructing, qualifying, transporting and installing subsea produced water separators often exceeds potential value gains in production. This is especially true for mature, marginal or deep-water fields. To make the business case of subsea produced water separation more attractive, there is a need for novel low-cost technologies suitable for standardization and modularization.

In this PhD work, a novel concept for subsea oil-water bulk separation has been developed, a prototype of the developed concept has been constructed, and the concept has been evaluated both experimentally and numerically.

The first phase of the research consists of a thorough state of the art review of available subsea produced water separator technologies. Drawbacks with existing technologies are outlined and focus areas for future technology developments are identified. Based on these findings, a new subsea produced water bulk separator concept, based on separation in multiple parallel pipes, is developed.

For experimental testing, a down-scaled prototype of the separator concept has been constructed along with a low pressure two-phase oil-water test facility. The prototype consists of two 150.6 *mm* internal diameter pipes in parallel, with a total horizontal length of 6.1 *m*. Four experimental campaigns have been executed, focusing on performance and operational envelope mapping, design feature evaluation, flow distribution, control strategy development and effect of upstream inlet choking and addition of surfactants. Experimental fluids are Exxsol$^{\text{TM}}$ D60 and distilled water with added NaCl. Separator performance is determined by flow rate, density, temperature and pressure measurements, and pictures of flow phenomena and established inlet droplet distributions are gathered for supplementary analysis.

Experimental results show that the prototype exhibits good performance for a wide range of inlet flow rates and water cuts. Based on results, design refinements are suggested and implemented, including preferred location for water extraction and an improved separator inlet configuration. An uneven flow splitting phenomenon is identified for certain flow conditions, which can be detrimental to operability and separator performance. Moreover, a robust control strategy to maintain satisfactory separator performance at varying inlet conditions is developed and implemented. Finally, quantification of performance variation due to more realistic inlet conditions are reported by studying the effect inlet choking and active interfacial agents has on separator performance.

A computational fluid dynamics model of the prototype has been developed utilizing the commercial software Ansys CFX. The model assumes two-phase flow, where one phase is fully dispersed in the other as spherical droplets with uniform diameters. Phasic continuity and momentum equations are solved for each phase, included interfacial momentum transfer terms. Numerical model output displays fair agreement to experimental results for water-continuous regimes at the separator inlet. For oil-continuous inlet regimes, agreement was not satisfactory. The numerical model can be used for further refinement of the concept design.

The presented research constitutes a scientific contribution to the oil and gas industry in the form of a developed, tested, and refined subsea oil-water bulk separator concept. This has been achieved by completing a thorough experimental and numerical study of oil-water separation and flow dynamics in parallel pipe geometries. The presented results indicate that the developed concept is attractive for further evaluation, and that it can form a basis for the development of next generation subsea produced water separators, overcoming outlined challenges with current technologies.

Declaration

This dissertation is submitted to the Norwegian University of Science and Technology (NTNU) for partial fulfilment of the requirement for the Philosophiae Doctor degree. The doctoral work was performed at the Department of Geoscience and Petroleum (IGP), NTNU, Trondheim, Norway, in the period July 2016 to June 2019. The work was supervised by Associate Professor Milan Stanko and co-supervised by professors Sigbjørn Sangesland and Gisle Øye.

I hereby declare that except where specific reference is made to the work of others, the contents of this dissertation are original and have not been submitted in whole or in part for consideration for any other degree or qualification in this, or any other university. This dissertation is my own work and contains nothing which is the outcome of work done by others, except as specified in the text and Acknowledgements.

Håvard Slettahjell Skjefstad
October 2019

Acknowledgements

First and foremost I would like to express my sincerest gratitude to my main supervisor, Associate Professor Milan Stanko, for giving me the opportunity to work on this project. I have truly enjoyed our frequent discussions and lasting collaboration, and you have been an ever trusting source of knowledge, insight and inspiration. I would also like to thank my two co-supervisors, Professors Sigbjørn Sangesland and Gisle Øye, for good advice, knowledge and support throughout these years.

I would like to thank SUBPRO for financial support and for allowing me to be a part of the exciting and rewarding research that defines the centre. To all my fellow SUBPRO colleagues, thank you for fruitful discussions, rewarding collaboration and delightful social activities.

For my colleagues and friends at the department of Geoscience and Petroleum, thank you for a great work environment, exciting lunch discussions and frequent coffee breaks. I am particularly grateful to my office mate Mariana Diaz, and our next door neighbours, Gilberto Nuñez and Diana González. Thank you for the collaboration, discussions and support. A special thanks to Senior Engineers Noralf Vedvik and Steffen Wærnes Moen for the assistance in planning and construction of the experimental facilities. I have enjoyed our long days in the workshop, and your company and good spirits will be missed. I would also like to thank Staff Engineers Terje Bjerkan, Håkon Myhren and Roger Overå for general support and assistance at various stages in the development.

To my family and loved ones, thank you for your everlasting support and encouragement in all my endeavours.

List of publications

Conference papers

Paper I: H. S. Skjefstad and M. Stanko. Subsea water separation: a state of the art review, future technologies and the development of a compact separator test facility. In *18th International Conference on Multiphase Production Technology.* BHR Group, 2017.

Paper II: H. S. Skjefstad and M. Stanko. An experimental study of a novel parallel pipe separator design for subsea oil-water bulk separation. In *SPE Asia Pacific Oil and Gas Conference and Exhibition.* Society of Petroleum Engineers, 2018.

Journal articles

Paper III: H. S. Skjefstad and M. Stanko. Experimental performance evaluation and design optimization of a horizontal multi-pipe separator for subsea oil-water bulk separation. *Journal of Petroleum Science and Engineering,* 176:203-2019, 2019.

Paper IV: S. J. Ohrem, H. S. Skjefstad, M. Stanko, and C. Holden. Controller design and control structure analysis for a novel oil-water multi-pipe separator. *Processes*, 7(4):190, 2019.

Paper V: H. S. Skjefstad, M. Dudek, G. Øye and M. Stanko. The effect of upstream inlet choking and surfactant addition on the performance of a novel parallel pipe oil-water separator. *Journal of Petroleum Science and Engineering*, [Submitted manuscript], 2019.

Table of contents

List of figures

List of tables

Nomenclature

Roman Symbols

A	Area	$[m^2]$
a	Constant	$[-]$
b	Constant	$[-]$
c	Force coefficient	$[kg/(m^3 s)]$
d	Droplet diameter	$[m]$
dP	Differential Pressure	$[Pa]$
ER	Extraction Rate	$[-]$
h	Height	$[m]$
K	Controller gain	$[min/L]$
N	Number of samples	$[-]$
n	Number of particles	$[-]$
P	Pressure	$[Pa]$
R	Radius	$[m]$
S	Standard deviation	
T	Temperature	$[^\circ C]$
t	Time	$[s]$
V	Volume	$[m^3]$
WC	Water Cut	$[-]$
X	Sample value	

Greek Symbols

α	Volume fraction	$[-]$
β	Phase identifier	
ε	Separation efficiency	$[\%]$
γ	Phase identifier	
μ	Dynamic viscosity	$[Pa \cdot s]$
∇	Nabla operator	
ω	Error	
ρ	Density	$[kg/m^3]$
σ	Interfacial tension	$[N/m]$
τ	Derivative time constant	$[s]$

Superscripts

D	Drag
L	Lift
T	Transposed
TD	Turbulent dispersion
VM	Virtual mass

Subscripts

1	Location identifier on P&ID
2	Location identifier on P&ID
3	Location identifier on P&ID
β	Phase identifier
C	Calibrated
c	Cell
D	Deviation
γ	Phase identifier

i	Number identifier	
in	Inlet	
M	Measurement	
m	Mixture	
o	Oil	
p	Particle	
Q	Quantization	
R	Random	
r	Ratio	
S	Systematic	
T	Transducer	
tot	Total	
w	Water	
oo	Oil outlet	
wo	Water outlet	
$\bar{X}$	Sample mean	

Other Symbols

C_D	Drag coefficient	$[-]$
$\mathbf{D}$	Drag force vector	$[N]$
d_{32}	Sauter mean diameter	$[m]$
d_{43}	De Brouckere mean diameter	$[m]$
d_{v50}	50 % volume based median diameter	$[m]$
Eo	Eötvös number	$[-]$
$\dot{m}$	Mass Flow	$[kg/s]$
$\mathbf{M}$	Interfacial force vector	$[N]$
$\dot{Q}$	Volume Flow	$[m^3/s]$

Re	Reynolds number	$[-]$
$\mathbf{S}$	External body force momentum source vector	$[N]$
$\bar{t}$	Student's t-distribution t value	$[-]$
$\mathbf{U}$	Velocity vector	$[m/s]$
$\bar{X}$	Sample mean	

Acronyms / Abbreviations

ADC	Analog To Digital
CFD	Computational Fluid Dynamics
DAQ	Data Acquisition System
DPS	Dual Pipe Separator
ER	Extraction Rate
ID	Internal Diameter
IGP	Department of Geoscience and Petroleum
LSB	Least Significant Bit
MPPS	Multiple Parallel Pipe Separator
NCS	Norwegian Continental Shelf
NTNU	Norwegian University of Science and Technology
OD	Outer Diameter
OPC	Open Platform Communication
P&ID	Pipe and Instrumentation Diagram
PI	Proportional-integral
PLC	Programmable Logic Controller
PVC	Ployvinyl Chloride
PVM	Particle Video Microscopy
PV	Process Variable
SP	Set Point
UV	Ultraviolet

Chapter 1

Introduction

1.1 Background

Produced water is a bi-product in oil and gas production, and for mature fields, it often surpasses produced oil in terms of quantity. A review of technologies for oil and gas produced water treatment published in 2009 [14], reported a global produced water production rate of 250 million barrels per day (three times the amount of produced oil). Looking to the Norwegian continental shelf (NCS), 175 million standard cubic meters of produced water was reported for 2017, amounting to about two times the amount of produced oil (92 million standard cubic meters) [23]. As more fields mature, the amount of produced water is expected to increase, and produced water management is thus a topic of increasing importance for the oil and gas industry.

For offshore fields, the majority of produced water is discharged to the ocean. At the NCS, 77 % of produced water was discharged in 2017 [23], while the remainder was re-injected to sub-surface. Prior to disposal, produced water must be separated from the oil and gas and treated. On the NCS, the upper allowable oil content in discharged produced water is 30 mg/L [23]. This limit is set to prevent pollution. For re-injection, the typical oil in water target is around 100 mg/L [7], which is to hinder formation plugging and issues with reduced injectivity. In traditional offshore production facilities, incoming fluids are firstly separated in a bulk separator stage, with a second downstream separation stage for produced water treatment. The bulk separation stage is normally a vessel type gravity separator, where gas oil and water are separated into individual streams based on their density difference. The water leaving the bulk separation stage has a typical oil content of 500-1000 mg/L [4], and must be treated further to reach the specified targets for re-injection or discharge. The treatment is typically performed with hydrocyclones (enhanced gravity separation) and/or gas flotation units where dispersed oil is removed by attachment to gas bubbles.

Subsea produced water separation consists of performing bulk oil-water separation and subsequent produced water treatment on the seabed. The technology has emerged as a viable option for meeting challenges arising from increased produced water rates. The following sections will outline the benefits of subsea produced water separation, as well as current challenges for the technology.

1.1.1 Benefits of subsea produced water separation

The benefits of subsea separation can be outlined as three separate aspects. These are: Topside de-bottlenecking, increased and more energy efficient production, and improved separation conditions.

Topside de-bottlenecking

In traditional offshore oil and gas topside processing, the bulk separation stage has a specified maximum capacity in terms of liquid and gas handling rates. These rates are defined to provide sufficient residence time for gravitational segregation of the phases and to ensure that extracted produced water meets required purity for downstream water treatment equipment. The downstream produced water treatment facilities have their respective design flow rates, defined to meet required oil in water levels for discharge or re-injection. Parallel to the water processing, separated oil and gas are treated to desired specifications. Both the produced water treatment and hydrocarbon production trains are designed for expected maximum production during the field lifetime.

During the operational lifetime of a field, produced water rates will in some cases reach the design capacity of the installation. This can for instance be caused by early water breakthrough from the aquifer, or prolonged operation of mature fields. In the first case, an early or unexpected increase in produced water might result in the design capacity being reached prior to expectation. It will then be necessary to choke back production, initiating an early field decline phase. In the case of mature field operation, the hydrocarbon production rate declines, and the produced water rate increases. Old production platforms are often kept in operation longer than the design lifespan. This is possible as long as the safety profile is maintained, and a positive cash flow is generated [8]. For these installations, the increasing produced water rate can ultimately become a problem, as it reaches the design capacity of the installation. It will again become necessary to choke back production in order to meet the capacity constraint. For both these cases, produced water has become a bottleneck in production, and the hydrocarbon production rate is dictated by the amount of water that can be processed. When this happens, the flow of sellable oil and gas is reduced, causing economic losses. An additional result is that a substantial part of the topside hydrocarbon processing capacity will be left unused. Revamping of topside facilities is a possible solution, but is often limited by access, available space and load capacity of the installation [8].

Subsea separation of produced water can reduce the load on topside installations, freeing up topside capacity, allowing for prolonged and increased production. It also offers the possibility of better utilizing existing production capacity by allowing new tie-ins to existing installations.

Increased and more energy efficient production

Subsea produced water separation also results in increased production rates. Removing produced water at the seabed reduces the hydrostatic pressure loss associated with seabead to topside transportation. By reducing the water cut of the production stream, the overall mixture density will decrease, resulting in reduced pressure loss in the risers. This will allow production at lower reservoir pressures, increase production rates, and allow an increased total recovery rate for the field.

A subsequent effect of removing produced water at the seabed is more energy efficient production. The cycle for topside processing of produced water was outlined in the previous section. Removing produced water close to the wellhead will allow the use of smaller downstream components, such as pipelines, valves, pumps, and topside processing equipment. This will reduce the cost and weight of offshore structures. In addition, if produced water can be directed to re-injection subsea, without being looped topside with subsequent boosting back to the seabed, further savings and more energy efficient production can be expected. As power is a limited resource offshore, this is an important benefit of subsea produced water separation.

Improved separation

Oil and water dispersions are typically formed by the mixing and agitation through constrictions, choke valves and pumps associated with transportation from reservoir to topside bulk separators [35]. The droplet size and characteristics of the resulting dispersion are dictated by the magnitude and duration of shear stresses the mixture had been subject to, the physical and interfacial properties of the fluids, and the presence of surface active components. The speed at which this dispersion separates is greatly dependant on the size of dispersed droplets, and at the rate of which small droplets coalesce (merge into larger droplets). In crude-oil systems, surface active components such as asphaltenes, resins or napthenic acids can adsorb at the oil-water interface, stabilizing formed droplets [11]. This hinders droplet coalescence, and greatly increases required residence time in the separator.

The amount of surface active components that adsorb at the oil-water interface is a function of exposure time and change in solubility conditions associated with subsea to topside transportation. Separating close to the wells can benefit oil-water separation efficiency, as droplet surfaces are more fresh [5]. Separating close to the wells will also result in a higher pressure and temperature for the wellstream, which lowers liquid and emulsion viscosities and further secures a larger oil-water density difference. This will further improve oil-water separation efficiency [5]. Finally, separating close to the well means less mixing and agitation, reducing dispersion formation.

1.1.2 Challenges with subsea produced water separation

Up to this point, the focus has been on the generic case of subsea produced water separation, including both bulk separation and water treatment. For the further discussion, focus will be given to the bulk separation stage only.

Traditional topside bulk separator installations are horizontal gravity vessels. This design enables good tolerance for slug flow and varying inlet conditions, and is a well known and qualified technology for liquid-liquid separation. However, when it comes to subsea installations, the traditional vessel design poses certain challenges. For a given pressure rating, the required vessel wall thickness increases with diameter [19]. This will cause large diameter vessels at large water depths to become heavy and expensive to manufacture. A subsequent challenge with size and weight is the cost of transportation and installation. Installation weight dictates which installation vessels that can be used, influencing project cost [17]. Being reliant on specific high capacity installation/intervention/retrieval vessels with limited availability is costly. This will also increase potential revenue losses at unplanned interventions/retrievals, as the vessel response time increases with decreased availability [17]. As a result, subsea separation relying on traditional gravity vessels can become too costly, not supported by expected production gains. This is especially true for mature fields, where remaining resources are limited. Developing lighter and more compact separator technologies (compared to traditional vessel designs) is therefore an important step in making the business case of subsea produced water separation more attractive. For instance, limiting module weight to 60 tons gives access to a much wider fleet of installation/intervention vessels, which reduces overall project cost [19].

However, reducing the size of a separator will naturally impose challenges. Generally, a reduced separator volume will negatively impact separator efficiency, reduce the operational envelope, and decrease tolerance for fluctuating inlet conditions [17]. This will further increase the risk of non-conforming inlet conditions for downstream water processing equipment, which can cause oily discharges and loss of revenue. A limitation in the operational envelope will cause further challenges in terms of technology qualification. When developing new separator technologies, extensive and expensive qualification campaigns are needed in order to accurately predict performance and operational constraints. Developing custom solutions for specific field conditions is thus not economically efficient, requiring large investments in testing and qualification for each specific technology. A final challenge is seen in system control, where more compact designs will require faster response times to deal with system transients and secure efficient and safe operation.

In order to make the business case of subsea produced water separation more attractive there is a need for more compact and lighter separator technologies that are both robust and safe to operate. Separator efficiency must be acceptable over a large operational range, the design must be suitable to standardization and modularization, and viable control principles must be evaluated. The topic of more compact separator development is what will be addressed in this dissertation. The focus is on bulk oil-water separation, and how the bulk separator stage can be designed to meet identified challenges.

1.2 Research goal and objectives

The goal of this PhD is to develop and test a novel oil-water separator concept for subsea produced water bulk separation. The developed concept is to meet identified challenges with current subsea oil-water bulk separator technologies, and by that make future subsea produced water separator developments more attractive.

In the development process, the proposed concept is to be evaluated both experimentally and numerically, and design improvements are to be made. Additionally, a control strategy for the separator concept is to be developed, and a fundamental analysis of the oil-water flow dynamics in the separator is to be performed.

In order to achieve the outlined goal, the following research objectives have been identified:

1. Perform a thorough state of the art review of existing principles for subsea oil-water bulk separation
2. Identify challenges with existing solutions and specify focus points for new technology development
3. Based on specified focus points, develop and design a novel concept for subsea produced water bulk separation
4. Design and construct a two-phase oil-water experimental facility to test the developed concept
5. Design and construct a prototype of the developed separator concept
6. Perform prototype experiments evaluating separator performance and design features
7. Perform prototype experiments evaluating flow mechanics and phase distribution in the separator
8. Propose and evaluate control strategies for the separator concept
9. Perform numerical simulations of the separator concept and validate model with experimental results

The research objectives have been carried out, and are presented as published conference papers, journal articles and dissertation chapters. Tasks 1-2 are covered by Paper I. Paper II addresses tasks 2-5. Tasks 6 and 7 are addressed in Paper III and V. Paper IV presents the separator control strategy development (task 8), while task 9 is presented as a separate dissertation chapter.

1.3 Limitations and considerations

The studies performed as part of this PhD are limited to low pressure two-phase oil-water experiments. Studies are further limited to the bulk separation stage, not focusing on downstream water treatment processes. The developed and presented separator concept is a concept suggestion, not a complete and validated separator design. It should be further emphasised that the performance data collected and presented throughout this dissertation are based on experiments with model oil and water. Performance with real crude oil will deviate from reported data. In addition, up-scaled performance data are based on simplified estimates, and have not been verified with experimental testing.

1.4 Dissertation structure

This dissertation has been structured to cover the outlined research objectives in a natural order, providing a chronological description of the separator development and testing. The following list outlines the contents of each dissertation chapter:

- Chapter 1: This chapter presents the background and underlying importance of the selected research topic. Further, the research objectives are presented and the dissertation structure is outlined
- Chapter 2: This chapter consists of a conference paper (Paper I [29]) that gives a thorough overview of the state of the art in subsea produced water bulk separation technologies
- Chapter 3: This chapter gives an overview of the experimental work that has been carried out throughout the PhD period. This includes separator concept development, prototype construction, lab facility design, construction and commissioning, and details of four completed experimental campaigns
- Chapter 4: This chapter consists of a conference paper (Paper II [30]) that presents the developed separator concept, the constructed experimental facility and preliminary test data for the separator prototype
- Chapter 5: This chapter consists of a journal paper (Paper III [31]) that presents the results of experimental campaigns one and two. The campaigns investigate separator design features and maps separator performance
- Chapter 6: This chapter consists of a journal paper (Paper IV [24]) that presents the results of experimental campaign three. The campaign investigates separator control strategies

- Chapter 7: This chapter consists of a journal paper (Paper V) that presents the results of experimental campaign four. The campaign investigates the effect inlet choking and surfactants has on separator performance

- Chapter 8: This chapter presents work done on modelling of the separator concept

- Chapter 9: This chapter presents a summary of conclusions and proposals for future work

Published conference papers and journal articles are included as respective chapters embedded in the dissertation structure. For this reason, Chapter 2 and Chapters 4-7 have their respective separate figure and table numbering, nomenclature, acronyms, and reference lists. The list of figures, tables, nomenclature and acronyms which is part of the dissertation front matter are thus to be used for Chapter 1, Chapter 3, Chapter 8 and Chapter 9. The same applies to the list of references at the end of the dissertation.

1.5 Declaration of authorship

In general, the candidate is the main author of presented conference papers and journal articles. Main authorship means the candidate has been responsible for designing, performing and analyzing the work presented in the paper, in addition to writing the manuscript. Co-author contributions are mainly manuscript input and structuring, general quality control, input on experimental design and input on result analysis. There are two exceptions from the outlined description:

- Paper IV: The main author of the article is fellow PhD Candidate Sveinung Johan Ohrem. The main author has written the majority of the manuscript, and is credited the development of the adaptive controller algorithm, the relative gain array analysis, performed step response calculations and calculation of controller parameters. The candidate is a co-author to this paper, and main contributions include:

  - Test facility design and construction
  - Rig operation and design of test sequence, test cases and operational conditions
  - Design and construction of the level measurement configuration
  - Control variable selection
  - Writing of manuscript sections 2.1-2.3

  Remaining work has been shared by both authors, including running of experiments, implementation of controllers and analysis of data. The contributions of the remaining co-authors are according to the initial description

- Paper V: One of the co-authors for the article is Postdoctoral fellow Marcin Dudek. The contribution from the Postdoctoral fellow extends beyond the outlined co-author contributions on the following:
  - Choice of surfactant to be used in the study
  - Performing bottle test experiments for determination of appropriate surfactant concentration
  - Performing fluid property determination experiments (density, viscosity, interfacial tension)
  - Contributing to analysis of droplet distribution data
  - Manuscript contributions on Section 1 and 2.4

  Other co-author contributions are according to the initial description

Two commercially available software solutions have been used to generate data presented in this dissertation. The first is Ansys CFX, a computational fluid dynamics solver, which has been used for the modelling part of the study. The second is an image analysis software developed by SOPAT GmbH, which is used for counting and reporting of droplet sizes. The author claims no contribution to the development of either software.

Chapter 2

State of the art review, Paper I

This chapter consists of Paper I, which gives a thorough introduction to existing subsea produced water bulk separator technologies, along with an overview of new technologies which are currently under development. The paper gives a general introduction to the subsea produced water separation business case, and goes into detail on why more compact separator technologies are desired. Further, aspects of respective separator design approaches are discussed, outlining potential challenges and future areas for improvement. The paper also presents an initial outline of the constructed oil-water test facility.

H. S. Skjefstad and M. Stanko. Subsea water separation: a state of the art review, future technologies and the development of a compact separator test facility. In *18th International Conference on Multiphase Production Technology.* BHR Group, 2017.

Subsea water separation: a state of the art review, future technologies and the development of a compact separator test facility

H S Skjefstad, M Stanko
Norwegian University of Science and Technology,
Department of Geoscience and Petroleum, Norway

ABSTRACT

Subsea water removal has emerged as a viable option to prolong the lifetime of brown field installations, increase recovery and generate increased return for operators. This paper presents a thorough literature review of both current subsea liquid-liquid separation installations as well as state of the art technologies currently being developed for field application. The applicability of respective technologies to identified business cases is discussed, including principle of operation, size and efficiency considerations, as well as technology readiness level. The details and layout of a newly constructed oil-water test loop to develop and design compact separators will also be presented.

INTRODUCTION

During an oil field's operational lifetime, the quantities of produced water in the production stream will steadily increase. Eventually, produced water will emerge as the main extracted fluid, and the rate will steadily increase until production is no longer economically viable. A review of oil and gas produced water treatment from 2009 (1) reported a global produced water production of 250 million barrels per day, accounting to a produced water to hydrocarbon ratio of 3:1. Looking to the NCS (Norwegian Continental Shelf), a total produced water quantity of 190 million m^3 was reported for 2015, accounting for more than twice the amount of produced oil (2). This ratio will steadily increase as more fields are reaching their mature stage, and illustrates the need for produced water management.

Offshore, most old production platforms are kept in operation even after having reached their design lifespan. This is possible as long as the unit maintains its' safety profile, generates a positive cash flow, and increases the overall recovery rate of the field (3). For these installations, produced water is posing a problem as design water treatment capacity is being overreached by the increasing produced water rate, creating a bottleneck in production. While revamping of topside facilities is a possible solution, this is often limited by access, available space and load capacity of the production unit (3). Subsea water removal has thus emerged as a viable option to prolong the lifetime of brown field installations, increasing production rate, increasing recovery rate and generating increased return for the operators. In addition to brown field applications, subsea water removal can be attractive for green field installations. New developments are characterized by deeper water, longer transport distances, marginal fields and colder surroundings. In order to make these developments economically feasible, subsea processing is needed.

This paper will provide an overview of existing subsea liquid-liquid separation solutions, discuss their area of applicability and identify possible shortcomings. New, proposed solutions will be looked into, including technologies currently being developed for field application as well as proposed separator designs from patents and literature. Before discussing the different designs, a more detailed description of the benefits of subsea water removal will be given, in addition to why compact designs are being sought in development.

BACKGROUND

Benefits of subsea water removal

The benefits of subsea water removal are best illustrated when compared to a conventional production solution. A typical FPSO (Floating Production, Storage and Offloading)-based development concept is given in Figure 1. This is the currently preferred solution for water depths beyond 200 meters, as discussed and illustrated in DNV GL's strategic research and innovation position paper, 2015 (4).

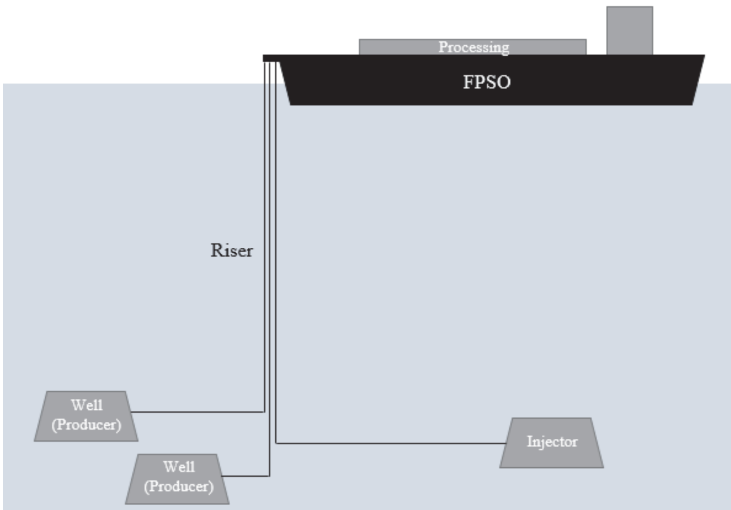

Figure 1: Conventional FPSO-based development concept

Well fluids are routed to an FPSO where the hydrocarbons are processed, collected and/or exported. The leftover fluid from production, water, is treated topside and discharged to sea or boosted back down to the seabed for re-injection. The driving force enabling production is the pressure difference between the wellhead and first stage separator at the FPSO. The wellhead pressure is a function of the reservoir pressure, friction loss in the flow lines/risers, hydrostatic pressure loss and the receiving pressure at the FPSO. As long as the pressure difference overcomes the pressure loss in the flow lines/risers, production can occur naturally. However, as a field matures, reservoir pressure will decline, subsequently reducing the wellhead pressure. This will cause production to decrease and eventually inapt to cover the cost of operation. Looking to Figure 1, a simplified expression for the hydrostatic pressure loss in the riser, assuming oil and water as the only riser fluids and no slip, can be given as:

$$\Delta P = (\alpha\rho_w + (1-\alpha)\rho_o)gh \qquad 1$$

Where α is the water cut, ρ_w and ρ_o the respective fluid densities and h the riser height. With water being the heaviest component produced, reducing the amount of produced water in the liquid column will reduce the pressure loss allowing increased production rates and increased overall recovery. An additional benefit can be seen when considering the topside water treatment facility. The majority of produced water is released to sea. On the NCS, of the 190 million m^3 of produced water reported in 2015, 78% was disposed to sea (2). In order to be disposed, the water must meet strict oil in water (OiW) requirements, which for the NCS is less than 30 ppm (2). An illustration of a topside water processing facility is given in Figure 2.

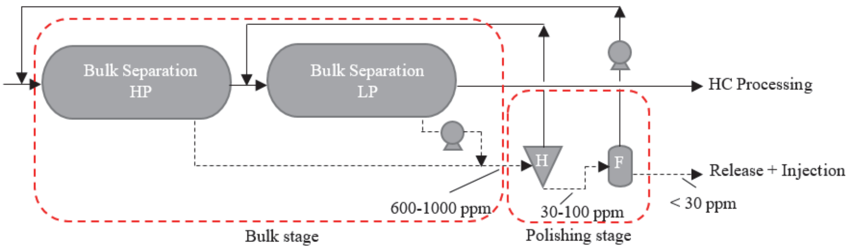

Figure 2: Illustration of topside processing facility

The first processing step consists of a high-pressure (HP) and low-pressure (LP) bulk separation stage, where OiW is reduced to approximately 1000 ppm. A downstream polishing stage, consisting of hydrocyclones (H) and flotation devices (F), ensures required quality is reached. The water treatment facility has a maximum design capacity which when reached will become a bottleneck in production. This means that topside facilities eventually will have available capacity in the hydrocarbon processing train being left unused, as the incoming production flow is limited by the amount of water that can be removed. By removing produced water on the seabed, topside capacity constrained infrastructure can be utilized by increasing production rates, or allow tiebacks to the facility.

Subsea separator design

Drivers

Topside installations utilize large vessels as the receiving first stage bulk separator, the principle of operation being separation by gravity. This enables good tolerance to slug flow and varying flow conditions, allows a large interfacial area for liquid-liquid separation, and enables desired flexibility in terms of flow rate and control. When looking to subsea installations, the traditional gravity separator configuration invites some challenges. For a given pressure rating, required wall thickness increases with diameter (5, 6). This entails large diameter vessels at large water depths become heavy and expensive to manufacture. A further challenge with size and weight is transportation and installation of equipment. Installation-weight set limits to which installation ships can be used, influencing project cost (7). Being reliant on a specific intervention vessel with limited availability for installation/retrieval is costly. It also increases potential revenue losses at unplanned shutdowns as the response time increase with decreased availability (7). As outlined by Kristiansen et al. (5), limitation of module weights to 60 tons gives access to a much wider fleet of installation/intervention vessels, given that module footprint is limited to the on-deck moonpool size. This will reduce project cost, reduce response time, and increases overall availability. Modular installations will also promote standardization of equipment. Qualifying subsea separator technology is an expensive and time-consuming process, which puts specific requirements on separator performance in order to justify the investment. Having standardized solutions will lower the CAPEX connected to separator installations, which ideally can increase the number of business cases suited for subsea separation implementation.

Challenges

In general, a reduced volume will negatively impact the separation efficiency, as well as decrease the tolerance to fluctuating flows (7). This will again increase the risk of non-conforming outlet conditions, which can affect downstream processing equipment and cause loss of revenue. The designed operational range is another challenge arising from compact design. Where vessel separators offer full turndown capabilities, a compact separator's efficiency might be highly sensitive to changes in flow velocity or composition. A challenge arising from limitations in operational range and applicability is the degree of technology standardization. Developing customized solutions for specific reservoir applications is not economically efficient, as it requires substantial testing and qualification for each developed technology. As discussed by Moraes et al. (3) operators might in addition be skeptical to making this investment, as the proved success of new solutions will make the technology available to competitors not having paid for its' development.

Approaches

A good reference technology when discussing compact separator construction is the well-known gravity separator. Separation by gravity occurs if the density of dispersed particles/droplets differ from that of the ambient liquid, and results in sedimentation if the dispersed medium's density is greater than that of the ambient, or creaming if the opposite is true. A well-known equation governing the creaming/sedimentation velocity (u) of spherical particles/droplets is given by Stokes law:

$$u = \frac{2(\rho_s - \rho_f) g {r_s}^2}{9\mu_f} \tag{2}$$

Here, ρ_s and ρ_f represent the particle/droplet and ambient fluid's respective densities, g the gravitational acceleration, r_s the particle/droplet radius and μ_f the ambient fluid's viscosity. Coupling this with required residence time in the separator, $t_{res} = H_L/u$, $H_L$being the required settling/creaming length, and expressing the throughput as a function of separator cross sectional area (A) and mixture velocity $U_m = q/A$, q being the volumetric flow, the following relation for the separator volume (V) can be derived:

$$\frac{L}{U_m} = \frac{LA}{q} = \frac{V}{q} = t_{res} \rightarrow V = \frac{H_L q}{u} = \frac{9 H_L q \mu_f}{2(\rho_s - \rho_f) g {r_s}^2} \tag{3}$$

This simplified analysis visualizes four different approaches to reduce the separator volume:

1. **Lower amount of throughput**: Reduce q (upstream gas-liquid separation)
2. **Reduce required settling length**: Reduce H_L (decrease vessel diameter)
3. **Increase separation driving forces**: Increase acting acceleration g (introduction of centrifugal acceleration)
4. **Enhancing coalescence**: Increase droplet radius r_s (application of coalescence enhancing technologies such as electrostatic coalescers)

The described approaches form the basis for current compact separator designs, which will be presented and discussed in a later section.

BUSINESS CASE IDENTIFICATION

Currently, the strongest business case for subsea water removal is connected to challenges with produced water levels and capacity constrained infrastructure topside. Removing water subsea will allow utilization of topside processing capacity by routing additional production streams to the platform/FPSO. This is seen by reviewing already installed subsea produced water separators, where de-bottlenecking of topside water processing has been the main driver for installation (8, 9).

A second business case is found in green field developments where topside processing is not economically feasible. This can be a result of remote and marginal fields, deep waters and cold surroundings (10). Especially remote, low energy field developments are in need of pressure support and produced water management. The distance to existing processing facilities can be substantial and water-processing capacity at receiving facilities limited.

The stages of separation required depends on how the produced water is to be disposed. A bulk stage can be sufficient for disposal reservoir injection, while secondary separation, as outlined in Figure 2, is necessary to reach required water quality for production reservoir injection or direct release. While water quality is important, additional consideration must be given to required quality of separated oil. The quality of oil is often sacrificed to achieve sufficient quality of water. Accepted water rates in transported oil is dictated by available processing-capacity topside, which will vary depending on the business case considered. Ensuring a clean oil phase will in addition reduce challenges associated with flow assurance, as formation of hydrates can be minimized, and reduce challenges with corrosion, resulting from the presence of high salinity produced water. The level of separation needed is thus an important factor in determining available business cases for subsea water removal. A common feature for all configurations is the need for bulk stage separation. For this reason, the technologies to be reviewed in this paper will be limited to the bulk stage, starting with a more thorough overview of existing installations.

CURRENT INSTALLATIONS

Currently installed subsea bulk water separators has been a result of required de-bottlenecking of downstream processing equipment topside, including the Troll and Tordis installations (8) and the Marlim field development (9, 11, 12). This section will present the respective installations, the means of separation and operational experiences.

Troll Pilot

Separator design

The Troll separator is a horizontal three-phase gravity separator installed at a water depth of 340m. A novel design feature is the utilization of a cyclonic inlet device, having several specified separation enhancing functionalities (13). Oil and gas is extracted at a shared outlet for topside transportation, while water is rerouted for reinjection. The separator diameter is 2.8m with a length of 9m tan/tan (length of cylindrical section), the total length being 11.8m. The separator has an integrated sand removal system, consisting of two set of pipes located at the bottom of the separator, one for flushing of the shell and one for sucking out the particle carrying water. The system is operated by a booster unit deployed from surface support if needed. The separator is fully integrated with the pipe/valve manifold system, making retrieval challenging. The overall dimensions of the installation is 17x17x8 m with a total weight of 350 tons (14). Oil-water interface level is measured by a nucleonic system and control is achieved by speed variation of the water injection pump. An inductive device was installed as backup. The liquid capacity for the separator is specified as 63000 bpd, with a maximum OiW content of 1000 ppm and an upper water in oil (WiO) content of 10% (8).

Operational experience

The separator station was put into regular operation in August 2001 (8). Since then, the station has only been subject to a few shutdowns. From 2008 to 2016, Troll Pilot performed with 100% availability (14). Samples of the separated water displayed a separation efficiency exceeding design, with individual sample results ranging from 15 to 500 ppm (13). The station has contributed to significant oil production increase at the Troll C facility, with an estimated enabled water injection of 5.6 million m^3 as of 2010 (8). In 2008, increased production was calculated to approximately 2000 barrels of oil per day (14).

Tordis Subsea Separation, Boosting and Injection (SSBI) Station

Separator design

The Tordis separator is a semi-compact horizontal gravity separator installed at a water depth of 210m. It is designed with a high length to diameter ratio for optimized oil/water separation (8). The term semi-compact is used because of a novel gas-bypass cyclonic inlet configuration where gas is by-passed the main separator body and commingled with the oil at the separator outlet for multiphase boosting. This allows a more compact design of the gravity-settling vessel, as the total throughput has been significantly reduced. Produced water was planned for injection in a disposal reservoir (Utsira). The project aimed to increase the recovery from 49% to 55% equivalent to an additional oil production of 35 million barrels (8, 15). The sand handling system is a batch configuration, which starts with a sand jetting arrangement generating vortexes to fluidize and remove sand. The sand slurry is directed to a sand handling module after which the sand is discharged into the produced water line downstream the injection pump. Driving forces for the sand handling system is provided by high-pressure water from downstream the injection pump. The separator at Tordis SSBI is installed as one of ten separate modules, easing retrieval. The separator is 17m long (tan/tan) with a diameter of 2.1 m (16). The liquid capacity for the separator is specified as 189000 bpd, with a maximum OiW content of 1000 ppm and an upper WiO content of 56700 bpd, being the limit of topside water treatment capacity (8).

Operational experience

Tordis SSBI station was started up in October 2007. The system performed above expectation, producing OiW levels below design of 1000 ppm as well as having a high uptime (8). Due to complications with the disposal well, production from the SSBI station had to be shut down in May 2008. From July 2013, the Tordis separation station was back in operation. However, the produced water is now transported back to the Gullfaks C platform for treatment, as there is no available disposal well for local subsea water injection (10).

SSAO Marlim

Separator design

The SSAO Marlim is a subsea separator installed at a water depth of 870m in the Marlim field, Campos basin, Brazil. The pilot system had to consider new compact separation technology, as the conventional gravity separator would not be applicable at the water depths considered (12). No disposal reservoir was available for produced water injection, meaning produced water had to be injected into the producing reservoir, which put strict requirements on oil and particle content in the separated water. This led to the addition of water polishing and de-sander modules ensuring particle and oil content lower than 10 and 100 ppm respectively (9). In Figure 3, a process diagram of the separator design is given. The figure is based on a separation process illustration given in (11). Bold solid lines represent HC/Multiphase flow (red for gas, green for oil, black for production stream), bold stippled lines represent produced water (blue), and weak solid lines represent solid extraction (brown).

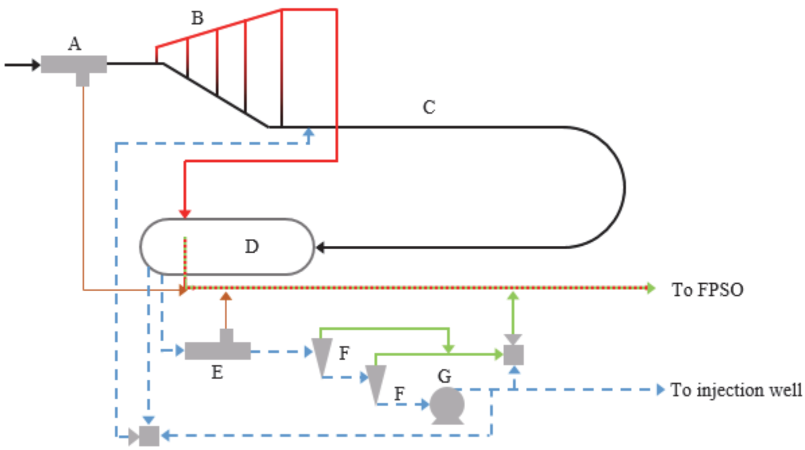

Figure 3: Illustration of Marlim separation process

A multiphase de-sander (A) reduces the amount of sand entering the other separator components. Downstream the de-sander a gas liquid separation segment “gas harp” (B), reduces the GVF to a maximum of 30% (9). The remaining fluids enter a pipe separator for oil/water separation (C). The pipe separator is approximately 60 meters long (11), and is connected to an outlet separator (D) where the phases are collected. The pipe separator and connected outlet vessel was designed to achieve an OiW content of maximum 1500 ppm (17). Oil with residual water and the separated gas is directed topside, while water is further treated. The polishing system consists of a de-sander (E), reducing the particle concentration to 10 ppm, and two stages of de-oiling hydrocyclones (F) ensuring an OiW content of less than 100 ppm (9). Reject flow from the de-sanders is injected to the multiphase flowline. The design expectancy was for 70% of produced water to be separated and injected, and the system was designed for a minimum WC of 70% in the incoming well-stream (17). Sand removal was performed by traditional sand jetting in the collection vessel, while a recirculation loop from downstream the injection pump to the pipe separator inlet was used for flushing of the pipe separator. Sand was transported with the hydrocarbons topside. The SSAO Marlim has a modular design, consisting of 10 retrievable modules, adding up to a total station size of 29x10.8x8.4m (LxBxH), and an overall assembly weight in air of 392 tons(11).

Operational experience

The injection and production wells were successfully connected to topside through the subsea installation in March 2012, followed by pump module installation in July 2012. Startup of the separation station was delayed because of the actual water cut being far below the expected value. Given the system design rate of 70% WC, a certain water rate was needed in order to run the flushing mechanism and water-polishing loop. This resulted in the station being bypassed the first months after installation (17). The system was brought online in February 2013, after a decision was made to recirculate water from downstream the injection pump to the inlet of the pipe separator ensuring operation within the design envelope. In March 2013, specified subsea produced water requirements were reached, and water was injected into the Marlim reservoir (17).

SUBSEA SEPARATION TECHNOLOGIES

Referring to Equation 3, existing installations display two approaches to making a bulk separator more compact, and thus attractive, for subsea installation. The first is for Tordis, where gas bypasses the main separator body, allowing a more compact vessel design. The second is the pipe principle utilized at Marlim, reducing settling length and allowing gravitational separation at large water depths. Looking to the literature, there are several proposed concepts for subsea bulk-water removal. This section will present a state of the art review of different bulk-water separation technologies, discussing their area of application and possible limitations in design.

Compact gravity

Compact gravity is the principle of separation as described for the Tordis installation. Gas is removed in a cyclonic inlet configuration, bypassing the gravity settling section, reducing the overall size of the installation. The concept is field proven with a reported separation efficiency below 1000 ppm oil in water, and has proven a viable technology for shallow water installations. The concept is based on the traditional gravity separator, but a reduced vessel size is made possible by inlet gas removal. A different approach to compact gravity separators is the spherical separator solution currently being developed as a JIP by Sulzer, previously ASCOM. The separator has a spherical shell, which allows for thinner walls and a more compact design compared to a cylindrical vessel installation. The shell is fitted with a spiraling baffle, allowing the liquid flow to utilize the maximum of the spherical volume, resulting in required residence times being reached (18). The design is envisioned as separate gas-liquid and liquid-liquid solutions working in series.

Considerations

Although the separator is more compact than conventional gravity separators, the overall vessel size is still large. As referenced, the separator installed at Tordis measures a tan/tan length of 17m with a diameter of 2.1m. This result in large and bulky separator modules, which weight will drastically increase with depth considered for installation. A calculative example of required shell thickness at 1500m water depth is given by Michaelsen in (19). A vessel diameter of 2.8m is estimated to require of wall thickness of 140mm carbon steel, resulting in a total weight for a 10m long separator of 100 tons. In comparison, a 1.5m diameter vessel will require a thickness of 47mm and a 0.5m diameter vessel a thickness of 25mm. In 2003 ABB proposed a long and slender gravity separator design with internals to promote the compact gravity principle for deep-water installations (19). The internals considered are electrostatic coalescence for enhanced droplet coalescence and di-electrophoresis for furtherer promotion of separation.

Pipe separator

When looking to separation in pipes, several alternative designs exists. The following technologies are solutions that to the author's knowledge have been or are currently being tested for subsea application. The extent to which respective technologies have been qualified may differ from reported results in the literature. Some patented and proposed solutions will also be included, discussing areas of interest for further development.

Horizontal pipe

Separation in a horizontal pipe is the principle of separation utilized for the SSAO Marlim installation. As such, the technology has already been field proven, and qualified for deep-water installation. The reduced diameter results in a shorter droplet traveling distance, enabling shorter residence times, which promotes a more compact design. The smaller pipe diameter will however result in larger flow velocities compared to a conventional gravity separator, meaning flow dynamics become more important in design. Although little to no results on the actual performance of the Marlim pipe separator is publically available, the concept was tested and reported by StatoilHydro (20), displaying OiW qualities below 600 ppm. A similar system has been developed and tested by ExxonMobil, including performance testing with added electrostatic coalescence (21, 22). A complete system overview is given in (21). Reported size of the pipe separator was a length to diameter ratio of 80.4. Testing of the separator was performed at low water cuts (10-40%) with light, medium and heavy crudes, with and without applied electrostatic coalescence. Reported results vary over the test regimes, but a separation efficiency below 1000 ppm OiW is displayed at the pipe separator outlet for multiple test points when electro coalescence is applied. Electrostatic coalescence did also drastically reduce the WiO content at the oil outlet, with reported readings being reduced from 24.8% to 2.7% for selected test points (22). The oil-water interface level was identified as an important control parameter for separator efficiency. Low interface levels lead to emulsion being extracted at the water phase outlet, drastically decreasing separator efficiency. An envisioned flow capacity per separation train of 60000 bpd is reported by ExxonMobil, with allowable water cuts ranging from 0 to 90% in the incoming flow (21).

Separation in pipes has also been the subject of several patents. A proposed concept for a pipe separator with improved separation efficiency is given by Gramme et al. (23, 24). Here, a water lock formed by an inclined pipe section is included in the design, allowing easier extraction of the water phase. Oil and gas passes this inclination, for separate extraction. The addition of a water lock can reduce the challenge of emulsion carry under in the water phase, as described by ExxonMobil, and offers a lightweight alternative to the collector vessel as utilized on SSAO Marlim.

Multipipe

An interesting extension of the pipe separator principle, allowing separation in pipes at lower velocities, is separation in multiple pipe sections. Saipem is currently designing and testing a separator system utilizing this multi-pipe principle (25). The separator is constructed of parallel spools, where the feed is split into several feedlines stretching down the length of the separator, which then expands into a larger diameter spool where separation takes place. The working principle of the SpoolSep is illustrated in Figure 4, which is based on a depiction given by Shaiek et al. (26). The SpoolSep has successfully completed a first step scaled testing campaign at low pressure and temperature with air, tap water and model oil, displaying basic functionality of the concept (26). Reported results displayed an OiW quality at the outlet in the range 500-2000 ppm depending on flow velocity, with WiO levels below 8%. Results showed a decline in efficiency with increasing velocities, and a sensitivity to water holdup level, where a holdup above 50% affects the drainage at the stand pipe outlet, decreasing separation efficiency (26). The water-oil interface level is controlled by a water injection pump. Sand removal is performed by directing all production flow to one spool, flushing out accumulated sand. The required fluid velocity for solid removal was investigated, and for velocities above

0.8 m/s, the sand was found to flow as a suspension in the liquid. The design case consisted of eight spools working in parallel, with total spool lengths of 50m, offering a design capacity of 49k-92k bpd, with WiO and OiW qualities of 15% and 1000 ppm respectively (26).

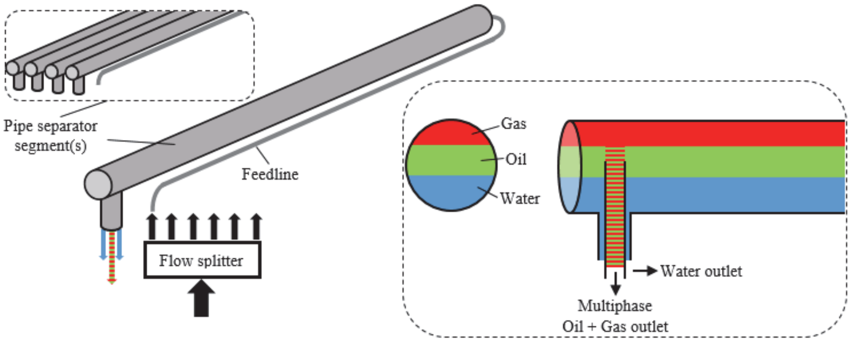

Figure 4: Illustration of SpoolSep working principle

Inclined pipe
A different approach to separation in pipe segments is to utilize inclination to achieve separation. Seabed Separation AS is currently developing a separation system that utilizes the inclined pipe principle. The design is explained in detail in patents (27, 28), and can in short be described as a dual pipe configuration where well fluids is fed through an inner tube which has a plurality of perforations enabling gravitational settling of sand and water in the bottom of the outer tube. The separator is known as the Dual Pipe Separator (DPS), and the concept has been subject to low pressure and temperature tests to investigate the effect of different design parameters on separation efficiency. As described in (28), the DPS is envisioned to work as a separator system of multiple inclined separators, offering adaption possibilities to change in fluid properties and differing oil wells. Arrangement can be either serial, to ensure that separation efficiency reaches specification, or in parallel to accommodate a wide variety of flow rates. The concept was recently presented at the Tekna Separation Technology conference in Stavanger (29), discussing further development plans and preliminary separator performance. An illustration of the DPS concept is given in Figure 5. Low pressure oil water tests were run with three 8 m long pipes in parallel, displaying an OiW content of 2,5% at optimized modifications, and WiO qualities of less than 0,5% for all tests (29).

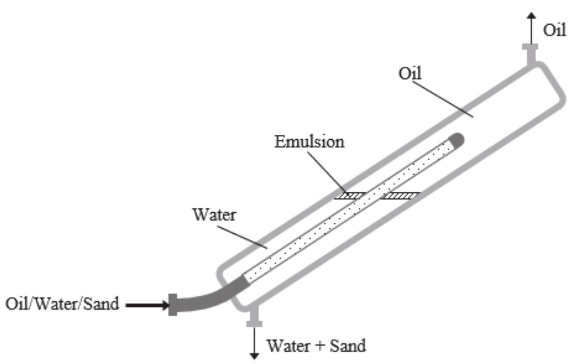

Figure 5: Operational principle of the DPS

Separation in inclined pipes has also been investigated at the department of Geoscience and Petroleum, NTNU. Performed research was part of the DGRASS/DEMO 2000 Program and looked into separation of water from a two/three phase mixture by utilizing distributed taping in an inclined separation tube. Experiments were low pressure, with model oil and water, and are reported by Rivera (30, 31).

Another concept utilizing an inclined pipe for separation is described in patent (32) from Schlumberger. In a similar manner to the inclined pipe principle investigated at NTNU, and the pipe solution proposed by Gramme et al (23, 24), this design utilizes gravity-based separation in pipe flow combined with an inclined pipe section to slow down the denser phase, creating an extending sump which can be extracted. Instead of having sequential tapping, this principle utilizes one tapping point, which flowrate is regulated by the position of the sump tail. The position of the tail is sensed, and tapping rate regulated accordingly. An illustration of the principle is given in Figure 6, as presented in (32).

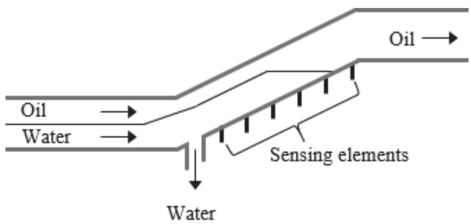

Figure 6: Patented concept by Schlumberger

Considerations
Separation in a pipe is field proven through Marlim, and extended testing by ExxonMobil at high pressure further promotes the technology in combination with electrostatic coalescence. Existing solutions are however bulky, consisting of long pipes, challenging the development of compact module designs as well as standardized solutions. Operational experience from Marlim illustrated potential risks of having systems designed for strictly water continuous flow regimes, as this can lead to potential shut down of the system. An alternative is seen in the multipipe configuration, which allows lower flow velocities, shorter pipes, and standardization of separate pipe segments to be used for a variety of field applications. The design specification dictates the number of pipes, which allows a final solution to be constructed of pre-qualified components. Although the concept is favorable in terms of standardization, the multipipe concept developed by Saipem is not compact, with envisioned spool sections of 50 meters in length. A potential solution for reducing the size is to develop concepts with upstream gas-liquid separation, allowing more compact and shorter pipe segments to be utilized for liquid-liquid separation. The concept can be further extended to include effects of inclination as previously discussed and possible phase locking mechanisms for eased extraction. This will also enable a more sensitive sensing regime for water levels, as it can be measured in extension of the hypotenuse caused by inclination, as illustrated in Figure 6. As both ExxonMobil and Spoolsep displayed sensitivity to water hold-up, the development of better-suited tapping mechanisms is attractive.

Inline cyclonic separator
Inline cyclonic separation technology is currently the most compact alternative delivered. The design relies on high centrifugal forces within a pipe segment to achieve separation. Inline separator solutions has been developed for multiple application areas, including gas-liquid separation, solids removal and liquid-liquid separation (16). Although no

inline liquid-liquid separators for bulk water removal has been installed subsea, the technology has been field tested at Gullfaks for topside qualification with promising results (33-36). There are several suppliers developing inline technology, whereas two were selected for the Gullfaks qualification tests. The two respective technologies will be presented in this section, together with their identified operational performance and limitations. A third supplier of cyclonic inline liquid-liquid separation technology is Sulzer, who has developed a twinline bulk deoiler. The technology is briefly presented in (37), but no detailed performance data was included.

InLine DeWaterer
The InLine Dewaterer is a cyclonic oil-water separator delivered by TechnipFMC. The working principle is that mixed oil-water flow enters the pipe in an inlet compartment, after which it flows through an internal liner where a swirl element imposes rotation. The swirling motion generates a centripetal acceleration, forcing oil and residual gas to the center of the liner, while water and sand is directed to the liner outer wall. As for conventional hydrocylones, the lighter phase is extracted through a reject flow, and the heavy phase through the underflow (35). An illustration of the working principle is given in Figure 7, as reported in (35).

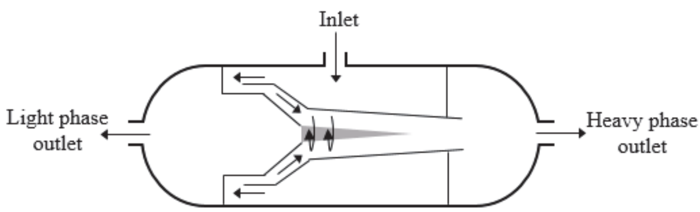

Figure 7: Working principle of InLine DeWaterer

The illustrated design is of a single liner in a surrounding pipe spool. Several liners can be combined in a larger spool/vessel for increased flow capacity. The unit tested at Gullfaks was a single liner with a flow capacity of 25m^3/h. Reported results displayed promising performance, and can be reviewed in detail in (34). At 60% water removal, 75% of test points displayed OiW levels below 500 ppm and 95% below 1000 ppm. The unit displayed a break point in performance where further increase of the water removal rate resulted in a drastic decrease in separator efficiency. Best results were seen for low flow rates, 50% of design, where the breakpoint occurred at 90% water removal. At higher flow rates, the water removal is limited to 80%. As long as the unit operated with water continuous flow, no significant effect of water cut on separation efficiency was observed. The referenced results are for low gas loadings, GVF < 5%. Separation efficiency was seen to decrease rapidly with increasing GVF. The reported pressure drop for the unit at design was 2 bar (34, 35).

Wx Separator
The Wx is an oil-water cyclonic separator developed and delivered by Caltec Limited (36). The design of the Wx separator follows the same principles as Caltec's gas-liquid compact separator named I-SEP, which is illustrated in Figure 8, based on reported design in (36). Multiphase flow enters the separator in an inlet involute, where a swirling motion is generated. The fluids are then separated in the separation chamber before the heavy phase is extracted in an outlet involute and the lighter phase in a separate light phase outlet.

The offshore trials at Gullfaks were completed with a $25m^3/h$ (3770 bpd) unit. Caltec has further developed three basic designs, Wx-6, Wx-12, and Wx-25 processing 6250, 12500 and 25000 bpd respectively. The unit can handle flow rates from 50-110% of design without reduction in water quality. With a water removal rate of 50-70% a water quality below 1000 ppm could be obtained. The breakpoint for the Wx separator was observed to occur around 70% water removal. Measurements below 500 ppm were obtained for 30% of the measuring points, with the majority being in the range 500-1000 ppm (34). The Wx technology displayed good tolerability for gas at the inlet, showing no deterioration in water quality with a GVF up to 20%. A similar pressure drop as for the DeWaterer was observed.

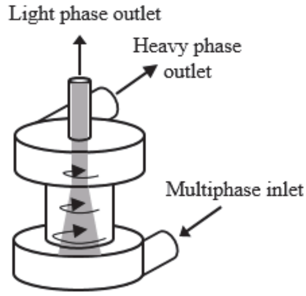

Figure 8: I-SEP separation principle

Considerations

The tests for both commercial cyclonic inline technologies were performed with actual well fluids from Gullfaks C. Both technologies have thus been qualified for real operating conditions for topside application. The experienced operating envelope was 50 to 110-130% of design, depending on technology, with a water removal rate of up to 70-80%. The specified operational envelope can provide an oil in water content lower than 1000 ppm, which corresponds to the design quality of the Troll and Tordis installations. For lower ppm's, water removal should be limited to 60%.

In regards to bulk water removal, both technologies are only qualified for water continuous flow. This limits the application to brownfield developments, where water content is sufficiently high, or requires a constant recirculation of water to maintain needed operational conditions. Reported results do not describe transient behavior, which can influence in situ water quality experienced by downstream equipment. However, the concepts displayed robustness in terms of water cut influence on separation efficiency. This indicates that a conservative water removal rate can be set in order to ensure acceptable oil in water quantities at the reject. A conservative removal rate will however result in a large amount of water being present in the transported oil, which may put restrictions on suitable business cases for implementation. An imagined example of a production well containing 70% produced water and a water removal efficiency of 60% will result in a water in oil content at light phase outlet of 48%. An interesting possibility is combining the inline technology with buffer vessels to either reduce transients prior to separation or provide additional downstream separation. Using the inline technology as a component in a combined system can increase the area of applicability. Such a solution was recently proposed by FMC at the Separation Technology 2016 conference in Stavanger (38), where the DeWaterer was included as a downstream separation step to a compact gravity vessel. Saipem has also developed and tested a combined system for liquid-liquid separation named the 3C cyclone (39). The design consists of a first stage liquid-liquid hydrocyclone, with a downstream vessel for pressure regulation, eased control and additional separation.

Alternative technologies

There are several alternative technologies being developed for oil water separation. A range of special wettable materials is under continuous development, and a thorough review of current state of the art is given by Xue et al. (40). The article presents recent developments in superhydrophobic and superoleophilic materials for oil removal, superhydrophilic and superoleophobic materials for water removal and lastly a range of controllable separation principles by the use of magnetism or electrically induced filters.

Separation by acoustics is another interesting concept being reported in the literature. A standing wave pattern is excited in a fluid by ultrasonic waves, creating a number of pressure nodes and antinodes. Dispersed quantities in the fluid will then be subject to acoustic forces, leading to a concentration of dispersed media in either pressure nodes or antinodes dependent on the fluid properties. The concept has previously been reported for separation of suspended particles by i.e. Benes et al. (41) and Shi et al. (42), and has also proved successful in separating and harvesting microalgae, as reported by Bosma et al. (43). In terms of oil water separation, the technique can be used to enhance coalescence, as dispersed droplets are forced together in respective nodes. Ultrasonic separation of oil-water emulsion was investigated and reported by Nii et al. (44), where irradiation by 2MHz ultrasound to prepared emulsions led to immediate flocculation of oil droplets, causing a significant increase in rising rate compared to that of oil droplets in the prepared emulsion. The concept has also recently been proposed as a downhole separation method to be used for oil field applications (45), indicating potential of separation of both particles and dispersed oil droplets form water. Separation by acoustics offers an alternative to the current electrostatic coalescence technology, with a wider area of application. It offers the possibility of solids extraction, as well as providing coalescence for both oil in water and water in oil dispersions. The working principle has only been investigated small-scale, and further investigations is needed in order to determine its' potential for actual field application.

SUMMARY, TRENDS AND TECHNOLOGY READINESS

Reviewed technology display a series of promising developments for liquid-liquid subsea separation. A continuous evolvement is seen from the early Troll pilot installation, where a three-phase gravity separator was utilized; into the more compact Tordis bypass configuration and finally the pipe separation principle at Marlim, allowing gravitational separation at large water depths. New developments display an increased focus on standardized component developments, which can be used as building blocks for a complete system design. This is seen by looking to the SpoolSep design presented by Saipem, and Seabed Separation's DPS. In terms of separator efficiency, qualified concepts have already displayed OiW quantities below 1000 ppm, being equivalent to topside bulk separator requirements. The Marlim development and ExxonMobil's pipe separator also display the applicability of subsea water polishing, opening the possibilities for reservoir injection and direct release. In terms of WiO qualities, reviewed technologies display varying performance. While ExxonMobil display WiO levels as low as 2.7% with the use of electrostatic coalescence, inline cyclonic technologies can experience more than 40% water in separated oil, making WiO levels an important differentiator when selecting equipment for field development. Another limiting factor can be required turndown ratio, where gravitational vessel/pipe developments are preferred compared to cyclonic equipment, which at default design is limited to 50% of design capacity. Separation by gravity appears to be the favored means of separation in both existing and new developments. This can be seen for all currently installed cases. A possible explanation for this is the lacking experience with cyclonic liquid-liquid separators as primary separation equipment (3). The technology is applied topside for water dominated flow, but there is limited information on oil-dominated conditions, which can lead to unforeseen scenarios unwanted subsea (3).

In terms of technology readiness, the literature offers few exact specifications. Utilizing the API technology readiness level (TRL) scale, which is divided into seven sections, where seven is proven and integrated technology, and zero an unproven idea/concept, reviewed concepts can be ranked according to reported development in qualification. Fully qualified technology includes compact gravity and horizontal pipe separation, as these are already field proven concepts. For inline cyclonic separators, the technology has been qualified for topside operation, however, in terms of subsea application, FMC reported their DeWaterer to a TRL of 3 at the Separation Technology conference in Stavanger (38). Low pressure and temperature tests has been reported for multipipe and inclined pipe concepts, while separation enhancing technologies such as acoustic irradiation for subsea oil-water separation is still in early stage development. Figure 9 gives an illustrative overview of the progress in development of each major technology discussed. Apart from referenced TRL levels, the illustration is only aimed at giving an approximate overview of the progressive development, and individual rankings may vary from what is reported here.

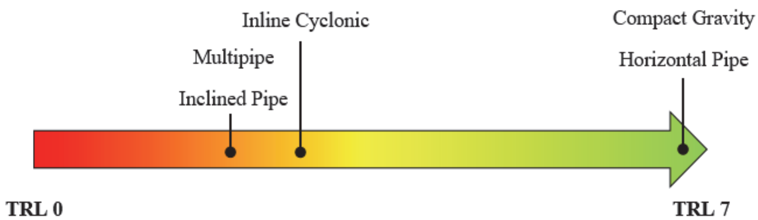

Figure 9: Illustration of TRL for subsea application of discussed technologies

TEST FACILITY DEVELOPMENT

In order to investigate new compact separator designs, a multiphase test facility for oil-water separation is currently under construction at the Norwegian University of Science and Technology. The project is part of the recently initiated research center SUBPRO, focusing on technology advancements within subsea production and processing. The P&ID for the facility is given in Figure 10, and testing of concept ideas will start 2H 2017.

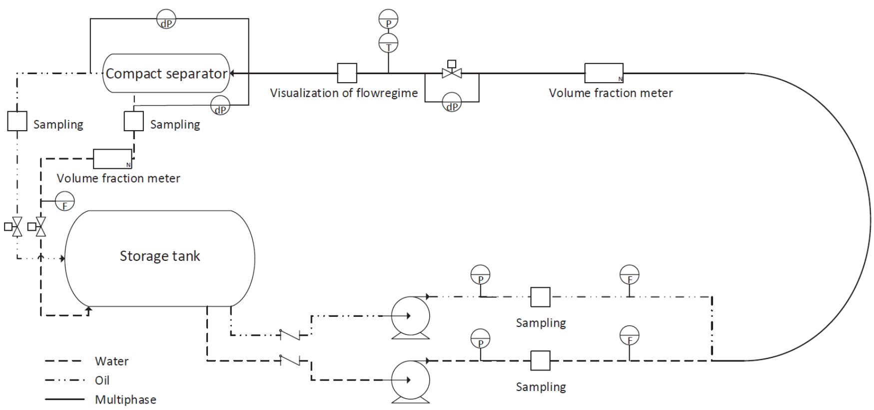

Figure 10: P&ID of designed multiphase test facility

The facility has a storage tank designed to room six cubic meters of fluid and provide baseline separation. A pump manifold consisting of four centrifugal pumps will supply boosting, where two pumps are connected to the rig at any given time. The design allows flow rates in the range 100-2100 L/min for the water phase and 100-1700 L/min for the oil. A return line from pump manifold outlet to inlet can be installed, allowing flow rates down to 50L/min. Respective flow rates are limited by separation efficiency in the storage tank, which is estimated to be 1000 L/min of each phase. Pump speed is controlled by frequency converters, and installed flowmeters allow adjustment of water cut (WC) to desired specification. Applied pipes are 75mm diameter transparent PVC, allowing visualization of developed flow regime. Pressure rating of piping is PN10 (10bar). Oil and water is combined at a comingling point, which is followed by a 12m long pipe section leading to the compact separator module. The line is fitted with a capacitance volume-fraction meter to allow verification of WC in the planned operating range (10-90%), and pressure and temperature sensors are installed to determine fluid properties. The addition of a butterfly valve with pressure loss measurement is considered for controlled dispersed regime generation, as presented by Fossen and Schumann (46). Differential pressure sensors are installed to measure the respective pressure drops over the compact separator module, and electrically controlled valves allow adjustment of extraction flow rates to facilitate control of separator performance. The compact separator water-extraction line is fitted with a sampling point and a downstream flow meter for accurate determination of separator efficiency. The addition of a second water fraction meter for continuous water quality monitoring is currently being considered, and is included as part of the design. Additional sampling points are included at key locations for accurate determination of fluid properties and composition. Test fluids are ExxsolD60 and distilled water with modified salinity (3.5vol% NaCl). A higher viscosity oil and addition of air for three-phase flow is considered for further testing of promising concepts.

Developed compact separator concepts will be designed to overcome challenges outlined with current technologies, offering separator solutions that are robust, effective and that facilitates easy installation and retrieval. Successful development will allow wider application of a technology that provides increased returns, increased recovery and more energy-efficient production.

ACKNOWLEDGMENTS

This work was carried out as a part of SUBPRO, a Research-based Innovation Centre within Subsea Production and Processing. The authors gratefully acknowledge the financial support from SUBPRO, which is financed by the Research Council of Norway, major industry partners and NTNU.

REFERENCES

1. Fakhru'l-Razi, A., et al., *Review of technologies for oil and gas produced water treatment.* Journal of hazardous materials, 2009. 170(2): p. 530-551.
2. NorskOiljе&Gass, *Environmental work by the oil and gas industry - Facts and development trends*, in *Environmental Report*. 2016. p. 17.
3. da Silva, F.S., et al. *Subsea Versus Topside Processing-Conventional and New Technologies*. in *OTC Brasil*. 2013. Offshore Technology Conference.

4. Kuhnle, T.I., *All Subsea - Creating value from subsea processing*, in *Underwater Technology Conference (UTC)*. 2015, DNV GL.
5. Kristiansen, O., Ø. Sørensen, and O. Nilssen. *CompactSep™-Compact Subsea Gas-Liquid Separator for High-Pressure Wellstream Boosting*. in *Offshore Technology Conference*. 2016. Offshore Technology Conference.
6. EN, B., *13445-3: 2009.* BSI British Standards. Unfired pressure vessels-Part, 2009. 3.
7. Hannisdal, A., et al. *Compact separation technologies and their applicability for subsea field development in deep water*. in *Offshore Technology Conference*. 2012. Offshore Technology Conference.
8. Davies, S.R., et al. *Experience to date and future opportunities for subsea processing in StatoilHydro*. in *Offshore Technology Conference*. 2010. Offshore Technology Conference.
9. Capela Moraes, C.A., et al. *Marlim 3 Phase Subsea Separation System: Subsea Process Design and Technology Qualification Program*. in *Offshore Technology Conference*. 2012. Offshore Technology Conference.
10. Ramberg, R.M., H. Rognoe, and O. Oekland. *Steps to the Subsea Factory*. in *OTC Brasil*. 2013. Offshore Technology Conference.
11. Orlowski, R., et al. *Marlim 3 Phase Subsea Separation System-Challenges and Solutions for the Subsea Separation Station to Cope with Process Requirements*. in *Offshore Technology Conference*. 2012. Offshore Technology Conference.
12. Euphemio, M., et al. *Subsea Oil/Water Separation of Heavy Oil: Overview of the Main Challenges for the Marlim Field-Campos Basin*. in *Offshore Technology Conference*. 2007. Offshore Technology Conference.
13. Horn, T., W. Bakke, and G. Eriksen. *Experience in operating world's first subsea separation and water injection station at Troll Oil Field in the North Sea*. in *Offshore Technology Conference*. 2003. Offshore Technology Conference.
14. Bakke, W. and H.K. Sundt. *Troll Pilot - The world's first and longest-running subsea separation system*. [PowerPoint presentation] in *UTC*. 2016. Statoil/General Electric.
15. Mogseth, G. *Functional verification of the worlds first full field subsea separation system-TIORA*. in *Offshore technology conference*. 2008. Offshore Technology Conference.
16. Khoi Vu, V., et al. *Comparison of subsea separation systems*. in *Offshore Technology Conference*. 2009. Offshore Technology Conference.
17. de Oliveira, D.A., et al. *Comissioning and Startup of Subsea Marlim Oil and Water Separation System*. in *OTC Brasil*. 2013. Offshore Technology Conference.
18. Mika Tienhaara, B.L. *Subsea ultradeepwater compact multiphase spherical separation system*. in *Rio Oil & Gas Expo and Conference 2012*. 2012. Rio: ASCOM Separation.
19. Michaelsen, J. *Innovative technology for ultradeepwater gravity-based separators*. in *Offshore Technology Conference*. 2003. Offshore Technology Conference.
20. Sagatun, S.I., et al. *The Pipe Separator-Simulations and Experimental Results*. in *Offshore Technology Conference*. 2008. Offshore Technology Conference.
21. Grave, E. and M. Olson, *Design and Performance Testing of a Subsea Compact Separation System for Deepwater Applications.* Oil and Gas Facilities, 2014. 3(04): p. 16-23.
22. Olson, M., et al. *Performance Testing of an Integrated, Subsea Compact Separation System with Electrocoalescence for Deepwater Applications*. in *Offshore Technology Conference*. 2015. Offshore Technology Conference.
23. Gramme, P.E. and I. Haukom, *Pipe separator for the separation of fluids, particularly oil, gas and water*. 2009, US Patent 7516794 B2.

24. Gramme, P. and G.H. Lie, *Pipe separator with improved separation*. 2009, US Patent 0102369 A1.
25. Abrand, S., et al. *Subsea Gas-liquid And Water-hydrocarbon Separation: Pipe Solutions For Deep And Ultra Deepwater*. in *OTC Brasil*. 2013. Offshore Technology Conference.
26. Shaiek, S. and L. Grandjean. *SpoolSep for Subsea Produced Water Separation-Experimental Results*. in *Offshore Technology Conference*. 2015. Offshore Technology Conference.
27. Skovholt, O., *Inclined Tubular Separator for Separating Oil Well Substances*. 2015, US Patent 20,150,343,328.
28. Skovholt, O., *Method for Separating Substances Mixed in Fluids From Oil Wells*. 2015, US Patent 20,150,343,327.
29. Hovda, A.J. *Matching established know-how into a subsea process system providing a versatile solution for life of field operation*. [PowerPoint presentation] in *Tekna Separation Technology Conference*. 2016. Stavanger: Seabed Separation.
30. Rivera, R.M., et al. *Water separation from wellstream in inclined separation tube with distributed tapping*. in *SPE Annual Technical Conference and Exhibition*. 2006. Society of Petroleum Engineers.
31. Rivera, R.M., *Water separation from wellstream in inclined separation tube with distributed tapping*, in *Department of Petroleum Engineering and Applied Geophysics* 2011, Norwegian University of Science and Technology.
32. Berard, M., K. Babour, and I. Babelli, *In-line flow separation of fluids in a pipe separator*. 2013, Google Patents.
33. Knudsen, B.L., et al. *Field Test of Compact Cyclonic Technology for Separation of Gas/liquid and Oil/water at The Gullfaks Field*. in *Offshore Technology Conference*. 2010. Offshore Technology Conference.
34. Bjorkhaug, M., B. Johannesen, and G.S. Eidsmo. *Flow Induced Inline Separation (FIIS) De-watering tests at the Gullfaks Field*. in *SPE Annual Technical Conference and Exhibition*. 2011. Society of Petroleum Engineers.
35. Westra, R., et al. *Qualification of inline dewatering technology*. in *SPE Offshore Europe Oil and Gas Conference and Exhibition*. 2013. Society of Petroleum Engineers.
36. Rehman, A., S. Peeran, and D.N. Beg. *Compact In-Line Bulk Water Removal Technologies-A Solution to the High Water Cut Challenges*. in *SPE Kuwait Oil and Gas Show and Conference*. 2015. Society of Petroleum Engineers.
37. Schook, R. and D. Thierens. *Debottlenecking of Mature Field Production through the Use of Very Compact and Efficient Separation Equipment, Topside or Subsea*. in *Offshore Technology Conference*. 2011. Offshore Technology Conference.
38. McKenzie, L., W. Krogh-Moe, and S.H. Høy. *Development of Sepfut*. [PowerPoint presentation] in *Separation Technology 2016*. 2016. Stavanger: FMC Technologies.
39. Butin, N., et al. *A New Simple And Efficient Technology For Subsea Bulk Oil/Water Separation For Production Enhancement-3C Cyclonic Separator*. in *Offshore Mediterranean Conference and Exhibition*. 2011. Offshore Mediterranean Conference.
40. Xue, Z., et al., *Special wettable materials for oil/water separation.* Journal of Materials Chemistry A, 2014. 2(8): p. 2445-2460.
41. Benes, E., et al. *Ultrasonic separation of suspended particles*. in *Ultrasonics Symposium, 2001 IEEE*. 2001. IEEE.
42. Shi, J., et al., *Continuous particle separation in a microfluidic channel via standing surface acoustic waves (SSAW).* Lab on a Chip, 2009. 9(23): p. 3354-3359.
43. Bosma, R., et al., *Ultrasound, a new separation technique to harvest microalgae.* Journal of applied Phycology, 2003. 15(2-3): p. 143-153.

44. Nii, S., S. Kikumoto, and H. Tokuyama, *Quantitative approach to ultrasonic emulsion separation.* Ultrasonics sonochemistry, 2009. 16(1): p. 145-149.
45. Abdel-Fattah, A.I. *Acoustic Downhole Three-Phase Separation Method in Oil Field Applications*. in *Abu Dhabi International Petroleum Exhibition & Conference*. 2016. Society of Petroleum Engineers.
46. Fossen, M. and H. Schümann, *Experimental Study of the Relative Effect of Pressure Drop and Flow Rate on the Droplet Size Downstream a Pipe Restriction.* Journal of Dispersion Science and Technology, 2016.

Chapter 3

Methodology

This chapter gives an overview of the design and experimental work activities carried out throughout this PhD. This includes design of a novel oil-water bulk separator principle, prototype design and construction, design, construction and commissioning of an experimental oil-water test facility, and experimental campaigns carried out to test the developed separator concept. This chapter serves as an introduction for Chapters 4-7 which present results from the respective experimental campaigns in the form of published conference papers and journal articles.

3.1 Separator concept design

A thorough description of the separator concept design process is given in Paper II, Chapter 4. This section gives a brief overview of the development, as a general understanding of the separator concept and prototype design is needed for explaining performed experimental campaigns.

In Chapter 2, a detailed overview of existing oil-water separator technologies were given. Existing subsea produced water separator installations were presented, and new developments currently being tested were discussed. Current installations are the Troll [9, 18] and Tordis [9, 22] vessel type gravity separators, and the Marlim pipe separator [7, 25, 13, 10]. In Chapter 4, drawbacks and benefit of the respective design approaches will be discussed. The vessel type separators offer good operational capacity and range, while the pipe separator offers shorter droplet travelling distances and separation at large water depths. In terms of drawbacks, both design approaches are large and bulky, and the pipe separator has limited flow capacity.

As discussed in Chapter 1, mature field developments have limited remaining resources, and low cost separator installations are thus essential for promoting the business case of subsea produced water separation. Looking to current installations, focus areas for cost reduction can be outlined. Firstly, the size of the separator installation affects several cost factors. Material cost, production cost, transportation cost and installation cost will all be proportional to the size and weight of the overall installation. Developing more compact separator installations will reduce these cost factors. A second driver for cost is testing and qualification. All current installations have been subject to individual test and qualification campaigns. Continued custom made installations for new developments drives cost. Developing standardized designs which are applicable to a wide range of field operating conditions will again reduce overall cost. In order to develop standardized designs it is important to maintain a large operational capacity and a wide operational range, especially for more compact separator designs. Capacity and operational range are also important factors for safe and continuous operation, which reduces down-time, securing overall better returns for the investment.

The focus on more compact standardized separator concepts is clearly seen in new technology developments, which was presented in Chapter 2. Saipem is developing and testing a pipe based concept, the SpoolSep, consisting of several 50 *m* pipe spools in parallel [2, 28]. A different pipe based concept, the Dual Pipe Separator (DPS), is currently being developed by Seabed Separation AS. The separator concept consist of modular inclined pipe segments mounted in parallel [33, 34]. The modular design approach illustrated in both these concepts allows the construction of compact standardized separator modules, which can be combined in parallel and or series to provide the needed operational capacity and range for the installation in question.

Based on outlined cost drivers and favourable design aspects discussed in this section, the following focus points were established for the new separator concept development:

1. Compactness
2. Suitability for standardization
3. Capacity and operational range
4. Modular design

3.1.1 Separator concept

The developed separator concept was designed by the author, with input from the main supervisor. The finished design was presented for industry partners to asses interest for further development. Given positive feedback, the design was selected for the basis of further study.

A pipe separator was used as a starting point for concept development. The pipe separator offers gravity based separation (a well known and robust principle of separation) at large water depths. The smaller pipe diameter offers reduced droplet travelling distances, reduces required wall thickness at deep waters and allows cheaper production. The drawbacks of the current pipe separator design is presented in Chapter 4 and amounts to the following:

1. Size: The one pipe solution of the current design leads to high fluid velocities. As a result, the pipe must be long to ensure sufficient separation. The total length of the pipe used for the Marlim installation is 60 *m* [25]. Additionally, the current extraction solution is bulky, and adds to the overall module size.

2. Capacity: A second effect of the smaller pipe diameter and higher fluid velocity is a capacity constraint. The flow regime in the separator must not transition into the dispersed regime, which counteracts separation. For illustration, the predicted liquid capacity of the Marlim pipe separator was 22500 *bpd* [10], while the Troll and Tordis separators had specified liquid capacities of 63000 and 189000 *bpd* respectively [9].

In light of these drawbacks, it was decided to design a concept utilizing multiple horizontal pipe sections in parallel. This will increase the total cross-sectional area of the separator, reducing velocity, allowing shorter pipe segments to be used in the design and secures higher liquid capacity. Current horizontal multi-pipe developments are not compact. The SpoolSep design developed by Saipem consists of several 50 *m* long, 24 *inch* outer diameter (OD) pipe spools in parallel [2]. This is a 3-phase separator concept, explaining the large spool sizes. Applying up-stream gas removal will allow more compact pipe segments to be used in the design.

A preliminary study including initial simplified capacity and potential weight reduction estimates for a multi-pipe design was carried out to justify further development. In the study, complete up-stream gas-liquid separation was assumed. Results are given in Paper II [30], Chapter 4, and display a potential weight reduction for a nine pipe solution compared to a vessel type separator at 1000 *m* water depth of 67 %. Capacity estimates were performed on pipe sections ranging from 6-7 *m* in length. It was decided to restrict length such that retrievable pipe modules fit within a 6 *m* by 6 *m* horizontal footprint, as outlined by industrial partners as the restricted retrievable module size. Simplified initial capacity estimates for a 6.5 *m* long 450 *mm* internal diameter (ID) dual pipe arrangement displayed a total liquid capacity ranging from 7625-18977 *bpd* depending on inlet WC and applied droplet cut off diameter. Based on these promising initial estimations, a complete concept proposal was developed.

The designed separator concept has been given the name Multiple Parallel Pipe Separator (MPPS), and a 3D concept illustration of the design is given in Figure 3.1. A complete description and justification of the design is included in Chapter 4. For the benefit of the reader, a summary will be given here.

A multiphase production stream enters in a T-section header (1) that divides the incoming flow into individual branch streams. Gas is removed in descending pipe elements (2) that further splits the production stream into horizontal pipe segments. Inspiration for the gas-liquid separation principle is the gas-harp installed as part of the Marlim pipe separator [7]. In case of up-stream gas-liquid separation, an alternate design will be a horizontally aligned

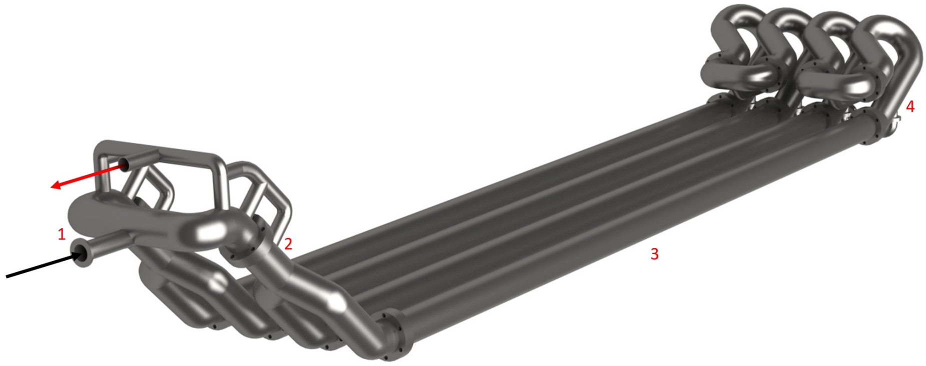

Fig. 3.1 Illustration of the MPPS concept

inlet section, dividing the production stream into respective separator branches. Downstream the inlet section, oil and water are separated in horizontal pipe sections (3). Horizontally aligned pipe sections minimize droplet travelling distance, and the multi-pipe approach ensures low fluid velocities, reducing required pipe section lengths. As previously outlined, current pipe separator designs have a bulky extraction design. The developed concept utilizes inclined pipe sections (4) for compact and controlled phase extraction. Water is extracted at the bottom of the inclined pipe sections, while oil flows up, over, and back down for separate extraction. A better illustration of the extraction section is given in Figure 3.2.

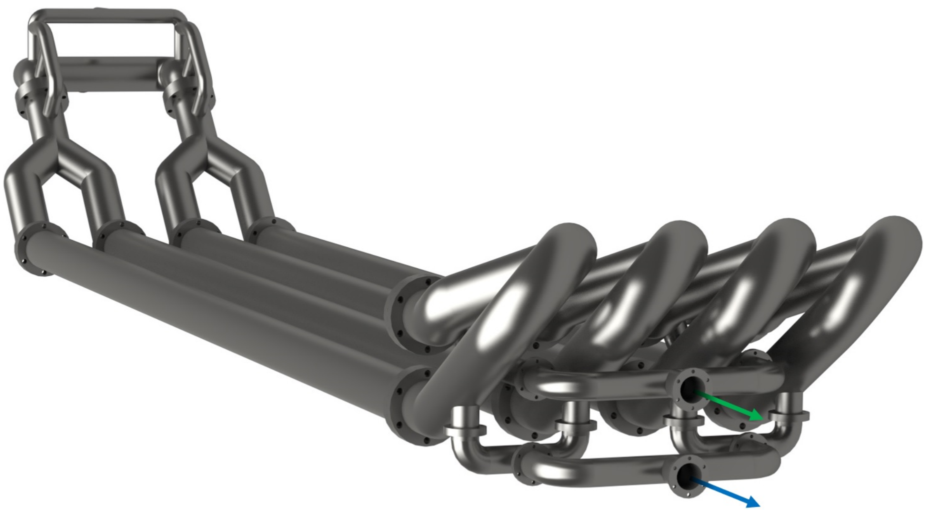

Fig. 3.2 Illustration of the MPPS extraction design

The upwards inclination slows down the water, working as a water lock, which builds up the water holdup. As a result, the water layer at the end of the pipe sections will be high irrespective of the inlet WC, reducing the risk of oil carry under in extracted water. The design was inspired by a proposed pipe separator design by Gramme et al. [16, 15], an in-line flow separator design by Berard et al. [3] and previous work at IGP, NTNU on oil-water separation in an inclined separation tube by Rivera et al. [26]. All cited solutions are for single pipe configurations. The novelty of the proposed extraction design is applying a similar principle for a multi-pipe arrangement, and connecting the outlets in a shared extraction point. The latter ensures self-regulation of the water layers in the respective pipe sections, easing separator control.

An important part of the design is the modular design approach allowing flexibility in capacity and operational range. The forming of the extraction section is such that secondary pipe sections can be connected in series if needed. Illustrations in Figures 3.1 and 3.2 display a solution with four pipes in parallel. This can also be increased depending on necessity. The scalability of the design is illustrated in Figure 3.3, where an eight pipe system with series connection is depicted.

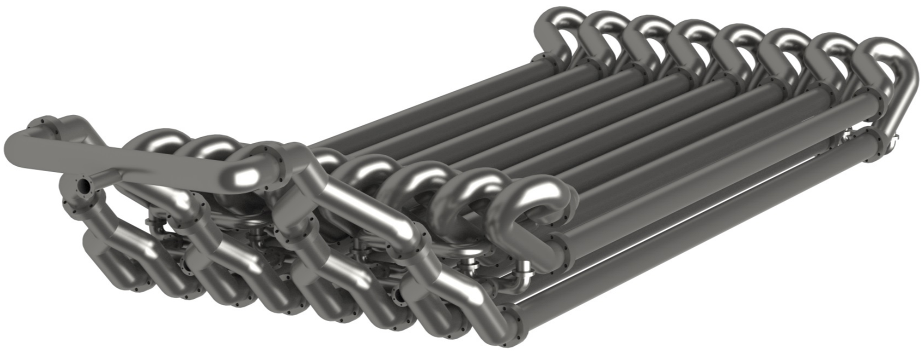

Fig. 3.3 Illustration of parallel and series mounting of MPPS segments

3.1.2 Prototype design

A prototype was constructed in order to experimentally investigate the MPPS functionality. The prototype was designed by the author, with input from the main supervisor. Construction of the prototype was completed by the author, in collaboration with Senior Engineer Noralf Vedvik and Master student Martin Holberg Marthinussen.

A 3D model of the constructed prototype is given in Figure 3.4. The prototype consists of two pipes in parallel, a limitation set by available lab space. The prototype is constructed in Polyvinyl chloride (PVC), with transparent 150.6 mm ID pipe sections as illustrated. Flange joints and bends are in coloured PVC plastic. The total length of the prototype is approximately 6.1 m. Detailed dimensioning is included in Section 3.3.1.

Oil and water enters to the right of the figure ($\dot{Q}_{in}$) in the T-section header. Several inlet configurations have been constructed and tested. More information on this will follow in Section 3.3.2. The inlet flow is divided into two separate branches before entering descending pipe elements. No gas removal pipes are fitted to the descending pipe sections, as no gas

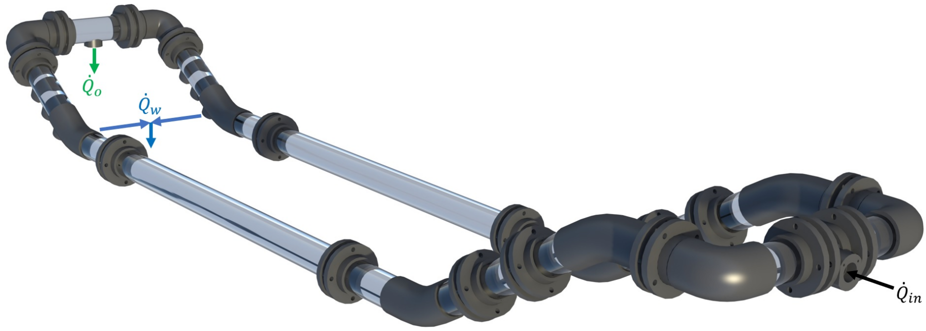

Fig. 3.4 Illustration of the MPPS prototype

supply is available in the current test facility. It was decided to include the descending sections in the prototype to allow future modification for 3-phase separation. Liquid-liquid separation takes place in the horizontal pipe elements before water is being extracted in a shared outlet at the bottom of the extraction section ($\dot{Q}_w$) and oil at the top ($\dot{Q}_o$). The prototype is constructed with several potential water extraction locations. More information on this will follow in Section 3.3.1. Initial inclination angle for the inlet and outlet sections were both set to 30 °. This corresponds with best efficiency configuration tested by Rivera et al. [26]. The MPPS prototype has a pressure rating of PN6 (6 *barg*).

3.2 Experimental facility

A two-phase oil-water test facility was designed and constructed as part of this PhD in order to test and validate the developed separator concept. The experimental facility was designed and dimensioned by the author in collaboration with Senior Engineer Noralf Vedvik, with input from the main supervisor. Acknowledgement is also given to Master student Espen Olaf Hestdahl for contributing to the design and construction of the pump manifold, and to Master student Ellen Kristine Knudsen Ellertsen for assisting in the development of the Particle Video Microscopy (PVM) insertion point. Instrumentation was selected and acquired by the author, with input from the main supervisor. The data acquisition system (DAQ) was designed and commissioned by the author in collaboration with Senior Engineer Steffen Wærnes Moen. The experimental facility is presented in Paper II, Chapter 4. However, a more thorough outline will be given here, including detailed specifications for the respective components, an outline of the DAQ system, calibration procedure and error estimation.

A pipe and instrumentation diagram (P&ID) of the constructed test facility is given in Figure 3.5. The facility, as presented in this section, is the final version of the test rig. The reported test facility in respective papers might vary slightly from the one presented here, depending on the stage in development at paper publication. Variation is limited to test fluid specifications and number of reported sensors. The respective sensor specifications outlined here are valid for all performed and reported experiments in this dissertation.

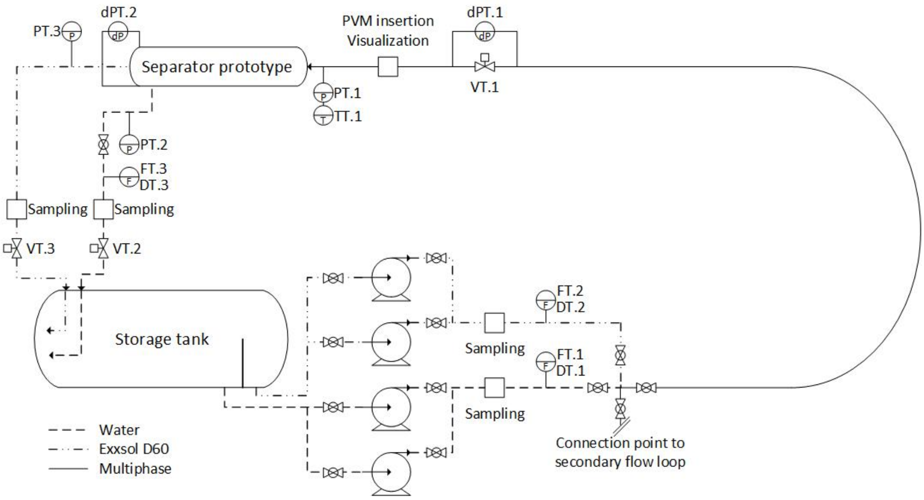

Fig. 3.5 Experimental facility P&ID

3.2.1 Storage tank

The storage tank is a 1.2 m diameter, 5.5 m long horizontal gravity separator, providing baseline separation. The tank rooms 6 m^3 of test fluids, and design specification allows for continuous operation at individual flow rates up to 750 L/min with a specified cut off diameter of 150 μm. Test fluids are Exxsol^{TM} D60 and distilled water with added NaCl. A biocide (IKM CC-80) was added to the water for bacterial growth inhibition, and 0.015 g/L of the colourant Oil Red O ($C_{26}H_{24}N_4O$) was added to the Exxsol^{TM} D60 for easier phase distinction. The amount of biocide added, and level of water salinity is reported for each respective experimental campaign. For select experiments in test campaign four, 15 ppm of the surfactant Span$^{®}$85 was added to the Exxsol^{TM} D60. Again, details will be given in the experimental campaign outline.

The storage tank has two inlets, one for each of the MPPS prototype return lines. As indicated in Figure 3.5, storage tank inlets are directed towards the back wall of the storage tank, close to the oil-water interface. This is to reduce momentum in the tank flow direction, and to ensure short travelling distances for the respective phase dispersions. Measured from the bottom of the storage tank, centreline elevation for the inlets are 0.41 m and 0.64 m respectively. The tank has two outlets, separated by a 0.74 m tall weir plate. The weir plate ensures pure phase extraction, where water is extracted upstream the plate, and Exxsol^{TM} D60 is extracted downstream. Two plexiglas covered manholes (600 mm and 450 mm diameter) are installed close to the weir plate for observation of phase behaviour during operation and allowing entrance for maintenance. Chemical fumes are vented through a 110 *mm* diameter opening at the top of the tank, which also maintains an internal pressure of 1 *atm*. The tank is constructed in fiberglas reinforced polyester with an internal liner of DION 9100, securing good chemical resistance.

3.2.2 Pump manifold

The pump manifold consists of four centrifugal pumps. The respective storage tank outlets are connected to two pumps in parallel, allowing respective flow capacities of 100-2100 L/min (906-19026 *bpd*) and 100-1700 L/min (906-15402 *bpd*). Installed pumps and respective specifications are listed in Table 3.1.

Table 3.1 Pump specifications

Qty.	Model	Flow rate $[L/min]$	Power $[kW]$	Max. Head $[m]$
1	Pedrollo F65/200 AR	400-2100	22.0	57.5
1	Pedrollo F50/200 B	400-1700	15.0	52.0
2	Pedrollo F40/200 A	100-700	7.5	55.0

Pumps are controlled by installed 0-50 Hz frequency converters, where 50 Hz corresponds to a maximum *rpm* of 2900. Two pumps are operated at any given time in accordance with required flow rate range.

3.2.3 Piping and valves

The test rig is constructed over two floors. The storage tank and pump manifold are at the ground level. From the pump manifold outlet, two 63 *mm* ID flexible PVC hoses with internal polyurethane coating transport boosted fluids up to a second floor, constructed as a 12.3 *m* by 2.3 *m* platform. The hoses are here connected to their respective DN65 (67.8 *mm* ID) transparent PVC feed lines. Each flow line has a Coriolis flow meter installed. Detailed information on flow meters will follow in the next section. The line size is reduced to DN50 (57 *mm* ID) 0.5 *m* up and downstream installed flow meters. Downstream the DN50 pipe sections, line sizes are again increased to DN65, and the lines are merged in a Y-junction to a multiphase transport line. The multiphase transport line includes a 5 *m* long transparent DN65 pipe down the length of the platform, a flexible DN65 720 *mm* radius PVC hose turn, and a secondary 5.5 *m* long transparent DN65 pipe section down to the MPPS prototype inlet. This adds up to a total multiphase line length of 12.7 *m*. 2 *m* upstream the MPPS prototype inlet a full bore electrically controlled ball valve (VT.1) is installed to allow for inlet choking. In addition, 1 *m* downstream VT.1, there is an insertion point for PVM probe measurements.

Two return lines lead from the MPPS prototype outlets to the respective storage tank inlets. Both return lines are in DN65 PVC piping. The water return line is fitted with a third Coriolis flow meter, and a similar line size reduction to DN50 is applied up and downstream the installed flow meter. All piping has a pressure rating of PN10 (10 *barg*). This does not include the MPPS prototype, which has its separate pressure rating. Each return line is fitted with an electrically controlled valve (VT.2 and VT.3) for regulation of the MPPS prototype extraction rates and inlet pressure. VT.2 is a full bore ball valve, while VT.3 is a pneumatic membrane valve.

In addition to electrically controlled valves, a series of manually controlled full bore ball valves are fitted thought the flow loop. This includes valves in the pump manifold to isolate pumps not in use, valves to allow for single-phase operation and a valve to direct flow to a secondary flow loop. As water with added NaCl is used as test fluid, valves have also been included to allow for isolation and flushing of critical components, such as flow meters and pumps.

3.2.4 Instrumentation

Flow and density

Three Coriolis flow meters are used for flow rate and density measurements. The installed Coriolis flow meters are of the type Micro Motion F200 (two), from Emerson, and Sitrans FC430 (one), from Siemens. Both flow meters have a nominal line size of DN50, and respective details on flow capacity and measurement accuracy are listed in Table 3.2.

Table 3.2 Flow meter specifications

Model	Nom. flow	Max. flow	Error		
	$[kg/min]$	$[kg/min]$	ρ $[kg/m^3]$	$\dot{m}$ $[\%]$	$\dot{Q}$ $[\%]$
F200	869.33	1451.66	0.54	0.11	0.15
FC430	866.67	1178.33	0.54	0.11	0.15

Reported error includes linearity and repeatability. The mass flow ($\dot{m}$) and volume flow ($\dot{Q}$) accuracies are given as percentage of actual flow. Calibration certificates for the Coriolis flow meters are included in Appendix A.

The two F200 meters are installed at the respective feed streams, indicated by FT1/DT.1 and FT.2/DT.2 in Figure 3.5. These allow for accurate adjustment of desired total flow rate and inlet WC during testing, and monitoring of single phase purities. The last flow meter is installed downstream the MPPS prototype water extraction point, in the water return line (FT.3/DT.3), allowing for continuous monitoring of water extraction rate and separated water quality.

Pressure

The test rig has five pressure transducers installed. PT.1,2 and 3 in Figure 3.5 are flush mounted static gage pressure transducers. PT.1 measures the static gauge pressure at the inlet of the MPPS prototype, while PT.2 and 3 measures static gauge pressure at the entrance of the respective MPPS prototype return lines. dPT.1 and 2 are differential pressure transducers. dPT.1 measures the static pressure loss over VT.1, while dPT.2 is installed as a level indicator for the inclined extraction section. More information on the the mounting and functionality of dPT.2 will follow in Section 3.3.3. All installed pressure transducers are of the type Sitrans P310, and detailed information on selected range and manufacturer specified accuracy is listed in Table 3.3.

Table 3.3 P310 specifications

Tag	Unit	Range	Error [%]
PT.1	*barg*	0 – 6	≤ 0.075
PT.2	*barg*	0 – 6	≤ 0.075
PT.3	*barg*	0 – 6	≤ 0.075
dPT.1	*mbar*	0 – 2000	≤ 0.075
dPT.2	*mbar*	0 – 50	≤ 0.075

Listed error includes hysteresis and repeatability, and represents error in the linear characteristic of the pressure transducer outputs.

Temperature

Temperature measurements are performed at the MPPS prototype inlet (TT.1 in Figure 3.5). The installed temperature sensor is a Ni1000 TK5000 resistance measurement element. The sensor has a nominal resistance of 1000 *Ohm* at 0 $^{\circ}C$, and resistance values at different temperatures are tabulated by the manufacturer. In liquid, the sensor has a reported response time of $\leq 30\ s$.

3.2.5 Test parameters

In Table 3.4, all recorded parameters with corresponding tag names, measurement range and span are given. These parameters represents the raw data collected during experiments and are the basis of all further calculation. The listed parameters are also used as the basis for error estimation, each with its corresponding error component.

Measured fluid densities (DT.1/2/3) are used to calculate the respective line water cuts according to Eq. 3.1.

Table 3.4 Recorded parameters

Tag	Parameter	Unit	Range	Span
FT.1	$\dot{Q}_1$	L/min	0 – 1000	1000
FT.2	$\dot{Q}_2$	L/min	0 – 1000	1000
FT.3	$\dot{Q}_3$	L/min	0 – 1000	1000
DT.1	ρ_1	kg/m^3	750 – 1050	300
DT.2	ρ_2	kg/m^3	750 – 1050	300
DT.3	ρ_3	kg/m^3	750 – 1050	300
PT.1	P_1	$barg$	0 – 6	6
PT.2	P_2	$barg$	0 – 6	6
PT.3	P_3	$barg$	0 – 6	6
dPT.1	dP_1	$mbar$	0 – 2000	2000
dPT.2	dP_2	$mbar$	0 – 50	50
TT.1	T_1	$^{\circ}C$	-30 – 122	152

$$WC_i = \frac{\rho_{m_i} - \rho_o}{\rho_w - \rho_o} \tag{3.1}$$

Here, ρ_{m_i} is the measured fluid density, while ρ_o and ρ_w are temperature corrected reference densities of pure Exxsol^{TM} D60 and water (storage tank samples) analyzed prior to experiments. This method of calculating stream water cuts assumes a no slip condition through the Coriolis meters, and has been validated by provided manufacturer test data and validation experiments included in Appendix B. WC in the water and Exxsol^{TM} D60 feed lines are monitored in order to track occurring contamination of the feed streams. As the facility is a closed loop system, micron scaled droplets of Exxsol^{TM} D60 and water that do not fully separate in the storage tank will build up in the respective pure phases over time. This build-up is monitored, and is used for correcting the reported MPPS inlet WC and for validating comparability of experimental results. The corrected MPPS inlet WC is calculated according to Eq. 3.2

$$WC_{in} = \frac{WC_1\dot{Q}_1 + WC_2\dot{Q}_2}{\dot{Q}_1 + \dot{Q}_2} \tag{3.2}$$

Separator performance will be evaluated for varying total flow rates ($\dot{Q}_{tot} = \dot{Q}_1 + \dot{Q}_2$), inlet water cuts ($WC_{in}$) and extraction rates (ER). The ER is the rate of fluid extracted through the MPPS water outlet (FT.3) over the rate of flow through the water feed line (FT.1), as outlined in Eq. 3.3.

$$ER = \frac{\dot{Q}_3}{\dot{Q}_1} \tag{3.3}$$

Two measures are used for separator performance indication in this dissertation. The first is separator efficiency (ε), which is defined as the amount of pure water extracted from the MPPS prototype divided by the theoretical amount of pure water possible to extract at the given ER. The expression is given in Eq. 3.4.

$$\varepsilon = \frac{WC_3\dot{Q}_3}{ER(WC_{in}\dot{Q}_{tot})} \tag{3.4}$$

The second measure is defined as a WC ratio (WC_r). This measure compares the WC of extracted water from the MPPS prototype (WC_3) to the WC of water in the water feed line (WC_1), as given in Eq. 3.5.

$$WC_r = \frac{WC_3}{WC_1} \tag{3.5}$$

This measure gives an unbiased estimate of the MPPS prototype performance, not affected by occurring pure phase contamination. For WC_r equal to 1, the water extracted from the MPPS is of the same quality as the water leaving the storage tank (baseline separator).

3.2.6 Data Acquisition System

The DAQ system is set up with a Programmable Logic Controller (PLC), communicating with a computer through an Open Platform Communications (OPC) server. The sensor transducers are connected to the PLC through respective analog input modules working as analog to digital (ADC) converters. All Coriolis flow meter and pressure transducer outputs are configured as 4-20 mA analog signals. The signal outputs are sent to their respective ADC input modules, converted to digital values, sent to the PLC, then finally outputted as signed 16 bit values which are communicated to a computer through an OPC server. The installed ADC have a 13 bit resolution, which corresponds to a least significant bit (LSB) value of 1.95 μA. This gives a quantization (resolution) error of $\pm$ 0.98 μA, equal to $\pm$ 0.006 % of the specified sensor spans in Table 3.4. In addition, the ADC modules have a reported measurement error at 25°C of $\pm$ 0.05 % of full-scale value, equal to 0.06 % of the reported measurement span. The computer is running a LabVIEW VI, which receives the signed 16 bit values and converts them back into measured process variables. An illustration of the DAQ information flow is given in Figure 3.6.

A separate temperature reading module is installed for the Ni1000 TK5000 resistance element. The module has a temperature recording range of -30 °C to + 122°C, with a reported resolution of 0.1 °C. The measurement error at 25 °C is given as $\pm$ 0.2 % of full span value, i.e. $\pm$ 0.3 °C.

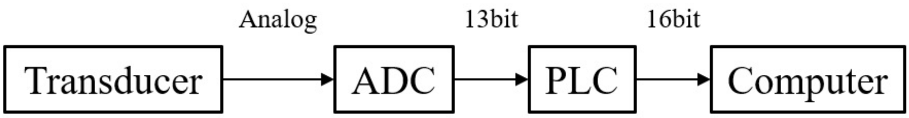

Fig. 3.6 Illustration of DAQ information flow

Installed pumps communicate digitally with the PLC, and can be controlled through the LabVIEW VI. Pump controllers were developed to assist with efficient adjustment of experimental test points. Details on the respective pump controllers are included in Appendix C.

3.2.7 Error estimation

Error estimation is performed for all experimental recordings in this dissertation. Considered error components are divided into systematic (ω_S) and random (ω_R) contributions. The systematic error components include manufacturer provided transducer error (Linearity/Hysterisis/Repeatability)(ω_T), quantization (resolution) error from the ADC (ω_Q) and reported measurement error of the respective analog input modules (ω_M). The random error component represents the random fluctuation of the respective process variables under experiments.

Systematic error

The respective systematic error components have been outlined in the previous sections. In Table 3.5, an overview of the components and resulting systematic errors are given. Calculations are performed with transducer spans as given in Table 3.4, and specified maximum values for flow rate and pressure measurements are used for calculation of ω_T. For performed experiments, recorded values (not maximum values) are used for calculation of ω_T, hence reported values in Table 3.5 will be larger than actual. The total systematic error component is a function of the respective local contributions and is calculated according to Eq. 3.6.

$$\omega_S = \sqrt{\omega_T{}^2 + \omega_Q{}^2 + \omega_M{}^2} \tag{3.6}$$

Calibration is performed prior to experimental campaign initiation to correct for any systematic shifts in received signals. If uncertainties in calibration are larger than reported transducer error (ω_T), the calibration uncertainty will replace ω_T when calculating ω_S. More information on the calibration procedure is given in Section 3.2.8.

Table 3.5 Systematic error components

Parameter	Unit	Error			
		ω_T	ω_Q	ω_M	ω_S
$\dot{Q}_1$	L/min	± 1.5e+00	± 6.0e-02	± 6.0e-01	± 1.6e+00
$\dot{Q}_2$	L/min	± 1.5e+00	± 6.0e-02	± 6.0e-01	± 1.6e+00
$\dot{Q}_3$	L/min	± 1.5e+00	± 6.0e-02	± 6.0e-01	± 1.6e+00
ρ_1	kg/m^3	± 5.4e-01	± 1.8e-02	± 1.8e-01	± 5.7e-01
ρ_2	kg/m^3	± 5.4e-01	± 1.8e-02	± 1.8e-01	± 5.7e-01
ρ_3	kg/m^3	± 5.4e-01	± 1.8e-02	± 1.8e-01	± 5.7e-01
P_1	$barg$	± 4.5e-03	± 3.6e-04	± 3.6e-03	± 5.8e-03
P_2	$barg$	± 4.5e-03	± 3.6e-04	± 3.6e-03	± 5.8e-03
P_3	$barg$	± 4.5e-03	± 3.6e-04	± 3.6e-03	± 5.8e-03
dP_1	$mbar$	± 1.5e+00	± 1.2e-01	± 1.2e+00	± 1.9e+00
dP_2	$mbar$	± 3.8e-02	± 3.0e-03	± 3.0e-02	± 4.9e-02
T_1	$°C$	-	± 1.0e-01	± 3.0e-01	± 3.2e-01

Random error

The random error includes random fluctuations in process variables and signal noise. Performed separator performance estimates in Paper II, III and V are run as steady state tests, with a large sample size. Mean values of respective parameters ($\bar{X}$) are used for calculations outlined in Section 3.2.5. The central limit theorem is utilized to calculate a 95 % confidence interval for the respective sample means, given by $\pm\bar{t}S_{\bar{X}}$. Here, $S_{\bar{X}}$ is the standard deviation of the calculated sample mean, and $\bar{t}$ is determined on the basis of degrees of freedom in the respective sample. The recorded number of samples (N) for steady state experiments reported in this dissertation is equal to 300, hence a $\bar{t}$ value of 1.96 has been used for confidence interval calculation. The calculated confidence interval for respective parameters represents the random error associated with the given variable. The steps in calculating the random error are given in Eqs. 3.7-3.10.

$$\bar{X} = \frac{\sum_{i=1}^{N} X_i}{N} \tag{3.7}$$

$$S = \frac{\sum_{i=1}^{N} (X_i - \bar{X})^2}{N-1} \tag{3.8}$$

$$S_{\bar{X}} = \frac{S}{\sqrt{N}} \tag{3.9}$$

$$\omega_R = \pm\bar{t}S_{\bar{X}} \tag{3.10}$$

Total error

The total error (ω_{tot}) for the respective parameters in Table 3.4 is a function of the calculated systematic (ω_S) and random (ω_R) error components.

$$\omega_{tot} = \sqrt{\omega_S^2 + \omega_R^2} \tag{3.11}$$

Error propagation is used in order to calculate the error of derived expressions in Eqs. 3.1-3.4. The method was outlined by Kline and McClintock in 1953, and is described by Moffat in [21]. Each calculated expression is a function of the parameters outlined in Table 3.4. Each of these parameters have a calculated error (ω_{tot}). For the purpose of further explanation, ω will represent the calculated ω_{tot}. For an expression (Y) being a function of the variables (x_1, x_2, x_3), with variable specified errors of (ω_{x_1}, ω_{x_2}, ω_{x_3}), the resulting total error can be calculated as outlined in Eq. 3.12.

$$\omega_Y = \sqrt{\left(\frac{\partial Y}{\partial x_1}\omega_{x_1}\right)^2 + \left(\frac{\partial Y}{\partial x_2}\omega_{x_2}\right)^2 + \left(\frac{\partial Y}{\partial x_3}\omega_{x_3}\right)^2} \tag{3.12}$$

Reference densities of Exxsol$^{\text{TM}}$ D60 and water used in Eq. 3.1 are functions of recorded temperature (T_1). The errors associated with these densities are thus estimated based on the total error of T_1 (ω_{T_1}). More information on reference density estimations will be given in the nest section.

3.2.8 Calibration

The calibration procedure included calibration of relevant pressure and temperature transducers, as well as a density measurement and resulting volume flow measurement correction.

Calibration of relevant pressure and temperature sensors was performed prior to experimental campaign 1 and 3. Campaigns 1 and 2, and campaigns 3 and 4, were run in close consecution, and no re-calibration of pressure and temperature sensors was deemed necessary in between these campaigns. However, density correction was performed prior to every experimental campaign.

The LabVIEW VI displays both un-calibrated and calibrated values. All recorded values are un-calibrated, and the respective calibration curves are added in the post processing.

Pressure Calibration

Pressure calibration was performed with a Druck DPI 612 portable pressure calibrator from GE. The calibration procedure is listed below:

1. Disconnect sensor from rig mounting and connect to portable calibrator. Calibration is done with the sensor connected to the rig DAQ system

2. The calibrator pressure is equalized with atmosphere, and the zero point for the sensor is set
3. The calibrator pressure is increased according to specified calibration intervals. The adjustment is manual with an accuracy of $\pm$ 0.3 *mbar*
4. At every interval, three 60 *s*, 10 *Hz* recordings are made
5. A calibration curve is calculated based on recorded points

Calculation of the calibration curve is done by plotting recorded sample means versus calibrator values (true values) for the whole calibration range. A linear curve is fitted to the data points, and the calibration curve is given by the trend line equation. The result is an equation for the calibrated pressure value (P_C) given as a linear function of the measured pressure value (P_M).

$$P_C = aP_M + b \tag{3.13}$$

This calibration corrects for any occurring systematic shift caused by the DAQ system in addition to sensor drift.

An overview of the calibration range and intervals for the respective pressure sensors are given in Table 3.6. The table also includes the maximum $S_{\bar{X}}$ calculated for all performed calibrations, and lowest coefficient of determination for the respective curve fittings.

Table 3.6 Pressure calibration specifications

Parameter	Unit	Cali.Range	Interval	$Max(S_{\bar{X}})$	R^2
P_1	*barg*	0 – 4	1	2.3e-04	1.00
P_2	*barg*	0 – 4	1	1.6e-04	1.00
P_3	*barg*	0 – 4	1	1.7e-04	1.00
dP_1	*mbar*	0 – 1000	100	6.2e-02	1.00
dP_2	*mbar*	0 – 7	1	1.3e-03	1.00

Temperature Calibration

Temperature calibration was performed with a 9102S Handheld Dry-Wells temperature calibrator from Fluke Calibration. the calibration procedure is listed below:

1. Disconnect sensor from rig mounting and connect to portable calibrator. Calibration is done with the sensor connected to the rig DAQ system
2. The calibrator temperature is set to desired start value

3. The calibrator temperature is increased according to specified calibration intervals. The adjustment is automatic, where a setpoint is specified for the desired temperature, and the temperature is regulated to within $\pm$ 0.25 $°C$ of the specified value

4. At every interval one 60 s, 1 Hz sample is recorded

5. When the maximum calibration value is reached, the process is repeated from maximum to minimum calibration value

6. A calibration curve is calculated based on recorded points

Calculation of the calibration curve is done by plotting recorded sample means versus calibrator values (true values) for the whole calibration range. A linear curve is fitted to the data points, and the calibration curve is given by the trend line equation. The result is an equation for the calibrated temperature value given as a linear function of the measured temperature value. This calibration corrects for any occurring systematic shift caused by the DAQ system in addition to sensor drift.

The calibration range was set to 15.0-25.0 $°C$ for post campaign 1 calibration. For calibration done prior to campaign 3, the calibration range was modified to 12.5-22.5 $°C$. In both cases the selected calibration interval was 1.0 $°C$.

Density Correction

All installed Coriolis meters are delivered with calibration certificates. However, due to significant fluctuations in facility ambient temperature, corrections to the density measurement must be made. Deviation from reported calibration temperature increases measurement error. As indicated by meter documentation, increase in error for mass flow measurements are equal to $\pm$ 0.0007 % per 1 $°C$ deviation from reported calibration temperature, hence insignificant. However, the error in density measurement increases with $\pm$ 0.1 kg/m^3 per 1 $°C$ deviation from calibration temperature, and must be corrected in order to maintain satisfactory accuracy.

The first step in the correction procedure is collecting storage tank samples of Exxsol^{TM} D60 and water. From acquired samples, a density curve over a specified temperature range is established. Density measurements were performed with an Anton Paar DMA^{TM} 5000M densitometer. A temperature span is selected, and density is recorded at 2.5 $°C$ intervals in the selected span, totalling at five points. Recordings are performed twice for each phase, one starting at the maximum temperature going down, and one starting at the minimum temperature going up. The mean value is used for deriving the respective density curves. The densitometer has a reported accuracy of 0.007 kg/m^3 and a reported temperature accuracy of 0.01 $°C$. Several precision classes are available when performing measurements. The selected precision class has the following stability requirements, which must be satisfied before a recording is made:

- Density: $< 0.005\ kg/m^3$ for 60 s
- Temperature: $< 0.005\ ^\circ C$ for 10 s

Density curves were established prior to experimental campaign 1, 3 and 4. Samples were also taken and analyzed after campaigns 2, 3 and 4 to monitor any shift in phase densities over the testing period. The resulting density curves will be functions of temperature, and are used to calculate the respective reference densities (ρ_o and ρ_w) in Eq. 3.1, with the corrected T_1 recording as input.

The next step in the correction process is to establish a correction curve for the respective Coriolis meters. The pump manifold is modified such that one pump supplies water to both feed lines. The Exxsol^{TM} D60 return line is closed, and only water is circulated in the test loop. All three Coriolis meters are now measuring the density of the same fluid at the same temperature. After all air is flushed from the system, and steady state operation is ensured, three 5 Hz, 60 s recordings of the fluid temperature T_1 and the respective meter densities (ρ_1, ρ_2, ρ_3) are made. The procedure is initiated early in the morning, when ambient temperature is low. The fluid temperature will gradually increase over time as a result of increasing ambient temperature and energy input from the pump. For every 0.5 $^\circ C$ temperature increase, a new recording is made.

The number of points recorded varies for the respective campaigns. For campaign 1, three points were recorded. For the remaining campaigns, a minimum of five points were recorded. The variation in number of points is dictated by expected temperature variation in the test facility while testing.

Recorded results are used to plot a density versus temperature curve for the respective flow meters. Average densities at the respective temperature points are used in plotting. The temperature reading is corrected according to performed temperature calibration prior to plotting. A plot is also made of the densitometer-established water reference density at the same temperature points. The deviation at each point (ρ_D) is calculated, and a deviation curve is plotted. The curve is fitted according to the least squares method. For campaigns 1 and 2, a linear deviation curve was used, while a second degree polynomial was used for campaign 3 and 4.

Two types of deviation curves were tested. The first approach calculated the deviation as recorded value subtracted the reference value ($\rho_i(T_1) - \rho_w(T_1)$). This results in a temperature dependant deviation which must be subtracted the respective meter readings to give the true value.

$$\rho_{C_i}(T_1) = \rho_i(T_1) - \rho_D(T_1)_i \tag{3.14}$$

The second approach calculated the deviation as reference value divided the recorded value. This results in a temperature dependant correction factor which must be multiplied the respective meter readings.

$$\rho_{C_i}(T_1) = \rho_i(T_1)\rho_D(T_1)_i \tag{3.15}$$

The approaches were tested by running pure Exxsol^{TM} D60 in the loop, and looking at which approach gave results closest to the Exxsol^{TM} D60 reference value. The first approach proved most accurate, displaying densities well within the specified $\pm$ 0.5 kg/m^3 error band.

This correction procedure was carried out before every experimental campaign, and the resulting density correction curves were used in the post processing. The validity of the corrections were tested prior to experimental initiation by operating the rig at low total flow rates, and visually checking corrected density readings against calculated reference values. Experimental testing was initiated if observed error was lass than specified error range of $\pm$ 0.5 kg/m^3.

The volume flow output ($\dot{Q}_i$) from the respective Coriolis meters are a function of internally recorded mass flow rate ($\dot{m}_i$) and density (ρ_i) measurements. As a result, the flow reading which is outputted to the DAQ system is based on the un-corrected density measurement. For this reason, a correction is also made to recorded flow readings. The volume flow rate is a function of the mass flow rate and density:

$$\dot{Q}_i = \frac{\dot{m}_i}{\rho_i} \tag{3.16}$$

The mass flow reading, which is not affected by the temperature variations, can thus be expressed as a product of the un-calibrated values of flow rate and density ($\dot{m}_i = \dot{Q}_i\rho_i$). The corrected volume flow rate can then be calculated by dividing the mass flow rate reading by the corrected density value:

$$\dot{Q}_{C_i} = \frac{\dot{Q}_i\rho_i}{\rho_{C_i}} \tag{3.17}$$

3.3 Experimental campaigns

In order to complete the research tasks outlined in Section 1.2, four experimental campaigns were designed and carried out as part of this dissertation. The campaigns were to investigate separator design features, evaluate separator performance, study flow mechanics inside the separator and develop a separator control strategy.

In Figure 3.7, dimensions of the developed prototype are given. The figure also includes markings that will be referenced in the respective experimental campaign sections. Three locations are outlined and numbered from 1 to 3. These are locations where pictures of occurring flow phenomena are captured. In addition, three tapping locations (T_1, T_2, T_3) are identified. These represent possible water extraction point locations along the ascending extraction pipe.

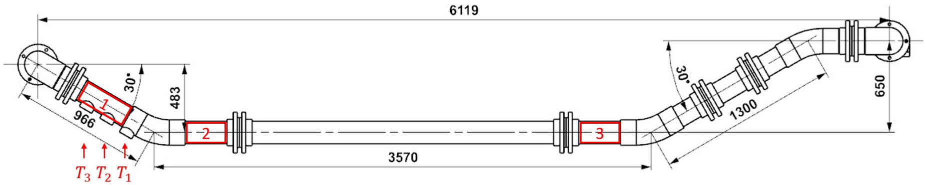

Fig. 3.7 MPPS prototype dimensions

3.3.1 Campaign 1

Test campaign 1 was designed to investigate the effect different water extraction locations have on separator performance. As outlined in Figure 3.7, three water extraction locations were constructed. The spacing between the respective tapping locations is 170 mm.

Test fluids used for campaign 1 are Exxsol^{TM} D60 with 0.015 g/L Oil Red O, and distilled water with 3.4 $wt\%$ NaCl and 1000 ppm of the biocide IKM CC-80. Test fluid properties are listed in Paper II and III.

The test matrix used for campaign 1 is given in Table 3.7. This matrix is first completed with water extracted through tapping location 1, with location 2 and 3 blocked. The matrix is then repeated using tapping location 2 and lastly 3. Calculated separation efficiencies were then compared to identify the preferred water extraction point. In addition to performance estimates, pictures were taken in order to visualize and characterize occurring flow phenomena in the extraction pipes. Pictures in campaign 1 were taken at location 1 outlined in Figure 3.7. The test procedure was as follows:

- Desired total flow rate and inlet WC adjusted for the separator inlet
- The flow rate through the water return line was adjusted to match desired ER
- The system was allowed to reach steady state
- A 60 s, 5 Hz sampling file was recorded
- Pictures of flow phenomena were taken at the tapping location
- Procedure repeated for next test point

By monitoring measured variable transients, a period of five times the prevailing residence time in the MPPS prototype was found sufficient for steady state approximation.

At least one day of rest was allowed between each round of testing. This to allow for complete phase separation in the storage tank, securing comparable initial conditions for the respective separator configurations.

Table 3.7 Campaign 1 test matrix

$\dot{Q}_{tot}$ $[L/min]$	WC_{in} $[\%]$	ER $[\%]$
250	30/50/70	50 70 90 100
500	30/50/70	50 70 90 100
750	30/50/70	50 70 90 100

Results from experimental campaign 1 are presented in Paper III. Some initial results are also included in Paper II. The tapping point identified as the best extraction point in this campaign was used for all further testing.

3.3.2 Campaign 2

Test campaign 2 was designed to map the performance of the developed MPPS prototype over a wide range of inlet flow rates, water cuts and extraction rates. Furthermore, the campaign was to study the effect different inlet configurations had on separator performance, as well as how the respective inlet options influenced flow distribution and behaviour in the separator pipes.

Three inlet design were tested in this campaign. The different configurations are illustrated in Figure 3.8, and consist of a normal inlet, a tangential inlet and a tangential inlet with novel phase re-arranging internals. Test fluids used in campaign 2 are the same as used in campaign 1.

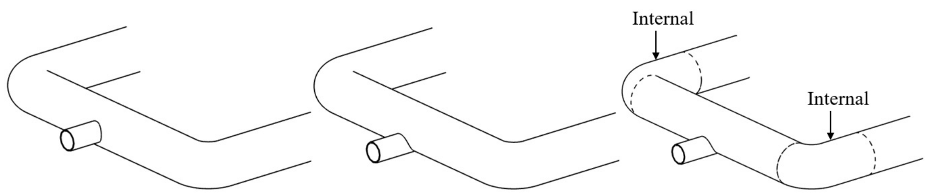

Fig. 3.8 Inlet configurations (Normal (left), Tangential (middle), Tangential w/ internal (right))

For the normal inlet, the multiphase feed-pipe enters at the centre of the inlet T-section. For the tangential inlet, the multiphase feed-pipe enters tangentially, at the bottom of the inlet T-section. This induces a swirling motion in the MPPS inlet, promoting initial separation by centripetal forces. The novel internals were designed to boost the performance of the tangential inlet configuration. The tangential inlet will promote a core and annular ring phase distribution in the MPPS inlet. However, when the flow enters the horizontal pipe sections, separation will be gravity driven, promoting a vertically segregated phase distribution. The transition from a core divided to a horizontally divided phase distribution can cause re-mixing of the phases. The internals are designed to redirect the flow from a core-distribution to a stratified distribution up-stream the descending pipe sections, thus avoiding potential re-mixing of the phases. Details on internal functionality, design and placement are included in Paper III, Chapter 5. The developed internals were designed by the author, and produced by the rapid prototype company 3A Prototype.

The test matrix for campaign 2 is given in Table 3.8. The campaign was run for all three inlet configurations, starting with the normal inlet, then the tangential inlet and finally the tangential inlet with internals configuration.

The test procedure was the same as outlined for experimental campaign 1. One exception is the picture location, which for campaign 2 was location 2 in Figure 3.4.

Table 3.8 Campaign 2 test matrix

$\dot{Q}_{tot}$ $[L/min]$	WC_{in} $[\%]$	ER $[\%]$
300	30/50/70/90	50 70 90
350	30/50/70/90	50 70 90
400	30/50/70/90	50 70 90
450	30/50/70/90	50 70 90
500	30/50/70/90	50 70 90
550	30/50/70/90	50 70 90
600	30/50/70/90	50 70 90
650	30/50/70/90	50 70 90
700	30/50/70/90	50 70 90

Results from experimental campaign 2 are presented in Paper III. The inlet configuration providing the best separator performance was used for all further testing.

3.3.3 Campaign 3

The goal of test campaign 3 was to develop a control strategy for the separator concept. This is a study that was performed in collaboration with PhD student Sveinung Johan Ohrem.

As outlined in Section 3.2, two electrically controlled valves (VT.1/2) are installed at the respective separator outlets. The goal for the controller is to adjust valve openings such that the extracted water maintains a specified purity, but at the same time ensures an as high as possible extraction rate. This campaign studies which parameters are best controlled with which valves, and what parameter should be used for controlling the separator performance. Two approaches were tested in terms of separator performance control. The first approach is to use one of the valves for controlling the separator pressure (PT.1), while the other is controlling the measured WC_r in the water extraction line. Both variables are controlled by opening and closing the respective valves. The second approach controls the separator efficiency by utilizing a proxy water level measurement setup for the inclined extraction pipe (dPT.2). The principle of proxy level measurement is outlined in Figure 3.9. A differential pressure transmitter (dPT.2) is connected between the top and bottom of the ascending extraction pipe. As outlined in the figure, both connector lines are filled with water. This means that the reading from the transmitter will be zero when the section is fully filled with water, and increase depending on the amount of Exxsol^{TM} D60 present in the incline. As for the first control approach, one valve will control the level reading, and the other will control the separator pressure.

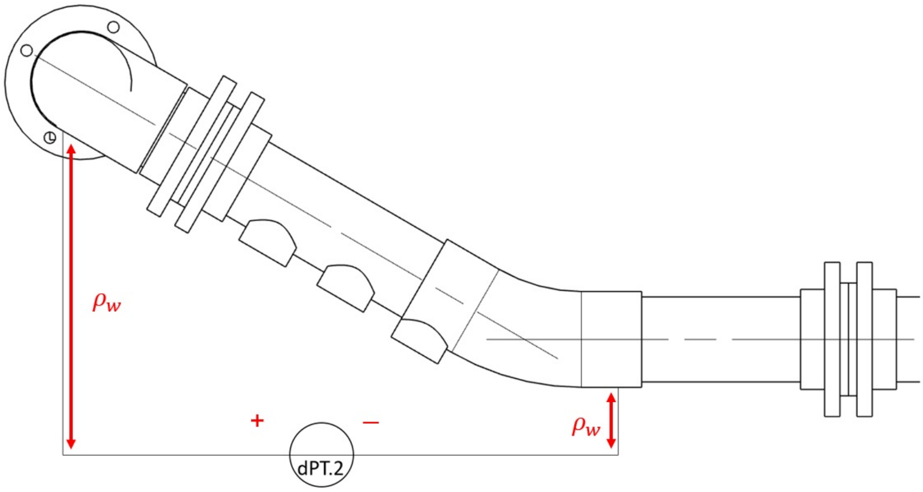

Fig. 3.9 Illustration of dPT.2 level indication principle

Two control structures are investigated for the respective control strategies. The first is a standard Proportional-integral (PI) controller, while the second is a model reference adaptive controller developed by PhD student Sveinung Johan Ohrem.

Controller options and strategies are compared by running a set inlet sequence designed to emulate real field operating scenarios. The test matrix for campaign 3 is outlined in Table 3.9.

Table 3.9 Campaign 3 test matrix

$\dot{Q}_{tot}$ $[L/min]$	WC_{in} [%]	Time s	Scenario
350	60	0-480	Nominal condition
350	80	480-840	Water breakthrough
400	74	840-900	New well introduced, step 1
450	67	900-960	New well introduced, step 2
500	60	960-1020	New well introduced, step 3
450	40	1020-1380	Old well shut down

In between test campaigns 2 and 3 the storage tank was emptied, cleaned and re-filled with test fluids. The Exxsol^{TM} D60 used in campaign 3 is the same as used for campaigns

1 and 2. The water used fro campaign 3 is freshly prepared and has a salinity of 3.2 *wt%* NaCl, with an added biocide (IKM CC-80) concentration of 750 *ppm*. Test fluid properties, together with campaign 3 results, are presented in Paper IV, Chapter 6.

3.3.4 Campaign 4

Test campaign 4 was designed to investigate the effect inlet choking and addition of surfactant had on the developed MPPS concept. Postdoctoral Fellow Marcin Dudek has been contributing to the work performed in this campaign. The study reports separator performance for a limited test matrix, for three inlet choke settings, with and without 15 *ppm* of the surfactant Span®85. Test fluids used in campaign 4 are the same as used for campaign 3, but with added surfactant for select experimental points. Test fluid properties are given in Paper V, Chapter 7. The test matrix for the study is given in Table 3.10.

Table 3.10 Campaign 4 test matrix

$dPT.1$ $[mbar]$	$\dot{Q}_{tot}$ $[L/min]$	WC_{in} $[\%]$	ER $[\%]$
	300	30/50/70	50 70 90
-	400	30/50/70	50 70 90
	500	30/50/70	50 70 90
	300	30/50/70	50 70 90
50	400	30/50/70	50 70 90
	500	30/50/70	50 70 90
	300	30/50/70	50 70 90
100	400	30/50/70	50 70 90
	500	30/50/70	50 70 90

Reported dPT.1 pressure is the pressure loss over the inlet choke valve (VT.1). The complete matrix is first run without added surfactant, than re-run with 15 *ppm* of Span®85 dissolved in the Exxsol™ D60.

Supplementary to performance estimates, PVM pictures were recorded for droplet distribution analyzis and photographies of the flow distribution and phenomena in the separator pipes were taken (location 2 and 3 in Figure 3.7).

The PVM probe utilized in this study was a PVM V819 probe from Mettler Toledo. The probe provides real time in situ digital gray scale images for droplet size measurement. The technology uses a high resolution CCD camera and internal illumination to obtain high quality images. A reflector cap was fitted to the end of the probe for better image quality. An illustration of the utilized PVM probe is given in Figure 3.10, and detailed specifications can be found in Paper V.

PVM pictures were taken for all flow rates and water cuts, at the 50 % ER point. The PVM probe was inserted in the previously mentioned PVM insertion point, at a 45° angle.

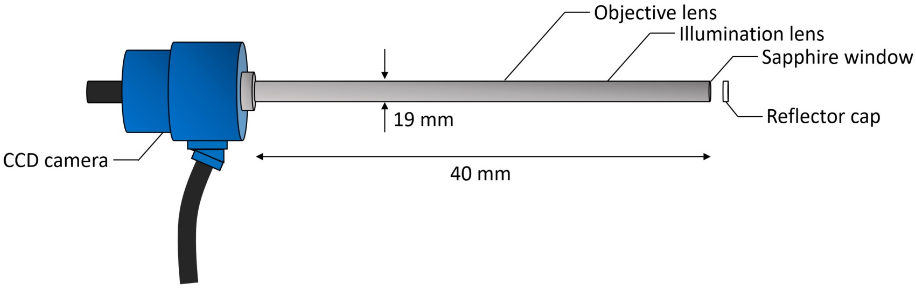

Fig. 3.10 PVM probe specifications

Pictures were taken at two heights, 0.15 and 0.85 ID from the top of the internal feed pipe wall. PVM probe placement is illustrated in Figure 3.11.

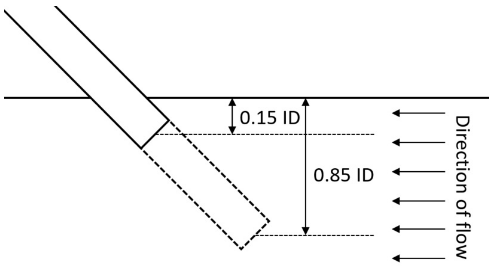

Fig. 3.11 PVM probe placement

The following test procedure was followed for all test points in campaign 4:

1. Total flow, WC_{in} and ER adjusted to desired values
2. Inlet choke valve adjusted for desired dPT.1 value
3. System operated for five times the corresponding MPPS residence time to reach steady state behaviour. Respective residence times vary from approximately 30 to 50 s
4. When ER equal to 50 %, PVM inserted at respective heights and 100 pictures taken
5. PVM removed
6. If PVM pictures taken, subsequent steady state operation period of five times the corresponding MPPS prototype residence time
7. Picture taken of the inlet flow regime
8. Separator performance logged
9. Pictures taken of flow distribution at entrance and exit of horizontal pipe segments

Results from experimental campaign 4 are presented in Paper V.

3.3.5 Summary

For the benefit of the reader, a summary of the respective campaign study objectives and where results are presented is given in Table 3.11.

Table 3.11 Summarized overview of experimental campaigns

Study objective	Campaign	Paper
Identify preferred location for water extraction	1	III
Perform mapping of separator performance and evaluate inlet design options	2	III
Develop a control strategy for the presented separator concept	3	IV
Investigate the effect inlet choking and surfactant addition has on separator performance	4	V

Chapter 4

Separator concept design and test facility construction, Paper II

This chapter consists of Paper II, which discusses drawbacks of existing subsea produced water technologies, highlights strategic focus areas for new developments, and presents the developed separator concept. Justifications for the separator design are given, and the test facility and separator prototype that has been constructed for experimental evaluation of the concept is presented. The paper reports initial performance data for the developed separator prototype, and gives details on a discovered uneven splitting phenomenon in the separator branches of forming dispersion layers.

H. S. Skjefstad and M. Stanko. An experimental study of a novel parallel pipe separator design for subsea oil-water bulk separation. In *SPE Asia Pacific Oil and Gas Conference and Exhibition.* Society of Petroleum Engineers, 2018.

Society of Petroleum Engineers

SPE-191898-MS

An Experimental Study of a Novel Parallel Pipe Separator Design for Subsea Oil-Water Bulk Separation

Håvard Slettahjell Skjefstad and Milan Stanko, Norwegian University of Science and Technology

This paper was prepared for presentation at the SPE Asia Pacific Oil & Gas Conference and Exhibition held in Brisbane, Australia, 23–25 October 2018.

Abstract

As oil fields mature, the produced water content of the production stream will often increase over time, and produced water management will eventually become a bottleneck in production. Subsea separation of produced water enables prolonged lifetime of brown field installations, increased recovery rates and more energy efficient production. In addition, implementation of subsea water separation will also enable future tie-ins to existing facilities, and reduce the need for new and expensive transport lines. Existing installed subsea produced water bulk separator technologies are limited to gravity and compact gravity vessels, such as Troll and Tordis, and the Marlim pipe separator. These are large installations, which are costly to manufacture, transport and install. In addition, the gravity and compact gravity vessels are not suited for deep-water installations, and there is a need for novel solutions to both reduce the weight and size of bulk water separators, making the technology more attractive for new business cases.

In order to investigate improved subsea bulk water separation technologies, a multiphase oil-water test loop has been developed at the Norwegian University of Science and Technology (NTNU). Facility test fluids are ExxsolD60 and distilled water with wt%3.4 NaCl. In this paper, a new separator design, utilizing multiple parallel pipes will be presented. The design allows reduction of required wall thickness at large water depths, shorter residence times and hence a shorter separator length compared to traditional gravity based technologies. Initial performance data of a constructed medium scale prototype will be reported, including separation efficiency estimations over a range of flow rates, water cuts (WC) and water extraction rates (ER). Tested flow rates vary from 250L/min to 750L/min at 30%, 50% and 70% WC. Water extraction rates are varied from 50% to 100% of the inlet water rate.

Based on this initial test campaign, the concept proves promising, displaying good separation efficiencies (>98%) for both water continuous and oil continuous inlet flows at moderate flow velocities. At higher flow rates, performance decreases, and water extraction rates must be limited in order to maintain high efficiencies. Photos of flow conditions at the water outlet are included, providing a visualization of the occurring two-phase flow phenomena inside the separator.

The presented concept adds to an expanding portfolio of proposed subsea separation solutions, and displays a new way of utilizing parallel pipes to achieve oil-water bulk separation.

Introduction

For mature oil fields, produced water is gradually taking over as the main extracted reservoir fluid, causing challenges in production. On the Norwegian Continental Shelf, 181million standard cubic meters of produced water was reported for 2016 (NOROG 2017). This accounts for more than twice the amount of produced oil. Today, produced water is transported topside where it is separated, cleaned and ultimately re-injected for pressure support or disposed to sea. Over time, the design water-treatment capacity of topside installations will eventually be reached. This causes a bottleneck in production, and leaves a substantial part of the hydrocarbon processing capacity left unused. In addition, the high amount of water in the well stream will cause loss of pressure in transportation, lowering production rates as a result.

By removing produced water at the seabed, more energy efficient production systems can be developed, and spare topside capacity can better be utilized by new tie-ins to existing facilities. In addition, production rates can be increased, and the need for new subsea transport lines reduced.

In this paper, a new design for a subsea produced water bulk separator will be presented. The design is aimed at overcoming shortcomings in current installations, providing the industry with a cheaper, more compact, flexible and modular separator design, which can help lower the cost of subsea water separation and further promote the business case. Results from an initial round of testing will be presented, along with a detailed overview of a newly developed multiphase test facility.

Field-proven existing technologies

There are several concepts for subsea bulk-water removal already in use, and further concepts currently being developed for commercialization. This section will give a brief overview of existing solutions as well as concepts that to the author's knowledge are currently under development. Benefits and drawbacks of respective designs will be discussed, providing a basis of understanding for the proposed qualities of the new separator concept. As this section will be limited to a brief overview of selected technologies, the reader is directed to (Skjefstad and Stanko 2017) if a more thorough introduction to subsea produced-water separation technologies is desired. In Skjefstad and Stanko 2017, the reader will also find more detailed information on the progress in development of discussed new concepts.

Troll. The Troll Pilot separator is a horizontal three-phase gravity separator. It is installed at a water depth of 340m and has a specified liquid capacity of 63000bpd. The separator has a diameter of 2.8m, a tan/tan length (length of cylindrical section) of 9m and a total length of 11.8m. The separator is fully integrated with the pipe/manifold system, and the whole installation has overall dimensions of 17×17×8m with a total weight of 350tons (Bakke and Sundt 2016). The separator has an integrated dual-pipe sand removal system, where one pipe is flushing the shell, and one extracting particle carrying water. The driving power for the system is an electrically driven booster unit deployed from surface support. A novel design feature for the separator is a cyclonic inlet device ensuring enhanced separation capabilities (Horn et al. 2003). The separator has a specified maximum oil in water (OiW) content of 1000ppm at the water outlet, and an upper water in oil (WiO) content of 10% (Davies et al. 2010).

Tordis. The Tordis separator is a horizontal semi-compact gravity separator. It is installed at a water depth of 210m and has a specified liquid capacity of 189000bpd (Davies et al. 2010). The terms semi-compact is used because of the novel cyclonic internal which allows gas to bypass the main separator body. This reduces the volumetric throughput of the vessel, which allows a more compact construction. The separator has a diameter of 2.1m, and is 17m long (tan/tan). Solids buildup is prevented by a sand jetting arrangement that generates vortexes to fluidize and remove sand. The separator is located in a separate module, which eases retrieval compared to the Troll Pilot separator. The separator has a specified maximum OiW content of 1000ppm at the water outlet, and the design WiO content was specified as maximum 56700bpd, which was the limit for available topside water treatment capacity (Davies et al. 2010).

Marlim. The Marlim separator is a separation system installed at a water depth of 870m, and had to be developed from new compact technologies as standard gravity vessels were not applicable for the water depths in question (Euphemio et al. 2007). This description will be limited to the bulk-water removal stage of the installation. The first component is a multiphase de-sander, which limits the amount of sand entering downstream components. From the de-sander, the flow enters a gas-liquid separator segment denoted as a "gas harp". This is designed to limit the downstream gas volume fraction (GVF) to 30% (Capela Moraes et al. 2012). Remaining fluids enter a pipe separator, which is a 60m long pipe (Orlowski et al. 2012), where liquid-liquid separation takes place. The stream then enters a collection vessel, which is reported as a small gravity vessel separator, for fluid extraction. The system was designed for a minimum inlet WC of 70%, and with a predicted liquid capacity of 22500bpd (de Oliveira et al. 2013).

Limitations, new developments and future focus points

The reviewed existing solutions can be divided into two groups of concept designs. The gravity vessel and compact-gravity vessel approach of Troll and Tordis, and the pipe separator approach utilized at Marlim. When developing new separator solutions, it is important to have a good understanding of current design approaches and to identify focus areas for improvement. The existing approaches have benefits and drawbacks, which will be discussed separately.

Compact-gravity vessel. The concept has already been field proven, and is a viable concept for shallow-water installations. Although being more compact than the traditional gravity vessel separator, the overall vessel size is still large. The size of the separator will result in bulky and heavy separator modules, which are expensive to transport and install. Another consideration is that the weight of these separators will drastically increase with increasing water depth. This results from the need for increased wall thickness of the vessel, making the compact gravity concept less attractive for deep-water installations. The topic of shell-thickness will be re-visited later in this paper to illustrate potential benefits of further reducing the separator diameter. A summary of benefits and drawback of a compact-gravity design is given in Table 1.

Table 1—Pros and cons for Compact-gravity vessel

PROS	CONS
Known and qualified design Large operational envelope Robust Gas-bypass	Overall bulky Large separator modules Heavy for deep water installations

Pipe separation. Separation in a single horizontal pipe is a concept that has been thoroughly tested and verified over the years, and performance data has been reported by StatoilHydro (Sagatun et al. 2008), and by ExxonMobil (Grave and Olson 2014, Olson et al. 2015). The reduced diameter offers a shorter droplet traveling distance, subsequently enabling reduced residence times compared to a gravity or compact gravity vessel. A secondary effect of the small diameter is that the design becomes more attractive for deep-water installations; a reduced diameter means thinner walls are required, which has a significant potential in overall weight reduction when compared to a vessel design. The reduced diameter will however lead to higher fluid velocities, and long pipes are thus required in order to achieve satisfactory separation efficiencies. Additionally, due to the reduced diameter, pipe liquid-liquid flow phenomena such as slip between the water and oil velocities can occur, affecting the separation performance.

The small diameter is the cause of certain drawbacks seen in the design. Too high fluid velocities will result in phase re-entrainment and negatively affect separation efficiency. To the authors knowledge, pipe separators are limited to maximum mixture flow velocities in the range 0.7-1m/s, allowing occurring slip to help break emulsion, but not cause re-entrainment. A small diameter will also make collection and extraction challenging, as is seen for the Marlim separator, where a downstream collection vessel is used for controlled phase extraction, increasing the overall footprint and weight of the separator module. In addition, as specified for the Marlim separator station, the pipe design is also aimed at water continuous flow conditions, which narrows the operational envelope of the installation. An overview of discussed pros and cons are given in Table 2.

Table 2—Pros and cons for horizontal single-pipe separation

PROS	CONS
Known and qualified design Reduced diameter for deep water installation Pipe code manufacturing Emulsion breakage by slip conditions	Long pipe Large foot-print Large separator modules Separate extraction vessel Limited flow capacity

An alternative to the single pipe separator is seen in Saipem's developed SpoolSep concept. The SpoolSep is constructed of several long pipe spools working in parallel, offering complete three-phase separation at large water depths. The working principle of the SpoolSep is illustrated in Figure 1, which is based on a depiction given by Shaiek et al. (Shaiek and Grandjean 2015).

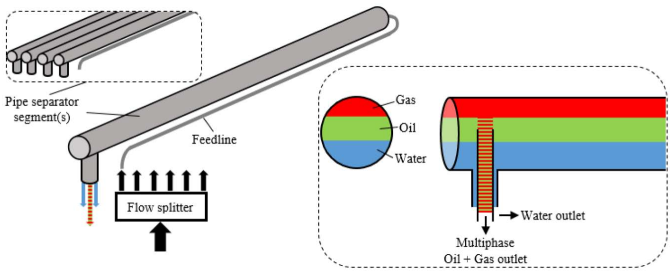

Figure 1—Illustration of SpoolSep working principle

The design removes the capacity constraint of a one-pipe solution, and offers increased flexibility by its modular design approach. The design case for the SpoolSep consist of a series of 24inch outer diameter (OD) pipes in parallel, with individual pipe lengths of 50m (Abrand et al. 2013). The reduced fluid velocity, and reduced settling distance offered by a multipipe solution means that individual pipe lengths can be significantly reduced compared to a single pipe solution. However, this is not the case for SpoolSep, which can be seen in connection with being a three-phase separator, meaning gas will take up a large part of the separator body, increasing fluid velocities.

In addition to separation in horizontal pipe segments, concepts has been designed utilizing inclination to achieve separation. One such concept is the Dual Pipe Separator (DPS), which is currently being developed by SeabedSeparation AS. The design is illustrated in Figure 2, and can be explained as a dual pipe solution where well fluids enter an internal perforated pipe, allowing water and sand to settle at the bottom of the pipe, and oil at the top. The design can be reviewed in detail in patents (Skovholt 2015a, 2015b). The design is envisioned to work as a system of several DPS in either parallel or series, offering great adaption possibilities for installation. A modular design also ensures reduced installation and transportation costs, promoting the business case for subsea separation.

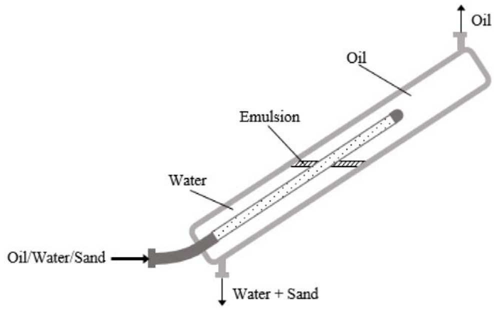

Figure 2—Illustration of DPS working principle

Areas of improvement. From discussed advantages and drawbacks of existing designs, and attractive features introduced in technologies under development, a set of focus areas for new developments can be outlined.

1. Compactness:
   All currently installed subsea bulk water separators are large installations. Reducing the footprint and weight of separator modules will reduce cost related to production, transportation and installation, making the overall business case of subsea water separation more attractive.
2. Capacity/Range:
   Robust solutions based on gravity vessels exists for shallow-water installations, enabling a large operational envelope with high flow capacity. When developing solutions that are more compact it is important to uphold this feature, which is currently not the case for developed deep-water installations.
3. Standardization
   The three existing installations for subsea water separation required their respective test and qualification programs, partly due to fundamental differences. Therefore, developing subsea separation solutions that can be qualified for a wide range of field operating conditions will greatly reduce the overall cost of future projects.
4. Modularization/Adaptivity:
   Modularization and adaptive design approaches is something that ensures the above mentioned areas of focus. Final separator solutions can be made up of pre-qualified compact separator modules, where the resulting design can be adapted according to required capacity and performance specifications. Modularization is a focus area seen in new proposed design developments such as the SpoolSep by Saipem or the DPS by SeabedSeparation.

Concept design

A pipe separator is used as a starting point for the new concept design. This is because it relies on gravity, a well-known driving force for separation, and enables separation at large water depths. Identified drawbacks for the pipe separator are footprint, module-size, limited capacity and a bulky extraction solution. To address these deficiencies, multiple pipes in parallel will be used in the new design, increasing the capacity, and reducing the required pipe lengths needed for separation.

Initial design considerations

A preliminary study of a multipipe design approach was performed in order to justify further development. This includes investigation of possible weight reduction, as well as simplified initial capacity estimates.

Weight reduction. Simplified initial estimations were performed in order to compare the size and weight of a multipipe approach to a standard vessel approach. The geometric relations and relevant derivations are provided in Appendix A.

If the cross sectional area and total volumetric flow rate is set equal for both approaches, a multipipe arrangement allows an increase in interfacial length, a reduction in residence time, and therefore, a reduction in separator length, all by a factor of $\sqrt{n}$, where n is the number of pipes used in parallel.

In addition, the potential weight reduction can be illustrated by plotting the estimated weight of a multipipe arrangement to the weight of vessel design. In Figure 3, the reference is a 2.1m diameter vessel installed at a water depth of 1000m, with a resulting wall thickness of 110mm. Again, relevant derivations are found in Appendix A.

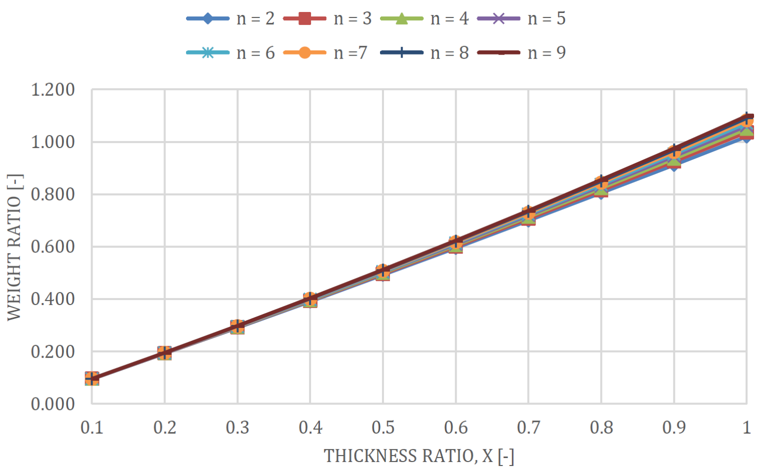

Figure 3—Weight ratio of a multipipe design with n pipes vs a 2,1m diameter vessel with 110mm wall thickness

It can be observed that a significant reduction in separator weight can be expected given the gained reduction in thickness from reduced diameter. A nine-pipe solution would result in a thickness ratio of 0.34 resulting in an overall weight reduction of approximately 67%. Thickness estimates were based on British Standard EN 13445-3:2009.

Simplified capacity estimates. Simplified capacity estimates were made in order to get an idea of expected flow limitations for gravity driven separation in short horizontal pipe segments. Investigated pipe lengths were in the range 6-7m, which allows cheaper and more accessible transportation vessels to be used for installation.

Estimates are based on basic Navier Stoke's residence time calculations, where the pipe diameter, WC and droplet cut off diameter is given as input. The calculation procedure and relevant derivations are given in Appendix B. The allowable total volumetric flow capacity was calculated for three pipe diameters (150mm, 300mm, 450mm), and droplet cut off diameters were varied between 150μm, 175μm and 200μm. In Table 3, results are given for a pipe length of 6.5m, for a range of water cuts.

Table 3—Simplified total flow capacity estimates at respective droplet cut off diameters and pipe diameters

Internal pipe diameter [mm]	Cut off diameter [μm]	Total liquid flow capacity [L/min] (bbl/day)			
		WC 30%	WC 50%	WC 70%	WC 90%
150	150	281*(2542)*	370*(3353)*	393*(3558)*	307*(2783)*
	175	382*(3459)*	504*(4563)*	535*(4843)*	418*(3788)*
	200	499*(4518)*	658*(5960)*	698*(6326)*	546*(4948)*
300	150	561*(5083)*	740*(6705)*	786*(7117)*	614*(5566)*
	175	764*(6919)*	1008*(9127)*	1069*(9686)*	836*(7576)*
	200	998*(9037)*	1316*(11921)*	1397*(1265)*	1092*(9895)*
450	150	842*(7625)*	1110*(10058)*	1179*(10675)*	922*(8349)*
	175	1146*(10378)*	1511*(13689)*	1604*(14530)*	1255*(11363)*
	200	1497*(13555)*	1974*(17881)*	2095*(18977)*	1639*(14848)*

Previous research at NTNU. The principle of separation in pipe segments has previously been investigated at the Department of Geoscience and Petroleum (IGP), NTNU. This includes development of a prototype for separation in an inclined pipe with distributed tapping (Rivera et al. 2006), and simulations of said concept (Stanko 2014). The idea was that the water layer at the bottom of the pipe would be slowed down by the upwards inclination, reducing its velocity, thus increasing the layer height. The water layer is then tapped steadily and continuously to separate it from the upwards moving flow. Experiments were performed with 30°, 45° and 60° upwards inclination. Reported results displayed best separation efficiency for 30° inclination. Numerical simulations further indicated lower inclination, and even downwards inclination as promising configurations. CFD simulations were reported to over-predict separation efficiency, indicating the need for experimental testing and subsequent model tuning for design optimization.

Concept proposal

The proposed concept has been given the name Multiple Parallel Pipe Separator (MPPS). A 3D preliminary conceptual design is depicted in Figure 4.

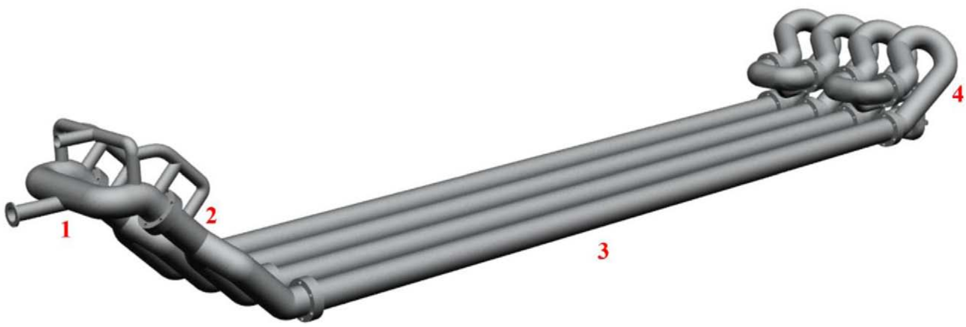

Figure 4—Illustration of MPPS design principle. Numerals 1-4 discussed in following text

The inlet (1) consists of an inlet T-section header that splits the incoming production stream into individual branch steams. An alternative design evaluated is to use a tangential inlet to ensure low mixing at the entrance while providing increased separation effect from centrifugal forces. This is the design seen in Figure 4. In this configuration, the heavier phase will be pushed towards the pipe walls while the lighter phase will concentrate in the center. For this reason, an additional internal device is included in the tangential inlet design proposal, located immediately downstream the T-section, to collect the fluids and reroute them into a layered configuration suitable for gravitational separation.

A set of descending pipe elements (2) is placed next, that split the production stream further into horizontal segments. The descending pipes have extraction points in the upper part connected to ascending pipes for gas removal (as previously employed at the Marlim installation (Capela Moraes et al. 2012)). Additionally, according to simulations performed by Stanko (Stanko 2014), the downwards inclination might have the additional advantage of promoting separation and establish a stratified layer.

Downstream the inlet section the flow enters a horizontal mid-section (3), where the main part of the liquid-liquid separation, driven by gravitational forces and density difference, takes place. As discussed earlier, the reduced pipe diameter and horizontal pipe configuration ensures a minimal droplet traveling distance and hence residence time, which subsequently allows short pipe segments to be utilized.

The final element of the separator is the upwards inclined extraction section (4). A water-rich stream is drained through a tapping point located at the bottom of the pipe. The oil-rich stream flows up, over, and back down for separate extraction or additional separation. Because of the reduced diameter, control and monitoring of the water holdup can be a challenge. As previously discussed, the inclined section induces an increase of the water holdup, which will improve water extraction at lower water cuts. The water level in the separator is to be controlled by detection and regulation of an extending water "tail" in the inclined section. This type of extraction method has previously been proposed for a single pipe solution by Schlumberger (Berard et al. 2013), illustrated in Figure 5. The idea of utilizing inclined pipe elements for oil-water separation was also, as mentioned earlier, previously investigated by Rivera (Rivera 2011).

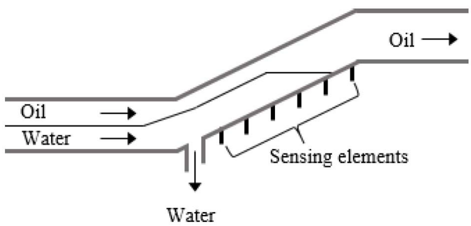

Figure 5—Patented concept by Schlumberger

In the proposed design, all parallel pipes are connected through their respective tapping points allowing eased system control and self-regulation in terms of flow distribution. This is illustrated in Figure 6 and Figure 7.

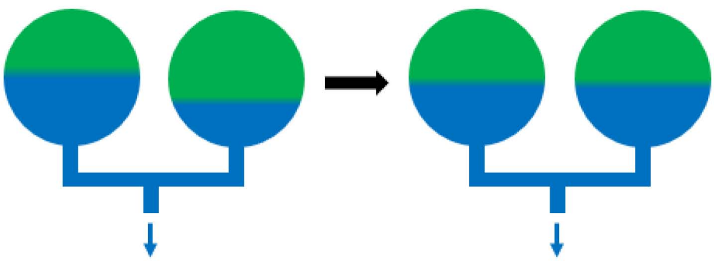

Figure 6—Self-regulation of phase distribution

Figure 7—MPPS extraction design

The outlet segment is envisioned in a way that allows easy series connection of several separator stages, without increasing the total horizontal footprint of the separator. This is made possible by a backwards skewed turn, and a following downward inclination, enabling stacking of several horizontal sections on top of each other. The number of pipes working in parallel can also be increased/reduced to match desired flow handling capacity. This has been illustrated in Figure 8, displaying eight pipes in parallel, with two horizontal sections in series. Gas removal has not been added to the illustration, but the concept is the same as in Figure 4. Focus is also given to modular design, and the idea is for pre-qualified pipe segments to be used for field installations. For example, a dual pipe section can be tested and qualified to a given flowrate. Final separator solutions can then be designed to match the required field specifications by combining pre-qualified components.

Figure 8—Illustration of MPPS in serial configuration

Test facility

An experimental facility has been constructed in order to quantify the performance of the developed concept. The constructed facility is a two-phase oil-water multiphase loop designed to test prototypes of compact bulk-water separator concepts. The facility was constructed in 2017 at the department of Geoscience and Petroleum, NTNU Trondheim, as part of the ongoing SUBPRO research program. A P&ID of the loop is given in Figure 9, displaying the main components of the system. Displayed tag names represent recorded variables, which are listed and explained later in Table 7.

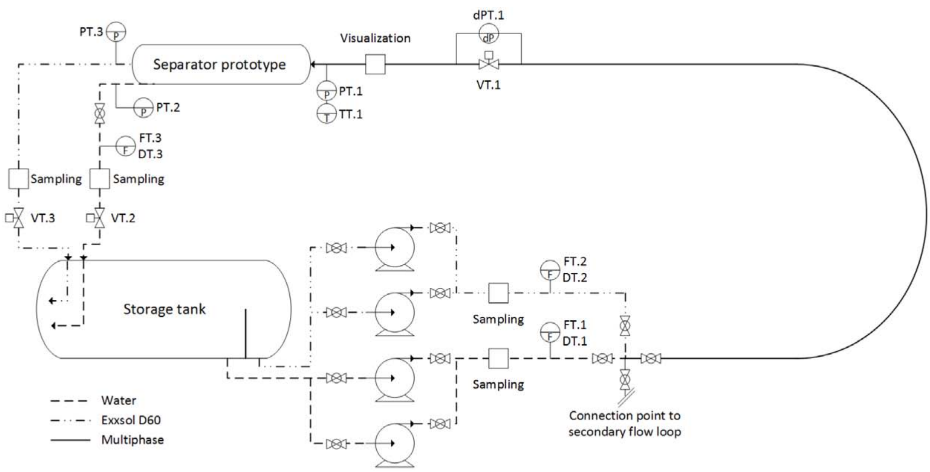

Figure 9—Multiphase flow loop P&ID

The storage tank is a 1.2m diameter, 5.5m long horizontal separator, providing baseline separation. The tank is designed to allow continuous operation at individual flowrates up to 750L/min with separation efficiency specified to a cut off diameter of $150\mu m$. Higher flowrates are tolerated in shorter time intervals, with the requirement of a subsequent shut down period to allow for complete phase separation. The tank rooms six cubic meters of test fluid, consisting of three cubic of distilled water with wt%3.4 NaCl, and three cubic of ExxsolD60. In order to allow for easier phase distinction, 0.015g/L Oil Red O (C26H24N4O) has been added to the ExxsolD60, turning it red. In addition, 1000ppm of the biocide IKM CC-80 has been added to the water to prohibit bacterial growth. Test fluid properties are given in Table 4.

Table 4—Test fluid properties at 23°C

TEST FLUID	DENSITY $[kg/m^3]$	VISCOSITY $[cP]$
Distilled water w/ wt%3.4 NaCl and 1000 ppm IKM CC-80	1020.7	0.99
ExxsolD60 w/ 0.025g/l Oil Red O	789.5	1.41

The storage tank has two inlets, one for each of the separator-prototype return lines. Return line outlets are located close to the oil-water interface, ensuring short traveling distances for the respective dispersed phases. The storage tank also has two extraction points, which are separated by a 0.74m tall weir plate. This ensures clean phase extraction, where water is extracted upstream the weir plate and ExxsolD60 is extracted downstream in a separate outlet. Chemical fumes disposal is performed through a 110mm diameter opening located at the top of the tank, which also maintains an internal pressure of one atm. The storage tank is constructed in fiberglass reinforced polyester with an internal liner of DION 9100, securing good chemical resistance.

The pump manifold consists of four centrifugal pumps, connected in parallel, providing an overall flow capacity of 100-2100L/min and 100-1700L/min for the respective phases. The installed pumps and their specification are listed in Table 5.

Table 5—Pump specifications

QUANTITY	MODEL	FLOW RATE $[L/min]$	POWER $[kW]$	MAX HEAD $[m]$
1	Pedrollo F65/200 AR	400-2100	22.0	57.5
1	Pedrollo F50/200 B	400-1700	15.0	52.0
2	Pedrollo F40/200 A	100-700	7.5	55.0

The pumps are controlled and regulated by frequency converters, with an applied range of 0-50Hz, where 50Hz constitutes maximum rpm of 2900. Two pumps are operated at any given time in accordance with desired flow rate range.

Three Coriolis flow meters are installed for flow and density measurements. The Coriolis meters are two Micro Motion F200 delivered by Emerson, and one Sitrans FC430 from Siemens. Both flowmeters have a nominal line size of DN50, and respective details on flow rate capacity and accuracy can be found in Table 6 (Emerson 2017, Siemens 2015).

Table 6—Flow meter specifications

MODEL	NOM. FLOW $[kg/min]$	MAX. FLOW $[kg/min]$	ERROR		
			Density $[kg/m^3]$	Mass flow [%]	Volume flow [%]
F200	869.33	1451.66	0.54	0.11	0.15
FC430	866.67	1178.33	0.54	0.11	0.15

Table 7—Recorded parameters

TAG	PARAMETER	UNIT
FT.1	$\dot{Q}_1$	L/min
FT.2	$\dot{Q}_2$	L/min
FT.3	$\dot{Q}_3$	L/min
DT.1	ρ_{m_1}	kg/m^3
DT.2	ρ_{m_2}	kg/m^3
DT.3	ρ_{m_3}	kg/m^3
PT.1	$P_{1_{stat}}$	$barg$
PT.2	$P_{2_{stat}}$	$barg$
PT.3	$P_{3_{stat}}$	$barg$
dPT.1	$dP_{1_{stat}}$	$barg$
TT.1	T_1	°C

Reported errors include linearity and repeatability, and are for the mass/volume flow measurements given as percentage of actual flow. The two F200 models are installed at the respective feed streams, indicated by FT.1/DT.1 and FT.2/DT.2 in Figure 9. This allows for accurate adjustment of desired WC during operation, and monitoring of single-phase purity. The last Coriolis meter is installed downstream the water outlet of the separator prototype, FT.3/DT.3, allowing continuous monitoring of extraction rate and separation efficiency.

Temperature measurement is performed with a Ni1000 TK5000 resistance measurement element. The sensor has a nominal resistance of 1000Ohm at 0°C, and resistance values at different temperatures are tabulated by the manufacturer. In liquid, the sensor has a reported response time of < 30s.

The multiphase test loop is constructed over two floors. The storage tank and pump manifold is located at the ground level. From the pump manifold, two flexible DN65 (75mm OD) reinforced PVC hoses transport boosted fluids to a second floor 12.3 × 2.3m platform, where they are connected to their respective DN65 transparent PVC feedlines. The line size is reduced to DN50 (63mm OD) 0.5m up- and downstream installed flowmeters. Downstream the DN50 pipe sections, line size is increased back to DN65, and the phases are comingled in a Y-junction. The multiphase transport line includes a 5.5m long transparent PVC straight pipe section down the length of the platform, a flexible 720mm radius transparent PVC hose turn, and a secondary 5m long transparent PVC pipe leading back up the platform to the separator prototype inlet. This ensures a total multiphase transport length of 13m prior to separator inlet. All piping in the flow loop is rated for PN10. This does not include the separator prototype itself, which pressure rating depends on individual design specification. The return lines are also constructed in DN65 PVC piping, with a similar reduction to DN50 up- and downstream the water return-line flow meter.

Three electrically controlled valves are installed at the rig. These are indicated as VT.1, VT.2, and VT.3 in the P&ID, Figure 9. VT.1 is a ball valve installed 2 meters upstream the separator prototype inlet. The valve is to allow for controlled dispersion generation, where dispersion size is affected by valve positioning as discussed and illustrated by Fossen and Schümann (Fossen and Schümann 2016). Valves VT.2 and VT.3 are installed for flow regulation. VT.2 is a ball valve, while VT.3 is a pneumatic membrane valve, allowing for fine-tuning of the flow split between the two separator prototype outlets.

Prototype and test procedure

A prototype of the proposed concept has been constructed and tested at the newly developed oil-water test facility. Limitations in available lab space restricted the prototype to two pipes in parallel, with an internal pipe diameter of 150mm (DN160). The goal of the testing was to display basic functionality of the proposed concept, and collect data on expected capacity constraints for a two-pipe section. An illustration of the prototype is given in Figure 10.

Figure 10—Constructed MPPS prototype

The oil-water stream enters at the inlet seen to the right in the figure ($\dot{Q}_{in}$). For baseline initial tests, a normal inlet configuration has been used. Tangential-inlet tests will be run in future experiments to study the effect of a low-mixing inlet with cyclonic effects. The inlet is split in the previously described T-section, before entering the descending pipe segments. Inclination at inlet and outlet are both set to 30° for the initial prototype design, which corresponds to best efficiency configuration according to (Rivera et al. 2006). As can be seen in Figure 10, inclined sections are constructed with flange joints, allowing testing of variable section lengths. There is currently no gas-supply available at the test loop, and therefore no gas removal pipes are included in the initial prototype design. The water-extraction pipe sections are fitted with three possible water-tapping locations, the bottom being illustrated in Figure 10 ($\dot{Q}_{e_w}$), and oil is extracted in a shared outlet connecting the two parallel pipes ($\dot{Q}_{e_o}$). The oil outlet has been simplified in comparison with the concept sketches. A T-section is fitted to the desired water extraction point, so that water is also extracted in a shared outlet. The extraction points not in use are blocked. Dimensions for the prototype is given in Figure 11.

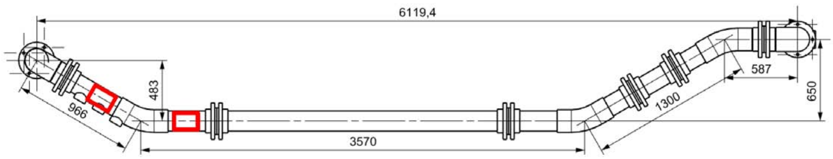

Figure 11—Initial prototype dimensions (mm)

Results included in this paper will be limited to a baseline performance test using the bottom water tapping point, as well as visualization of flow phenomena in the separator at selected test points. Visualization is performed at locations indicated with a red rectangle in Figure 11. A future publication will include testing and comparing separation performance of the three water-tapping locations, and the normal vs. tangential inlet configurations.

Test procedure

Recorded parameters with their corresponding tag names are given in Table 7. These parameters represent the raw data collected and are the basis of all further calculation. These parameters are also used as the basis of error estimation, each with its corresponding error component. Measurements are done continuously, with a sampling frequency of 5Hz. The sampling time is set to 60s, which results in 300 samples being taken for each test point. Experiments are run at steady state, and a run time of five times the prevailing residence time was found sufficient for steady state classification.

Measured fluid densities are used to calculate the respective feed water cuts according to Eq.(1).

$$WC_i = \frac{\rho_{m_i} - \rho_o}{\rho_w - \rho_o} \tag{1}$$

Here, ρ_{m_i} is the mixture density at DT.1/2/3 respectively, ρ_o is the temperature corrected established density of ExxsolD60 and ρ_w is the temperature corrected established salt-water density (ρ_o=-0.732T_1 + 806.29 [kg/m^3], $\rho_w = -0.004T_1^2 - 0.11T + 1025.4\ [kg/m^3]$, 15°C<$T_1$<25°C). Calculated water cuts are used to estimate the actual WC at the separator inlet, as given in Eq.(2).

$$WC_{in} = \frac{WC_1\dot{Q}_1 + WC_2\dot{Q}_2}{\dot{Q}_1 + \dot{Q}_2} \tag{2}$$

This formulation is used to account for imperfect separation in the storage tank, which due to the closed loop nature of the system will result in gradual pollution of the incoming water and oil streams. The separation efficiency is then expressed as the rate of water extracted from the separator to the theoretical amount of water that can be extracted at the given extraction rate (ER), as given in Eq.(3).

$$\epsilon = \frac{WC_3\dot{Q}_3}{ER\left(WC_{in}(\dot{Q}_1 + \dot{Q}_2)\right)} \tag{3}$$

The ER, Eq.(4), is defined as the rate of fluid extracted through the MPPS prototype water outlet, FT.3, to the rate of total fluid that enters the system from the water feed line FT.1.

$$ER = \frac{\dot{Q}_3}{\dot{Q}_1} \tag{4}$$

The test matrix used for baseline performance mapping is given in Table 8.

Table 8—Baseline performance test matrix

TOTAL LIQUID FLOWRATE [L/MIN]	WC [%]	ER [%]			
250	30/50/70	50	70	90	100
500	30/50/70	50	70	90	100
750	30/50/70	50	70	90	100

Results

In Figure 12 - Figure 14, calculated separation efficiencies for the respective test points are given. The reported efficiencies and extraction rates are calculated values from Eq.(3) and (4) respectively.

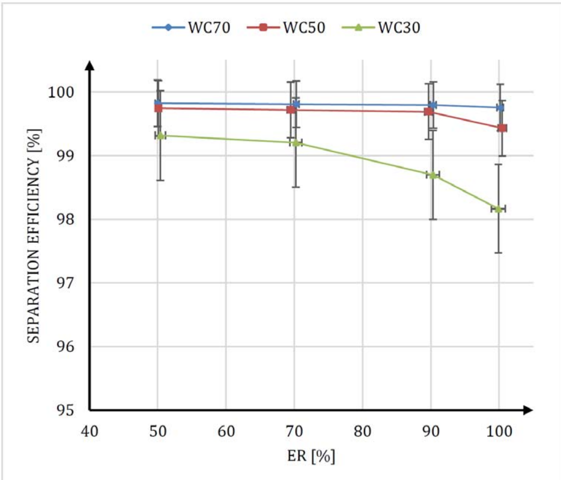

Figure 12—Performance data at $\dot{Q}_{tot}$ = 250L/min

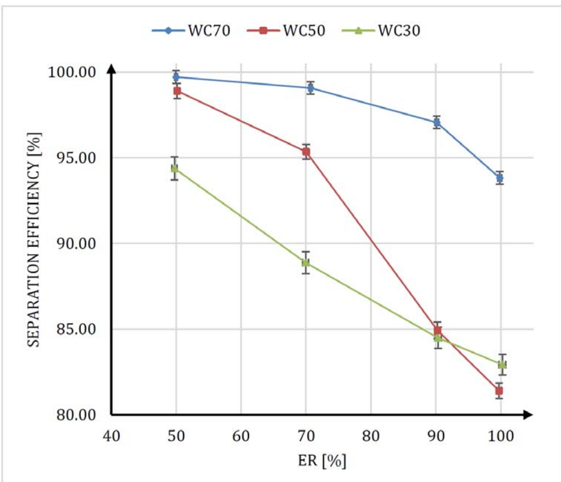

Figure 13—Performance data at $\dot{Q}_{tot}$ = 500L/min

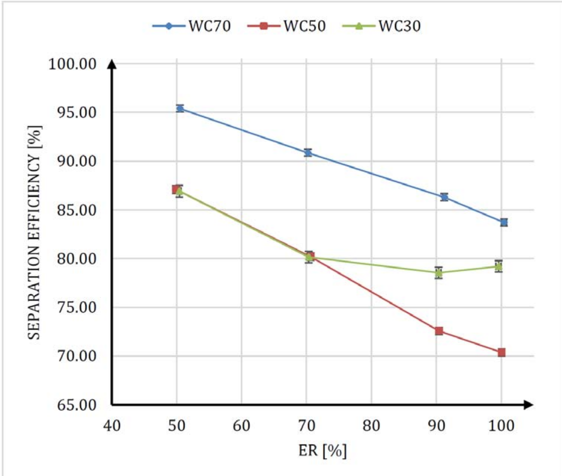

Figure 14—Performance data at $\dot{Q}_{tot}$= 750 L/min

From measured results, excellent separation efficiencies (98%-100%) are observed for the low flowrate case of 250L/min (U_m = 0.12*m/s*). For WC 70% and 50%, excellent separation efficiencies are achieved for all ER. For a WC of 30% a slight drop in separation efficiency is observed at high extraction. When increasing the flowrate to 500L/min (*Um* = 0.23*m/s*), a larger effect on separation efficiency from decreasing WC and increasing ER is observed. For the case of 70% WC, good separation efficiency can be maintained by limiting the ER to 70%. For a WC of 50%, a further limitation in ER to 50% is required in order to maintain good separation efficiency. For a WC of 30% a steady decrease in separation efficiency is observed, and this WC range appears to be the most challenging operational area. A further increase of the total flowrate to 750L/min (U_m = 0.35*m/s*) results in a strong overall reduction in separation efficiencies.

A decrease in performance with reduced WC seems to be related to the re-entrainment of oil droplets into the established water layer at the extraction point. In Figure 15, a photo of occurring flow phenomenon at the extraction section for a flow rate of 250L/min at 70% WC, 90% ER is given. The water extraction point is indicated with a white arrow. It is observed that the oil phase flows in a periodic pulse-like manner, and small oil droplets are dispersed in the top part of the established water layer.

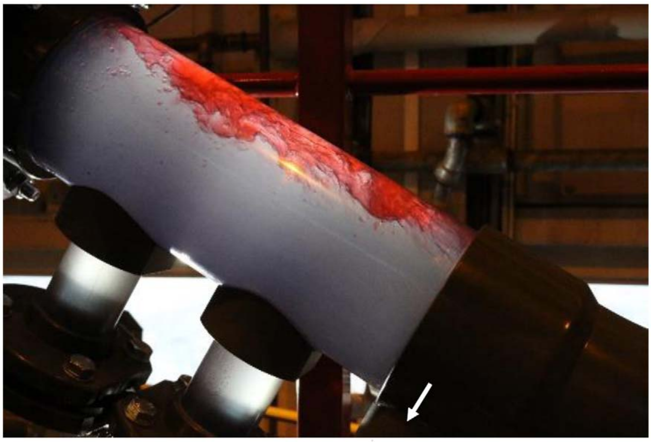

Figure 15—Flow phenomenon in extraction pipe for $\dot{Q}_{tot}$ = 250L/min, WC = 70%, ER = 90%

In Figure 16, the observed flow phenomenon for the same test point, but with WC = 30% is displayed. A more intense re-distribution of oil droplets is observed.

Figure 16—Flow phenomenon in extraction pipe for $\dot{Q}_{tot}$ = 250L/min, WC = 30%, ER = 90%

In Figure 16, the height of water at the extraction point is close to 70% of the pipe diameter. This is an effect of the inclined extraction section, securing a buildup of the water layer. A water height equal to 70% of the pipe diameter corresponds to an area fraction of 75%, which means the area for the oil phase is 25%. The non-slip water holdup is 30% (equal to the WC at the separator inlet), which means that there is a "slip" ratio of seven between the oil and water flow velocities (i.e. the oil flows seven times quicker than the water). This increased slip-velocity could be a significant contributor to the observed increase in re-entrainment of oil droplets into the water layer.

For higher mixture flowrates (i.e. 500-750L/min), the deterioration of separator performance looks to be related to the formation of a fine dispersion layer in the separator pipes. The initial onset of this layer was observed at a total flowrate of 350L/min in the WC range 30-50%, which corresponds to a mixture velocity of $U_m = 0.16 m/s$. The height of this dispersion layer was observed to increase with decreasing inlet WC, as is illustrated in Figure 17 and Figure 18.

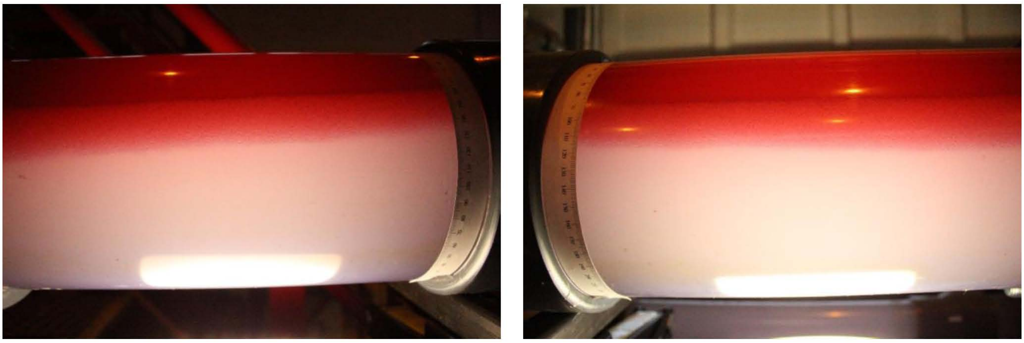

Figure 17—Left and right separation pipes at Q = 500L/min, WC = 70%, ER = 90%

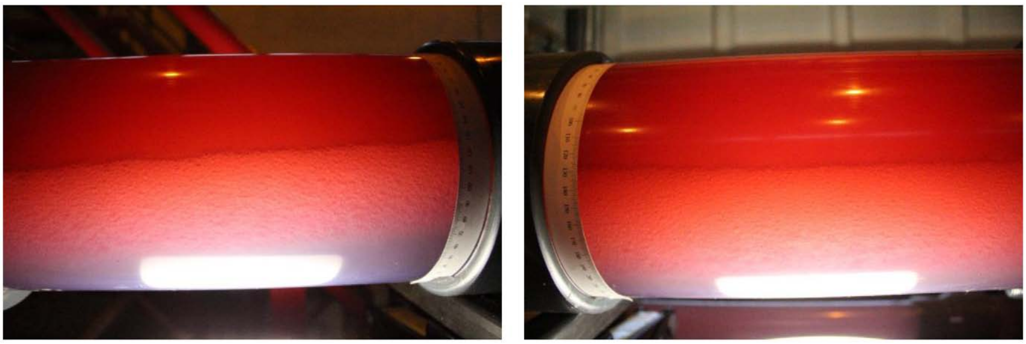

Figure 18—Left and right separation pipes at Q = 500L/min, WC = 30%, ER = 90%

For the majority of test points, both separation branches exhibited identical flow configuration and characteristics, where any formed dispersion layer was split equally between both branches. However, for some cases (medium-high inlet flow rates, inlet WC of 50% and 70%, with low-medium ER), the flow distribution changes. The formed dispersion layer is initially present in both pipes, but as the system reaches steady state, the dispersion layer will migrate completely into one pipe over time. This is shown In Figure 19, where the same operating point as in Figure 17 is run, but the extraction rate has been reduced to 50%. The experiments were repeated several times and there was no preferential branch for dispersion layer accumulation. It seemed to occur randomly.

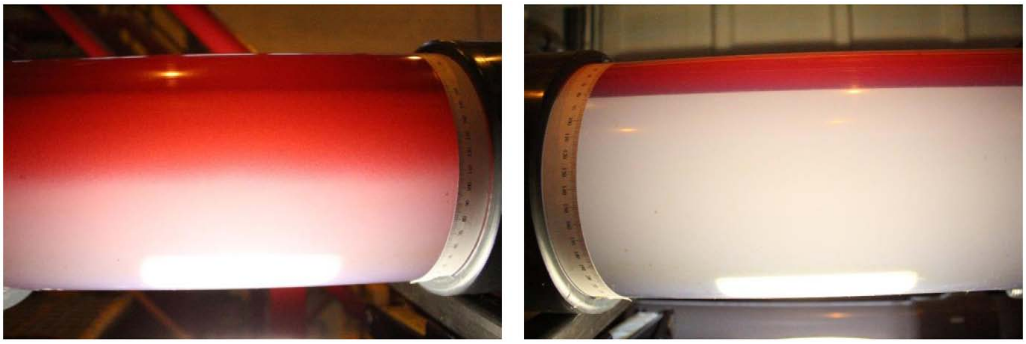

Figure 19—Left and right separation pipes at Q = 500L/min, WC = 70%, ER = 50%

Conclusions

This paper has presented the details of a novel oil-water separator concept (the MPPS) suitable for subsea applications. The concept was conceived and defined by analyzing and studying existing field-proven subsea separation facilities, current concepts under development, and previous work performed at the Institute of Geoscience and Petroleum, NTNU.

An initial baseline performance test of the proposed concept was performed. In addition, observed flow phenomena for selected test points have been presented and discussed, aiming to improve the understanding of oil-water separation in multiple pipes. Presented results displayed overall excellent performance for a flowrate of 250L/min. At this flowrate, close to 100% of the incoming water could be extracted while maintaining high separation efficiencies. When increasing the flowrate to 500L/min, a reduction in extraction rates down to 50-70% was needed to maintain good separation efficiencies. The efficiency drops with decreasing WC, as well as for increasing ER.

Two factors have been identified as potential reasons for the drop in efficiency at lower water cuts. The first is re-entrainment of oil-droplets into the water phase because of increased slip velocity between the oil and water layer occurring at low water cuts in the extraction section. The second phenomenon is the formation of a dispersion layer hindering complete separation of the phases. Initial onset of this dispersion layer was observed close to 350L/min in the WC range 30% – 50%. At high extraction rates, this dispersion layer distributes evenly between the two pipes of the separator prototype. When reducing the ER, the forming dispersion layer was observed to migrate into one pipe, while the second pipe remained with pure oil-water phases. This effect was observed for water cuts 70% and 50%, while the dispersion remained evenly distributed for a WC of 30%.

Overall, the application of a multipipe system for subsea oil-water bulk separation has been proven promising, and further testing of the concept will include a study of optimal tapping point location, as well as optimal inlet configurations to maximize separator performance.

Acknowledgments

This work was carried out as a part of SUBPRO, a Research-based Innovation Centre within Subsea Production and Processing. The authors gratefully acknowledge the financial support from SUBPRO, which is financed by the Research Council of Norway, major industry partners and NTNU. The authors would also like to thank senior engineers Noralf Vedvik and Steffen Wærnes Moen for valuable help and input during construction of the presented test facilities, as well as Martin Holberg Marthinussen for thickness estimate calculations.

Nomenclature

Symbol	Description	SI unit	Conversion
A	Cross sectional area	$[m^2]$	-
A_w	Area fraction water	$[-]$	-
A_o	Area fraction oil	$[-]$	-
g	Gravitational acceleration	$[m/s^2]$	-
h	Water height	$[m]$	$1000[mm]$
L	Length	$[m]$	-
R	Radius	$[m]$	$1000[mm]$
r	Radius	$[m]$	$1000[mm]$
S	Interfacial layer width	$[m]$	-
T	Temperature	[°C]	-
t_{res}	Residence time	$[s]$	-
U	Velocity	$[m/s]$	-
V	Volume	$[m^3]$	-
W	Weight	$[kg]$	-
wt%	Weight percentage	$[-]$	-
ϵ	Separation efficiency	$[-]$	
μ	Viscosity	$[Pa \cdot s]$	$1000[cP]$
$\dot{Q}$	Volume flow	$[m^3/s]$	$60000[L/min]$
ρ	Density	$[kg/m^3]$	-
θ	Angle	$[rad]$	$180/\pi[\circ]$

Subscript	
a	Continuous phase
d	Dispersed phase
i	1, 2, …, n
m	Mixture
mat	Material
o	Oil
r	Rising
s	Settling
tot	Total
w	Water

References

Abrand, S., Shaiek, S., Anres, S. J. et al. 2013. Subsea Gas-liquid And Water-hydrocarbon Separation: Pipe Solutions For Deep And Ultra Deepwater. Proc., OTC Brasil.

Bakke, W. and Sundt, H. K. 2016. Troll Pilot - The world's first and longest-running subsea separation system. Proc., UTC.

Berard, M., Babour, K., and Babelli, I. 2013. In-line flow separation of fluids in a pipe separator, *Google Patents (Reprint)*.

Capela Moraes, C. A., da Silva, F. S., Marins, L. P. M. et al. 2012. Marlim 3 Phase Subsea Separation System: Subsea Process Design and Technology Qualification Program. Proc., Offshore Technology Conference.

Davies, S. R., Bakke, W., Ramberg, R. M. et al. 2010. Experience to date and future opportunities for subsea processing in StatoilHydro. Proc., Offshore Technology Conference.

de Oliveira, D. A., Pereira, R. d. S., Capela Moraes, C. A. et al. 2013. Comissioning and Startup of Subsea Marlim Oil and Water Separation System. Proc., OTC Brasil.

Emerson. 2017. *Micro Motion F-Series Flow and Density Meters, Product Data Sheet PS-00603, Rev. Y (Reprint)*.

Euphemio, M., Oliveira, R., Nunes, G. et al. 2007. Subsea Oil/Water Separation of Heavy Oil: Overview of the Main Challenges for the Marlim Field-Campos Basin. Proc., Offshore Technology Conference.

Fossen, M. and Schümann, H. 2016. Experimental Study of the Relative Effect of Pressure Drop and Flow Rate on the Droplet Size Downstream a Pipe Restriction. *Journal of Dispersion Science and Technology (just-accepted)*.

Grave, E. and Olson, M. 2014. Design and Performance Testing of a Subsea Compact Separation System for Deepwater Applications. *Oil and Gas Facilities* **3** (04): 16–23.

Horn, T., Bakke, W., and Eriksen, G. 2003. Experience in operating world's first subsea separation and water injection station at Troll Oil Field in the North Sea. Proc., Offshore Technology Conference.

NOROG. 2017. *2017 Enviromental Report - Environmental work by the oil and gas industry, facts and development trends*.

Olson, M., Grave, E., Juarez, J. et al. 2015. Performance Testing of an Integrated, Subsea Compact Separation System with Electrocoalescence for Deepwater Applications. Proc., Offshore Technology Conference.

Orlowski, R., Euphemio, M. L. L., Euphemio, M. L. et al. 2012. Marlim 3 Phase Subsea Separation System-Challenges and Solutions for the Subsea Separation Station to Cope with Process Requirements. Proc., Offshore Technology Conference.

Rivera, R. M. 2011. *Water separation from wellstream in inclined separation tube with distributed tapping*. PhD, Norwegian University of Science and Technology.

Rivera, R. M., Golan, M., Friedemann, J. D. et al. 2006. Water separation from wellstream in inclined separation tube with distributed tapping. Proc., SPE Annual Technical Conference and Exhibition.

Sagatun, S. I., Gramme, P., Horgen, O. J. et al. 2008. The Pipe Separator-Simulations and Experimental Results. Proc., Offshore Technology Conference.

Shaiek, S. and Grandjean, L. 2015. SpoolSep for Subsea Produced Water Separation-Experimental Results. Proc., Offshore Technology Conference.

Siemens. 2015. *Flow Measurement - SITRANS F C, Product Data Sheet (Reprint)*.

Skjefstad, H. S. and Stanko, M. 2017. Subsea water separation: a state of the art review, future technologies and the development of a compact separator test facility. Presented at the 18th International Conference on Multiphase Production Technology, Cannes, France. 2017/12/13/.

Skovholt, O. 2015a. *Inclined Tubular Separator for Separating Oil Well Substances*, US Patent 20,150,343,328 (Reprint).

Skovholt, O. 2015b. *Method for Separating Substances Mixed in Fluids From Oil Wells*., US Patent 20,150,343,327 (Reprint)

Stanko, M. E. W. 2014. *Topics in Production Systems Modeling: Separation, Pumping and Model Based Optimization*.

Appendix A

Weight reduction

Simplified initial estimations were performed in order to compare the size and weight of a multipipe approach to a standard vessel approach. In Figure A-1, dimensions for a vessel and a series of parallel pipes are given.

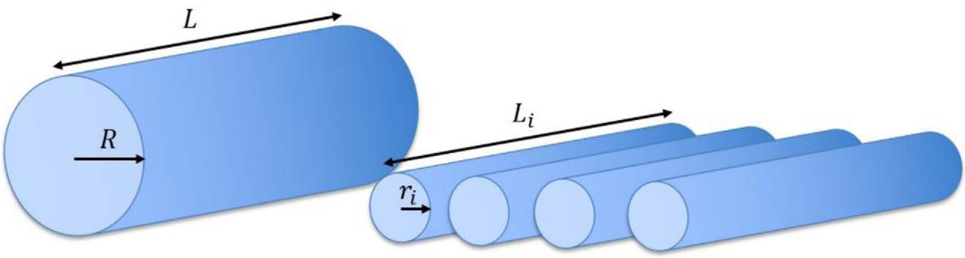

Figure A-1—Vessel and pipe dimensions

From these dimensions, the cross-sectional area (A) and volume (V) of the vessel and the same (A_i, V_i) for the combined number of pipes (n) can be derived:

$$A = \pi R^2 \tag{5}$$

$$V = \pi R^2 L \tag{6}$$

$$A_{i_{tot}} = nA_i = n\pi r_i^2 \tag{7}$$

$$V_{i_{tot}} = nV_i = n\pi r_i^2 L_i \tag{8}$$

By looking at a case where the total cross-sectional area of parallel pipes are equal to the cross-sectional area of the vessel, and assuming an equal total flow rate ($\dot{Q}$) for both cases, the velocity through the vessel separator (U_m) would be equal to the individual velocities in the respective pipes (U_{m_i}). It is here assumed that incoming process-stream is split equally and flows with a uniform flow velocity. This can be shown by the following relation:

$$U_m = \frac{\dot{Q}}{A} = \frac{\frac{\dot{Q}}{n}}{\frac{A}{n}} = \frac{\dot{Q}_i}{A_i} = U_{m_i} \tag{9}$$

Here, $\dot{Q}$ is the total flow rate of oil and water, while U_m/U_{m_i} is the mixture velocities found by dividing the total flow rate with the respective total cross-sectional area. The following relations can then be derived, where subscript w signifies water:

$$A = A_{i_{tot}} \rightarrow R = r_i\sqrt{n} \tag{10}$$

$$U_w = U_{w_i} \rightarrow A_w = \frac{\dot{Q}_w}{\dot{Q}_{w_i}} A_{w_i} = nA_{w_i} \tag{11}$$

Using the geometric relations identified in Figure A-2, certain comparisons in terms of interfacial area, holdup, residence time and required separator length can then be made.

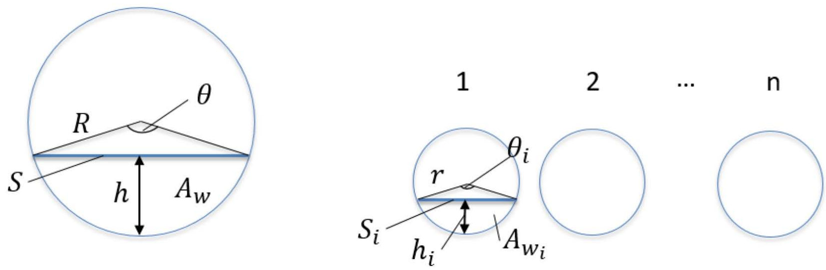

Figure A-2—Vessel and pipe relations

From Eq.(10) and (11), the following relation between θ and θ_i can be derived:

$$A_w = \frac{R^2}{2}(\theta - \sin(\theta)) = \frac{nr^2}{2}(\theta_i - \sin(\theta_i)) = \frac{R^2}{2}(\theta_i - \sin(\theta_i)) \rightarrow \theta = \theta_i \tag{12}$$

Utilizing the result of Eq.(12), the following relations for interfacial length (S), setling distance (h), residence time (t_{res}) and separator length (L) can be made:

$$S = 2Rsin\left(\frac{\theta}{2}\right), \quad S_{i_{tot}} = n2rsin\left(\frac{\theta}{2}\right) = \sqrt{n}2Rsin\left(\frac{\theta}{2}\right) = \sqrt{n}S \tag{13}$$

$$h = R\left(1 - \cos\frac{\theta}{2}\right), \quad h_i = r\left(1 - \cos\frac{\theta}{2}\right) = \frac{R}{\sqrt{n}}\left(1 - \cos\frac{\theta}{2}\right) = \frac{h}{\sqrt{n}} \tag{14}$$

$$t_{res} = \frac{h}{u}, \quad t_{res_i} = \frac{h_i}{u} = \frac{h}{u\sqrt{n}} = \frac{t_{res}}{\sqrt{n}} \tag{15}$$

$$L = t_{res}U_m, \quad L_i = t_{res_i}U_{m_i} = \frac{t_{res}U_m}{\sqrt{n}} = \frac{L}{\sqrt{n}} \tag{16}$$

The variable u is the setling/rising velocity given by Stokes' Law as:

$$u = \frac{2(\rho_d - \rho_a)gr_d^2}{9\mu_a} \tag{17}$$

Where ρ_d and ρ_a refers to the dispersed and continuous phase respective densities, g is the gravitational acceleration, r_d is the dispersed phase's spherical radius, and μ_a is the continuous phase's viscosity.

It is thus evident that by utilizing a multipipe design we can achieve an increase in interfacial length (S), and a reduction in required settling distance (h), residence time (t_{res}) and separator length (L). All by a factor equal to the square root of the number of pipes utilized.

Taking this a step further, an estimation for the potential reduction in separator weight can be calculated. By adding a thickness to the vessel and pipes illustrated in Figure, t and t_i respectively, the weight of the cylindrical vessel shell (W), and combined weight of the pipe shell sections ($W_{i_{tot}}$) can be given as:

$$W = V_{mat}\rho_{mat} = (\pi L(R + t)^2 - \pi LR^2)\rho_{mat} = \pi Lt(2R + t)\rho_{mat} \tag{18}$$

$$W_{i_{tot}} = nV_{mat_i}\rho_{mat} = n\pi L_i t_i(2r + t_i) = \sqrt{n}\pi Lt_i\left(2\frac{R}{\sqrt{n}} + t_i\right) \tag{19}$$

It should be noted that these estimations are limited to the weight of the cylindrical shell, not included the front and back walls. Combining Eq.(18) and Eq.(19), an expression for the weight ratio between the two designs can be derived, where x represents the thickness ratio t_i/t.

$$\frac{W_{i_{tot}}}{W} = \frac{\sqrt{n}\pi L t_i \left(2\frac{R}{\sqrt{n}} + t_i\right)}{\pi L t(2R + t)} = \frac{t_i\left(2R + \sqrt{n}t_i\right)}{t(2R + t)} = \frac{x\left(2R + \sqrt{n}xt\right)}{2R + t} \tag{20}$$

The potential weight reduction can then be illustrated by plotting Eq.(20) for an imagined reference vessel design. In Figure A-3, the reference is a 2.1m diameter vessel installed at a water depth of 1000m, with a resulting wall thickness of 110mm.

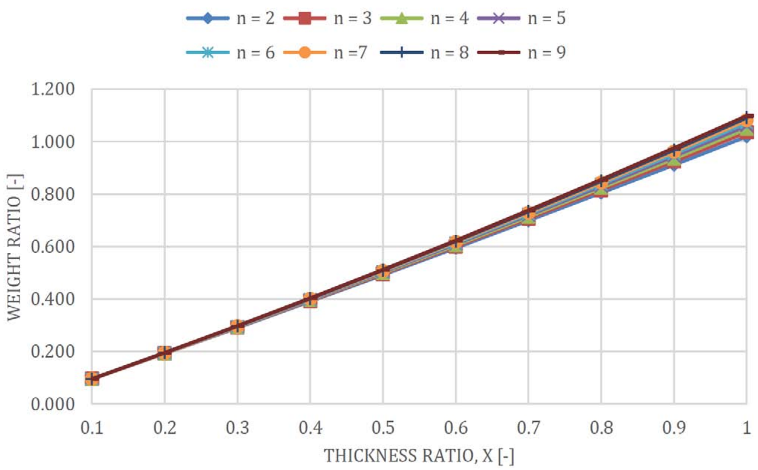

Figure A-3—Weight ratio of a multipipe design with n pipes vs a 2.1m diameter vessel with 110mm wall thickness

It can be observed that a significant reduction in separator weight can be expected given the gained reduction in thickness from reduced diameter. A nine-pipe solution would result in a thickness ratio of 0.34 resulting in an overall weight reduction of approximately 67%. Thickness estimates were based on British Standard EN 13445-3:2009.

Appendix B

Simplified capacity estimates

Simplified capacity estimates were made in order to get an idea of expected flow limitations for gravity driven separation in short horizontal pipe segments. Investigated pipe lengths were in the range 6-7m, which allows cheaper and more accessible transportation vessels to be used for installation.

Estimates are based on basic Navier Stoke's residence time calculations, with fluid properties as given in Table B-1.

Table B-1—Fluid properties for capacity estimates

Fluid	Density [kg/m3]	Viscosity [cP]
Water	1020	1
Oil	790	1.4

A cut off droplet diameter was chosen to calculate the settling (u_s)/rising (u_r) velocity of a water/oil droplet respectively. Three cut-off diameters were chosen, $150\mu m$, $175\mu m$ and $200\mu m$. The settling velocities are calculated with Eq.(21) and (22).

$$u_r = \frac{2(\rho_w - \rho_o)gr^2}{9\mu_w} \tag{21}$$

$$u_s = \frac{2(\rho_w - \rho_o)gr^2}{9\mu_o} \tag{22}$$

Here μ represents the viscosity for the respective phases, r is the droplet radius corresponding to the given cut-off diameter and g is the gravitational acceleration. The water height (h) at a given WC and pipe diameter (D) is then calculated. A no-slip condition is assumed, meaning that the area fraction of a given pipe cross-sectional area (A) taken up by either phase is equal to the WC.

$$A = \frac{\pi D^2}{4} \tag{23}$$

$$A_w = A \times WC \tag{24}$$

Looking back to Figure A-2, the water height can then be found by iterating Eq.(25), then solving Eq.(26).

$$\theta = \frac{8A_w}{D^2} + \sin(\theta) \tag{25}$$

$$h = \frac{D}{2}\left(1 - \cos\left(\frac{\theta}{2}\right)\right) \tag{26}$$

The calculated water height is then used to calculate the required residence time in the pipe, and by using the pre-defined pipe length, a predicted flow rate is given. For all water cuts, two residence times are calculated. The first is the time it takes for a small droplet of water to travel from the top of the pipe to the established water layer (t_{res_s}). The second is the time it takes for a small droplet of oil to travel from the bottom of the pipe to the established oil layer (t_{res_r}). The maximum of these times are then used to find the total liquid flow capacity.

$$t_{res_s} = \frac{D - h}{u_s}, \quad t_{res_r} = \frac{h}{u_r}, \quad t_{res} = \max(t_{res_s}, t_{res_r}) \tag{27}$$

$$\dot{Q} = \frac{L}{t_{res}} A \tag{28}$$

In Table B-2, results are given for a pipe length of 6.5m, at different pipe diameters and cut-off diameters for a range of WC. Results are given for a dual pipe configuration, meaning calculated flowrate according to Eq.(28) is multiplied by a factor of two.

Table B-2—Simplified total flow capacity estimates at respective droplet cut off diameters and pipe diameters

Internal pipe diameter [mm]	Cut off diameter [μm]	Total liquid flow capacity [L/min] (bbl/day)			
		WC 30%	WC 50%	WC 70%	WC 90%
150	150	281*(2542)*	370*(3353)*	393*(3558)*	307*(2783)*
	175	382*(3459)*	504*(4563)*	535*(4843)*	418*(3788)*
	200	499*(4518)*	658*(5960)*	698*(6326)*	546*(4948)*
300	150	561*(5083)*	740*(6705)*	786*(7117)*	614*(5566)*
	175	764*(6919)*	1008*(9127)*	1069*(9686)*	836*(7576)*
	200	998*(9037)*	1316*(11921)*	1397*(1265)*	1092*(9895)*
450	150	842*(7625)*	1110*(10058)*	1179*(10675)*	922*(8349)*
	175	1146*(10378)*	1511*(13689)*	1604*(14530)*	1255*(11363)*
	200	1497*(13555)*	1974*(17881)*	2095*(18977)*	1639*(14848)*

Chapter 5

Separator performance evaluation and design improvement, Paper III

This chapter consists of Paper III, which presents results from two completed separator design feature studies. The studies investigate optimal location for water extraction, and maps separator performance with three different separator inlet configurations. The paper presents an expected up-scaled operational envelope for the developed concept, which is based on calculated performance of the constructed prototype.

H. S. Skjefstad and M. Stanko. Experimental performance evaluation and design optimization of a horizontal multi-pipe separator for subsea oil-water bulk separation. *Journal of Petroleum Science and Engineering*, 176:203-219, 2019.

Journal of Petroleum Science and Engineering 176 (2019) 203–219

Contents lists available at ScienceDirect

Journal of Petroleum Science and Engineering

journal homepage: www.elsevier.com/locate/petrol

Experimental performance evaluation and design optimization of a horizontal multi-pipe separator for subsea oil-water bulk separation

Håvard S. Skjefstad*, Milan Stanko

Department of Geoscience and Petroleum, Norwegian University of Science and Technology, S. P. Andersens veg 15A, PTS1, 7031, Trondheim, Norway

A R T I C L E I N F O

Keywords:
Compact separation
Pipe separation
Oil-water separation
Subsea separation
Modular design
Energy efficient production

A B S T R A C T

Subsea separation of produced water increases the recovery rates for brown field installations. Removing produced water on the seabed increases production rates, removes topside produced water bottlenecks and enables better utilization of existing topside facilities. Existing subsea bulk water separator technologies are limited to gravity and compact gravity vessel types, as seen on Troll and Tordis, and the pipe separator installed at Marlim, which are large, heavy and costly installations. In order to make the business case for subsea produced water separation more attractive, there is a need to reduce the weight and areal footprint of separator designs. It is also important to develop separator solutions that can be qualified for a wide range of field operating conditions.

This paper presents the experimental testing of a novel produced water separator design, the Multiple Parallel Pipe Separator (MPPS). The design uses multiple horizontal pipe segments in parallel for liquid-liquid separation, with inclined outlet pipe segments for increased water holdup and eased water extraction. Experiments are performed on a two-pipe prototype.

A limited test matrix was run to investigate the best location for water extraction. Three tapping locations were tested. Experiments displayed oil re-entrainment along the inclined extraction pipe, and the best extraction point was found to be close to the horizontal to inclined transition.

Using the identified tapping location, a detailed performance mapping was performed at total flow rates from 300 to 700 L/min and water cuts ranging from 30 to 90%. The performance mapping was performed with three different inlet configurations, a normal inlet, a tangential inlet, and a tangential inlet accompanied with novel phase re-arranging internals. Best separator performance was achieved for the tangential inlet with internals configuration, displaying efficiencies in the range 78.8–100%.

A dispersion layer was observed in the separator pipes for total flow rates above 350 L/min. At low water extraction rates, this forming dispersion layer was observed to migrate completely into one of the two separator branches at random. The uneven splitting of the dispersion layer was observed to strengthen when changing from a normal to a tangential inlet configuration. The installation of phase-rearranging internals eliminated the uneven splitting of the dispersion layer, resulting in an even phase distribution between the two separator branches.

1. Introduction

Produced water management is an important consideration for mature oil fields. In most cases, produced water gradually replaces hydrocarbons as the main extracted fluid. A review of oil and gas produced water treatment technologies from 2009 (Fakhrul-Razi et al., 2009) reports a global produced water production of 250 million bpd. At the time, this corresponded to a produced water to hydrocarbon ratio of 3:1. On the Norwegian Continental Shelf (NCS), production of 181 million standard cubic meter of produced water was reported for 2016 (NOROG, 2017). This accounts for more than two times the amount of produced oil.

Produced water is normally transported with the production stream topside where it is separated and cleaned. Depending on the installation, the water is then either re-injected for pressure support, or disposed to sea. Increased produced water rates eventually cause challenges for offshore installations, especially when the lifespan of installations are extended beyond design specification. This is a situation that occurs frequently (da Silva et al., 2013). As the field matures, produced water production will increase, eventually reaching design capacity and becoming a bottleneck in production. Subsea separation of produced water enables de-bottlenecking of topside facilities, allowing

* Corresponding author.
E-mail address: havard.s.skjefstad@ntnu.no (H.S. Skjefstad).

https://doi.org/10.1016/j.petrol.2019.01.027
Received 1 October 2018; Received in revised form 4 January 2019; Accepted 6 January 2019
Available online 09 January 2019
0920-4105/

increased production rates and new tie-ins to existing facilities.

An important consideration for subsea separation is that cost must be low enough to justify investment. Brown fields have limited remaining reserves, which means limited return rates for the operator. Subsea separation is thus often considered too capex-intensive to be profitable, as discussed by Moraes et al. (da Silva et al., 2013). It is therefore important to develop cost-effective subsea separator technologies, making the business case for subsea separation more attractive.

Existing subsea liquid-liquid separator solutions are the gravity vessel separators at Troll (Horn et al., 2003) and Tordis (Davies et al., 2010), and the Marlim pipe separator (Capela Moraes et al., 2012) (Orlowski et al., 2012). Vessel type separators are well known from topside application. They are robust, have good slug dampening capabilities and have a large operational envelope. However, for subsea applications, the diameter of a gravity vessel will cause challenges. Large water depths means thick vessel walls, which result in large and heavy installations. This increases the overall cost of the installation. The Marlim pipe separator was designed for deep water application, where the reduced pipe diameter is more suited for the increased hydrostatic pressure. However, the one-pipe solution of the Marlim separator is still a large installation. The reported pipe length is 60 m (Orlowski et al., 2012), and the design includes a vessel-type geometry downstream the pipe for fluid extraction which again adds to the overall weight and complexity of the installation. Additionally, the one-pipe solution of the Marlim installation has limited flow capacity, and is restricted to water continous inlet flows (de Oliveira et al., 2013).

An alternative to the one pipe solution is seen in Saipem's SpoolSep concept (Shaiek Grandjeanet al., 2015). The design consist of several long pipe spools working in parallel, and is designed for complete three-phase separation at large water depths. SpoolSep removes the capacity constraint of a one-pipe solution, and its modular design approach offers more flexibility in development and installation. However, the SpoolSep is still a large and heavy installation, with design spool specifications of 50 m length, and outer diameter (OD) of 24 *inches*. Results from a scaled down prototype test of the SpoolSep was reported in (Shaiek Grandjeanet al., 2015), displaying oil in water quantities in the range 500–2000 *ppm*.

Other alternative bulk water separator designs have been reported in the literature. Rivera et al. (2006) built and tested an inclined pipe separator with sequential tapping for bulk separation of oil and water. Separation efficiencies in the range 95–100% were reported for favourable flow regimes. A different concept was presented by Zeng et al. (2016), proposing a design utilizing two parallel-connected paths, one with high local resistance and one with high frictional resistance, for oil-water separation.

As described, there are existing solutions for subsea separation of produced water. However, current designs result in large, heavy and costly installations. In addition, all current installations required their respective test and qualification programs (partly due to fundamental differences), again adding to the overall cost. In order to make subsea separation of produced water economically attractive, there is a need to reduce the weight and areal footprint of separator designs. It is equally important to develop separator solutions that can be qualified for a wide range of field operating conditions. This paper presents the experimental testing of a newly developed oil-water bulk separator concept named the Multiple Parallel Pipe Separator (MPPS). The concept utilizes multiple pipes in parallel, offering reduced settling times and a more compact, modularized and adaptive separator design compared to existing subsea bulk-water separator installations.

2. Separator concept

The new design has been given the name Multiple Parallel Pipe Separator (MPPS), and was recently presented at the 2018 SPE Asia-Pacific Oil & Gas Conference and Exhibition (Skjefstad and Stanko, 2018). In (Skjefstad and Stanko, 2018), the reader can find justifications for the separator concept design as well as calculative examples of possible weight reduction compared to a vessel type separator. The weight reduction potential was illustrated for a 1000 m water depth installation, where a multi-pipe arrangement displayed a possible weight reduction of 67% compared to a vessel type separator (Skjefstad and Stanko, 2018). An illustration of the concept is given in Fig. 1.

The concept utilizes multiple horizontal pipe segments in parallel for liquid-liquid separation. The inlet (1) is a T-section header that splits the incoming production stream into individual branch streams. Two

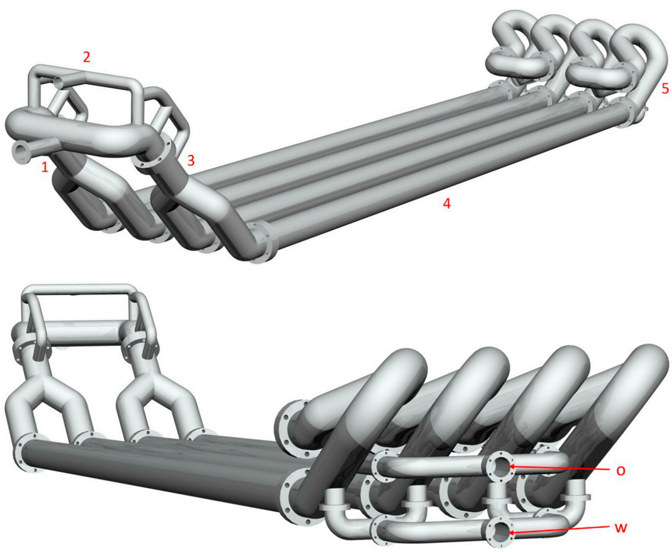

Fig. 1. Illustration of the MPPS concept design.

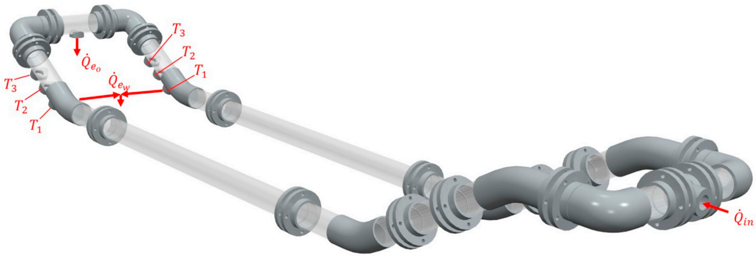

Fig. 2. Illustration of the constructed MPPS prototype.

inlet configurations have been designed, one normal and one tangential. The tangential inlet is intended to enhance separation by means of centrifugal forces, as well as ensure a low mixing inlet. This configuration will push the heavier phase towards the pipe wall, while the lighter phase will concentrate in the pipe centre. A set of novel internals has been developed for the tangential inlet configuration. The internals are designed to rearrange the fluids from a core divided phase distribution to a stratified flow configuration upstream the connected downward section (3). Detailed information on the respective inlet designs will be given later in Section 3.5.2. The set off descending pipe elements (3) that follow the inlet T-section is to further split the production stream into horizontal pipe elements. The inlet T-section with internals can alternatively be configured for gas-liquid separation, in which case extraction pipes for gas (2) are fitted to the top part of the descending pipe elements. This design approach is previously proven for a one-pipe solution at the Marlim installation (Capela Moraes et al., 2012). Next follows the horizontal pipe segments (4), where the main part of the liquid-liquid separation takes place. Extraction of water (w) is performed in an inclined extension of the horizontal pipes (5), where water is slowed down, securing a large holdup for eased and controlled extraction. The remaining oil rich stream flows up the inclined section and back down for separate extraction (o). The design of the extraction section is such that several horizontal pipe sections can be mounted in series without increasing the areal footprint of the separator. All extraction pipes are connected to a shared outlet, one for water and one for oil, securing self-regulation of the system.

3. Test procedure

3.1. Prototype design

A prototype was constructed to investigate the separation performance of the concept, the internal oil-water flow dynamics, and determine its operational map. The prototype consists of two DN150 (150.6 *mm* ID) transparent PVC pipes in parallel, and is shown in Fig. 2.

The inlet section is on the right in the figure, where the flow is split in the T-section, leading to the respective horizontal pipe sections. As mentioned, two inlet configurations have been constructed. One normal inlet, as is shown in the figure, and one tangential inlet. Both inlets will be tested to investigate the effect the inlet configurations has on separator performance and flow split dynamics. A 30° decline follows the inlet split. The current test facility has no gas supply, and therefore no gas removal pipes have been installed. After the downward section, the two parallel horizontal pipe sections follow. This is where the main part of the liquid-liquid separation is to take place. At the end of the horizontal sections, the pipes are inclined at a 30° angle. This is to secure a large water holdup for eased extraction. For details on design justifications, the reader is directed to (Skjefstad and Stanko, 2018). Along the inclined outlet sections, three tapping locations for water has been constructed. This is to investigate the optimal location for extracting water. In Fig. 2, the bottom tapping location is marked in red with the denotation $\dot{Q}_{e_w}$. As illustrated, a T-section is fitted to the designated tapping point, so that extraction is performed from both pipe sections through a common extraction line. This extraction line will be referenced as the water return line in the following section. For the remainder of this paper, the marked tapping location (located closest to the horizontal section) will be referenced as tapping location 1 (T1), while the middle will be T2, and the last T3. The extraction point for oil is marked as $\dot{Q}_{e_o}$, again being a shared outlet for both pipe sections. In Fig. 3, the dimensions of the prototype is given. The spacing between tapping locations is 170 *mm*.

3.2. Test facility

The test facility is a two phase oil-water flow loop with ExxsolD60 and distilled water with added *wt%* 3.4 NaCl as experimental fluids. 0.015 g/L of the colourant Oil Red O ($C_{26}H_{24}N_4O$) has been added to the ExxsolD60 for phase distinction, and 1000 *ppm* of the biocide IKM CC-80 was added to the water for bacterial growth inhibition. Fluid properties at 23 °C are given in Table 1, and an overview of the test fluids separability and dispersion characteristics can be found in Section 3.4.

A P&ID of the test facility is given in Fig. 4. The loop consists of a 1.2 *m* diameter - 5.5 *m* long storage tank for baseline separation. The residence time in the storage tank is approximately 27 times the residence time in the presented MPPS prototype. Fluid head is provided by a pump manifold downstream the storage tank. The pump manifold consist of 4 pumps in parallel, with a total flow capacity of 100–2100 L/min for the water phase and 100–1700 for the ExxsolD60. Pumps are controlled and regulated by 0–50 *Hz* frequency converters, 50 *Hz* constituting a maximum *rpm* of 2900. Two flexible DN65 (67.8 *mm* ID) PVC hoses lead from the pump manifold up to a second floor to two DN65 transparent PVC feed lines. Each feed line is fitted with a Coriolis flow meter for density and flow rate measurement. The line size is reduced to DN50 0.5 *m* up- and down-stream installed flow meters. The feed lines merge in a Y-junction and the multiphase transport line

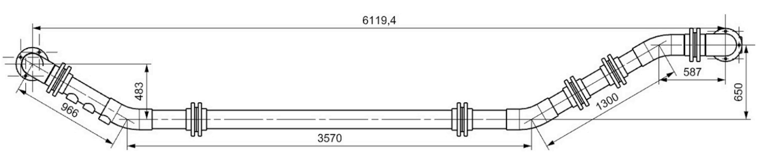

Fig. 3. Prototype dimensions [mm].

Table 1
Fluid properties at 23 °C.

Fluid	Density $[kg/m^3]$	Viscosity $[cP]$
Water w/ $wt\%$3.4 NaCl and 1000 ppm IKM CC-80	1020.75	0.99
ExxsolD60 w/ 0.015 g/L Oil Red O	789.45	1.41

includes a 5.5 m long straight transparent DN65 (67.8 mm ID) PVC pipe, a 720 mm radius 180° flexible DN65 PVC hose turn, and a secondary 5 m long straight transparent DN65 PVC pipe leading back to the presented MPPS prototype inlet. Temperature and pressure are recorded directly upstream the inlet, and an electrically controlled ball valve with added dP measurement is installed 2 m upstream the MPPS prototype inlet to allow for inlet choking. A valve opening of 100% was applied for all test points presented in this study, meaning no pressure loss was induced over the installed inlet valve. The loop has two return lines, one for water and one for ExxsolD60. The water return line has a third Coriolis meter installed, allowing continuous monitoring of oil in water (OiW) content and extraction flow rate. The water return line is in addition fitted with an electrically controlled ball-valve, while the ExxsolD60 return line is fitted with a pneumatic membrane valve for fast and accurate fine-tuning of extraction rate. Pressure is recorded in both extraction lines. All piping in the flow loop is rated for PN10, except the separator prototype, which is PN6.

A more detailed description of the lab facilities is given in (Skjefstad and Stanko, 2018).

3.3. Instrumentation and test parameters

The installed Coriolis meters are two Micro Motion F200 (FT.1 and FT.2) and one Sitrans FC430 (FT.3). The flow meters have a maximum flow of 1452 kg/min and 1178 kg/min respectively. Reported error for mass flow is 0.11% of actual, for volume flow it is 0.15% of actual, and for density, 0.54 kg/m^3.

Installed pressure transducers are of the type Sitrans P310. The gauge pressure transducers have a specified range of 0–6 $barg$ with a reported maximum error of 0.075%. The dP transducer has a span of 0–2 $barg$ with the same error specification. Temperature measurement is performed with a Ni1000 TK5000 element, which in the installed module has a temperature range of– 30 °C to + 122 °C with a resulting measurement error of ± 0.3 °C.

Table 2
Recorded parameters.

Tag	Parameter	Unit
FT.1	$\dot{Q}_1$	L/min
FT.2	$\dot{Q}_2$	L/min
FT.3	$\dot{Q}_3$	L/min
DT.1	ρ_1	kg/m^3
DT.2	ρ_2	kg/m^3
DT.3	ρ_3	kg/m^3
PT.1	P_1	$barg$
PT.2	P_2	$barg$
PT.3	P_3	$barg$
dPT.1	dP_1	$barg$
TT.1	T_1	°C

The flow, density and pressure measurements are subject to two additional error components in the experimental set-up. A quantization error resulting from a 13 bit analogue to digital converter (ADC), and a data acquisition (DAQ) error equal to 0.05% of full span.

All recorded parameters are given in Table 2. These are the basis of all further calculation. Parameters are recorded continuously with a set sampling frequency of 5 Hz. Sampling time for all test points are 60 s, giving 300 samples.

Density measurements are used to estimate the water cut (WC) of the flow passing through the respective Coriolis meters. Calculation is

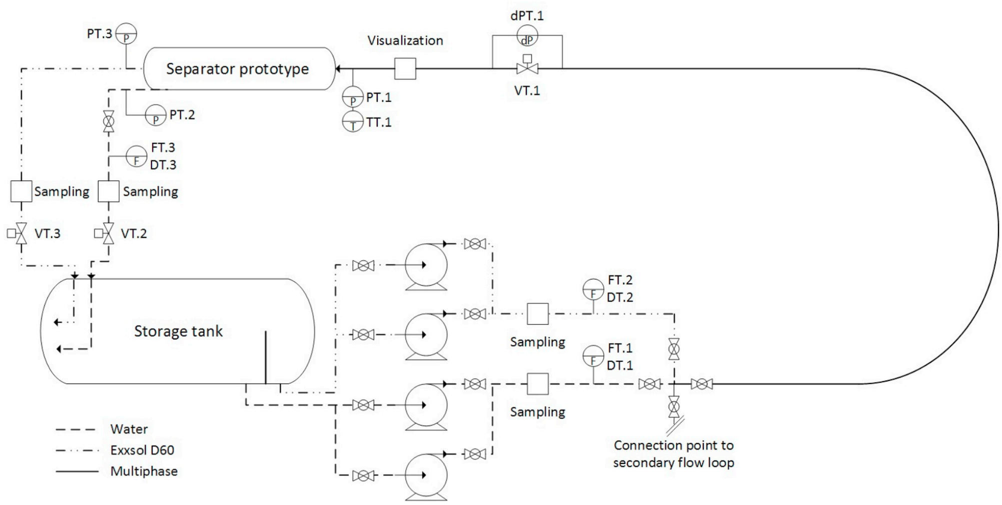

Fig. 4. Lab facility P&ID.

done according to Eq. (1), where ρ_i is the recorded density, and ρ_o and ρ_w are the pre-established temperature corrected densities of ExxsolD60 and Water. The reference densities for ExxsolD60 and Water were determined for a temperature range of $15-25\ ^\circ C$, and the respective expressions are given in Eqs. (2) and (3). Recorded temperature at the MPPS inlet (TT.1) is used for reference density determination. The stated approach to determine WC assumes a homogeneous distribution of ExxsolD60 and Water in the Coriolis meters. This assumption is supported by diameter reductions upstream the Coriolis meters, diameter reductions in the Coriolis meters, and an averaging over the 300 samples taken at each test point.

$$WC_i = \frac{\rho_i - \rho_o}{\rho_w - \rho_o} \tag{1}$$

$$\rho_o = -0.732T_1 + 806.29 \quad [kg/m^3] \tag{2}$$

$$\rho_w = -0.004T_1^2 - 0.11T_1 + 1025.40 \quad [kg/m^3] \tag{3}$$

The calculated WC of the water and ExxsolD60 feed lines are then used to calculate the actual WC of the compact separator inlet stream. Calculation is performed according to Eq. (4), where $\dot{Q}_1$ and $\dot{Q}_2$ are the flow rates through the Water and ExxsolD60 respective feed lines. This ensures an accurate estimation of WC regardless of occurring phase contamination arising from the circulation of fluids in the test facility.

$$WC_{in} = \frac{WC_1\dot{Q}_1 + WC_2\dot{Q}_2}{\dot{Q}_1 + \dot{Q}_2} \tag{4}$$

Separation efficiencies will be estimated at set extraction rates (ER). The ER is defined as the mixture flow rate through the water return/extraction line to the rate of incoming flow through the water feed line, as given in Eq. (5).

$$ER = \frac{\dot{Q}_3}{\dot{Q}_1} \tag{5}$$

The separation efficiency is given as the rate of water extracted to the amount of water theoretically possible to extract at the given ER. The expression is given in Eq. (6).

$$\varepsilon = \frac{WC_3\dot{Q}_3}{ER(WC_{in}(\dot{Q}_1 + \dot{Q}_2))} \tag{6}$$

As previously mentioned, there will be phase contamination over time, with small amounts of ExxsolD60 being dispersed in the inlet water and vice versa. This will have a negative effect on the efficiency reading. For this reason, the ratio of WC at the water extraction line to the WC at the water feed line is also monitored. A value close to unity shows good separator performance and is unbiased in terms of ExxsolD60 contamination. The WC ratio is calculated according to Eq. (7).

$$WC_{ratio} = \frac{WC_3}{WC_1} \tag{7}$$

Errors of calculated properties are found by error propagation as outlined in (Kline and McClintock). The expressions are broken down into their constituent parameters, as listed in Table 2. A confidence interval of 95% has been used for all error estimations. Mean values of recorded parameters are used in calculation. The standard deviation of the sample means are used for confidence interval estimations, resulting in an interval of ± 1.96 times the standard deviation of the respective sample means. Errors accounted for in performed calculations are:

- Instrument error (Linearity/Repeatability/Hysteresis)
- Quantization error (From ADC)
- DAQ error (from DAQ system)
- Random error (Confidence interval of measurement)

Table 3
Test matrix for tapping location study.

$\dot{Q}_{tot}\,[L/min]$(Um [m/s])	$WC_{in}\,[\%]$	$ER\,[\%]$
250 *(0.12)*	30/50/70	50 70 90 100
500 *(0.23)*	30/50/70	50 70 90 100
750 *(0.35)*	30/50/70	50 70 90 100

3.4. *Test fluid characterization*

Simplified bottle tests were performed in order to give an overview of the test fluids separability and dispersion characteristics. Five 80 *ml* samples were prepared, respective water cuts being 70%, 60%, 50%, 40% and 30%. The samples were then filled in a 47 *mm* ID, 80 *ml* beaker, where a magnetic stirring pin was used to mix the ExxsolD60 and Water. Mixing was performed at 1400 *rpm* for 2 minutes. Time was then recorded from end of mixing to a clear two-phase interface had formed. Time recording was repeated three times for each sample.

Observed dispersion characteristics and separation behaviour identified the inversion point for the dispersion to be between 30 and 40% WC. For the 40–70% WC samples, a water layer established quickly in the bottom of the beaker, while a dispersion was visible in the top part of the beaker where an oil layer gradually formed. For the 30% WC sample, an oil layer quickly established in the top part of the beaker, while a dispersion layer was visible in the bottom part, where a water layer gradually formed. The time of separation, given as a total average for all samples, was 64 *s*.

3.5. *Experimental campaign*

This paper will report the results of two completed experimental campaigns. The first was a study to identify the effect on separator performance from alternating the location of water extraction/tapping along the inclined extraction section. The second was aimed at mapping separator performance and investigate the effect different inlet configurations had on calculated efficiency. An additional part of the second campaign was mapping of occurring flow patterns at the MPPS inlet.

3.5.1. *Tapping location study*

The test matrix used for the tapping location study is given in Table 3. The given flow rate $\dot{Q}_{tot}$ is the total flow rate at the MPPS inlet ($\dot{Q}_1 + \dot{Q}_2$ from Table 2). $\dot{Q}_1$ and $\dot{Q}_2$ are adjusted to match the desired total flow and inlet WC. In addition, the corresponding mixture velocity (U_m) inside the parallel pipe sections is given, assumed an even flow split and zero interphase slip. This matrix was run for each of the three water tapping locations. The calculated separation efficiency was then compared to identify the preferred water extraction point. All tests in the tapping location study were performed with a normal inlet configuration.

In addition to efficiency calculations, pictures were taken in order to visualize and characterize the occurring flow phenomena in the extraction pipes.

The test procedure was as follows:

- Desired flow rate and WC was set at the separator inlet
- The rate through the water extraction outlet was adjusted to match the desired ER
- The system was allowed to reach steady state
- A 60 s sampling file was recorded
- Pictures of flow phenomena were taken at the tapping location
- Procedure repeated for next test point

By monitoring transients of measured variables, a period of five times the prevailing residence time in the separator prototype was found sufficient for reaching a steady state regime.

3.5.2. Performance mapping study

The goals of the performance mapping study were to quantify separator performance for several combinations of inlet rates, water cuts and extraction rates. Furthermore, the effect of the different inlet configurations were to be studied, and a mapping of the occurring flow patterns at the MPPS inlet was to be made.

Flow pattern mapping was achieved by visual inspection of the flow pattern directly upstream the MPPS inlet in the 67.8 mm ID multiphase transport line. Mapping was performed from 10 to 90% WC at 10% increments, and for total flow rates ranging from 250 to 700 L/min with 50 L/min steps. Six different flow patterns were identified, and they can be viewed in Fig. 5. Flow pattern identification was based on illustrations given by Trallero et al. (1997), with the addition of a seventh flow pattern (Dispersion of water in oil and oil).

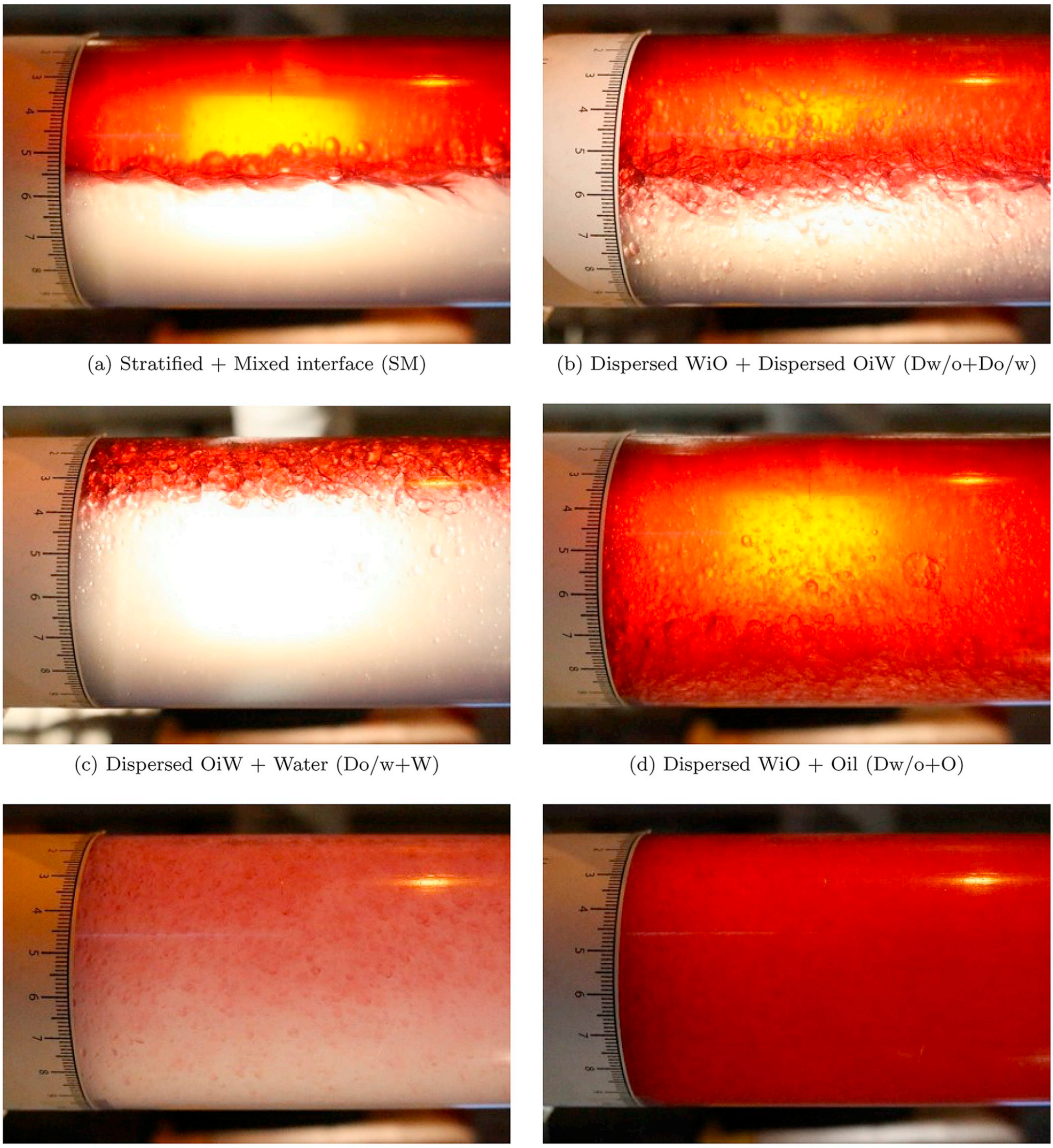

(a) Stratified + Mixed interface (SM)

(b) Dispersed WiO + Dispersed OiW (Dw/o+Do/w)

(c) Dispersed OiW + Water (Do/w+W)

(d) Dispersed WiO + Oil (Dw/o+O)

(e) Dispersed OiW (Do/w)

(f) Dispersed WiO (Dw/o)

Fig. 5. Identified flow patterns upstream the MPPS inlet.

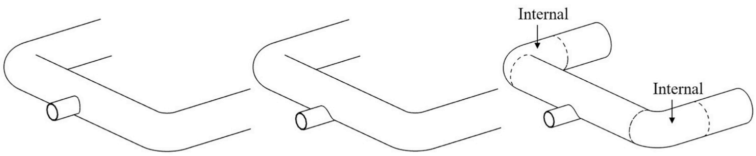

Fig. 6. Inlet configurations. From left to right: Normal, Tangential, Tangential w/internal.

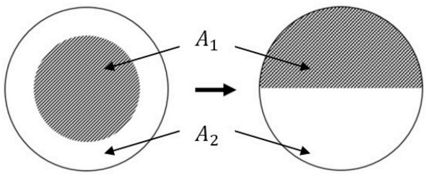

Fig. 7. Internal functionality.

Three inlet configurations have been tested in the performance mapping study, including a normal inlet configuration, a tangential inlet configuration, and a tangential inlet with installed novel internals. The different inlet configurations are illustrated in Fig. 6.

The novel internals were developed to boost the separation performance of the tangential inlet configuration. A Tangential inlet will create a swirl at the separator inlet, promoting oil and water to separate and arrange in a core and annular ring distribution. When the flow enters the horizontal pipe section, separation will be gravity driven, thus promoting a vertically segregated phase distribution. To avoid remixing of the phases, the internals redirects the flow from core-distributed to stratified upstream the descending inlet pipe elements. The internals are also acting as flow straighteners, so that the initially induced swirl does not negatively affect separation in the downstream horizontal pipe sections. The described functionality of the internals is illustrated in Fig. 7. For the current internal design, A_1 is equal to 70% of the pipe cross-section area, while A_2 is equal to 30%. This division was chosen so that internal functionality was ensured for water cuts as low as 30%. It is likely that the optimal area ratio will depend on the inlet WC, however, due to manufacturing and budgetary constraints, this has not been studied in the present work. The internals have a total length of 557 mm, and they are installed as illustrated in Fig. 6. The combination of the tangential inlet with internals, and subsequent separation in horizontal pipes is to secure good separation efficiency at both high and low flow rates.

The experimental matrix used for the performance mapping study is given in Table 4. This matrix was run for each respective inlet configuration. Tests were also run for 10% WC, however, due to significant measurement error arising at low water flow rates, these test points were excluded from the presented results. As for the tapping study campaign, the given flow rate $\dot{Q}_{tot}$ represents the total flow rate at the MPPS inlet, and the corresponding mixture velocity (U_m) is the mixture velocity inside the parallel pipe sections assumed an even flow split and zero interphase drag. The test procedure is the same as listed in Section 3.5.1. Pictures are however taken at the end of the horizontal section to characterize the phase split, instead of capturing the flow phenomena at the tapping location. The performance mapping study is performed with the tapping location displaying best performance from the initial tapping location study.

Table 4
Test matrix for performance mapping study.

$\dot{Q}_{tot}$ [L/min](Um [m/s])	WC_{in} [%]	ER [%]
300 *(0.14)*	30/50/70/90	50 70 90
350 *(0.16)*	30/50/70/90	50 70 90
400 *(0.19)*	30/50/70/90	50 70 90
450 *(0.21)*	30/50/70/90	50 70 90
500 *(0.23)*	30/50/70/90	50 70 90
550 *(0.26)*	30/50/70/90	50 70 90
600 *(0.28)*	30/50/70/90	50 70 90
650 *(0.30)*	30/50/70/90	50 70 90
700 *(0.33)*	30/50/70/90	50 70 90

Table 5
Contamination of inlet feed streams.

$\dot{Q}_{tot}$ [L/min]	Average feed stream WC [%]					
	Normal inlet		Tangential inlet		Tangential inlet /w internals	
	WC_1	WC_2	WC_1	WC_2	WC_1	WC_2
300	99.9	0.1	100.0	0.2	100.0	0.3
350	99.8	0.1	99.9	0.3	99.9	0.3
400	99.7	0.2	99.9	0.3	99.9	0.4
450	99.6	0.2	99.8	0.3	99.8	0.4
500	99.5	0.2	99.6	0.4	99.7	0.5
550	99.3	0.3	99.5	0.5	99.5	0.5
600	99.1	0.4	99.3	0.6	99.4	0.5
650	99.1	0.4	99.1	0.7	99.2	0.7
700	99.0	0.5	99.0	0.7	99.1	0.7

The purity of the feed streams were monitored and compared in order to quantify the comparability of the performance data for the respective inlet configurations. The average WC at the Water and ExxsolD60 feed streams for each total flow rate and inlet configuration are given in Table 5.

In (Skjefstad and Stanko, 2018), an uneven splitting phenomenon was reported for the normal inlet configuration. The uneven splitting phenomenon was related to the forming of a dispersion layer in the separator pipes, and how this layer over time migrated to one of the two separator prototype branches at low extraction rates. This phenomenon will be further investigated in the performance mapping study as part of phase split characterization, looking at how the uneven splitting phenomenon is affected by changing the inlet configurations.

4. Results

4.1. Tapping location study

Efficiency data for the tapping study is given in Figs. 8 and 9. The plots display separation efficiency vs. ER, at a given inlet WC for all three tapping locations. Presented results include data for total flow rates of 250 L/min and 500 L/min. Data for 750 L/min has been left out, but display the same trend as for 500 L/min.

In Fig. 8, data for $\dot{Q}_{tot}$ = 250 L/min at 70%, 50% and 30% WC are given.

For 70% WC, little effect of tapping location is observed. For high ER, a small decrease in efficiency for T3 occurs. T1 and T2 overlap within the indicated error range. For 50% WC, a more distinct influence of the tapping location is observed. Worst performance is observed for T3, which drops away from T1 and T2 at 70% ER. T1 and T2 is equal up to 90% ER, where T2 decreases slightly in performance. For 30% WC, the same trend as for 50% WC is observed. T3 has the worst performance, while T1 and T2 are equal at low to medium ER, but T1

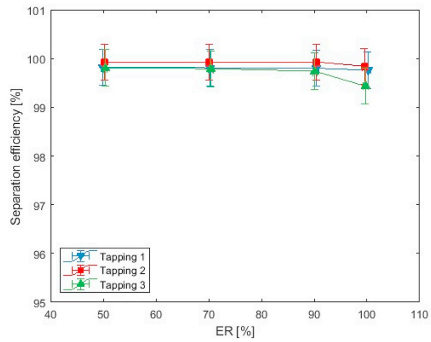

(a) Efficiency at $\dot{Q}_{tot} = 250\ L/min$, WC = 70%

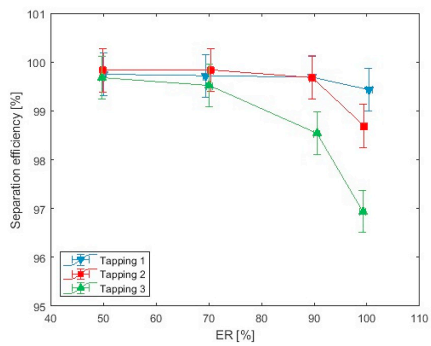

(b) Efficiency at $\dot{Q}_{tot} = 250\ L/min$, WC = 50%

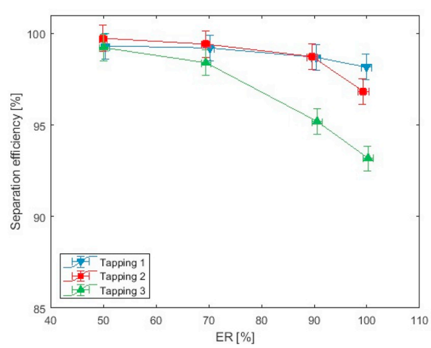

(c) Efficiency at $\dot{Q}_{tot} = 250\ L/min$, WC = 30%

Fig. 8. Efficiency at $\dot{Q}_{tot} = 250\ L/min$.

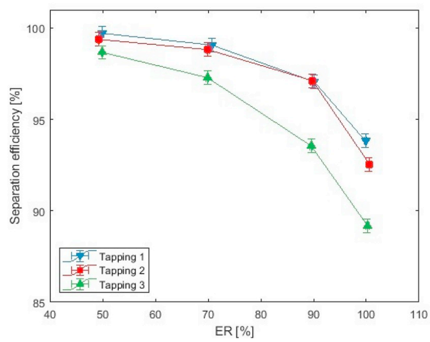

(a) Efficiency at $\dot{Q}_{tot} = 500\ L/min$, WC = 70%

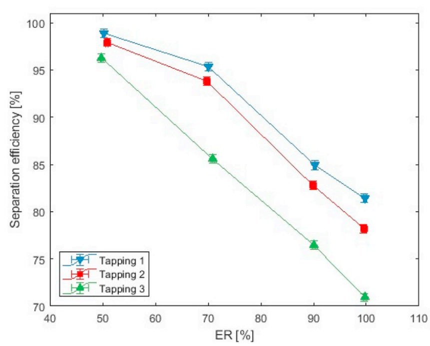

(b) Efficiency at $\dot{Q}_{tot} = 500\ L/min$, WC = 50%

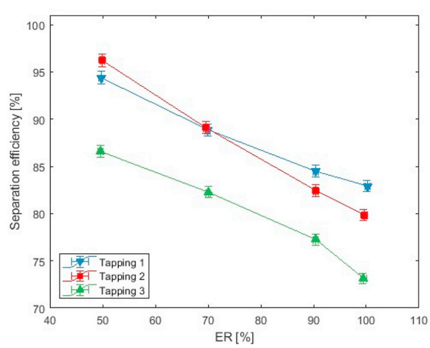

(c) Efficiency at $\dot{Q}_{tot} = 500\ L/min$, WC = 30%

Fig. 9. Efficiency at $\dot{Q}_{tot} = 500\ L/min$.

performs better at maximum extraction.

Data for the 500 L/min flow rate test points are given in Fig. 9.

For 70% WC, a similar trend as for the 250 L/min test points is observed. T1 and T2 are close to equal up to 90% ER, where T2 drops slightly in performance. T3 display worst performance for all ER. For 50% WC, T1 is observed to provide best results for all ER, followed by T2 then T3 (a significant drop in performance is observed for T3). At 30% WC it is again evident that T3 gives the worst performance. For low ER, T2 gives slightly better performance than T1, but for increasing ER, T1 again provides the best separation efficiency.

From presented results it is clear that utilizing T3 gives a significant drop in performance compared to T1 and T2. Between T1 and T2, T1 resulted in marginally better performance, especially for higher ER. From presented data it can be concluded that extraction of water should be performed close to the bottom of the inclined extraction section, as performance decreased by moving the tapping point further up the inclined outlet pipe.

The observed drop in performance at low WC and high ER is supported by observed flow phenomena in the inclined outlet pipe. In Fig. 10, one of the two inclined outlet pipes is displayed at the operating

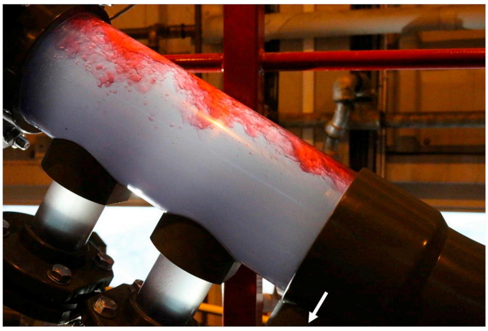

Fig. 10. Flow distribution near tapping point at $\dot{Q}_{tot} = 250\ L/min$, WC = 70%, ER = 90 %.

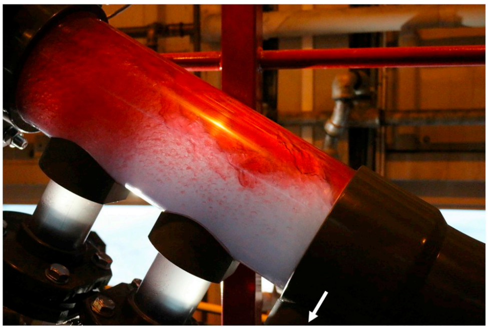

Fig. 11. Flow distribution near tapping point at $\dot{Q}_{tot} = 250\ L/min$, WC = 30%, ER = 90 %.

point $\dot{Q}_{tot} = 250\ L/min$, WC = 70%, ER = 90%. Tapping point one is being used in the figure, indicated by a white arrow.

It can be seen that the inclination of the outlet pipe induces a large water holdup. In addition, it is observed that the ExxsolD60 is not flowing in a stratified manner, but rather in intermittent slugs. This appears to cause re-entrainment of small ExxsolD60 droplets which can be seen along the inclined pipe section.

In Fig. 11, the flow phenomenon at the same operating point, but for WC = 30% is depicted. A large holdup of water is observed even though the inlet WC is only 30%. Close to the tapping point, a water height of close to 70% of the pipe diameter is observed. A water height of 70% corresponds to a hold up (area fraction) of 75%, which with an inlet water fraction of 30% leads to a slip factor of 7 between the water and ExxsolD60 flow velocities. This is believed to be the cause of the increased re-entrainment which is observed from Figs. 10 and 11. The increased re-entrainment along the inclined outlet pipe also explains the drop in performance observed for T2 and T3, which was most significant at lower WC.

4.2. Performance mapping

Results from the performance mapping study is presented in the following subsections. The first subsection reports the recorded flow pattern map directly upstream the MPPS inlet. This is representative for all three inlet configurations. The following sections report performance data for the respective inlet design options. Based on results from the tapping location study, T1 was used for all test points. Results include a full color plot performance matrix for the test range specified in Table 4, as well as pictures and discussion of occurring flow

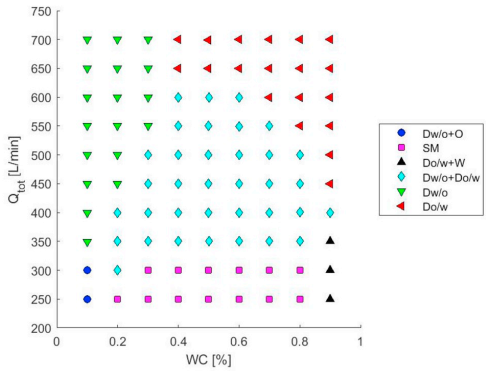

Fig. 12. Established flow pattern map upstream the MPPS inlet.

phenomena. All pictures presented in this section are taken at the end of the two horizontal pipe sections, directly upstream the inclined extraction pipes. To better illustrate the operational envelope of the separator prototype, contour lines have been added to the presented color plots. Contour lines for the efficiency plots have been set at 98%, and contour lines for the WC ratio plots at 99%. The operational envelope will be specified as the test points that fall within both contour lines.

4.2.1. Flow pattern map

The established flow pattern map is given in Fig. 12. The map reports occurring flow patterns directly upstream the MPPS inlet in the multiphase feed pipe. The map is given for total flow rate at the separator inlet vs. WC. The corresponding inlet (feed pipe) mixture velocities for the respective test points range from 1.15 m/s ($\dot{Q}_{tot} = 250\ L/min$) to 3.23 m/s ($\dot{Q}_{tot} = 700\ L/min$).

Observed flow patterns in the range $\dot{Q}_{tot} = 650$–$700\ L/min$ for water cuts ranging from 30 to 50% were difficult to distinguish from each other. The identified inversion point between oil in water dispersion (Do/w) and water in oil dispersion (Dw/o) was therefore based on reported bottle tests in Section 3.4.

4.2.2. Normal inlet

Color plots of separation efficiency and WC ratio for the normal inlet configuration are given in Fig. 13. Data is presented as a total flow rate vs. WC matrix, one for each extraction rate, representing all test points outlined in Table 4.

From given results it is evident that separation efficiency decreases at reduced WC and increased ER. The 30–50% WC range is observed to be the most challenging for operation, and both ER and flow rate must be reduced to maintain satisfactory performance in this operational range. Maximum separation efficiency is found in the high WC low total flow rate region, where several test points show 100%. Minimum separation efficiency is seen for $\dot{Q}_{tot} = 700\ L/min$, WC = 50%, ER = 50%, at 74.5%. Maximum error in efficiency is found at the operating point $\dot{Q}_{tot} = 300\ L/min$, WC = 30%, ER = 50%, being $\pm 0.71\ pp$. Minimum error is $\pm 0.35\ pp$, seen at $\dot{Q}_{tot} = 700\ L/min$, WC = 90%, ER = 90%. The error in WC ratio is steady around $\pm 0.35\ pp$ for all operating points. An operational envelope has been derived from added contour lines, and is given in Table 6. When determining the envelope, the cut off in terms of WC ratio is set at 99% $\pm 0.3\ pp$.

A dispersion layer is observed to appear in the horizontal pipes at $\dot{Q}_{tot} = 350\ L/min$, WC = 50%. Layer thickness increases with flow rate. The layer is observed in the WC range 30–90%, with highest volume fraction in the 30–50% WC range. For 30% and 70% WC, it first appears at $\dot{Q}_{tot} = 400\ L/min$, while it is delayed to $\dot{Q}_{tot} = 500\ L/min$ for 90% WC. Dispersion layer thickness for 90% WC is insignificant compared to the lower WC test points.

Journal of Petroleum Science and Engineering 176 (2019) 203–219

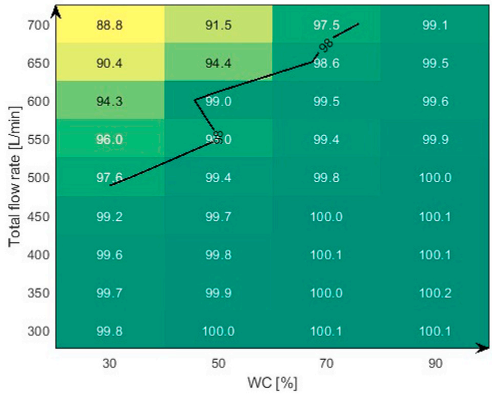

(a) Efficiency [%] at ER = 50%

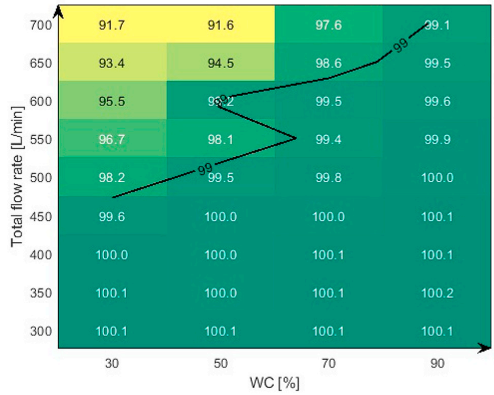

(b) WC ratio [%] at ER = 50%

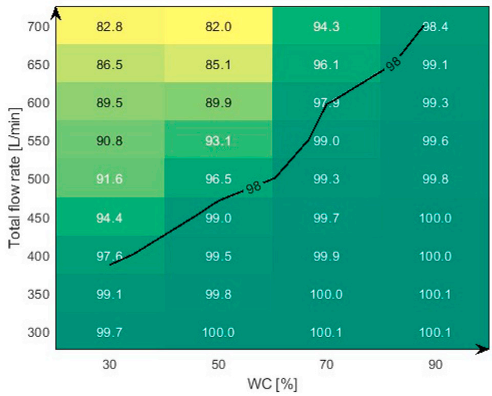

(c) Efficiency [%] at ER = 70%

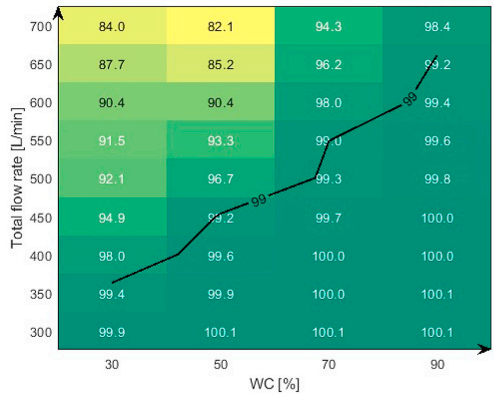

(d) WC ratio [%] at ER = 70%

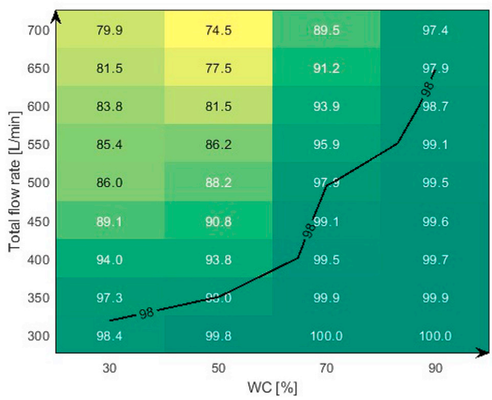

(e) Efficiency [%][%] at ER = 90%

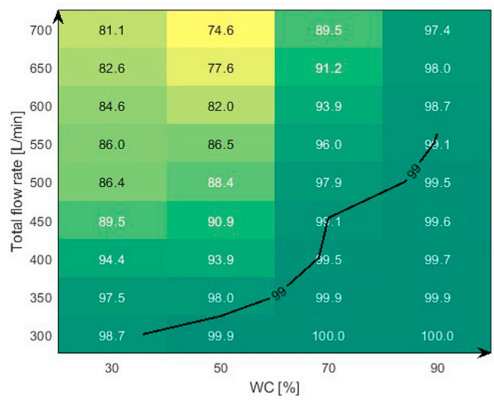

(f) WC ratio [%] at ER = 90%

Fig. 13. Efficiency and WC ratio results for the normal inlet configuration.

Table 6
Normal inlet operational envelope.

ER[%]	$\dot{Q}_{tot}$ [L/min](Um [m/s])			
	30% WC	50% WC	70% WC	90% WC
50	450*(0.21)*	500*(0.23)*	600*(0.28)*	700*(0.33)*
70	350*(0.16)*	450*(0.21)*	550*(0.26)*	650*(0.30)*
90	300*(0.14)*	300*(0.14)*	450*(0.21)*	600*(0.28)*

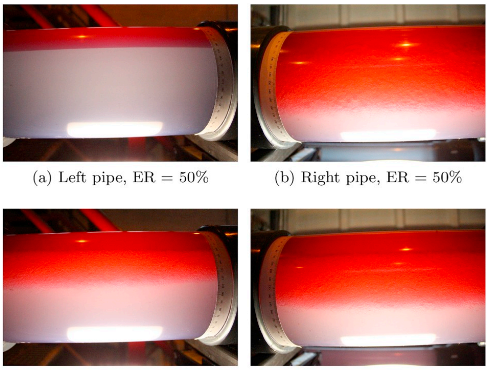

(a) Left pipe, ER = 50% (b) Right pipe, ER = 50%

(c) Left pipe, ER = 90% (d) Right pipe, ER = 90%

Fig. 14. Normal inlet flow phenomena at $\dot{Q}_{tot}$ = 450 L/min, WC = 50 %.

The discussed uneven splitting phenomenon is first observed at $\dot{Q}_{tot}$ = 400 L/min, WC = 50%/70%, ER = 50%. As mentioned in Section 3.5.2, the observed phenomenon occurs at low ER, where the formed dispersion layer migrates into one of the two parallel pipes leaving the other with pure ExxsolD60 and water phases. Increasing the ER promotes a more even split of the layer. The phenomenon is depicted in Fig. 14, displaying occurring phenomenon at $\dot{Q}_{tot}$ = 450 L/min, WC = 50% for 50% and 90% ER. The pipe in which the dispersion layer migrates seems to be random, and has been observed to take place in both pipes. The uneven splitting phenomenon is observed to occur in the flow range $\dot{Q}_{tot}$ = 400–550 L/min, for WC = 50–90%. No uneven splitting is observed at 30% WC. An even split of the dispersion layer is observed for all ER outside this flow range.

In Fig. 15 the established dispersion layers at the different water cuts (30, 50, 70 and 90%) are given. Pictures are for $\dot{Q}_{tot}$ = 500 L/min, ER = 50%. The same test points will be depicted for the tangential inlet configurations. The thick dispersion layers observed for 30% and 50% WC are believed to cause the drop in performance observed for this operational range.

4.2.3. *Tangential inlet*

Color plots of separation efficiency and WC ratio for the tangential inlet configuration are given in Fig. 16.

From given results it is again seen that separation efficiency decreases at reduced WC and increased ER. The 30–50% WC range is still observed to be the most challenging for operation, and both ER and flow rate must be reduced to maintain satisfactory performance in this operational area. As for the normal inlet case, the operational envelope of the separator was determined by setting a cut off for the WC ratio at 99% ±0.3 *pp*. Results are given in Table 7. By comparing Figs. 13 and 16 and Tables 6 and 7, it can be observed that the tangential inlet slightly increases the operational envelope of the separator. The errors in reported separation efficiency and WC ratio are the same as for the normal inlet configuration.

As in the case of the normal inlet configuration, a dispersion layer starts to appear at $\dot{Q}_{tot}$ = 350 L/min, WC = 50%. Layer thickening and

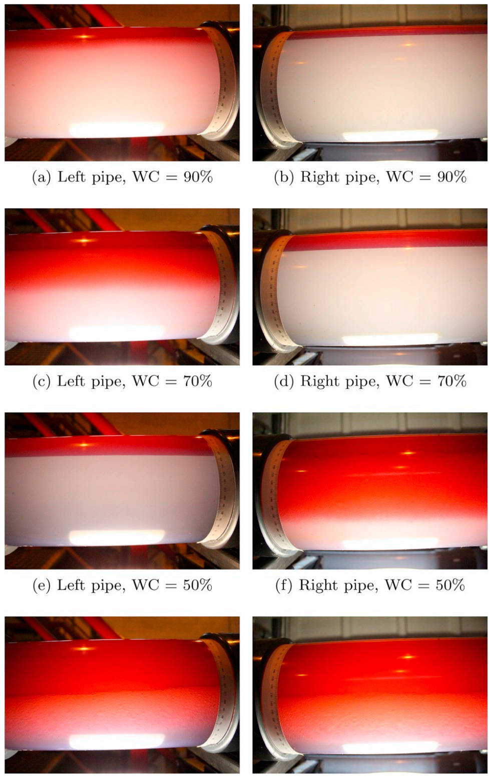

(a) Left pipe, WC = 90% (b) Right pipe, WC = 90%

(c) Left pipe, WC = 70% (d) Right pipe, WC = 70%

(e) Left pipe, WC = 50% (f) Right pipe, WC = 50%

(g) Left pipe, WC = 30% (h) Right pipe, WC = 30%

Fig. 15. Dispersion layer formation and splitting with normal inlet at $\dot{Q}_{tot}$ = 500 L/min, ER = 50 %.

formation at respective WC is equal to reported findings from the normal inlet case. For a normal inlet, the reported uneven splitting phenomenon was observed for a limited range of WC and flow rates. With a tangential inlet, migration of the dispersion layer at low ER is observed for all test points where a dispersion layer has formed. Again, increasing the ER promotes a more even split of the layer, but a distinct uneven split is however still visible for the tangential inlet case. The phenomenon is depicted in Fig. 17, displaying occurring phenomenon at $\dot{Q}_{tot}$ = 450 L/min, WC = 50% for 50% and 90% ER. Again, the pipe in which the dispersion layer migrates seems to be random.

In Fig. 18, the established dispersion layers at respective WC are given. Pictures are restricted to $\dot{Q}_{tot}$ = 500 L/min, ER = 50%. Comparing to Fig. 15, a slight reduction in dispersion layer thickness is observed. This can be a contributing factor to the increased operational envelope seen for the tangential inlet case. In addition, the occurring splitting at 30% WC can be a contributing factor to the decreased performance observed for 30% WC at 90% ER.

4.2.4. *Tangential inlet with internals*

Color plots of separation efficiency and WC ratio for the tangential inlet with internals configuration are given in Fig. 19.

The same trend in separation efficiency as for the normal and tangential inlet configurations is observed. The operational envelope for the tangential inlet w/internals has been derived in the same way as for the two previous cases, and is given in Table 8. Comparing Fig. 19 to 13 and 16, and Table 8 to Tables 6 and 7, it can be observed that a

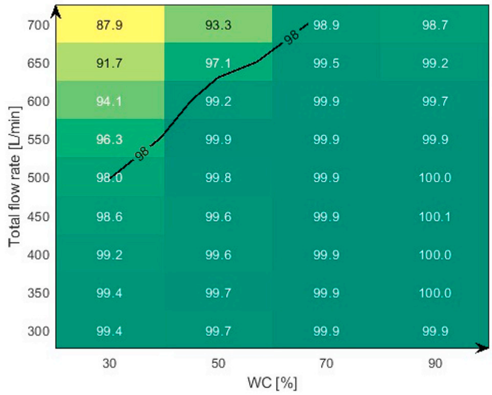

(a) Efficiency [%] at ER = 50%

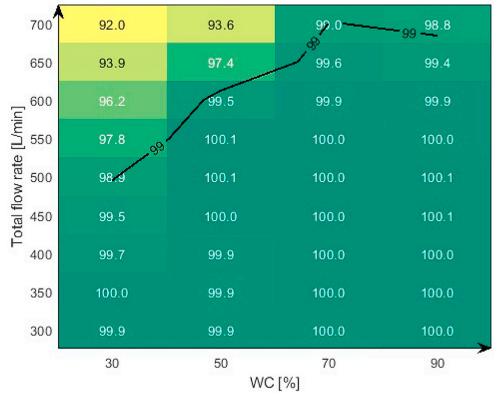

(b) WC ratio [%] at ER = 50%

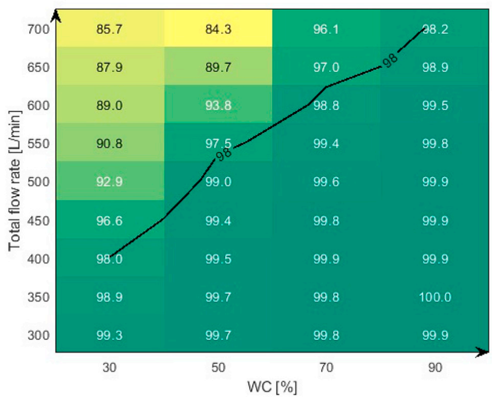

(c) Efficiency [%] at ER = 70%

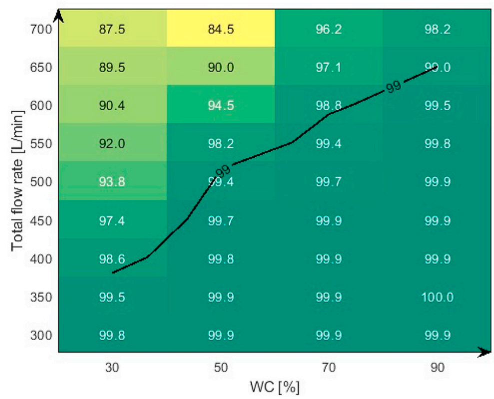

(d) WC ratio [%] at ER = 70%

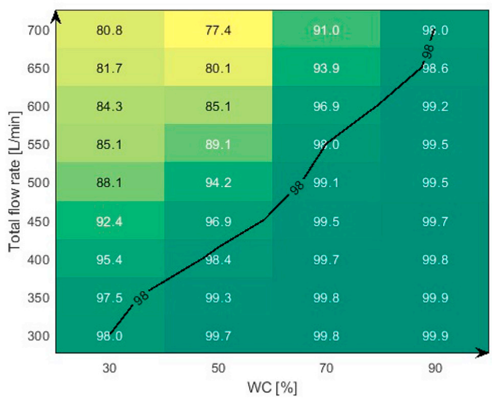

(e) Efficiency [%] at ER = 90%

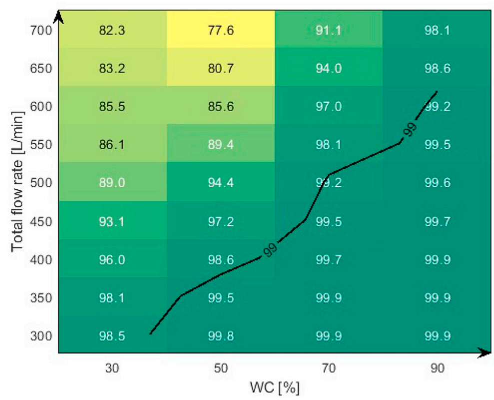

(f) WC ratio [%] at ER = 90%

Fig. 16. Efficiency and WC ratio results for the tangential inlet configuration.

Table 7
Tangential inlet operational envelope.

ER[%]	$\dot{Q}_{tot}$ [L/min](Um [m/s])			
	30%*WC*	50%WC	70%WC	90%WC
50	500*(0.23)*	600*(0.28)*	700*(0.33)*	700*(0.33)*
70	350*(0.16)*	500*(0.23)*	600*(0.28)*	650*(0.30)*
90	<300*(0.14)*	350*(0.16)*	500*(0.23)*	600*(0.28)*

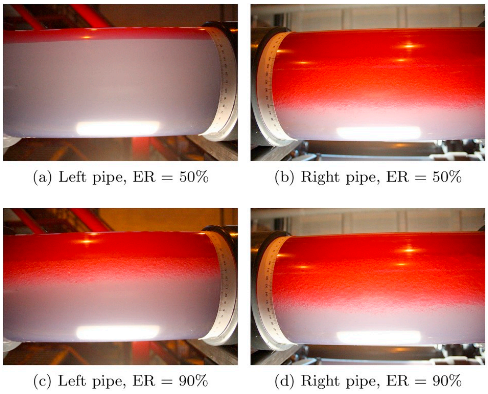

(a) Left pipe, ER = 50% (b) Right pipe, ER = 50%
(c) Left pipe, ER = 90% (d) Right pipe, ER = 90%

Fig. 17. Tangential inlet flow phenomena at $\dot{Q}_{tot}$ = 450 L/min, WC = 50 %.

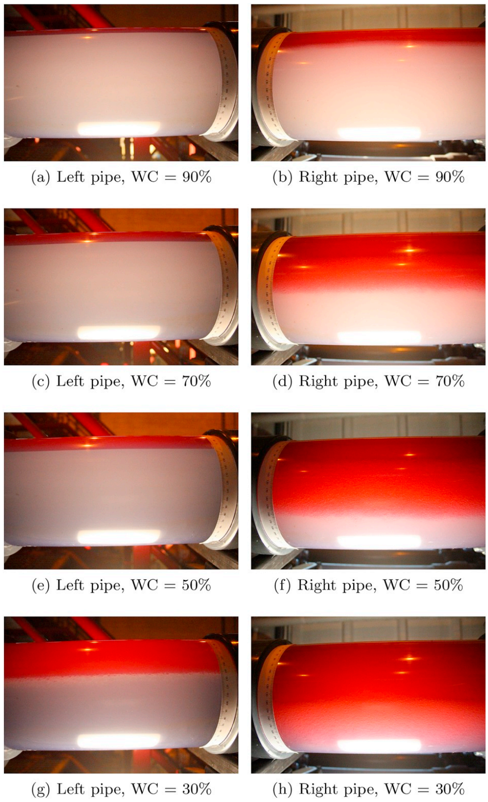

(a) Left pipe, WC = 90% (b) Right pipe, WC = 90%
(c) Left pipe, WC = 70% (d) Right pipe, WC = 70%
(e) Left pipe, WC = 50% (f) Right pipe, WC = 50%
(g) Left pipe, WC = 30% (h) Right pipe, WC = 30%

Fig. 18. Dispersion layer formation and splitting with tangential inlet at $\dot{Q}_{tot}$ = 500 L/min, ER = 50 %.

tangential inlet/w internals allows the largest operational envelope of the tested configurations. The error is the same as for the normal inlet configuration.

Dispersion layer appearance is observed at $\dot{Q}_{tot}$ = 400 L/min, WC = 50%, slightly higher than for the two previous inlet configurations ($\dot{Q}_{tot}$ = 350 L/min). In the WC range 30–70%, layer thickening and formation is equal to reported findings from the normal/tangential inlet cases. For 90% WC there is no observation of the dispersion layer. The reported uneven splitting phenomenon occurring for the normal and tangential inlet configurations is not observed when internals are installed. The dispersion layer is equally split between both pipes for all test points, including low and high ER. This is shown in Fig. 20, displaying pictures of the oil-water distribution at $\dot{Q}_{tot}$ = 450 L/min, WC = 50% for 50% and 90% ER.

In Fig. 21, the established dispersion layers at respective WC for the tangential inlet configuration/w internals are given. Pictures are restricted to $\dot{Q}_{tot}$ = 500 L/min, ER = 50%. Comparing Figs. 21 to 15 and 18, it is clear that the added internals results in a reduced dispersion layer thickness. It is again evident that there is a correlation between dispersion layer thickness and separation efficiency.

4.3. Discussion

Results from the tapping location study indicated T1 as the preferred extraction point for the Water. This was seen in connection with re-entrainment of ExxsolD60 droplets along the inclined extraction pipe. The inclination of the extraction pipe causes an increase in the Water holdup, which again causes a significant slip between the Water and ExxsolD60 phase velocities. This slip is believed to be a contributing factor to the observed re-entrainment. The current angle of inclination of the extraction pipes is 30°. This was based on experiments run by Rivera et al. (2006), where the separation of oil and water in an inclined pipe was tested. Further optimization of the extraction pipe inclination is relevant for future work. A reduced inclination will lead to lower water holdup, but also reduced slip. Finding a good trade-off between water holdup and low oil re-entrainment is relevant for the studied MPPS separator design.

Presented performance mapping results indicate that the operational envelope is negatively affected by formation of a dispersion layer in the horizontal pipe sections of the separator. The observed dispersion layer starts to form at total flow rates in the range $\dot{Q}_{tot}$ = 350–400 L/min for a WC equal to 50%. Dispersion layer formation is most severe in WC range 30–50%, which corresponds with the region of lowest separator performance. This belief is further strengthened as the operational range is observed to increase as the dispersion layer thickness is reduced when moving from a normal to a tangential inlet.

The observed increase in performance when moving from a normal inlet to a tangential inlet with internals is illustrated in Figs. 22–24. The graphs report the average WC ratio over all flow rates at respective water cuts for the three different inlet configurations. Fig. 22 displays the results for 50% ER, Fig. 23 for 70% ER and Fig. 24 for 90% ER.

For 50% ER, the three inlet designs perform evenly. The maximum difference in performance at 50% ER is observed for the normal and tangential/w internal inlets at 50% WC, being 1.2 *pp*. For 70% and 90% WC, there is no noticeable difference. When increasing the ER, the differences become more apparent. In Fig. 23 both the tangential inlet (T) and tangential inlet/w internals (I) are seen to outperform the normal inlet (N) in the 30–50% WC range. A further increase to 90%

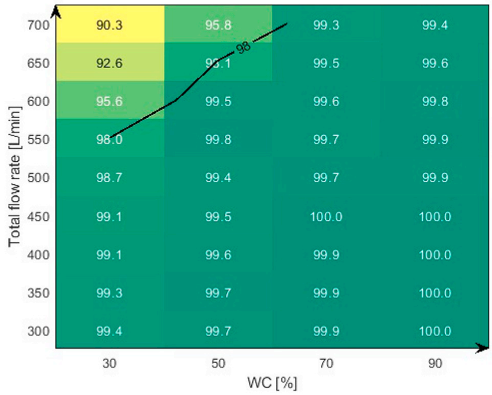

(a) Efficiency [%] at ER = 50%

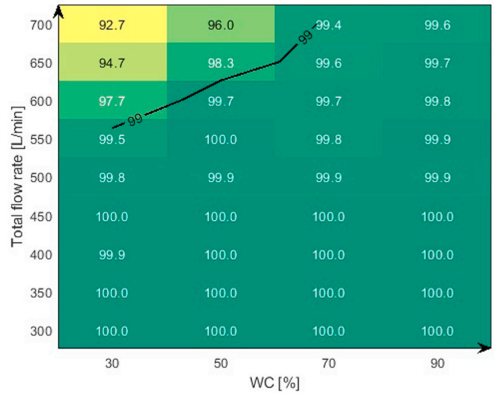

(b) WC ratio [%] at ER = 50%

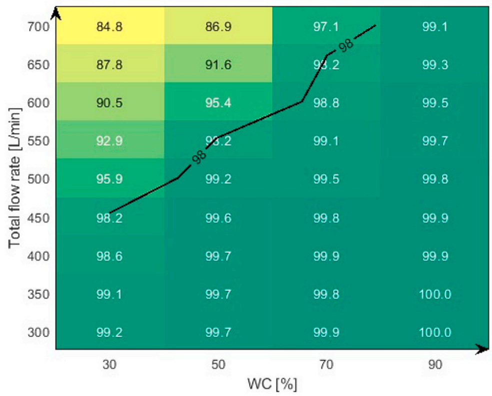

(c) Efficiency [%] at ER = 70%

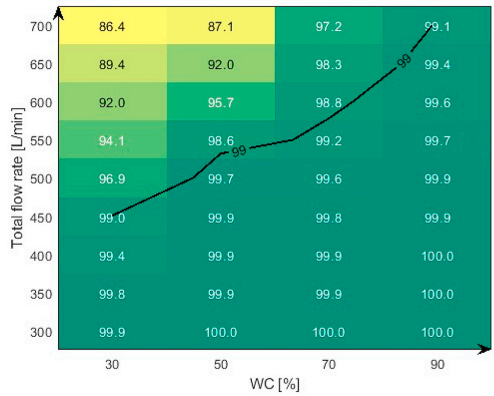

(d) WC ratio [%] at ER = 70%

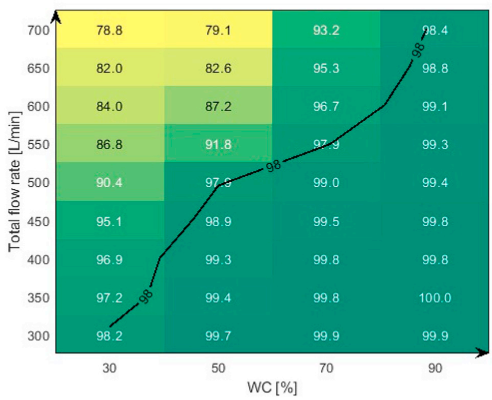

(e) Efficiency [%] at ER = 90%

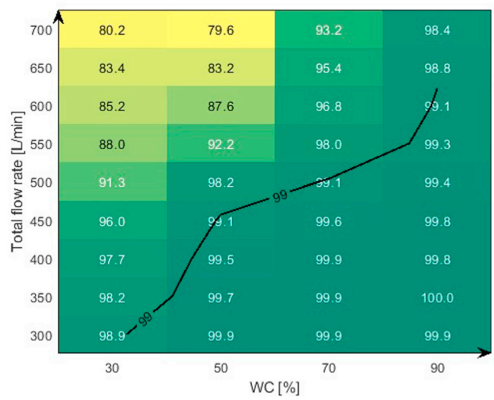

(f) WC ratio [%] at ER = 90%

Fig. 19. Efficiency and WC ratio results for the tangential inlet w/ internals inlet configuration.

Table 8
Tangential inlet w/internal operational envelope.

$ER\,[\%]$	$\dot{Q}_{tot}\,[L/min]$(Um [m/s])			
	30% WC	50% WC	70% WC	90% WC
50	550*(0.26)*	600*(0.28)*	700*(0.33)*	700*(0.33)*
70	450*(0.21)*	500*(0.23)*	600*(0.28)*	700*(0.33)*
90	300*(0.14)*	450*(0.21)*	500*(0.23)*	650*(0.30)*

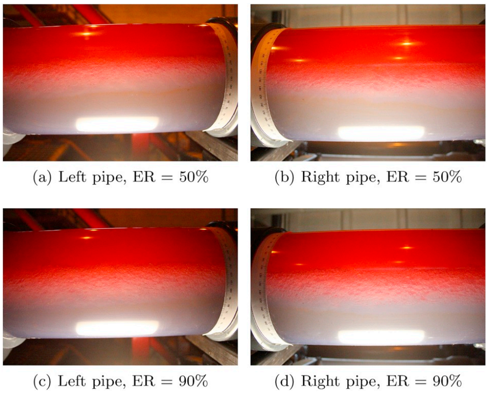

(a) Left pipe, ER = 50% (b) Right pipe, ER = 50%
(c) Left pipe, ER = 90% (d) Right pipe, ER = 90%

Fig. 20. Tangential inlet/w internals flow phenomena at $\dot{Q}_{tot}$ = 450 L/min, WC = 50 %.

extraction enhances this difference even more, also becoming noticeable at 70% WC. For 90% ER, the largest difference in WC ratio between the three inlet configurations is observed at 50% WC, being 88% (N), 91.4% (T) and 93.2% (I). The largest difference in performance between the three inlet configurations is observed in the operational range corresponding with highest degree of dispersion layer formation. This again indicates that the gain in performance seen from having a tangential inlet is mostly connected to reduced dispersion layer formation in the 30% to 50% WC region. The further increase in performance achieved from the developed internals have several explanations.

- Mitigation of the uneven splitting phenomenon, resulting in an evenly split phase distribution, with a clearly defined water layer at the bottom of both horizontal pipes
- A more efficient transition from a core distributed to a stratified phase division, avoiding remixing of phases downstream the separator inlet.
- Mitigation of the inlet swirl, avoiding remixing of phases downstream the separator inlet
- Increased coalescence of dispersed phase droplets in flow straightening chambers
- Reduced dispersion layer formation

The underlying cause of the observed uneven splitting phenomenon, and the associated randomness of its formation is as of date not clear to the authors. However, the seeming randomness of migration indicates the cause of the phenomenon to originate from fluid mechanic properties rather than mechanical properties of the prototype. A better understanding of the underlying cause of formation, and control of

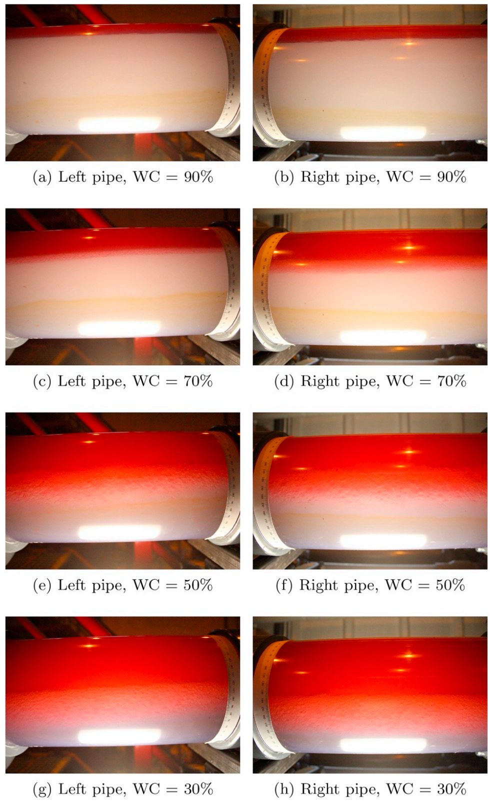

(a) Left pipe, WC = 90% (b) Right pipe, WC = 90%
(c) Left pipe, WC = 70% (d) Right pipe, WC = 70%
(e) Left pipe, WC = 50% (f) Right pipe, WC = 50%
(g) Left pipe, WC = 30% (h) Right pipe, WC = 30%

Fig. 21. Dispersion layer formation and splitting with tangential inlet w/internal at $\dot{Q}_{tot}$ = 500 L/min, ER = 50 %.

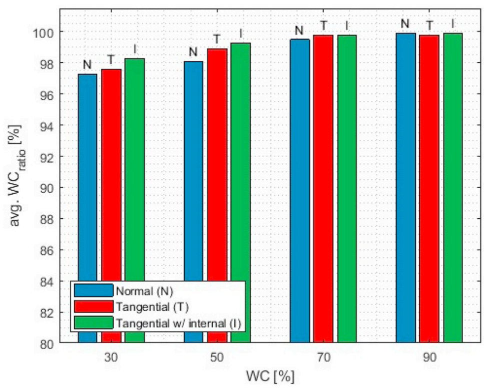

Fig. 22. Average WC_{ratio} for the different inlet configurations at respective water cuts for ER = 50 %.

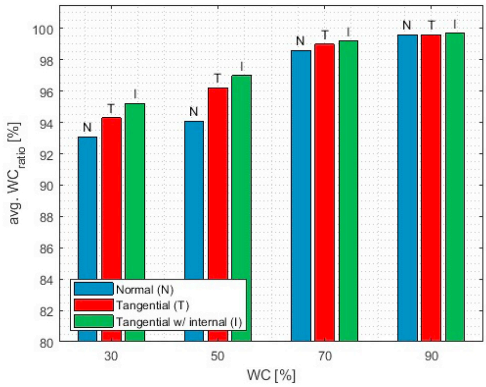

Fig. 23. Average WC_{ratio} for the different inlet configurations at respective water cuts for ER = 70 %.

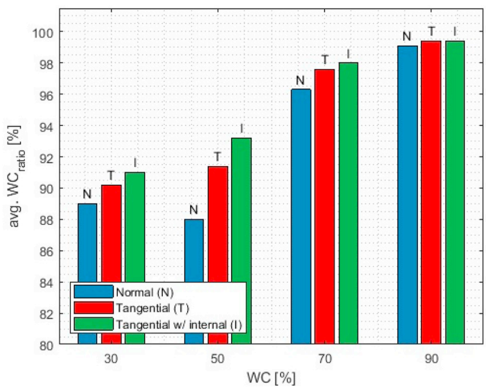

Fig. 24. Average WC_{ratio} for the different inlet configurations at respective water cuts for ER = 90 %.

where the dispersion layer migrates, opens up for several interesting possibilities in enhancing the performance of the proposed oil-water separator. The forming dispersion layer can be routed to a specific pipe for targeted intervention/breakage, while the remaining pipes are filled with clear oil and water phases.

On the other hand, installation of developed internals mitigated the observed uneven splitting phenomenon. Again, the cause of mitigation is unclear to the authors. A possible explanation for the absent migration of dispersion is that the internals add an additional pressure drop to the system. Further improvement of internal design is expected to yield even better performance results. The main point of improvement is adjusting the angle of internal flow straightening elements to allow a less turbulent transition from a swirling fluid motion to stratified flow. Current blades are straight, resulting in a large angle of attack between the blades and incoming flow. Blade angles should be adjusted to match design flow capacity. Minimizing turbulence in the internals can further reduce the amount of dispersion formed at the separator inlet, boosting separator performance.

Table 9
Up-scaled operational envelope for a two-pipe system.

$D\,[mm]$	$\dot{Q}_{tot}\,[L/min]$([bbl/day])			
	30%WC	50%WC	70%WC	90%WC
150	550 *(4982)*	600 *(5435)*	600 *(5435)*	650 *(5887)*
300	1100 *(9964)*	1200 *(10870)*	1200 *(10870)*	1300 *(11774)*
450	1650 *(14946)*	1800 *(16305)*	1800 *(16305)*	1950 *(17661)*

4.4. Up-scaling

Presented performance data are from a 150.6 mm ID dual pipe prototype. In a real system, the dimensions of the MPPS would be scaled-up. Up-scaling of results is therefore necessary in order to get an idea of expected performance in real field applications. The MPPS is designed to be a compact separator solution, and the prototype has been constructed to envisioned full-scale length. Up-scaling estimations will therefore be limited to diameter increase.

Estimated up-scaled performance will be based on simplified Stoke's law settling velocity calculations. It will be assumed that the WC in the pipes and slip between phases remain constant.

The required residence time in the separator can be calculated by an estimated droplet settling/creaming velocity (u), and the required settling/creaming length (h), as given in Eq. (8).

$$t_{res} = h/u \tag{8}$$

This can be used to estimate a required separator pipe length (L).

$$L = t_{res}\dot{Q}_{tot}/A = t_{res}U_m \tag{9}$$

Where $\dot{Q}_{tot}$ is the total volumetric flow rate, A is the total pipe cross sectional area and U_m is the mixture velocity in the separator.

An assumed up-scaled pipe diameter of factor f ($D \to fD$) will affect t_{res} and A in the following manner:

$$t_{res} = h/u, \quad D \to f\,D \to t_{res} = f\,h/u \tag{10}$$

$$A = \pi D^2/4, \quad D \to f\,D \to A = \pi f^2 D^2/4 \tag{11}$$

An up-scaled volumetric flow rate can then be derived from Eq. (9).

$$\dot{Q}_{tot} = \frac{LA}{t_{res}}, \quad D \to f\,D \to \dot{Q}_{tot} = \frac{f\,LA}{t_{res}} \tag{12}$$

It can thus be expected that an increase in diameter with a given factor will allow an increase in the flow rate by the same factor. This can be seen as a conservative estimate, as the respective superficial velocities will be reduced, allowing more favourable flow conditions. This is shown in Eq. (13) for the superficial water velocity (U_{sw}) as a function of the water flow rate ($\dot{Q}_w$) and the total water area in the separator pipes (A_w). Again, the assumptions are that the WC, holdup and slip remains constant when scaling up.

$$U_{sw} = \frac{\dot{Q}_w}{A_w}, \quad D \to f\,D \to U_{sw} = \frac{f\dot{Q}_w}{f^2 A_w} = \frac{\dot{Q}_w}{fA_w} \tag{13}$$

An up-scaled operational envelope is given in Table 9, where flow rates are presented in the unit of experimental testing (L/min) and in production units (bbl/day). Data is based on the reported operational envelope in Table 8. The ER is set to 90% for 90% WC, 70% for 70% WC and 50% for 50% and 30% WC.

Comparing these production rates to real field applications can give an idea of the total size of a potential MPPS installation. Reported liquid capacity of the Marlim pipe separator is 22500 bbl/day, and it was designed for a minimum inlet WC of 70% (de Oliveira et al., 2013). Based on up-scaled capacity estimates in Table 9, a similar capacity can be achieved by utilizing four 300 mm ID pipes in parallel. A larger installation, the Troll Pilot, has a reported liquid capacity of 63000 bbl/day (Davies et al., 2010). Again, by looking to Table 9, estimates show that an 8 pipe system of 450 mm ID pipes can give a total liquid capacity of 65220 bbl/day.

The authors want to emphasise that the performance data collected in this paper are based on experiments with model oil and water. Performance with real crude oil will deviate from reported data. In addition, up-scaled performance data are based on simplified estimates, and have not been verified with experimental testing.

5. Conclusion

5.1. Tapping location study

Presented results indicate that oil droplets are re-entrained into the established water layer when moving up the inclined extraction section of the separator. Water should therefore be extracted close to the horizontal alignment of the pipe.

5.2. Performance mapping study

The following conclusions can be drawn from presented results:

- Separator performance drops with decreased inlet WC and increased extraction rates
- The WC range 30–50% is observed to be most challenging in terms of maintaining good separation efficiency, exhibiting efficiencies in the range 75–100%
- Drop in performance in the 30–50% WC range is believed to be connected to the presence of a dispersion layer in the separator pipes. First observation of the layer is at total flow rates in the range 350–400 L/min (U_m = 0.16–0.19 m/s)
- An uneven splitting phenomenon is observed at low extraction rates where the established dispersion layer migrates fully into one branch of the separator
- Changing the inlet from a normal to a tangential configuration improves separator performance, especially in the 30–50% WC range. In this range, at 90% ER, the average increase in WC_{ratio} is 2.3 pp. Improvement of separator performance is seen in connection with a reduction in the forming dispersion layer
- A tangential inlet promotes a stronger uneven splitting of the forming dispersion layer
- Installation of phase re-arranging internals further improves the performance of the separator. Maximum improvement is seen at 50% WC, 90% ER, where the average WC ratio increased with 5.2 pp when moving from a normal inlet to a tangential inlet with internals
- Installation of the phase re-arranging internals additionally reduce thickness of the forming dispersion layers. The internals are also observed to eliminate the uneven splitting of the dispersion layer for the cases studied

Acknowledgements

This work was carried out as a part of SUBPRO, a Research-based Innovation Centre within Subsea Production and Processing. The authors gratefully acknowledge the financial support from SUBPRO, which is financed by The Research Council of Norway, major industry partners and NTNU, and the Department of Geoscience and Petroleum. The authors would also like to thank senior engineers Noralf Vedvik and Steffen Wærnes Moen for valuable help and input during construction of the presented test facility. Finally, the authors acknowledge the contribution of Ellen Kristine Ellertsen in the development of the presented inlet flow pattern map.

References

Capela Moraes, C.A., da Silva, F.S., Marins, L.P.M., Monteiro, A.S., de Oliveira, D.A., Pereira, R.M., Pereira, R. d. S., Alves, A., Raposo, G.M., Orlowski, R., et al., 2012. Marlim 3 phase subsea separation system: subsea process design and technology qualification program. In: Offshore Technology Conference. Offshore Technology Conference.

da Silva, F.S., Monteiro, A.S., de Oliveira, D.A., Capela Moraes, C.A., Marins, P.M., et al., 2013. Subsea versus topside processing-conventional and new technologies. In: OTC Brasil, Offshore Technology Conference.

Davies, S.R., Bakke, W., Ramberg, R.M., Jensen, R.O., et al., 2010. Experience to date and future opportunities for subsea processing in statoilhydro. In: Offshore Technology Conference. Offshore Technology Conference.

de Oliveira, D.A., Pereira, R. d. S., Capela Moraes, C.A., Baracho, V.P., de Souza, R.d.S.A., Euphemio, M.L.L., da Silva, F.S., Monteiro, A.S., Casanova, C.C., Duarte, D.G., et al., 2013. Comissioning and startup of subsea marlim oil and water separation system. In: OTC Brasil, Offshore Technology Conference.

Fakhrul-Razi, A., Pendashteh, A., Abdullah, L.C., Biak, D.R.A., Madaeni, S.S., Abidin, Z.Z., 2009. Review of technologies for oil and gas produced water treatment. J. Hazard Mater. 170 (2–3), 530–551.

Horn, T., Bakke, W., Eriksen, G., et al., 2003. Experience in operating world's first subsea separation and water injection station at troll oil field in the north sea. In: Offshore Technology Conference. Offshore Technology Conference.

S. Kline, F. McClintock, Describing Uncertainties in Single Sample Experiments, Mechanical Engineering.

NOROG, 2017. Environmental Report - Environmental Work by the Oil and Gas Industry, Facts and Development Trends. Tech. rep.. NOROG 2017.

Orlowski, R., Euphemio, M.L.L., Euphemio, M.L., Andrade, C.A., Guedes, F., Tosta da Silva, L.C., Pestana, R.G., de Cerqueira, G., Lourenço, I., Pivari, A., et al., 2012. Marlim 3 phase subsea separation system-challenges and solutions for the subsea separation station to cope with process requirements. In: Offshore Technology Conference. Offshore Technology Conference.

Rivera, R.M., Golan, M., Friedemann, J.D., Bourgeois, B., et al., 2006. Water separation from wellstream in inclined separation tube with distributed tapping. In: SPE Annual Technical Conference and Exhibition. Society of Petroleum Engineers.

Shaiek, S., Grandjean, L., et al., 2015. Spoolsep for subsea produced water separation-experimental results. In: Offshore Technology Conference, Offshore Technology Conference.

Skjefstad, H.S., Stanko, M., 2018. An experimental study of a novel parallel pipe separator design for subsea oil-water bulk separation. In: SPE Asia Pacific Oil and Gas Conference and Exhibition. Society of Petroleum Engineers.

Trallero, J., Sarica, C., Brill, J., et al., 1997. A study of oil-water flow patterns in horizontal pipes. SPE Prod. Facil. 12 (03), 165–172.

Zeng, Q., Wang, Z., Wang, X., Zhao, Y., Guo, X., 2016. A novel oil–water separator design and its performance prediction. J. Petrol. Sci. Eng. 145, 83–94.

Chapter 6

Separator control strategy, Paper IV

This chapter consists of Paper IV, which presents developed control strategies for the designed separator concept. The paper investigates two approaches for controlling the quality of extracted water, being direct control of the extracted water WC, or control of the level of water in the ascending extraction pipe. Two different control methods are tested and compared by running a set separator inlet sequence. This article is the result of collaboration work with PhD student Sveinung Johan Ohrem, and the author contribution is listed in Chapter 1.

S. J. Ohrem, H. S. Skjefstad, M. Stanko, and C. Holden. Controller design and control structure analysis for a novel oil-water multi-pipe separator. *Processes*, 7(4):190, 2019.

processes

MDPI

Article

Controller Design and Control Structure Analysis for a Novel Oil–Water Multi-Pipe Separator

Sveinung Johan Ohrem [1,*,†], Håvard Slettahjell Skjefstad [2], Milan Stanko [2] and Christian Holden [1]

1 Department of Mechanical and Industrial Engineering, Faculty of Engineering, NTNU Norwegian University of Science and Technology, 7491 Trondheim, Norway; christian.holden@ntnu.no
2 Department of Geoscience and Petroleum, Faculty of Engineering, NTNU Norwegian University of Science and Technology, 7491 Trondheim, Norway; havard.s.skjefstad@ntnu.no (H.S.S.); milan.stanko@ntnu.no (M.S.)
* Correspondence: sveinung.j.ohrem@ntnu.no
† Current address: Institutt for Maskinteknikk og Produksjon, NTNU, 7491 Trondheim, Norway.

Received: 8 March 2019; Accepted: 28 March 2019; Published: 2 April 2019

check for updates

Abstract: To enable more efficient production of hydrocarbons on the seabed in waters where traditional separator equipment is infeasible, the offshore oil and gas industry is leaning towards more compact separation equipment. A novel multi-pipe separator concept, designed to meet the challenges of subsea separation, has been developed at the Department of Geoscience and Petroleum at the Norwegian University of Science and Technology. In this initial study, a control structure analysis for the novel separator concept, based on step-response experiments, is presented. Proportional-integral controllers and model reference adaptive controllers are designed for the different control loops. The proportional-integral controllers are tuned based on the well-established simple internal model control tuning rules. Both control methods are implemented and tested on a prototype of the separator concept. Different measurements are controlled, and results show that the performance of the separator under varying inlet conditions can be improved with proper selection of control inputs and measurements.

Keywords: process control; separation; oil and gas

1. Introduction

In mature oil fields on the Norwegian Continental Shelf, the amount of water extracted in 2016 accounted for more than twice the amount of produced oil [1]. This produced water is transported topside for separation and cleaning. Eventually, the water treatment capacity of the topside facilities will be reached which causes a bottleneck in the production and leaves a substantial part of the hydrocarbon processing capacity left unused. Furthermore, a high amount of water in the well stream will cause a loss of pressure in the transportation pipelines, leading to a lower production. Removing the water on the seabed frees up capacity at the topside facility, which can be utilized for new tie-ins to existing fields.

In offshore oil and gas production, the processing of oil and gas on the seabed is also considered an enabler for more efficient liquid boosting, longer range gas compression from subsea to onshore, cost efficient hydrate management, more efficient riser slug depression, and access to challenging field developments [2].

Large vessels, referred to as gravity separators, are commonly used offshore for separation of oil, water and gas. These separators are robust and have a high performance, but they are not suited for use at ultra deep waters ($\geq$3000 m) due to the required size, which makes the installation and maintenance economically challenging [2]. Detailed descriptions on modelling and control of gravity separators can be found in [3,4].

A novel separator concept not relying on vessels, but rather on separation in multiple pipes (Figure 1), was recently developed [5]. This separator has been dubbed the MPPS, the Multiple Parallel Pipe Separator. The reduced diameter of the pipes compared to that of vessels makes the pipe separator better suited for installation at deeper waters. A prototype of the separator has been built at the Department of Geoscience and Petroleum at the Norwegian University of Science and Technology and the steady-state performance has been evaluated [6].

Currently, the separator laboratory does not have a control system and all valves are opened and closed manually via a LabView human–machine interface. Automatic control of key variables in the separator is important, as it helps counteract the effects of external disturbances, enables tracking of setpoints, enables optimal operation, and ensures that safety requirements are met.

The separator is equipped with several sensors providing measurements that may serve as controlled variables (CVs). Two valves are used as inputs, or manipulated variables (MVs). It is not straightforward to select a CV, as some variables may be more difficult to control and more sensitive to disturbances. This issue is addressed in Section 2.5 of this paper. Furthermore, some variables may be difficult or impossible to control directly, and, hence, finding a secondary variable that is easier to control and has an effect on the primary control variable can be very helpful.

In [7], a control design study was performed for a complete subsea separation system including a pipe separator. The liquid level in the pipe separator was chosen as the CV, and Proportional-Integral-Derivative (PID) controllers were used in all control loops. The authors state that controlling the system is challenging due to strong interactions between process components, constraints in valve openings and opening/closing speed of the valves. The study does not go into detail about the tuning of the controllers, nor is a control structure analysis presented.

The same is true for the work presented in [8]. Here, PID controllers, tuned by trial and error, was used to achieve the desired performance. The level of the oil/water interface in the pipe separator was controlled. The authors also stated that a control system should be able to adapt to varying operating conditions.

Other previous control-related work on pipe separators [9–11] do not go into detail on the selected control structure or control algorithm used. In this paper, the pairing of the MVs and CVs is analyzed. A detailed presentation of the Proportional-Integral (PI) controller tuning, and a comparison of the separator efficiency when using different candidate CVs is presented. Furthermore, model reference adaptive control is applied to a pipe separator. Adaptive control schemes have seen applications in process control [12] and offshore oil and gas production [13–15], but the authors have not been able to locate any prior published work on adaptive control of pipe separators.

Although the pipe separator used in this study is different from those used in [7–11], it is the authors' belief that the results are transferable and that the results presented here can serve as a basis for future control design of pipe separators.

This work contains an initial control structure analysis and an initial controller design for the MPPS. The purpose is to investigate, analyze and test several control structures, hence both a conventional PI controller and an adaptive controller is developed and tested in the laboratory. The PI controller tuning is based on the well-established simple internal model control (SIMC) tuning rules [16]. The performance of the different control structures and controllers are qualitatively and quantitatively compared and a basis for future work is established.

2. Materials and Methods

2.1. Separator Concept

The separator being tested in this paper is the Multiple Parallel Pipe Separator (MPPS), a multi-pipe arrangement for oil–water bulk separation. The concept was previously presented in [5,6], where the reader can find detailed information on design considerations and performance evaluation. Experiments are carried out on a two-pipe 150.6 mm ID prototype, which is depicted in Figure 1.

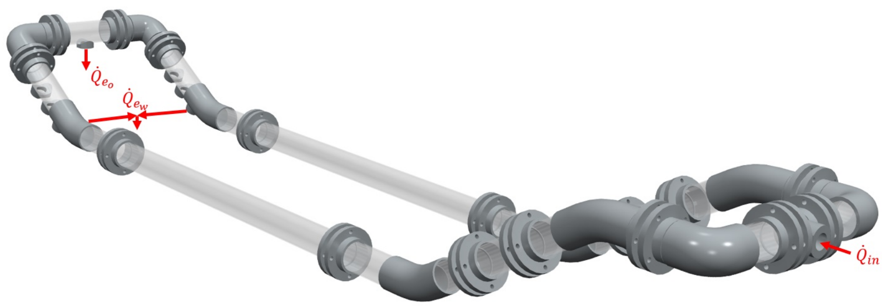

Figure 1. The Multiple Parallel Pipe Separator (MPPS) prototype.

An oil–water mixture enters at the separator inlet ($\dot{Q}_{in}$), where the flow is divided into two parallel and identical separator branches. The fluids pass through the horizontal pipe segments, where they separate and are then extracted through their respective outlets. Water is extracted through the water extraction line ($\dot{Q}_{e_w}$), while oil is extracted through the oil extraction line ($\dot{Q}_{e_o}$). As seen in Figure 1, an inclined extraction section is utilized in the design. This is to increase the water holdup in the horizontal pipe sections prior to extraction and to slow down and build up water close to the water extraction point.

The inlet has a tangential configuration and is fitted with novel phase-rearranging internals. Detailed information on the inlet configuration can be found in [6]. The total horizontal length of the separator prototype is 6.1 m.

2.2. Test Facility

The test fluids used in the separator are distilled water with added wt% 3.2 NaCl, and Exxsol D60 model oil. To prevent bacterial growth, 750 ppm of the biocide IKM CC-80 was added to the water. Furthermore, 0.015 g/L of the colorant Oil Red O has been added to the Exssol D60 for phase distinction. The test fluid properties are given in Table 1.

Table 1. Test fluid properties at 20 °C.

Fluid	Density (kg/m^3)	Viscosity (cP)
Water	1020.0	1.0
Exxsol D60	792.2	1.4

A piping and instrumentation diagram (P&ID) of the test facility is given in Figure 2. The storage tank is a gravity separator with a diameter of 1.2 m and a length of 5.5 m. It has a capacity of 6 m^3 and serves as a baseline separator. The gravity separator provides two clean phase outlets (water and Exxsol D60), which are connected to a pump manifold.

The pump manifold consists of four centrifugal pumps, two of which are used at any given time. The pumps used for the presented experiments each have a flow capacity of 100–700 L/min and a maximum head specification of 55 m. The pumps are controlled by 0–50 Hz frequency converters, where 50 Hz constitutes a maximum rpm of 2900. Two flow lines are connected to the pump manifold, one for each phase.

Both flow lines are fitted with a Coriolis flow meter measuring flow rate (FT.1/2) and density (DT.1/2). The flow meters allow accurate adjustment of the desired inlet flow and water cut (WC), as well as monitoring of phase purities.

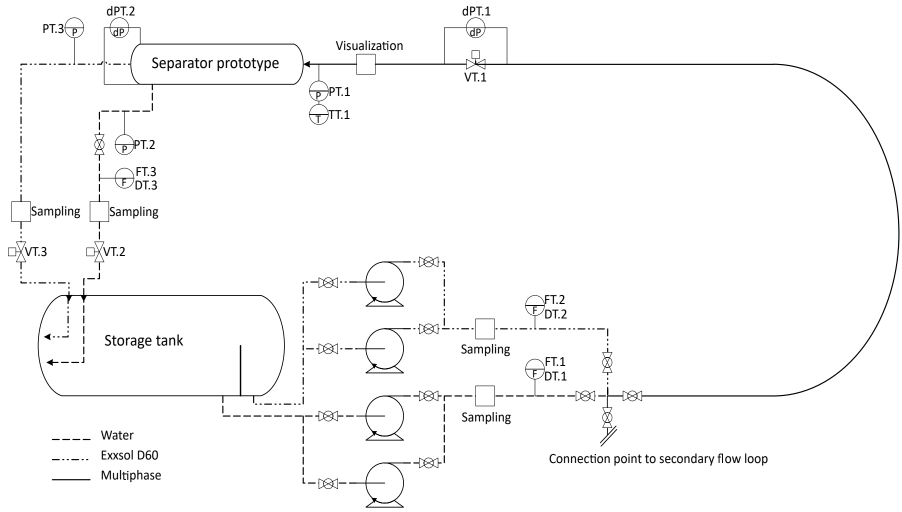

Figure 2. Lab facility piping and instrumentation diagram (P&ID).

Downstream from the Coriolis flow meters, the flow lines merge in a Y-junction to a multiphase flow line. The multiphase flow line is a 67.8 mm ID transparent polyvinyl chloride (PVC) pipe, which consists of a 5.5 m long straight section, a 720 mm radius 180° turn, and a secondary 5 m long straight section down to the inlet of the MPPS prototype.

Static gauge pressure (PT.1) and temperature (TT.1) are measured at the MPPS inlet. A ball-type inlet choke valve (VT.1) is fitted two meters upstream from the MPPS inlet. The differential pressure (dPT.1) is measured across the valve. For all presented experiments, VT.1 has been 100% open with zero pressure loss over the inlet choke valve.

Two return lines, one for water and one for Exxsol D60, are connected to the MPPS prototype. The return lines are fitted to their respective separator outlets $\dot{Q}_{e_w}$ and $\dot{Q}_{e_o}$. Static pressure transducers (PT.2/3) are fitted to each return line, and a third Coriolis flow meter (FT.3/DT.3) is mounted on the water return line. This allows tracking of the amount of water extracted from the separator, as well as calculation of the purity of the water extracted. Detailed information on logged and calculated parameters will follow in the next section.

A second dP transducer (dPT.2) is installed at the water extraction point of the MPPS prototype. This measures the dP over the inclined extraction pipe, serving as a proxy level indicator for water in the section. An illustration of the sensor mounting is given in Figure 3. The connector lines are filled with water, and the left side connection is the positive side, hence the dP measurement will be zero when the entire inclined section is filled with water and increase with the amount of oil present. The dP transducer is, unfortunately, working in the extreme end of its range and thus the measurements are quite noisy. Furthermore, low-frequency waves form in the pipeline leading up to the incline, causing a continuous disturbance on the dP measurement.

Lastly, both return lines are fitted with control valves for pressure and extraction rate control. The water return line is fitted with an electrically controlled ball valve (VT.2), while the oil return line is fitted with a pneumatic membrane valve (VT.3).

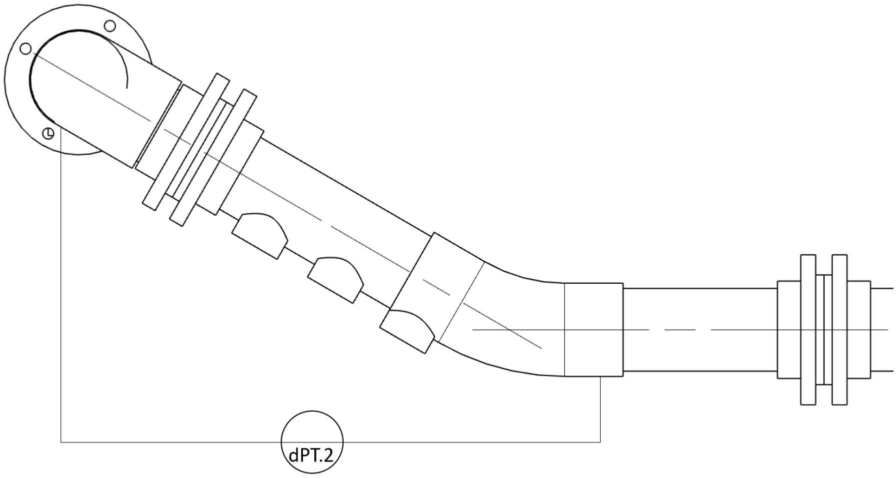

Figure 3. dPT.2 installation.

2.3. Test Parameters

All recorded test parameters are listed in Table 2. The table includes tag names, parameter names, parameter units and specified sensor range. The values for VT.2 and VT.3 are specified values sent to the valves by the controllers, not the actual measured position of the valves.

Table 2. Recorded parameters.

Tag	Parameter	Unit	Range
FT.1	$\dot{Q}_1$	L/min	0–1000
FT.2	$\dot{Q}_2$	L/min	0–1000
FT.3	$\dot{Q}_3$	L/min	0–1000
DT.1	ρ_1	kg/m^3	750–1050
DT.2	ρ_2	kg/m^3	750–1050
DT.3	ρ_3	kg/m^3	750–1050
PT.1	P_1	barg	0–6
PT.2	P_2	barg	0–6
PT.3	P_3	barg	0–6
dPT.2	dP_2	mbar	0–50
TT.1	T_1	°C	−30–122
VT.2	Valve 2	% Closed	0–100
VT.3	Valve 3	% Closed	0–100

As mentioned in Section 2.2, three Coriolis flow meters are used to adjust inlet flow rate and water cut, monitor phase purities, determine the amount of water extracted from the MPPS prototype, and the purity of the extracted water. The WC in the respective flow lines is determined by

$$\mathrm{WC}_i = \frac{\rho_i - \rho_o}{\rho_w - \rho_o} \ . \tag{1}$$

Here, ρ_i is the measured density at DT.1/2/3, while ρ_w and ρ_o are the pre-determined temperature-corrected densities of the water and Exxsol D60, respectively. For pure-phase feed streams, WC_1 should be equal to 100% while WC_2 should be equal to 0%. From calculated WC and measured flow rates, the actual WC in the multiphase transport line (WC_{in}) is calculated as

$$\mathrm{WC}_{in} = \frac{\mathrm{WC}_1\dot{Q}_1 + \mathrm{WC}_2\dot{Q}_2}{\dot{Q}_1 + \dot{Q}_2}, \tag{2}$$

where $\dot{Q}_1$ and $\dot{Q}_2$ are the water and oil flow, respectively, before mixing. When running experiments, $\dot{Q}_1$ and $\dot{Q}_2$ are adjusted such that the desired total flow and WC_{in} are reached.

The amount of water extracted from the MPPS prototype is determined by the extraction rate (ER). The ER is the flow rate through the water extraction line divided by the flow rate in the water feed line:

$$\mathrm{ER} = \frac{\dot{Q}_3}{\dot{Q}_1}, \tag{3}$$

where $\dot{Q}_3$ is the flow at the water outlet of the MPPS.

As the test loop is a closed system, the water and Exxsol D60 phases will be contaminated over time. Microscopic droplets of water will be dispersed in the oil and vice versa. In order to give a performance measurement that is independent of occurring contamination, the WC ratio is calculated. The WC ratio is equal to the WC at the water extraction line (WC_3) divided by the WC at the water feed line (WC_1):

$$\mathrm{WC}_r = \frac{\mathrm{WC}_3}{\mathrm{WC}_1}. \tag{4}$$

A WC_r equal to 100% means that the extracted water from the MPPS prototype is of equal quality to the water, leaving the baseline separator prior to being mixed with the oil. A WC_r of 100% is thus the upper limit on the purity that can realistically be achieved by the MPPS prototype.

2.4. System Identification

A dynamic model of the system is very helpful when designing controllers. A classical way to identify the dynamic relations between a manipulated variable and a control variable is to perform a step response experiment and calculate the transfer function. In this work, the procedure from [16] was followed, and it was assumed that the dynamic model between each input and output could be described by a first-order plus time delay transfer function on the form

$$\frac{y}{u} = G(s) = \frac{ke^{-\theta s}}{\tau s + 1}, \tag{5}$$

where y is the output, u is the input, and s is the Laplace variable. The transfer function variables describing the dynamic response, k, τ and θ are of special interest. These variables represent the plant gain, the time constant and the time delay, respectively. The plant gain provides the steady-state output of the plant, for a specific input, and is given by

$$k = \frac{\Delta y}{\Delta u}\ . \tag{6}$$

The time constant, τ, is the time it takes the output to reach 63% of the steady-state value, and the time delay, θ, is the amount of time it takes the input to cause a reaction on the output.

The step response experiments were performed with one valve at a time, with the other valve in a fixed position, and at a fixed inlet flow rate and inlet WC. The valve openings, inlet flow rate and inlet WCs are listed in Table 3.

Some of the measurements contained significant measurement noise, hence the measured values where filtered using a 1st order Butterworth filter before the parameter analysis was performed. The transfer function between each input and output was then calculated and validated by comparing it to the original response. If any deviations were present, the transfer function variables were tuned manually to improve the fit.

Table 3. Inlet conditions and changes in valve openings used in step response experiments.

Output	Δ VT.2 (% Closed)	VT.3 (% Closed)	Flow Rate (L/min)	WC_{in} (%)
WC_r	30	80	450	50
PT.1	30	70	450	50
dPT.2	30	70	450	50
Output	**Δ VT.3 (% Closed)**	**VT.2 (% Closed)**	**Flow Rate (L/min)**	**WC_{in} (%)**
WC_r	−30	20	450	50
PT.1	20	50	350	50
dPT.2	20	50	350	50

The step response experiments were performed on the two inputs VT.2 and VT.3, and three measurements were chosen as candidate CVs. The pressure PT.1 is a necessary CV for safety reasons. A measurement that gives a direct indication of the separator efficiency is the the water cut ratio WC_r, and hence this is also a candidate CV. The laboratory is not equipped with a level measurement sensor, instead the pressure drop dPT.2 over the incline is used for this purpose. The level is often used as an CV in previous work, as mentioned in the Introduction, and will also be a candidate CV in this work.

From the step response experiments, the following transfer functions were identified:

$$\frac{\mathrm{WC}_r}{\mathrm{VT.2}} = G_1(s) = \frac{0.2423e^{-10s}}{20.9s+1}, \tag{7}$$

$$\frac{\mathrm{PT.1}}{\mathrm{VT.2}} = G_2(s) = \frac{0.0026e^{-10s}}{14.1s+1}, \tag{8}$$

$$\frac{\mathrm{dPT.2}}{\mathrm{VT.2}} = G_3(s) = \frac{-0.0739e^{-10s}}{23.1s+1}, \tag{9}$$

$$\frac{\mathrm{WC}_r}{\mathrm{VT.3}} = G_4(s) = \frac{-0.5962e^{-4s}}{2s+1}, \tag{10}$$

$$\frac{\mathrm{PT.1}}{\mathrm{VT.3}} = G_5(s) = \frac{0.0156e^{-4s}}{8.3s+1}, \tag{11}$$

$$\frac{\mathrm{dPT.2}}{\mathrm{VT.3}} = G_6(s) = \frac{0.2722e^{-4s}}{13.2s+1}. \tag{12}$$

A comparison between the measured response, the filtered response, and the transfer function response is shown in Figure 4. Here, we see that some of the responses could be better described by a second-order transfer function. In particular, the transfer functions between VT.2 and the different outputs (note the second order dynamics in WC_r in Figure 4a not captured by $G_1(s)$ and the overshoot in dPT.2 in Figure 4e not captured by $G_3(s)$). However, for the control study in this work, it is assumed that a first order model is sufficient. The fluctuations present are purely caused by measurement and process noise.

2.5. Control Structure Analysis

The separator is a multiple input multiple output (MIMO) system with two inputs and several possible outputs. It is not straightforward to pair an input with an output, and hence a relative gain array (RGA) analysis ([17], Section 3.4) was performed. The RGA provides a measure of interactions between the inputs and outputs and [17,18] recommends pairing inputs and outputs such that the rearranged system has an RGA matrix close to identity. Furthermore, negative steady-state RGA elements should be avoided. The RGA for a square system on the form

$$y = G(s)u \tag{13}$$

is found by calculating the element-wise matrix product

$$\mathrm{RGA}(G) = G_0 G_0^{-T}, \tag{14}$$

where $G_0 = G(0)$ is the steady-state transfer function matrix of $G(s)$ in Equation (13).

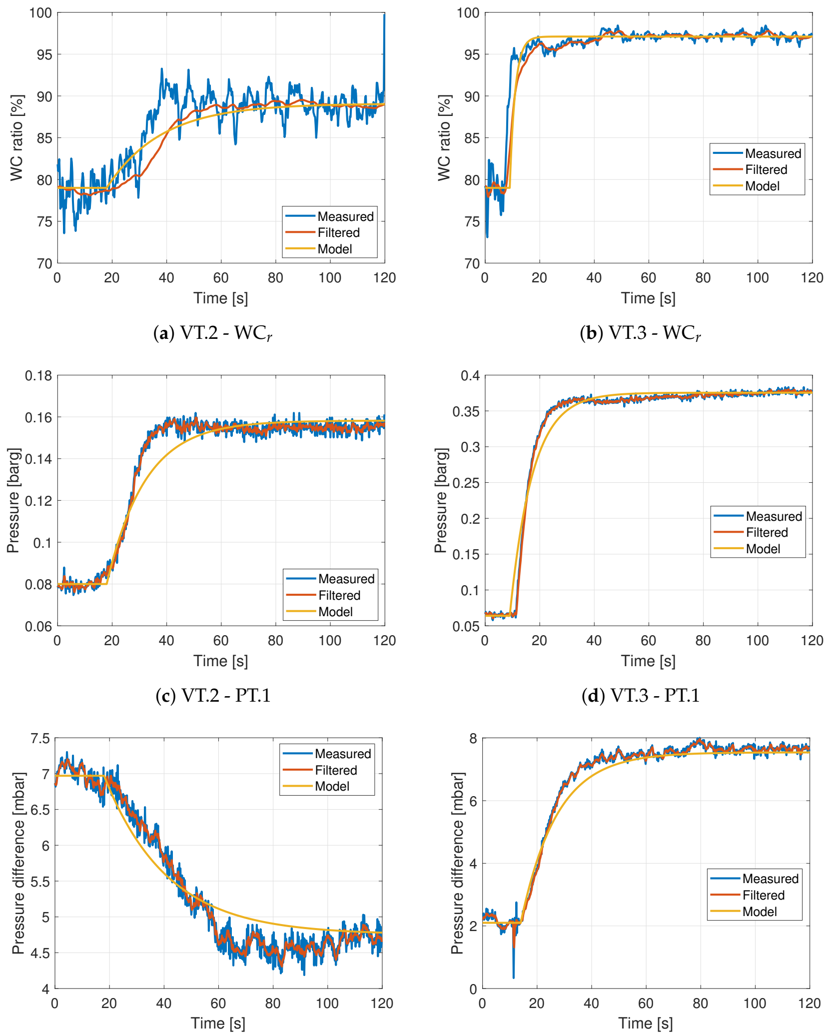

(**a**) VT.2 - WC$_r$ (**b**) VT.3 - WC$_r$

(**c**) VT.2 - PT.1 (**d**) VT.3 - PT.1

(**e**) VT.2 - dPT.2 (**f**) VT.3 - dPT.2

Figure 4. Step response comparison between measured signal, filtered signal and transfer functions.

Another parameter to consider when investigating the pairing of CVs and MVs is the Niederlinski index (NI) ([18], Section 2.2.1)

$$\mathrm{NI} = \frac{\det\left[G(0)\right]}{\prod_{i=1}^{n} g_{ii}(0)}, \tag{15}$$

where g_{ii} are the diagonal elements of $G(0)$. If the open-loop system is stable (which is the case here), one should select pairings corresponding to positive NI values [19]; otherwise, the closed-loop system will be unstable ([18], Th. 1). The RGA matrices and the NI for the separator is shown in Table 4. From the RGA analysis, it is clear that VT.2 should be paired with WC_r or dPT.2, and VT.3 with PT.1, as this corresponds to the pairing closest to 1. The NI is positive for both possible pairings, hence no pairing will lead to an unstable system.

Table 4. Relative gain array (RGA) and Niederlinski index (NI) for the separator.

Input	Output	RGA	NI
VT.2 VT.3	WC_r PT.1	$\begin{bmatrix} 0.7082 & 0.2918 \\ 0.2918 & 0.7082 \end{bmatrix}$	1.4121, 3.4269
VT.2 VT.3	dPT.2 PT.1	$\begin{bmatrix} 0.6185 & 0.3815 \\ 0.3815 & 0.6185 \end{bmatrix}$	1.6169, 2.6209

2.6. Controller Design

A multivariable system, such as the one investigated here, could benefit from a multivariable control scheme. However, since this is an initial control study, the developed controllers are decoupled, single-loop controllers.

2.6.1. PI Control

A PI controller has the form

$$u(s) = k_c \left(1 + \frac{1}{\tau_I s}\right)(r - y), \tag{16}$$

where k_c is the proportional gain, τ_I is the integral time in seconds, r is the reference and y is the measured output to be controlled. PI controllers are developed for the separator by applying the SIMC tuning rules [16]. The SIMC tuning rules states that the proportional gain and integral time of the PI controller should be chosen as

$$k_c = \frac{1}{k}\frac{\tau}{\tau_c + \theta}, \tag{17}$$

$$\tau_I = \min\left(\tau, (\tau_c + \theta)\right), \tag{18}$$

where k_c is the proportional gain, τ_I is the integral time, and τ_c is the desired closed-loop time constant, which is the only tuning parameter. For tight and robust control, Ref. [16] recommends choosing $\tau_c = \theta$. Although the RGA analysis recommended a specific pairing of inputs and outputs, PI controllers are developed and tested for all configurations. The parameters used in the PI controllers are found in Section 3.2.1.

A derivative part could have been added to the controllers, but this would have required a measurement of the derivative of the CV. This is not available but could have been calculated numerically. However, as the control objective is to keep the CVs at steady-state, the derivative of the CV would be close to zero when operating at steady-state and the contribution would only be from the measurement noise. Derivative action is uncommon in process control applications where the plants are stable with overdamped responses and first-order dominant dynamics (which is the case here), since the performance improvement is usually too small compared to the added complexity [17,20].

2.6.2. Adaptive Control

As an alternative to conventional PI control, a model reference adaptive controller (MRAC) ([21], Section 6.2.2) was implemented and tested for the two control configurations recommended by the RGA analysis, i.e., VT.3 controls PT.1 and VT.2 controls either WC_r or dPT.2.

When using MRAC, the controller parameters are automatically updated such that the error between the measured variable and the output of a reference model is reduced. This could be very beneficial if the process parameters change over time or at different operating points, which may lead to poor control when using a controller with fixed gains. The MRAC structure is different from a PI controller structure, i.e., there is no proportional and integral gain in the MRAC, but rather two parameters that try to approximate a value that causes the closed-loop system dynamics to be equal to the reference model dynamics. Hence, using the proportional and integral gain of a PI controller as initial values in an MRAC is not necessarily helpful. A schematic of the MRAC is shown in Figure 5.

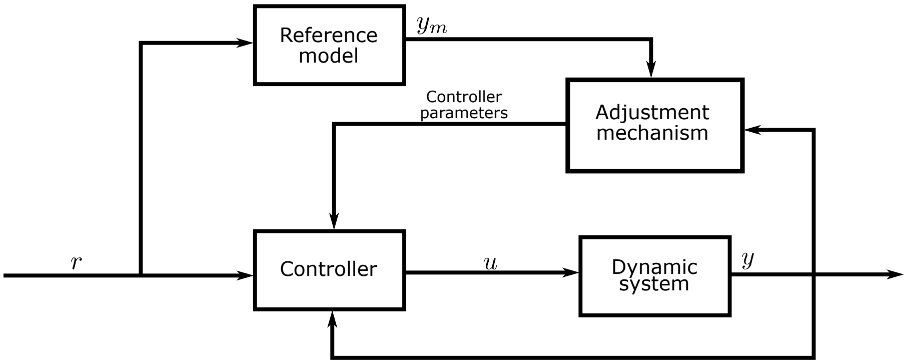

Figure 5. Model reference adaptive control (MRAC) schematic.

The MRAC has the form

$$u = -k_a(t)y + l_a(t)r, \tag{19}$$

where $k_a(t)$ and $l_a(t)$ are time-varying gains, updated by the adaptive laws

$$\dot{k}_a = \gamma_k e y \,\mathrm{sign}(k), \tag{20}$$

$$\dot{l}_a = -\gamma_l e r \,\mathrm{sign}(k), \tag{21}$$

where γ_k, γ_l are adaptation gains, y is the measured value to be controlled, r is the reference and $\mathrm{sign}(k)$ is either 1 or -1. The error signal $e = y - y_m$, where y_m is the output of the reference model

$$\dot{x}_m = a_m x_m + b_m r, \tag{22}$$

$$y_m = x_m, \tag{23}$$

where $a_m < 0$ and b_m are chosen by the operator and specify the desired closed-loop dynamics of the system.

The only system knowledge required by the MRAC is the sign of k. It can be shown ([21], Section 6.2.2) that, if $y = x$ is the state in a linear system, the controller given by Equations (19)–(23) causes $y \to y_m$ asymptotically for $\gamma_k, \gamma_l > 0$. The parameters used in the MRAC are found in Section 3.2.2.

3. Results

In total, six experiments were carried out in the laboratory: four experiments with PI controllers and two experiments with MRAC. When using PI control, all control pairings were tested, but with MRAC only the pairings recommended by the RGA analysis was carried out.

3.1. LabView Implementation

The laboratory is controlled through a computer running LabView 2015 (National Instruments, Austin, TX, USA) on Windows 7 (Microsoft, Redmond, WA, USA) with an Intel i7 4770S (Santa Clara, CA, USA), 3.1 GHz processor and 16 GB RAM. The PI controllers could be readily implemented in the LabView 2015 block diagram through existing PI controller blocks.

The MRAC, however, had to be implemented using an add-on for LabView called MathScript Module. This module allows the user to write code, and execute it at each iteration of the LabView program. To calculate the MRAC input in Equation (19), the differential equations in Equations (20)–(22) must be solved. This was done using first-order Euler integration with a step length of 0.0001 s. A dead band was introduced to the adaptation algorithms, i.e., the adaptation was stopped if the error was less than 5% of the setpoint for dPT.2 and PT.1 and less than 0.5% for WC_r.

3.2. Controller Tuning

3.2.1. PI Controllers

A transfer function model is only an approximation of the real system dynamics. It was assumed that the transfer functions were of first order. The controller parameters may require re-tuning if the transfer function models differ significantly from the real dynamics (they may change with operating point and inlet conditions) or if nonlinearities in the valve openings are not considered. Furthermore, there are interactions between the control loops; hence, a multivariable controller would probably be a better choice. This, however, has not been studied in this work.

It was found during initial testing that the choice of $\tau_c = \theta$ was too aggressive for VT.2 and, hence, $\tau_c = 30$ s was chosen for this valve. For VT.3, $\tau_c = \theta$ could only be used when controlling WC_r. Otherwise, $\tau_c = 10$ s was used. The controller parameters for the different PI controllers are listed in Table 5.

Table 5. PI controller parameters.

MV	CV	τ_c	k_c	τ_I
VT.2	WC_r	30 (s)	2.15 (-)	20.8 (s)
VT.2	PT.1	30 (s)	135.2 (1/barg)	14.1 (s)
VT.2	dPT.2	30 (s)	−7.82 (1/mbar)	23.1 (s)
VT.3	WC_r	4 (s)	−0.424 (-)	2.04 (s)
VT.3	PT.1	10 (s)	38.1 (1/barg)	8.28 (s)
VT.3	dPT.2	10 (s)	3.464 (1/mbar)	13.2 (s)

3.2.2. Model Reference Adaptive Controller

It was found during testing in the laboratory that the initial values $k_a(0)$ and $l_a(0)$ as well as the adaptation gains γ_k, γ_l had to be chosen with care. This is due to the fact that time delays and measurement noise was ignored when the controller was derived. The adaptive controller parameters used are listed in Table 6.

Table 6. Model reference adaptive controller (MRAC) parameter values.

Experiment	MV	CV	a_m (1/s)	b_m (1/s)	γ_k (1/s)	γ_l (1/s)	$k_a(0)$	$l_a(0)$
5	VT.2	WC_r	$-1/30$	$1/30$	0.00002	0.00002	0 (-)	0 (-)
	VT.3	PT.1	$-1/10$	$1/10$	100	100	50 (1/barg)	50 (1/barg)
6	VT.2	dPT.2	$-1/30$	$1/30$	0.01	0.01	0 (1/mbar)	0 (1/mbar)
	VT.3	PT.1	$-1/10$	$1/10$	20	20	50 (1/barg)	50 (1/barg)

3.3. Test Sequence and Control Objectives

All experiments presented here were performed on the same day. Prior to each experiment, the lab was operated at nominal inlet conditions for 5 min, i.e., a flow rate of 350 L/min and 60% WC. The valves were manually set to VT.2 = 30% closed and VT.3 = 70% closed. This led to an initial pressure PT.1 $\sim$ 0.1 barg, an initial $WC_r \sim$ 99% and an initial dPT.2 $\sim$ 1.9 mbar when the controllers were activated. The static pressure is initialized at 0.1 barg in order to see how the controllers, and especially the adaptive controllers, perform during an initial transient. A setpoint of 0.4 barg for PT.1 was necessary as the valve controlling the pressure could then operate in the middle of its range, and not saturate, when the inlet flow rate was high.

The inlet conditions were varied in order to emulate situations that may occur in a subsea oil/water separator. The inlet variables available for manipulation are the total liquid flow and the inlet WC. Table 7 shows the different inlet conditions and the scenarios they emulate.

The main control objectives in all experiments are to maintain the desired pressure PT.1 and to keep WC_r as high as possible. The latter is important in order to ensure that the water quality is high enough for the downstream water cleaning equipment. A setpoint of 99% is chosen for the WC_r. Looking only at WC_r may, however, be misleading, since it says nothing about how much water is extracted. For this, the ER is used. It is important to maintain a high ER while maintaining a high WC_r. If the ER is very low, almost no liquid is leaving the separator through the water outlet. In this case, the WC_r may be high, but a lot of water is leaving through the oil outlet.

In Experiments 1 and 2, the WC_r is controlled directly using either VT.2 or VT.3. In Experiments 3, 4 and 6, the dP between the bottom of the outlet incline and the top of the outlet incline is controlled. This serves as a proxy level measurement of the water level in the incline. When controlling the dP, and the level, by proxy, a buffer of water is built up in the incline, making the WC_r more robust to inlet variations. It was found through image analysis that a dP of 2 mbar gave stable oil and water layers (see the Appendix A) and the buffer volume was assumed sufficient. Hence, this setpoint is used in the controllers. Figure 6 shows a sketch of this.

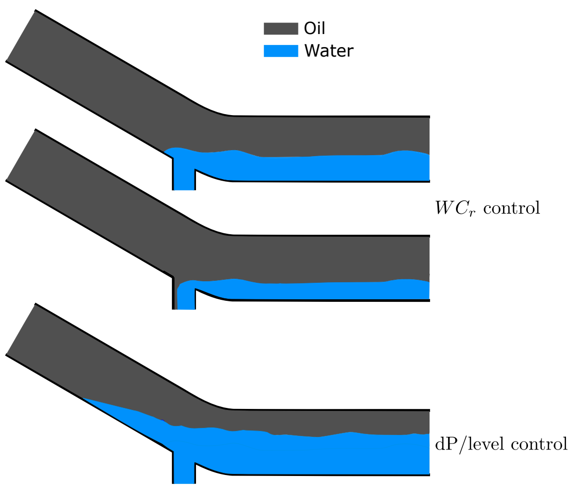

Figure 6. When controlling WC_r directly, no buffer volume of water is present in the inclined section. Hence, oil breakthrough into the water outlet is more frequent when comparing to the dP/level control.

Table 7. Inlet conditions used in all experiments.

Total Flow (L/min)	WC_{in} (%)	Time Stamp (s)	Situation
350	60	0–480	Nominal conditions
350	80	480–840	Water breakthrough
400	74	840–900	New well introduced, step 1
450	67	900–960	New well introduced, step 2
500	60	960–1020	New well introduced, step 3
450	40	1020–1380	Shut down of old well

3.4. Experiment 1. PI Control VT.2–PT1, VT.3–WC_r

Figure 7 shows the results of Experiment 1 where the recommended pairings from the RGA analysis were not used. Since both outputs depend on both inputs, both controllers need to work continuously to counteract the effects caused by the other controller. Furthermore, when WC_r is higher than the setpoint, the controller will close VT.3 to decrease WC_r. This causes the ER to increase above 100% and oil starts flowing through the water outlet. Due to time delays, this effect suddenly causes a drop in WC_r which then has to be counteracted. These drops in WC_r are clearly seen in Figure 7b.

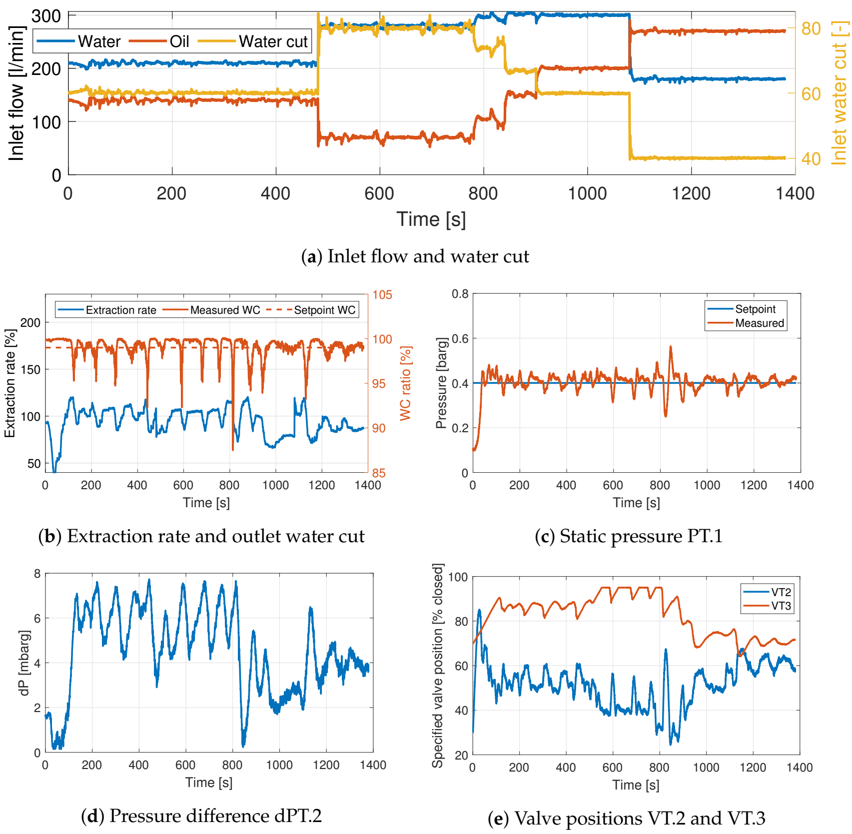

(**a**) Inlet flow and water cut

(**b**) Extraction rate and outlet water cut

(**c**) Static pressure PT.1

(**d**) Pressure difference dPT.2

(**e**) Valve positions VT.2 and VT.3

Figure 7. Experiment 1. PI controllers on VT.2 and VT.3 where VT.2 controls PT.1 and VT.3 controls WC_r.

The pressure controller is able to keep the pressure around the setpoint. The controller handles the steps in inlet flow and inlet WC quite well, but the effect of the other control loop is quite clear.

Processes **2019**, *7*, 190

Notice how the differential pressure dPT.2 oscillates (Figure 7d) due to the lack of control. The dP is quite high, indicating a large amount of oil in the incline. Numerical values for the performance can be found in Table 8.

3.5. Experiment 2. PI Control VT.2–WC$_r$, VT.3–PT.1

Figure 8 shows the results of Experiment 2. Here, the recommended pairings from the RGA analysis were used, and the results show that PT.1 is controlled much better than in Experiment 1. The variations in WC$_r$ are less frequent, but this is caused by the slow controller operating VT.2. As can be seen in Figure 8e, from $t \sim 500$ s to $t \sim 700$ s, the VT.2 valve opens very slowly. This causes the extraction rate to increase slowly (it increased much faster in Experiment 1) towards the point where a drop in WC$_r$ happens. This occurs at $t \sim 700$ s, causing the valve to close again. Since the variations in WC$_r$ happen less frequently, the effect on PT.1 from VT.2 opening and closing is also less than in Experiment 1, which may explain why PT.1 is better controlled in Experiment 2. It should be noted, however, that VT.3 is much faster than VT.2, hence the controller could possibly be able to counteract the influence of VT.2 even if the oscillations had been more frequent. The differential pressure dPT.2 oscillates here as well (Figure 8d), due to the lack of control and the dP is quite high, indicating a large amount of oil in the incline. Numerical values for the performance can be found in Table 8.

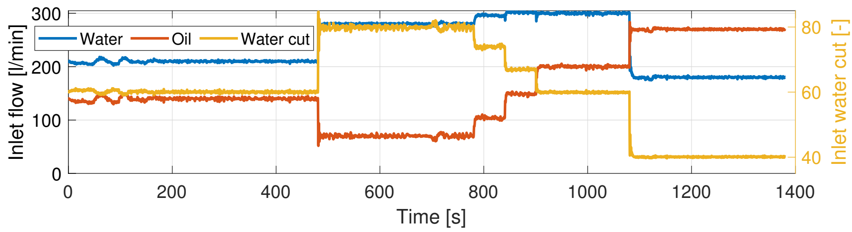

(**a**) Inlet flow and water cut

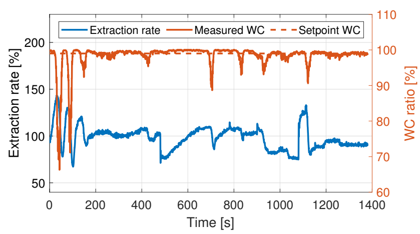

(**b**) Extraction rate and outlet water cut

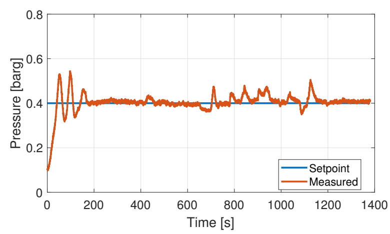

(**c**) Static pressure PT.1

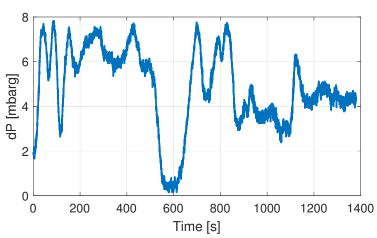

(**d**) Pressure difference dPT.2

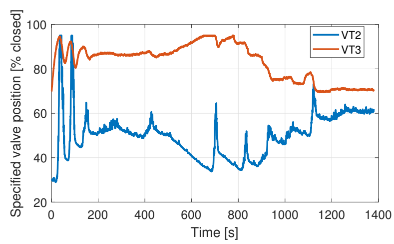

(**e**) Valve positions VT.2 and VT.3

Figure 8. Experiment 2. PI controllers on VT.2 and VT.3, with the pairing recommended by the RGA analysis.

The initial transient is quite oscillatory. This is caused by the large initial error in the PT.1 and the fact that no reference filter is used. After PT.1 stabilizes, so does WC_r. During the steps in inlet conditions, both controllers are able to keep the controlled variable close to the setpoint. The variations in PT.1 are smaller than in Experiment 1.

3.6. Experiment 3. PI Control VT.2–PT.1, VT.3–dPT.1

In this experiment, WC_r is not used in the controller. Instead, the dP is controlled to a fixed setpoint. Figure 9 shows the results. Here, we see that the behaviour of the WC_r and the ER is not as in Experiments 1 and 2. Since the dP is controlled, a buffer volume is established in the incline. This buffer volume functions as a filter for the disturbances occurring at the inlet. The WC_r has very few drops below 99% in this experiment (Figure 9b). Numerical values for the performance can be found in Table 8.

The effects of measurement noise in the dP transducer are clearly seen in Figure 9d.

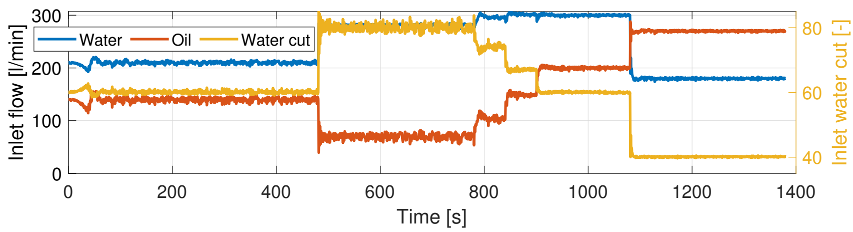

(**a**) Inlet flow and water cut

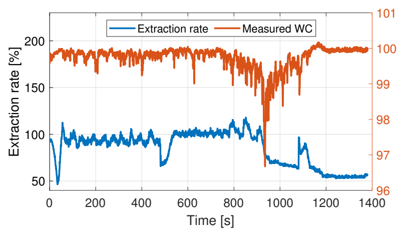

(**b**) Extraction rate and outlet water cut

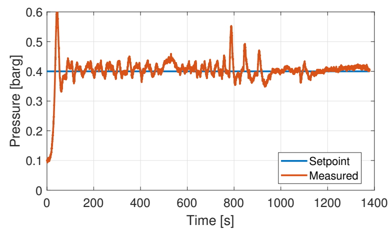

(**c**) Static pressure PT.1

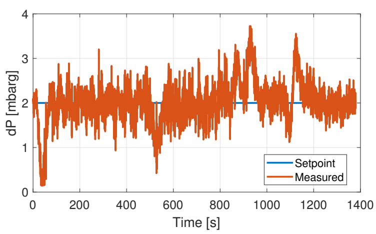

(**d**) Pressure difference dPT.2

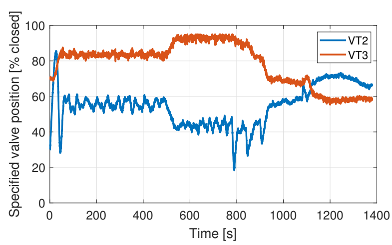

(**e**) Valve positions VT.2 and VT.3

Figure 9. Experiment 3. PI controllers on VT.2 and VT.3 with VT.2 controlling PT.1 and VT.3 controlling dPT.2.

3.7. Experiment 4. PI Control VT.2–dPT.2, VT.3–PT.1

This experiment uses the control configuration recommended by the RGA analysis. The results of the experiment are shown in Figure 10. The results are quite similar to those found in Experiment 3, but the oscillations in PT.1 during the disturbances are smaller. It is also clear that VT.2 is changing significantly more than VT.3 in Experiment 3. The variations and initial overshoot in dPT.2 are larger in this experiment, but this is caused by VT.2 being much slower than VT.3. The behaviour of the WC_r and the ER is quite similar to Experiment 3, but the undershoot at $t \sim 950$ s is smaller in this experiment. Numerical values for the performance can be found in Table 8.

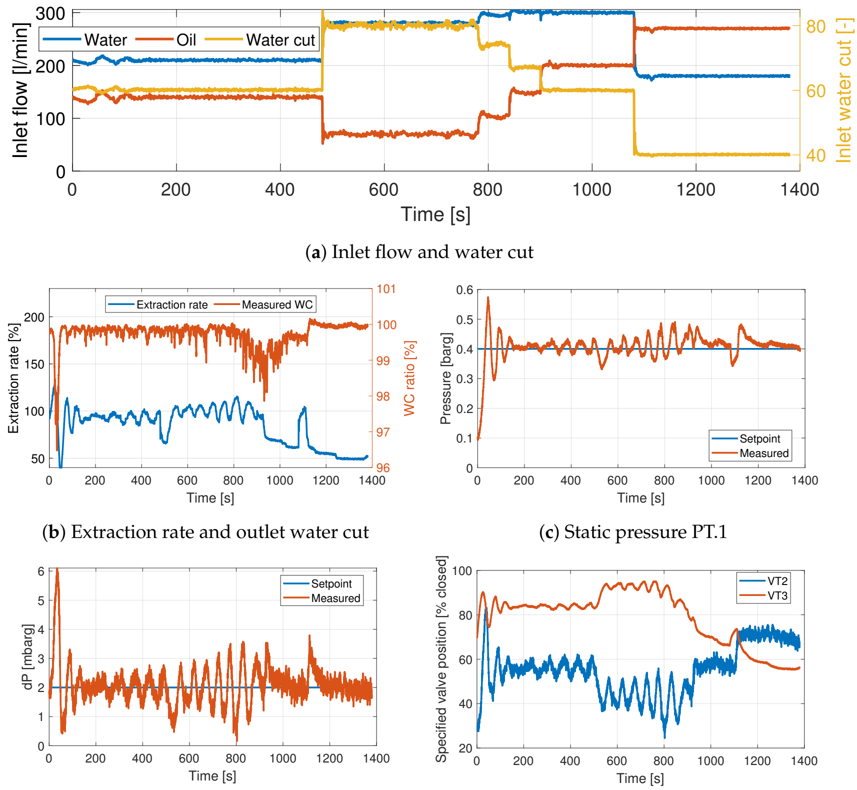

(**a**) Inlet flow and water cut

(**b**) Extraction rate and outlet water cut

(**c**) Static pressure PT.1

(**d**) Pressure difference dPT.2

(**e**) Valve positions VT.2 and VT.3

Figure 10. Experiment 4. PI controllers on VT.2 and VT.3 with VT.2 controlling dPT.2 and VT.3 controlling PT.1, as recommended by the RGA analysis.

3.8. Experiment 5. Adaptive Control VT.2–WC_r, VT.3–PT.1

The model reference adaptive controller was first tested on the recommended control configuration with VT.2 controlling WC_r and VT.3 controlling PT.1. The results are shown in Figure 11. The pressure is controlled very well when using the MRAC. Note that the reference signal in Figure 11c is the output of the reference model given in Equations (22) and (23), hence the signal is filtered and the initial response has much less overshoot compared to Experiment 2. The WC_r controller is quite slow, hence the extraction rate increases slowly to the level where the drops in WC_r occur. When the drops do happen, they are approximately equal to the drops experienced in Experiment 2.

The adaptive gains are shown in Figure 11f,g. The gains for VT.2 are initialized at 0, but the gains for VT.3 are initialized at 50. This was found through trial and error to be a good initial value for VT.3. Numerical values for the performance can be found in Table 8.

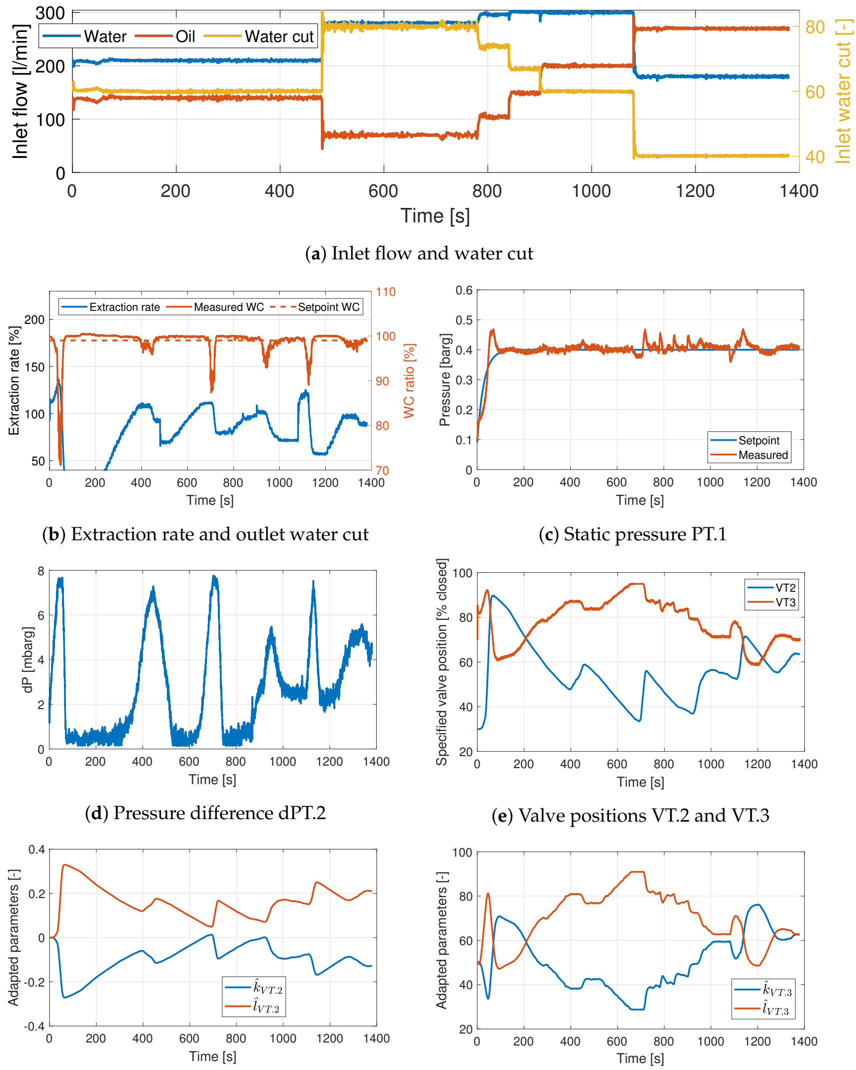

(**a**) Inlet flow and water cut

(**b**) Extraction rate and outlet water cut

(**c**) Static pressure PT.1

(**d**) Pressure difference dPT.2

(**e**) Valve positions VT.2 and VT.3

(**f**) Adapted parameters VT.2 controller

(**g**) Adapted parameters VT.3 controller

Figure 11. Experiment 5. MRAC on VT.2 and VT.3 with VT.2 controlling WC_r and VT.3 controlling PT.1, as recommended by the RGA analysis.

3.9. *Experiment 6. Adaptive Control VT.2–dPT.2, VT.3–PT.1*

The final experiment used MRAC for VT.2 and VT.3, with VT.2 controlling dPT.2 and VT.3 controlling PT.1. From Figure 12b, it is clear that the WC_r and ER have similar behaviour to that shown in Experiments 3 and 4. The pressure PT.1 is controlled quite well, though with some increases in oscillations compared to that observed in Experiment 5, caused by the need for a lower adaptation gain in this experiment.

The pressure difference controller has trouble bringing dPT.2 to the reference after the first change in inlet conditions happens at $t = 480$ s. This could be caused by the large initial overshoot caused by the zero initialization of the adaptive parameters. As can be seen from Figure 12f,g, the adaptive parameters start changing direction at $t = 480$ s, but, since γ_k and γ_l had to be chosen to be quite small because of the slow valve, the adaptation takes a long time. Furthermore, the changes in PT.1 is causing the pressure difference dPT.2 to change. Since the VT.2 controller (and valve) is so slow, it is unable to bring dPT.2 to the reference as can be seen in Figure 12d.

Numerical values for the performance can be found in Table 8.

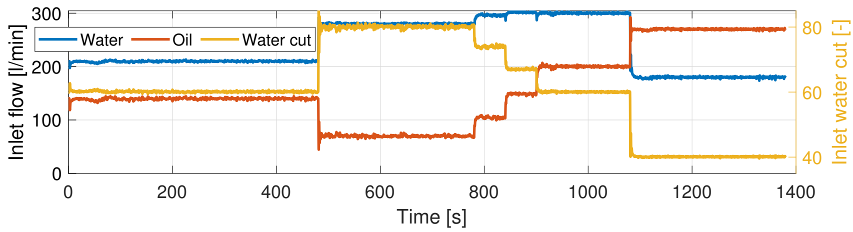

(**a**) Inlet flow and water cut

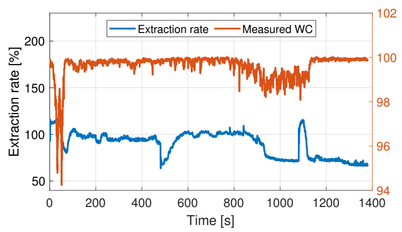

(**b**) Extraction rate and outlet water cut

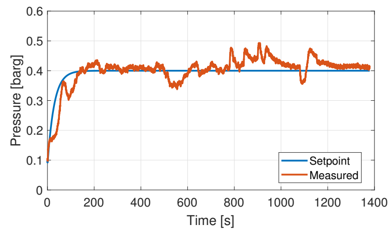

(**c**) Static pressure PT.1

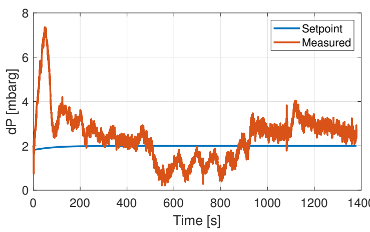

(**d**) Pressure difference dPT.2

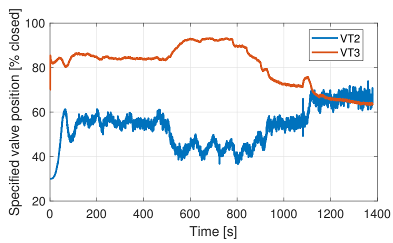

(**e**) Valve positions VT.2 and VT.3

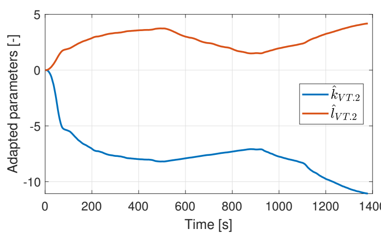

(**f**) Adapted parameters VT.2 controller

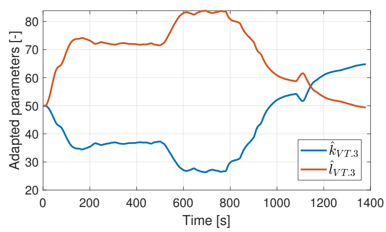

(**g**) Adapted parameters VT.3 controller

Figure 12. Experiment 6. MRAC on VT.2 and VT.3 with VT.2 controlling dPT.2 and VT.3 controlling PT.1, as recommended by the RGA analysis.

3.10. Numerical Comparison

Table 8 shows a numerical comparison of the values of interest from Experiments 1–6. The table includes the mean, root-mean-square (RMS), standard deviation (STD) and median, as well as the integrated absolute error (IAE) for the variables being controlled. The initial transient has an effect on all these numbers, hence the values are also calculated from t = 200 s rather than from t = 0 to exclude this effect. These values are showed in parentheses.

Table 8. Numerical comparison of Experiments 1–6. Values in parentheses are calculated after the initial transient is over, i.e., from $t = 200$ s.

Experiment	Variable	Mean	RMS	STD	Median	IAE
1	WC_r	99.09 (99.03)	99.09 (99.03)	1.17 (1.21)	99.43 (99.37)	1085.6 (929.2)
	PT.1	0.40 (0.41)	0.41 (0.41)	0.05 (0.03)	0.41 (0.41)	41.72 (29.03)
	ER	93.96 (94.64)	95.10 (95.5)	14.64 (12.73)	95.99 (95.86)	-
2	WC_r	98.38 (98.92)	98.44 (98.93)	3.46 (1.25)	99.25 (99.24)	1803.9 (901.44)
	PT.1	0.40 (0.40)	0.41 (0.41)	0.045 (0.02)	0.41 (0.41)	31.79 (17.09)
	ER	98.17 (96.7)	98.9 (97.3)	12.36 (10.5)	99.44 (98.32)	-
3	WC_r	99.73 (99.72)	99.73 (99.72)	0.33 (0.35)	99.85 (99.84)	-
	PT.1	0.40 (0.41)	0.40 (0.41)	0.048 (0.02)	0.41 (0.41)	31.27 (17.87)
	dPT.2	2.02 (2.07)	2.07 (2.10)	0.44 (0.40)	2.02 (2.04)	417.24 (336.46)
	ER	84.58 (83.80)	86.41 (85.78)	17.69 (18.34)	91.50 (90.97)	-
4	WC_r	99.72 (99.74)	99.72 (99.74)	0.37 (0.29)	99.83 (99.83)	-
	PT.1	0.41 (0.41)	0.41 (0.41)	0.047 (0.026)	0.41 (0.41)	39.34 (26.13)
	dPT.2	2.08 (2.03)	2.19 (2.10)	0.68 (0.52)	2.04 (2.04)	619.55 (459.9)
	ER	83.98 (82.63)	86.34 (85.01)	20.05 (19.97)	91.97 (91.47)	-
5	WC_r	98.83 (99.04)	98.88 (99.06)	2.89 (1.68)	99.74 (99.69)	1861.8 (1254.5)
	PT.1	0.40 (0.40)	0.40 (0.41)	0.04 (0.014)	0.40 (0.41)	23.78 (12.76)
	ER	78.71(84.67)	84.10 (86.92)	29.60 (19.65)	84.60 (87.71)	-
6	WC_r	99.59 (99.67)	99.60 (99.67)	0.55 (0.36)	99.80 (99.83)	-
	PT.1	0.40 (0.41)	0.40 (0.42)	0.053 (0.025)	0.41 (0.41)	43.25 (26.31)
	dPT.2	2.42 (2.16)	2.65 (2.30)	1.10 (0.79)	2.49 (2.36)	1222.3 (831.00)
	ER	89.61 (87.75)	90.60 (88.73)	13.38 (13.15)	94.50 (93.59)	-

4. Discussion

From the RGA analysis, it was found that VT.3 should control PT.1 in all cases. The numerical data from Experiments 1 and 2 (Table 8) shows that the control structure proposed by the RGA analysis improves the ER. The values for WC_r is slightly worse in Experiment 2, but if the initial transient is ignored the difference is reduced. The slow valve VT.2 is controlling WC_r in Experiment 2, which may explain why the values are worse, as it takes this valve more time to reduce the error compared to VT.3.

The numerical data from Experiments 3 and 4 (Table 8) show that controlling dPT.2 rather than WC_r improves the separator performance. The mean, median and RMS of the WC_r are higher and the STD is much lower in both Experiments 3 and 4 compared to Experiments 1 and 2. This comes at the cost of a lower extraction rate. This could probably be improved by finding a better setpoint for dPT.2. The differences between Experiment 3 (not RGA) and Experiment 4 (RGA) are very small when looking at WC_r. Experiment 4 has slightly lower values in mean, median and RMS and slightly higher in STD, but, if the initial transient is ignored, the values are slightly better than in Experiment 3 (except for median). Overall, Experiment 3 has slightly better values than Experiment 4. This is the opposite of what one might expect based on the results of the RGA analysis. The RGA analysis, however, is only based on steady state behaviour and does not consider time-delays or transients. The results may indicate that the transfer functions used in the RGA analysis are significantly different from the real dynamics, i.e., the model identification in Section 2.4 may be insufficiently accurate.

The performance of the adaptive controllers are approximately equal to the performance of the PI controllers. Experiments 5 and 6 must be compared with Experiments 2 and 4, respectively.

The WC_r is slightly higher in Experiment 5 compared to Experiment 2, but the ER is much lower in Experiment 5. This is caused by the very low adaptation gains chosen in Experiment 5, which causes VT.2 to close very slowly and, hence, less variations are present in WC_r. The pressure control, however, is slightly improved when using the adaptive controller.

The values from Experiment 6 are very similar to those from Experiment 4. The WC_r is slightly worse, but the ER is higher. The adaptive gains for the dPT.2 controller again had to be chosen very low, which causes sluggish control of dPT.2. This again affects the static pressure due to the interactions between the two CVs, and hence the performance is reduced for both dPT.2 and PT.1. Comparing Experiments 5 and 6, it is again clear that controlling dPT.2 rather than WC_r improves the efficiency.

According to the information shown in Table 8, the performance of the PI controller and the adaptive controller is approximately equal. However, aspects such as implementation and ease of operation should also be considered. The PI controllers could be easily implemented in the LabView block diagram, but the tuning required step response experiments and some trial and error. The MRAC, however, did not require a step response model, but the implementation required a custom script and the tuning was largely based on trial and error and the experience of the operators. The adaptation gain for the controller operating the slow valve VT.2 had to be very low, which may have negatively affected the end result. Improving the performance significantly with tuning, however, would be difficult due to the constraints imposed by the slow valve. Finding suitable adaptation gains and initial values for the MRAC was not trivial.

The SIMC tuning rules was chosen for the PI controllers, due to its simplicity and proven efficiency for first-order plus time delay systems [16], but other tuning methods specifically designed for tuning decentralized PI controllers with two inputs and two inputs exist [22,23]. These methods may reduce the interactions between the control loops and lead to tighter control during transients, at the cost of a more complex tuning procedure.

A multivariable controller (adaptive or not) would probably outperform both controllers as it would better compensate for the interactions between the control loops. Implementing this is suggested as future work.

A model predictive controller (MPC) would also be a natural next step. The MPC can calculate the optimal setpoints and inputs while also handling the input and variable constraints. Implementing an MPC is also suggested as future work.

5. Conclusions

This paper presented a control structure analysis and controller design for a novel multi-pipe separator concept developed at the Department of Geoscience and Petroleum at the Norwegian University of Science and Technology. The control structure analysis gives an indication of which outputs to pair with which inputs, and the controller design for the conventional PI controllers is based on the well established SIMC tuning rules. Step response experiments were performed to gather data for the dynamic models of the different input/output relations in the separator. The dynamic models were assumed to be of first order with a time delay, but second order models and models accounting for the interactions between the states would probably yield better results, considering the measured system responses. Model reference adaptive controllers were also developed for the separator. The performances of the PI and adaptive controllers were quite similar, but the adaptive controller does not require a step response model in the tuning procedure. Due to a lack of tuning rules, however, the adaptive controller was quite difficult to tune. Furthermore, the adaptation gains in the MRAC had to be chosen very small due to the slow control valve VT.2. A faster valve would probably improve the results.

It was found that controlling the dP over the incline in the separator, and the water/oil interface level, by proxy, yielded a more stable water cut ratio on the water outlet, which was the primary control objective. This is due to dP control establishing a buffer volume of water in the incline, unlike when controlling WC_r directly.

The separator is a multiple input, multiple output (MIMO) system and would probably benefit from a multivariable controller rather than two decoupled controllers. Model predictive control could potentially improve the results even more, as the separator is subject to several constraints and control objectives. Finding the optimal setpoints and outputs within the constraints is key for efficient operation. This is suggested for future work.

Author Contributions: Conceptualization, S.J.O., H.S.S., M.S. and C.H.; methodology, S.J.O. and H.S.S.; software, S.J.O. and H.S.S.; validation, S.J.O. and H.S.S.; formal analysis, S.J.O. and H.S.S.; investigation, S.J.O. and H.S.S.; resources, H.S.S. and M.S.; data curation, S.J.O. and H.S.S.; writing—original draft preparation, S.J.O. and H.S.S.; writing—review and editing, S.J.O., H.S.S., M.S. and C.H.; supervision, M.S. and C.H.

Funding: This research was carried out as a part of SUBPRO, a Research-based Innovation Center within Subsea Production and Processing. The authors gratefully acknowledge the financial support from SUBPRO, which is financed by the Research Council of Norway, major industry partners, and NTNU.

Conflicts of Interest: The authors declare no conflict of interest.

Abbreviations

The following abbreviations are used in this manuscript:

MPPS	Multiple parallel pipe separator
CV	Controlled variable
MV	Manipulated variable
SIMC	Simple internal model control
ppm	Parts per million
P&ID	Piping and instrumentation diagram
PVC	Polyvinyl chloride
MRAC	Model reference adaptive control
ER	Extraction rate
PID	Proportional, Integral, Derivative
WC	Water cut
PT	Pressure transmitter
dPT	Differential pressure transmitter
RMS	Root mean square
STD	Standard deviation
IAE	Integrated absolute error

Appendix A

The incline was photographed under varying inlet conditions and with varying pressure difference over the incline. The photos show that a pressure difference setpoint around 2 mbar will give stable oil and water layers and a decent water buffer in the incline. The photos are shown in Figures A1–A4.

Q_{tot} [l/min]	WC_{in} [%]	$dPT.2$ [mbar]	WC_r [%]	ER [%]
299.83	30.09	1.22	99.93	45.96
300.04	30.11	1.67	99.91	60.11
300.09	30.11	2.24	99.83	75.78

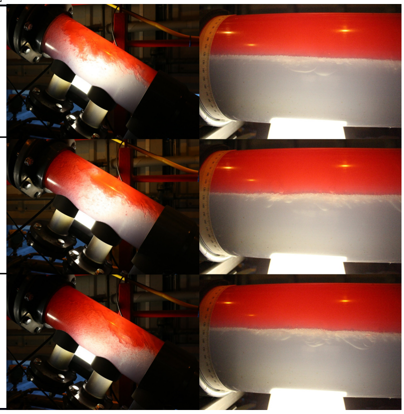

Figure A1. 300 L/min inlet flow and 30% water cut.

Q_{tot} [l/min]	WC_{in} [%]	$dPT.2$ [mbar]	WC_r [%]	ER [%]
299.99	70.04	1.26	99.91	97.11
299.92	70.07	1.76	99.90	99.26
299.72	70.10	2.31	99.88	99.88

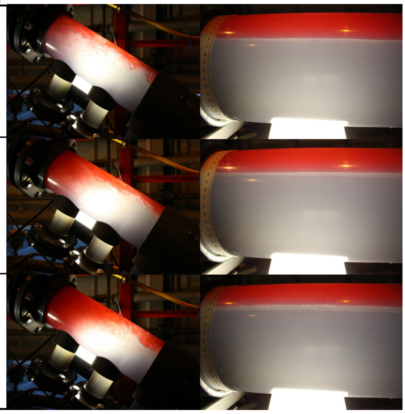

Figure A2. 300 L/min inlet flow and 70% water cut.

Q_{tot} [l/min]	WC_{in} [%]	$dPT.2$ [mbar]	WC_r [%]	ER [%]
499.94	30.25	1.76	100.02	12.18
499.98	30.11	2.21	100.0	24.55
499.96	30.08	3.25	98.12	58.36

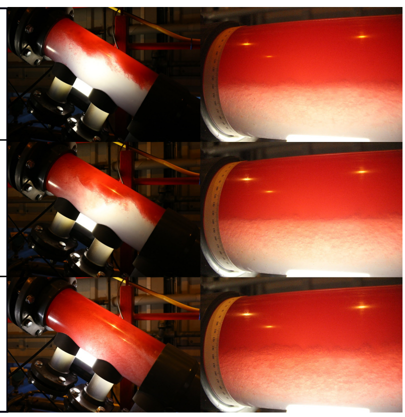

Figure A3. 500 L/min inlet flow and 30% water cut.

Q_{tot} [l/min]	WC_{in} [%]	$dPT.2$ [mbar]	WC_r [%]	ER [%]
499.99	69.83	1.16	99.47	75.44
499.91	69.89	1.70	99.17	80.89
500.15	69.81	2.16	98.80	86.72

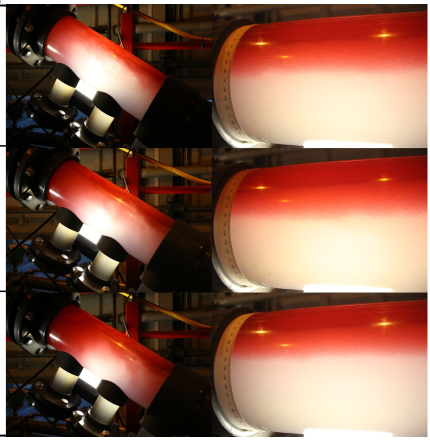

Figure A4. 500 L/min inlet flow and 70% water cut.

References

1. Norwegian Oil and Gas Association. *Environmental Report—Environmental Work by the Oil and Gas Industry, Facts and Development Trends*; Technical Report; Norwegian Oil and Gas Association: Stavanger, Norway, 2017.
2. Hannisdal, A.; Westra, R.; Akdim, M.R.; Bymaster, A.; Grave, E.; Teng, D.T. Compact separation technologies and their applicability for subsea field development in deep water. In Proceedings of the Offshore Technology Conference, Houston, TX, USA, 30 April–3 May 2012; Offshore Technology Conference: Houston, TX, USA, 2012.
3. Backi, C.J.; Skogestad, S. A simple dynamic gravity separator model for separation efficiency evaluation incorporating level and pressure control. In Proceedings of the 2017 American Control Conference (ACC), Seattle, WA, USA, 24–26 May 2017; pp. 2823–2828.
4. Backi, C.J.; Krishnamoorthy, D.; Skogestad, S. Slug handling with a virtual harp based on nonlinear predictive control for a gravity separator. *IFAC-PapersOnLine* **2018**, *51*, 120–125. [CrossRef]
5. Skjefstad, H.S.; Stanko, M. An Experimental Study of a Novel Parallel Pipe Separator Design for Subsea oil–water Bulk Separation. In Proceedings of the SPE Asia Pacific Oil and Gas Conference and Exhibition, Brisbane, Australia, 23–25 October 2018; Society of Petroleum Engineers: Richardson, TX, USA, 2018.
6. Skjefstad, H.S.; Stanko, M. Experimental performance evaluation and design optimization of a horizontal multi-pipe separator for subsea oil–water bulk separation. *J. Pet. Sci. Eng.* **2019**, *176*, 203–219. [CrossRef]
7. Pereira, R.M.; Campos, M.C.M.M.D.; de Oliveira, D.A.; de Souza, R.D.S.A.; Orlowski, R.; Duarte, D.G.; Raposo, G.M.; Lillebrekke, C.; Ljungquist, D.; Carvalho, A.; et al. SS: Marlim 3 Phase Subsea Separation System: Controls Design Incorporating Dynamic Simulation Work. In Proceedings of the Offshore Technology Conference, Houston, TX, USA, 30 April–3 May 2012; Offshore Technology Conference: Houston, TX, USA, 2012.
8. Li, Z.; Olson, M.; Rayachoti, V.; Gupte, P.; Pierre, F.; Gul, K. Subsea Compact Separation: Control System Design. In Proceedings of the Offshore Technology Conference, Houston, TX, USA, 5–8 May 2014; Offshore Technology Conference: Houston, TX, USA, 2014.
9. Olson, M.; Grave, E.; Juarez, J.; Gul, K. Performance Testing of an Integrated, Subsea Compact Separation System with Electrocoalescence for Deepwater Applications. In Proceedings of the Offshore Technology Conference, Houston, TX, USA, 4–7 May 2015; Offshore Technology Conference: Houston, TX, USA, 2015.
10. Grave, E.; Olson, M. Design and Performance Testing of a Subsea Compact Separation System for Deepwater Applications. *Oil Gas Facil.* **2014**, *3*, 16–23. [CrossRef]
11. Sagatun, S.I.; Gramme, P.; Horgen, O.J.; Ruud, T.; Storvik, M. The Pipe Separator-Simulations and Experimental Results. In Proceedings of the Offshore Technology Conference, Houston, TX, USA, 5–8 May 2008; Offshore Technology Conference: Houston, TX, USA, 2008.

12. Minh, V.T. Modeling and control of distillation column in a petroleum process. In Proceedings of the 2010 5th IEEE Conference on Industrial Electronics and Applications, Taichung, Taiwan, 15–17 June 2010; pp. 259–263.
13. Campos, M.; Takahashi, T.; Ashikawa, F.; Simões, S.; Stender, A.; Meien, O. Advanced anti-slug control for offshore production plants. *IFAC-PapersOnLine* **2015**, *48*, 83–88. [CrossRef]
14. Ohrem, S.J.; Holden, C.; Jahanshahi, E.; Skogestad, S. $\mathcal{L}_1$ adaptive anti-slug control. In Proceedings of the 2017 American Control Conference (ACC), Seattle, WA, USA, 24–26 May 2017; pp. 444–449.
15. Ohrem, S.J.; Kristoffersen, T.T.; Holden, C. Adaptive feedback linearizing control of a gas liquid cylindrical cyclone. In Proceedings of the 2017 IEEE Conference on Control Technology and Applications (CCTA), Mauna Lani, HI, USA, 27–30 August 2017; pp. 1981–1987.
16. Skogestad, S.; Grimholt, C. The SIMC method for smooth PID controller tuning. In *PID Control in the Third Millennium*; Springer: London, UK, 2012; pp. 147–175.
17. Skogestad, S.; Postlethwaite, I. *Multivariable Feedback Control: Analysis and Design*; John Wiley & Sons Ltd.: Hoboken, NJ, USA, 2007; Volume 2.
18. Wang, Q.G.; Ye, Z.; Cai, W.J.; Hang, C.C. *PID Control for Multivariable Processes*; Springer: Berlin, Germany, 2008.
19. Hovd, M.; Skogestad, S. Pairing criteria for decentralized control of unstable plants. *Ind. Eng. Chem. Res.* **1994**, *33*, 2134–2139. [CrossRef]
20. Visioli, A. *Practical PID Control*; Springer Science & Business Media: Berlin, Germany, 2006.
21. Ioannou, P.A.; Sun, J. *Robust Adaptive Control*; PTR Prentice-Hall: Upper Saddle River, NJ, USA, 1996; Volume 1.
22. Vázquez, F.; Morilla, F.; Dormido, S. An iterative method for tuning decentralized PID controllers. In Proceedings of the 14th IFAC World Congress, Beijing, China, 5–9 July 1999; pp. 491–496.
23. Huang, H.P.; Jeng, J.C.; Chiang, C.H.; Pan, W. A direct method for multi-loop PI/PID controller design. *J. Process Control* **2003**, *13*, 769–786. [CrossRef]

Chapter 7

Surfactant and inlet choking effect on separator performance, Paper V

This chapter consists of Paper V, which investigates how separator performance is affected by inlet choking and addition of surfactant to the system. Three inlet choke settings are tested, and performance is mapped with and without added surfactant. Supplementary investigation of inlet droplet sizes and flow phenomena are carried out to better understand observed performance trends. Postdoctoral Fellow Marcin Dudek has contributed to the work presented in this paper, and author contributions are listed in Chapter 1. The paper was submitted to the Journal of Petroleum Science and Engineering on May 22nd, and the paper included here is the initially submitted manuscript.

H. S. Skjefstad, M. Dudek, G. Øye and M. Stanko. The effect of upstream inlet choking and surfactant addition on the performance of a novel parallel pipe oil-water separator. *Journal of Petroleum Science and Engineering*, [Submitted manuscript], 2019.

The effect of upstream inlet choking and surfactant addition on the performance of a novel parallel pipe oil-water separator

Håvard S. Skjefstad[a,*], Marcin Dudek[b], Gisle Øye[b], Milan Stanko[a]

[a]*Department of Geoscience and Petroleum, Norwegian University of Science and Technology*
[b]*Department of Chemical Engineering, Norwegian University of Science and Technology*

Abstract

This paper reports the effect of inlet choking and addition of surfactant on the performance of a parallel pipe oil-water separator. These two issues can have a strong effect on oil-water separation in real hydrocarbon production systems.

Experiments were performed with Exxsol™ D60 and salt water. Three choke settings were tested for flow rates in the range 300-500 L/min, with three inlet water cuts and three water extraction rates. The test matrix was run with and without added surfactant. The oil-water distribution and behaviour within the separator is also studied. Droplet size measurements were performed at the separator inlet for droplet size distribution generation in the form of cumulative volume plots.

The study shows that inlet choking has an overall negative effect on separator performance, especially for water-continuous inlet regimes. The maximum decrease in performance due to choking was 14 *pp*, while it was 4 *pp* due to addition of surfactant.

Keywords: Oil-water separation, Droplet size distribution, Surfactant, Inlet choking, Separation efficiency

*Corresponding author
Email address: havard.s.skjefstad@ntnu.no (Håvard S. Skjefstad)

1. Introduction

Produced water management is a topic of increasing importance in the oil and gas industry. Produced water accompanies oil to surface, and in mature fields, often surpasses produced oil in terms of quantity. This is for instance seen on the Norwegian Continental Shelf, where 181 million standard cubic meters of produced water was reported for 2016, amounting to more than two times the amount of produced oil [1]. Produced water is the largest waste stream in oil production and contains a combination of organic and inorganic compounds, which when discharged may contaminate surface and underground water as well as soil [2]. In order to secure safe disposal of produced water, the water must be separated from the oil and treated. Developing more efficient oil-water separator technologies and separation processes are important steps for securing safe disposal of produced water.

Although initially present as two separated phases, the turbulence, mixing and agitation through constrictions, choke valves and pumps will lead to oil-water dispersions (emulsions) being formed during production [3]. These dispersions have to be separated during treatment processes before the fluids are exported (oil) or discharged/re-injected (water). In typical offshore topside processing, the fluids from an oil well are first separated in a gravity separator, where the gas, oil and water are segregated into individual streams based on their respective densities. Separated oil is pumped further to a secondary separator, often equipped with electrocoalescers to aid the growth of water droplets and speed up their sedimentation. At the same time, the produced water is treated in hydrocyclones (enhanced gravitational separation) or gas flotation units, where the removal of dispersed oil is supported by their attachment to gas bubbles. Even though the bulk gravity separator alone often is insufficient to reach the desired quality of crude oil and water [4], its performance plays a key role in the efficiency of the further treatment process. In general, high water content in the crude oil and/or oil content in the produced water downstream the bulk separator can lead to the need for increased residence times and/or circulating flow back to the bulk separator inlet. Consequently, the performance of the first-stage separator will determine the production capacity and for that reason be crucial for the entire petroleum production chain [5].

For a topside installation, the process stream is choked before entering the first stage bulk separator. This choking process serves as a large energy input to the stream, which causes subsequent dispersed-phase breakup into small droplets (emulsions). Emulsions are kinetically-stabilized liquid-liquid dispersions that are challenging to separate. What dictates the size of these droplets is the chemical composition and interfacial properties of the respective fluid components, and the level of energy input in the droplet formation process. In complex fluid systems, such as crude oil, the kinetics of coalescence between droplets is thus an important factor to the separation process. Merging of micron-sized droplets can greatly speed up creaming or sedimentation of droplets [6], as dictated by Stokes law of gravity separation, stating that the rising velocity is proportional to the square of the droplet radius. Coalescence, however, can also be hindered by the presence of crude oil-indigenous surface-active components (e.g. asphaltenes, resins or naphthenic acids), which can adsorb at the oil-water interface and stabilize the droplets against merging [7]. A second effect of topside transportation is lowering of pressure. For production streams containing dissolved CO_2, a reduction in pressure will result in an increase in pH. A pH increase will lead to higher surface charges on dispersed oil droplets, which further increases stability of the oil in water emulsions, hindering separation.

Knowledge of droplet size distributions and kinetics in oil-water dispersions/emulsions are thus important for sizing of separator equipment. Break up of two-phase oil-water flow and subsequent droplet distribution analysis has been reported in several publications in the past. In [8], Schümann et al. compared focus beam reflectance measurements (FBRM) and particle video microscopy (PVM) for droplet size measurement in oil-water dispersions. PVM measurements of known particle samples were shown to give correct droplet size distributions. Further, in [9], Fossen and Schümann investigated two-phase oil-water breakup over a butterfly valve at different pressure losses, water cuts and flow rates. However, the resulting effect on separator performance is rarely reported.

Separating oil and water on the seabed can mitigate some of the discussed issues of topside processing. By separating closer to the wells, and maintaining a high pressure, less problems with emulsion formation and emulsion stability is expected [10]. In addition, separating close to the well means less mixing and turbulence, and the energy losses associated with transporting the water to surface are reduced. However, inlet choking (e.g wellhead choking) and stabilizing surfactants might still affect separator performance. The direct effect inlet choking and stabilizing surfactants has on separator performance is rarely reported in the literature. The aim of this paper is therefore to investigate the direct effect inlet choking and stabilizing surfactant has on downstream bulk separator performance. Steady state measurements will be used to evaluate separator performance at varying inlet choke settings, water cuts and total flow rates, and pictures off occurring flow phenomena in the separator as well as droplet size distributions upstream the separator inlet will be used for supplementary evaluation. The results of this paper will give a better understanding of how up-stream disturbances affect oil-water bulk separator performance. Subsequently, the paper results can give an indication of the potential benefit of subsea separation, where upstream disturbances are reduced.

2. Methodology

2.1. Separator concept

Experiments are carried out on a parallel pipe bulk oil-water separator concept prototype. The separator design was based on a state of the art subsea separator technology review [11], and is presented in [12] and [13]. The concept has been named Multiple Parallel Pipe Separator (MPPS), and an illustration of the constructed prototype is given in Figure 1. A multiphase oil-water feed stream enters at the separator inlet ($\dot{Q}_{in}$). The inlet has a tangential configuration, promoting initial cyclonic separation. The fluids pass through a set of novel phase re-arranging internals, enforcing a radial to horizontal phase arrangement transition, before near complete separation is achieved in the horizontal pipe sections. Extraction of water ($\dot{Q}_{e_w}$) is performed in an upwards inclined pipe segment. The upwards inclination increases the water hold up at the extraction point, easing controlled extraction. Oil is extracted in its separate outlet ($\dot{Q}_{e_o}$). The prototype is constructed in 150.6 mm internal diameter (ID) transparent polyvinyl chloride (PVC) pipes, and has a total horizontal length of 6.1 m. Full dimensions of the prototype are given later in Figure 3. Detailed information on design justifications can be found in [12], while a detailed overview of the inlet design and internal functionality and placement is found in [13].

2.2. Test facility

The test facility is a two-phase oil-water flow loop. Test fluids are distilled water with added 3.2 $wt\%$ NaCl and Exxsol^{TM} D60 with 0.015 g/L Oil Red O for phase distinction. Additionally, 750 *ppm* IKM CC-80 has been added to the water for bacterial growth inhibition, and 15 ppm of the surfactant Span$^{®}$85 was added to the Exxsol^{TM} D60 for selected experimental points.

Figure 1: MPPS prototype

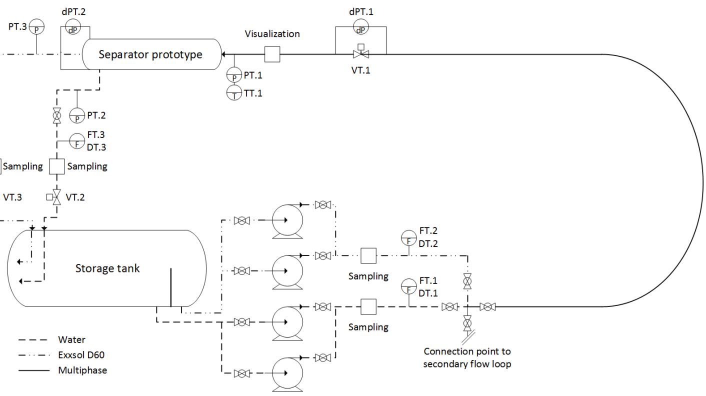

Figure 2: Test facility P&ID

Details on test fluid properties and behaviour is found in Section 2.4. A pipe and instrumentation diagram (P&ID) of the facility is given in Figure 2.

The storage tank is a 6 m^3 (1.2 m diameter, 5.5 m long) gravity vessel providing baseline separation. Downstream the storage tank, a pump manifold boosts the respective clean phases to desired flow rate and water cut (WC). The pumps used in these experiments are centrifugal pumps, with respective flow capacities of 100-700 L/min (55 m max head). The pumps are controlled by 0-50 Hz frequency converters, 50 Hz constituting a maximum rpm of 2900. The flow rate and phase purities (densities) are monitored by two installed Coriolis flow meters (FT.1/2 and DT.1/2). The feed streams then enter a Y-junction, where they merge to a multiphase flow line. The multiphase flow line is a 13 m long 67.8 mm ID transparent PVC pipeline, leading to the inlet of the constructed separator prototype. A full-bore ball valve (VT.1) is installed 2 m upstream the separator inlet. This valve is used for choking of the inlet flow. The pressure loss over the valve is monitored by a differential pressure sensor (dPT.1), measuring from directly upstream to 5 ID downstream the valve. 1 m downstream VT.1 a particle video microscopy (PVM) probe insertion point for droplet size distribution measurements is placed. Pressure (PT.1) and temperature (TT.1) are measured at the prototype inlet. Two return lines are connected to the prototype outlets ($\dot{Q}_{e_w}$, $\dot{Q}_{e_o}$). The water return line is fitted with a third Coriolis flow meter (FT.3/DT.3), allowing monitoring of extraction rate (ER) and the purity of the extracted water. Both return lines are 67.8 mm ID PVC pipes leading back to the storage tank. Pressure is measured in both lines (PT.2/3), and both lines have choke valves installed for extraction rate adjustment. The water return line is fitted with an electrically controlled ball valve (VT.2), while the oil return line has a pneumatic membrane valve (VT.3).

2.3. Test parameters and procedure

All experiments carried out in this paper are steady state tests. The test matrix is given in Table 1. Three inlet choke levels were tested. The first was open valve (the valve is a fullbore valve, hence no induced pressure loss over VT.1), then $dPT.1 = 50\ mbar$ and $dPT.1 = 100\ mbar$. Three total inlet flow rates ($\dot{Q}_{tot}$) were tested for each choke configuration, three inlet water cuts (WC_{in}) were tested for each flow rate, and three extraction rates were tested for each WC_{in}. The matrix was first completed with no added surfactant, then re-run with 15 *ppm* of the surfactant Span®85 added to the Exxsol™ D60. The total number of test points add up to 162.

Tests for one inlet choke configuration were carried out over one day. The system was then given one day resting before the next choke setting was tested. This was done to ensure complete phase separation in the storage tank in between testing, hence securing comparable initial conditions for the respective test configurations. The open valve tests were run first, followed by the 50 $mbar$ then 100 $mbar$ choke tests. The initial test point was $\dot{Q}_{tot} = 300\ L/min$, 30 % WC, 50 % ER. The matrix was systematically executed by increasing ER, then WC, then total flow rate, until the final test point of $\dot{Q}_{tot} = 500\ L/min$, 70 % WC, 90 % ER was reached.

All recorded parameters are listed in Table 2. Logging was performed at 5 Hz, with a log time of 60 s, giving a total of 300 samples per test point.

Table 1: Test matrix

$dPT.1$ $[mbar]$	$\dot{Q}_{tot}$ $[L/min]$	WC_{in} [%]	ER [%]
-	300	30/50/70	50 70 90
	400	30/50/70	50 70 90
	500	30/50/70	50 70 90
50	300	30/50/70	50 70 90
	400	30/50/70	50 70 90
	500	30/50/70	50 70 90
100	300	30/50/70	50 70 90
	400	30/50/70	50 70 90
	500	30/50/70	50 70 90

Mean values of recorded parameters are used for subsequent calculation. The three Coriolis meters were used to adjust the inlet flow rate and water cut, monitor phase purities, determine the amount of water extracted from the MPPS prototype, and the purity of the extracted water. The WC in the respective flow lines is determined by:

$$WC_i = \frac{\rho_i - \rho_o}{\rho_w - \rho_o} \tag{1}$$

Here, ρ_i is the measured density at DT.1/2/3, while ρ_w and ρ_o are the pre-determined temperature corrected densities of the water and Exxsol^{TM} D60. For pure feed streams, WC_1 should be equal to 100 % while WC_2 should be equal to 0 %. From calculated WC and measured flow rates, the actual WC at the MPPS prototype inlet (WC_{in}) is calculated.

$$WC_{in} = \frac{WC_1\dot{Q}_1 + WC_2\dot{Q}_2}{\dot{Q}_1 + \dot{Q}_2} \tag{2}$$

$\dot{Q}_1$ and $\dot{Q}_2$ are the respective water and Exxsol^{TM} D60 feed streams. When running experiments, $\dot{Q}_1$ and $\dot{Q}_2$ are adjusted such that the desired total flow ($\dot{Q}_{tot}$) and WC_{in} is reached. $\dot{Q}_{tot}$ is simply the sum of $\dot{Q}_1$ and $\dot{Q}_2$.

The amount of water extracted from the MPPS prototype is determined by the ER. The ER is the flow rate through the water extraction line (FT.3) divided by the flow rate in the water feed line (FT.1):

Table 2: Recorded parameters

Tag	Parameter	Unit
FT.1	$\dot{Q}_1$	L/min
FT.2	$\dot{Q}_2$	L/min
FT.3	$\dot{Q}_3$	L/min
DT.1	ρ_1	kg/m^3
DT.2	ρ_2	kg/m^3
DT.3	ρ_3	kg/m^3
PT.1	P_1	$barg$
PT.2	P_2	$barg$
PT.3	P_3	$barg$
dPT.1	dP_1	$mbar$
TT.1	T_1	$°C$

$$ER = \frac{\dot{Q}_3}{\dot{Q}_1} \tag{3}$$

As the test loop is a closed system, the water and Exxsol^{TM} D60 phases will be contaminated over time. Microscopic droplets of water will be dispersed in the oil and vise versa. In order to give a performance measurement that is independent of occurring contamination, a WC ratio (WC_r) is calculated. The WC ratio is equal to the WC at the water extraction line (WC_3) divided by the WC at the water feed line (WC_1).

$$WC_r = \frac{WC_3}{WC_1} \tag{4}$$

A WC_r equal to 100 % means that the extracted water from the MPPS prototype is of equal quality to the water leaving the baseline separator (storage tank).

Particle video microscopy (PVM) was used for droplet size measurement in this study. The probe utilized was a PVM V819 probe from Mettler Toledo. The probe provides real time in situ digital gray scale images for droplet size measurement. The technology uses a high resolution CCD camera and internal illumination to obtain high quality images. A reflector cap was fitted

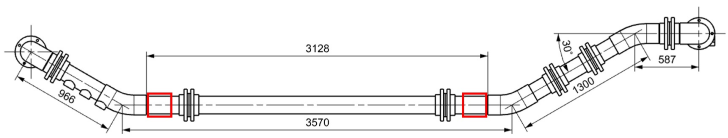

Figure 3: Prototype dimensions [mm] with illustrated picture location

to the end of the probe for better image quality. The selected reflector cap has a 4 mm spacing from the probe window. The field of view is 1075 x 825 μm, with a resolution of 2 μm. The output image from the PVM has a resolution of 1360 x 1024 $pixels$, giving a conversion factor of 0.8 $\mu m/pixel$.

PVM pictures were taken for all flow rates and water cuts, at the 50 % ER point. The PVM probe was inserted in the previously mentioned PVM insertion point, at a 45° angle. Pictures were taken at two heights, 0.15 and 0.85 ID from the top of the internal feed pipe wall. This gives a total of 18 picture series per inlet choke setting, and a grand total of 108 picture series. For every picture series, 100 pictures were taken at a frequency of 2 Hz. For future references, the 0.15 ID insertion point will be referenced as the top location, and the 0.85 ID point as the bottom location. These heights were chosen based on observed flow regimes at the separator inlet with open inlet choke, securing probe placement in the established water and oil layers for the 30 % and 70 % inlet WC test points respectively.

Photos of flow phenomena in the horizontal pipe sections were taken to improve the understanding of measured performance trends. Pictures were taken at the start and end of the respective pipe sections, as illustrated in Figure 3. The figure also includes overall dimensions of the MPPS prototype, as well as the distance between the picture points.

Additionally, pictures were taken directly upstream the MPPS inlet (in the 67.8 mm ID feed-pipe) for inlet flow regime determination.

The following test procedure was followed for all test points:

1. Total flow, WC_{in} and ER adjusted to desired values
2. Inlet choke valve adjusted for desired dPT.1 value
3. System operated for five times the corresponding MPPS residence time for steady state behaviour. Respective residence times vary from approximately 30 to 50 s
4. When ER equal to 50 %, PVM inserted at respective heights and 100 pictures taken

Table 3: Fluid properties @ 15°C

Fluid sample	ρ $[kg/m^3]$	μ $[cP]$	σ_{ow} $[mN/m]$
Water[b]	1021.05	1.20	16.1
Exxsol™ D60[b]	795.74	1.61	
Water[a]	1021.06	1.19	15.8
Exxsol™ D60[a]	795.76	1.61	
Water[b*]	1021.06	1.19	16.1
Exxsol™ D60[b*]	795.78	1.60	
Water[a*]	1021.04	1.21	16.2
Exxsol™ D60[a*]	795.75	1.59	

[a] After experiment
[b] Before experiment
[*] With 15 *ppm* Span®85

5. PVM removed
6. If PVM pictures taken, subsequent steady state operation period of five times the corresponding MPPS prototype residence time
7. Picture taken of the inlet flow regime
8. Separator performance logged
9. Pictures taken of flow distribution at entrance and exit of horizontal pipe segments

2.4. Fluid characterization

In order to validate comparability of results, fluid samples from the storage tank were collected before and after each test campaign for density, dynamic viscosity and interfacial tension (IFT) determination. Density measurements were performed with an Anton Paar DMA™ 5000M densitometer. Viscosities were measured with an Anton Paar Physica MCR 301 rheometer. Densities and viscosities were measured between 10-20°C with 2.5°C intervals. The mean values at 15°C are reported in Table 3. The IFT between the respective oil and water samples were measured with a DataPhysics SVT20 spinning drop video tensiometer at 15°C, and is also reported in Table 3. Each measurement was repeated twice. The standard deviation for the viscosity tests is in the range of 1 %, while it is between 1 and 4 % for the IFT measurements.

The measured reference density curves for water and Exxsol^{TM} D60 used in reported experiments are given in Eqs. 5 and 6.

$$\rho_w = -0.0048{T_1}^2 - 0.0722T_1 + 1023.2 \tag{5}$$

$$\rho_o = -0.7319T_1 + 806.72 \tag{6}$$

A series of IFT measurements were performed to characterize the interfacial properties of the studied system. It was found that the used Exxsol^{TM} D60 and water already exhibited interfacial activity, even before adding surfactant. By performing tests in which one of the phases was replaced with a clean sample of Exxsol^{TM} D60 or salt water (e.g. freshly prepared salt water with the Exxsol^{TM} D60 sampled from the test facility storage tank), it was observed that the IFT did not differ from the values obtained from the sampled Exxsol^{TM} D60 and water. All measurements were approximately 16 mN/m, which is remarkably close to other crude oil and brine systems reported in literature [14, 15]. By contrast, the IFT for a pure (non-sampled) salt water and Exxsol^{TM} D60 system was close to 40 mN/m. Measurements were also performed on a system without the biocide – pure salt water and pure Exxsol^{TM} D60 with the addition of the Oil Red O dye. These revealed higher IFT values (approximately 25 mN/m), and also considerably slower equilibration, compared to the systems with the biocide present. Therefore, it is suspected that the biocide added to the system, which appears to some extent be both oil- and water-soluble, is mostly responsible for the interfacial activity demonstrated in this system.

Additional IFT measurements and bottle tests were performed on the fluids before adding the surfactant to pre-determine its effect and avoid under- or overdosage. IFT measurements were done with the above-mentioned spinning drop tensiometer. The bottle tests were conducted by adding appropriate amounts of oil (with and without the surfactant) and water to a vial (with similar proportions as in the experimental matrix), mixing them at 10 000 rpm for 30 seconds and visually following the separation. All of these tests were performed in room temperature (approximately 23°C).

The IFT measurements with surfactant revealed that adding 10 ppm of surfactant to the Exxsol^{TM} D60 had virtually no effect on the IFT of oil and water, whereas the addition of 25 ppm of Span$^{®}$85 to the sampled oil phase caused the IFT to be lowered to 13.5 mN/m, and 50 ppm of the surfactant resulted in the IFT value of approximately 12 mN/m. Conducted bottle tests reflected these results. In the bottle tests, 10 *ppm* of surfactant did not significantly change the emulsion behaviour, compared to the system without the additive. After adding 25 *ppm* of the surfactant, the formation of a stable emulsion phase at 30 % and 50 % WC could be observed, which prolonged the separation process several times. This effect was multiplied when the higher concentration of surfactant (50 *ppm*) was tested, where the separation took more than one hour. In both cases, however, the separation was quite quick at the highest water cut. Based on the observed bottle test results and previous experience that over-dosage of surfactant can lead to extremely stable emulsions, it was decided that 15 *ppm* of the surfactant was a fitting concentration for the large scale separator tests.

2.5. Droplet size measurement

Recorded PVM pictures were used for calculating droplet size distributions. For each test point, all captured pictures were analysed with an image analysis software (SOPAT GmbH, Germany), automatically registering individual droplet diameters. Subsequently, recorded droplet diameters were used to generate cumulative volume fraction (Q_f) distributions (Eq.7) for the respective test points. In Eq.7, d_i is the individual recorded droplet diameters in the respective samples. Plots are given for d ranging from 1 to 600 μm, 600 μm being above d_{max} for all test points.

$$Q_f(d) = \frac{\sum \pi {d_i}^3/6 \quad for \quad d_i \leq d}{\sum \pi {d_i}^3/6 \quad for \quad d_i \leq d_{max}} \tag{7}$$

The SOPAT image analysis software is thoroughly outlined in [16], and has seen recent applications in [17] and [18].

In addition to cumulative volume fraction plots, the Sauter mean diameter (d_{32}) and the 50 % median volume based diameter (d_{v50}) are provided for additional trend analysis.

3. Results

3.1. Inlet flow regime

The flow regime at the inlet was mapped for all test points. Identification was based on illustrations given by Trallero et al. [19], and previous identification by the authors [13]. Four different flow regimes were identified: stratified mixed (SM), dispersed oil in water and dispersed water in

Table 4: Flow regime at MPPS inlet

$\dot{Q}_{tot}$ $[L/min]$	WC_{in} [%]	No choke	50 $mbar$ choke	100 $mbar$ choke
300	30	SM	Dw/o	Dw/o
	50	SM	Do/w	Do/w
	70	SM	Do/w	Do/w
400	30	SM	Dw/o	Dw/o
	50	SM	Do/w	Do/w
	70	SM	Do/w	Do/w
500	30	Do/w+Dw/o	Dw/o	Dw/o
	50	Do/w+Dw/o	Do/w	Do/w
	70	Do/w+Dw/o	Do/w	Do/w

oil (Do/w+Dw/o), dispersed oil in water (Do/w) and dispersed water in oil (Dw/o). Regimes for the respective test points are listed in Table 4.

Recorded flow regimes were similar for the no-surfactant and surfactant tests. Pictures of captured flow regimes are included in Appendix A.

3.2. Separator performance and flow phenomena

The calculated WC_r for the no-surfactant test points are given in Figure 4. The calculated WC_3 for the same test points are included in Appendix A, Figure A.17. In Appendix A, the reader will also find tables of all recorded data, with associated errors, for the respective test points. The maximum error in reported WC_r values is 0.4 *pp*. Included errors are linearity, hysteresis, quantization, data acquisition and random error in the measurements.

The effect of inlet choking is clearly visible when looking from Figure 4a, 4d, 4g (No choke), to Figure 4b, 4e, 4h (50 *mbar* choke) and Figure 4c, 4f, 4i (100 *mbar* choke). At 50 % ER, a slight decrease in performance is observed when applying inlet choking for an inlet WC of 50 % and a total flow rate of 500 L/min. For the same flow rate, a slight increase in performance is seen for 30 % WC_{in} when moving from no-choke to applied inlet choking. The same trend is observed when increasing the extraction rates. The reduction in performance is more severe for high total flow rates, high pressure drops over the choke, and medium inlet water cut. The maximum reduction observed in WC_r is 14 *pp* when compared against the no choking case. For low inlet water cut, the effect of inlet choking on WC_r is negligible or, for the high total flow rate case, improving separation with a maximum of 3 *pp*.

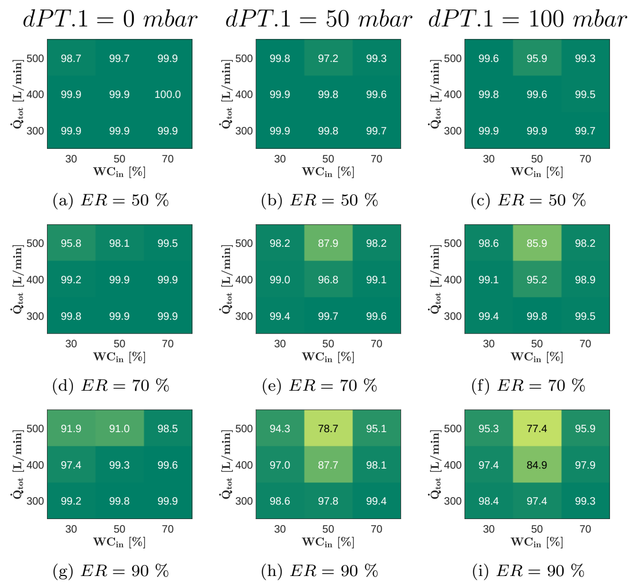

Figure 4: WC_r [%] results for $dPT.1$ = 0, 50, 100 $mbar$ and ER = 50, 70, 90 % for the no surfactant tests

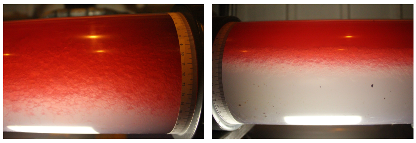

(a) Entry, no choke (b) Exit, no choke

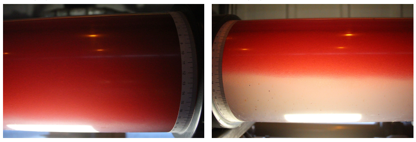

(c) Entry, 100 $mbar$ choke (d) Exit, 100 $mbar$ choke

Figure 5: Flow phenomena at the start and end of the horizontal pipe sections for the no-surfactant tests at $\dot{Q}_{tot} = 400\ L/min$, $WC_{in} = 50$ % and ER = 90 %. Pictures are given for no choke and 100 $mbar$ choke

Captured flow phenomena in the horizontal pipe sections supports observed trends in logged performance. In Figures 5 to 8, flow phenomena at the start and end of the horizontal pipe sections are given. Included pictures are for 30 % and 50 % inlet WC, with $\dot{Q}_{tot} = 400$ and 500 L/min, displaying flow phenomena with open inlet choke and for a dPT.1 pressure of 100 $mbar$. Flow phenomena were similar in both pipe segments, and for this reason, pictures of only one pipe have been included. Observed trends for the 70 % WC_{in} test points were the same as for the 50 % WC_{in}, and are not shown.

Figure 5 and 6 shows the flow distribution at 50 % inlet water cut.

From presented pictures it is clearly seen how inlet choking affects dispersion at both the start and end of the horizontal pipe sections. A clear increase in dispersion layer thickness is observed at the end of the horizontal pipe, and an increase in flow rate is observed to further increase both the layer thickness and the effect of inlet choking. A result of this increased dispersion layer is an increased chance of extracting the dispersion with the water at high extraction rates. This corresponds well with reported data in Figure 4, where a drastic decrease in WC_r at 90 % ER is observed for 50 % WC_{in} at $\dot{Q}_{tot} = 400$ and 500 L/min, the latter being worse. It should also be noted that the forming dispersion layer in the pipes is water-continuous. A clear/sharp boundary is observed between the pure oil layer and dispersion layer, while the boundary between the water and dispersion layer is more gradual.

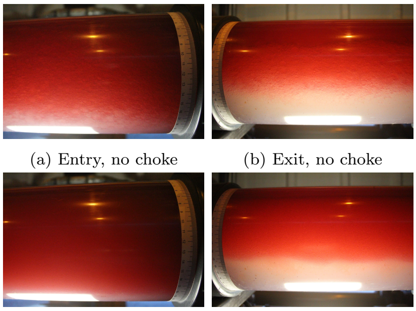

(a) Entry, no choke (b) Exit, no choke

(c) Entry, 100 $mbar$ choke (d) Exit, 100 $mbar$ choke

Figure 6: Flow phenomena at the start and end of the horizontal pipe sections for the no-surfactant tests at $\dot{Q}_{tot} = 500\ L/min$, $WC_{in} = 50\ \%$ and ER = 90 %. Pictures are given for no choke and 100 $mbar$ choke

A different behaviour is observed for the 30 % inlet WC test points (Figure 7 and 8)

From presented pictures there is little to no observed effect of inlet choking. For $\dot{Q}_{tot} = 400\ L/min$, both entry and exit of the horizontal pipe section looks unchanged. At $\dot{Q}_{tot} = 500\ L/min$ a slight decrease in the formed dispersion layer thickness is detectable for the 100 $mbar$ inlet choke case. This is again consistent with presented data in Figure 4. At 300 and 400 L/min, no significant effect of inlet choking is detected for the 30 % WC_{in} test points. However, at 500 L/min, an increase in WC_r is observed at high ER. Again, the formed dispersion layer at the exit of the separator pipes is seen to be water-continuous.

The calculated WC_r for the 15 ppm Span®85 test points display the same trends as for for the no-surfactant tests. A decline in WC_r is observed with increasing pressure drop over the inlet choke. However, an exception from the no-surfactant trend is observed for the 30 % inlet WC test points. For the system with no surfactant (Figure 4), an increase in WC_r was observed at $\dot{Q}_{tot} = 500\ L/min$ when the pressure loss over the inlet choke was increased. This is not the case after adding surfactant. For the surfactant case, the WC_r is stable when going from open choke to 50 $mbar$ pressure loss, and drops when increasing the pressure loss to 100 $mbar$. Plots of WC_r and WC_3 for the surfactant tests are included in Appendix A, Figure A.18 and Figure A.19. Again, the maximum error in reported WC_r values is 0.4 pp.

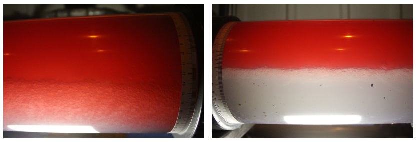

(a) Entry, no choke (b) Exit, no choke

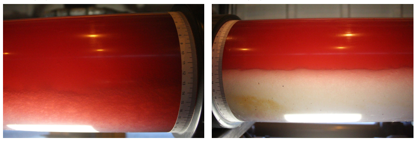

(c) Entry, 100 $mbar$ choke (d) Exit, 100 $mbar$ choke

Figure 7: Flow phenomena at the start and end of the horizontal pipe sections for the no-surfactant tests at $\dot{Q}_{tot} = 400\ L/min$, $WC_{in} = 30\ \%$ and ER = 90 %. Pictures are given for no choke and 100 $mbar$ choke

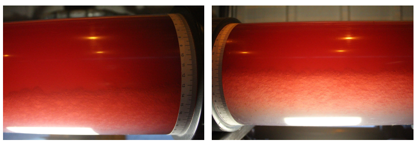

(a) Entry, no choke (b) Exit, no choke

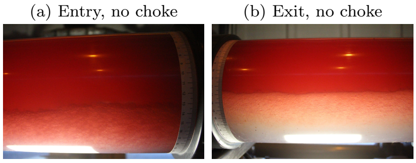

(c) Entry, 100 $mbar$ choke (d) Exit, 100 $mbar$ choke

Figure 8: Flow phenomena at the start and end of the horizontal pipe sections for the no-surfactant tests at $\dot{Q}_{tot} = 500\ L/min$, $WC_{in} = 30\ \%$ and ER = 90 %. Pictures are given for no choke and 100 $mbar$ choke

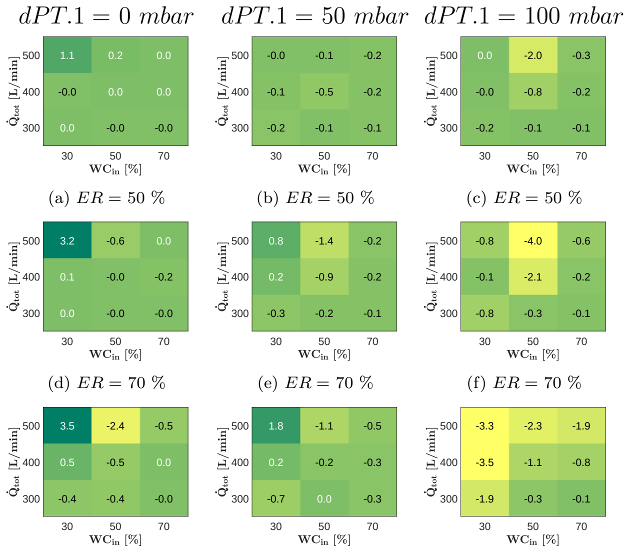

(a) $ER = 50$ % (b) $ER = 50$ % (c) $ER = 50$ %

(d) $ER = 70$ % (e) $ER = 70$ % (f) $ER = 70$ %

(g) $ER = 90$ % (h) $ER = 90$ % (i) $ER = 90$ %

Figure 9: Difference [*pp*] between the surfactant and no-surfactant WC_r results for $dPT.1 = 0$, 50, 100 $mbar$ and $ER = 50$, 70, 90 %

In Figure 9 the effect of adding surfactant is illustrated. The figure shows calculated WC_r for the surfactant tests (Figure A.18) subtracted the WC_r of the no-surfactant tests (Figure 4). The results are given in percentage points (*pp*), where a negative value indicates a decrease in performance, and a positive value indicates an increase in performance.

Adding surfactant has a general negative effect on the separator performance for the 50 % and 70 % WC_{in} test points. A maximum decrease of 4 *pp* is observed for $\dot{Q}_{tot} = 500\ L/min$, at 50 % WC_{in} and 70 % ER. However, an increase in performance is observed for the 30 % WC_{in}, $\dot{Q}_{tot} = 500\ L/min$ test point at the no choke and 50 $mbar$ choke settings.

In Figure 10 and 11, captured flow phenomena for the surfactant tests are shown. The figure displays flow phenomena at the horizontal pipe exit for the same test points as in Figure 5 to 8. Comparing these figures, there is no significant change detected from adding surfactant at a 50 % inlet WC, except a small increase in the dispersion layer for the no choke test points.

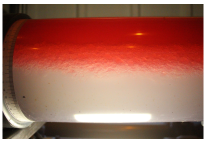

(a) $\dot{Q}_{tot} = 400\ L/min$, no choke

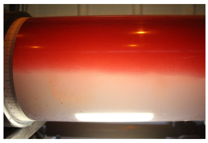

(b) $\dot{Q}_{tot} = 400\ L/min$, 100 $mbar$ choke

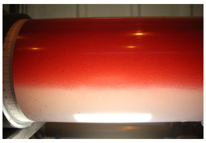

(c) $\dot{Q}_{tot} = 500\ L/min$, no choke

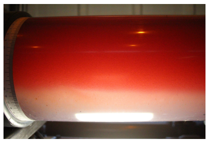

(d) $\dot{Q}_{tot} = 500\ L/min$, 100 $mbar$ choke

Figure 10: Flow phenomena at the exit of the horizontal pipe sections for the the 15 ppm Span®85 tests at $WC_{in} = 50$ % and ER = 90 %. Pictures are given for no choke and 100 $mbar$ choke

For the 30 % WC_{in} test points however, a small change is noted. For the no choke test point at $\dot{Q}_{tot} = 500\ L/min$, the formed dispersion layer is observed to be more "compact" and smaller in size compared to the no-surfactant test in Figure 8. At the same time, the 100 $mbar$ choke test points display a larger dispersion layer compared to the equivalent no-surfactant test points. This does again support results reported in Figure 9, where an increase in WC_r is seen for $\dot{Q}_{tot} = 500\ L/min$, 30 % WC_{in} no-choke, while a drop in WC_r is seen for all flow rates at 30 % WC_{in} at 100 $mbar$ inlet choking. Similarly to the no-surfactant tests, formed dispersion layer in the separator pipes is seen to be water-continuous.

3.3. Droplet distributions

Droplet distributions are presented as cumulative volume fraction vs. droplet diameter plots. Markers are included at 50 μm intervals. The plot gives a representation of the accumulated volume of all droplets up to a specified diameter, divided by the total volume of all droplets recorded. When comparing plots of test points with the same inlet WC, a shift to the left will indicate more, and smaller droplets being recorded, while a shift to the right indicates fewer and larger droplets being recorded. Plots are however sensitive to large drops, as the volume is a function of the diameter cubed. This means that a rightward shift can also be induced by a few large droplet

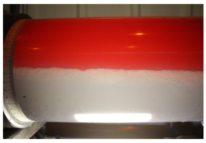

(a) $\dot{Q}_{tot} = 400\ L/min$, no choke

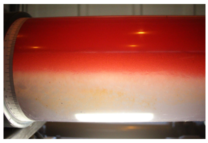

(b) $\dot{Q}_{tot} = 400\ L/min$, 100 $mbar$ choke

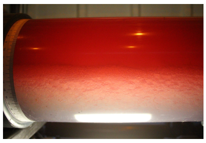

(c) $\dot{Q}_{tot} = 500\ L/min$, no choke

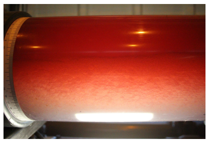

(d) $\dot{Q}_{tot} = 500\ L/min$, 100 $mbar$ choke

Figure 11: Flow phenomena at the exit of the horizontal pipe sections for the the 15 ppm Span®85 tests at WC_{in} = 30 % and ER = 90 %. Pictures are given for no choke and 100 $mbar$ choke

recordings, which does not necessarily represent the overall trend for the test point. In addition, plotted distributions represent the fraction of phases that are dispersed, and any continuous regimes are not captured by the distribution. This means that for test points with inlet regimes that are not fully dispersed, a cumulative volume fraction of 1 will not represent the actual fraction of the respective phase.

Based on reported flow regimes at the separator inlet, bottom location data (oil drops in water) are presented for the 50 % and 70 % WC_{in} test points, while top location data (water droplets in oil) are presented for the 30 % WC_{in} test points. The average number of droplets captured per test point (droplet diameters used for distribution calculation) was 2402 for the no-surfactant tests and 3457 for the surfactant tests. The overall minimum number of droplets captured for one test point was 874.

In Figure 12, results for 50 % WC_{in} at dPT.1 = 100 $mbar$ and increasing flow rates are given. It is clear that an increase in flow rate results in a leftward shift in the distribution. This indicates an increased fraction of smaller droplets, and hence more difficult separation conditions. For $\dot{Q}_{tot}$ = 400 and 500 L/min, the addition of surfactant is observed to cause a further shift to the left.

The same trend as in Figure 12 is observed for 50 $mbar$ choke and the 70

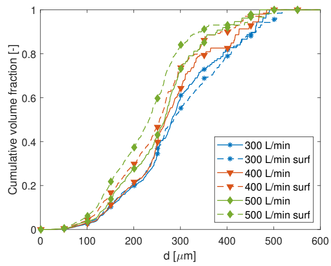

Figure 12: Cumulative volume fraction for $WC_{in} = 50$ %, $dPT.1 = 100\ mbar$

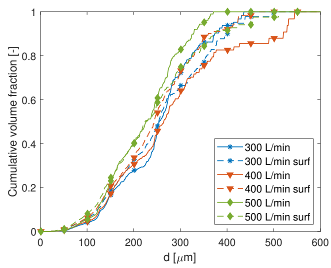

Figure 13: Cumulative volume fraction for $WC_{in} = 30$ %, $dPT.1 = 100\ mbar$

% WC_{in} test points, which distributions are included in Appendix A.

The distribution for 30 % WC_{in} at $dPT.1 = 100\ mbar$ is given in Figure 13.

In the sub 250 μm droplet diameter range, the trend is similar to the 50 % and 70 % WC_{in} test points. Above 250 μm, however, the trends are not as consistent. In the case of two flow rates (300 and 500 L/min), the addition of surfactant results in a rightward shift of the cumulative fractions, indicating that larger droplets are detected. An opposite observation is made for the remaining flow rate, where the additive is seen to decrease the water droplet sizes. It should be noted that in this case, a significant contribution from the above 500 μm droplets is present, which can influence the outcome of the plot, as previously discussed.

A different trend is observed for the no choke test points. Figure 14 displays the distribution for the 30 % WC_{in} cases.

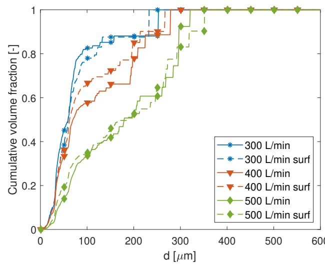

Figure 14: Cumulative volume fraction for $WC_{in} = 30$ %, no choke

The graph shows a shift to the right for increasing flow rates. Although higher flow rates usually mean higher turbulence levels, and hence smaller droplet sizes, it is in this case believed that the level of dispersion of both phases influence the results. For the no choke test points, the majority of the oil and water exists as continuous phases. At low flow rates, most of the dispersed droplets will be smaller droplets that were not separated out in the storage tank and thus recirculated in the test loop. At higher flow rates however, larger droplets will start to get entrained and dispersed in the respective continuous phases. This explanation is supported by flow regimes reported in Table 4, and in pictures given in Appendix A. A similar trend is seen for the 50% and 70 % WC_{in} test points. The recirculation of small droplets can be illustrated with simplified Stoke's law terminal creaming/sedimentation velocity estimations. Given reported fluid properties in Table 3, a tank diameter of 1.2 m (with 90 % liquid area) and an effective separation length of 5 m, a 50 μm diameter droplet will achieve a creaming/sedimentation distance of 0.23 m and 0.18 m respectively, for a total flow rate of 300 L/min. This is not sufficient to fully separate in the storage tank.

In Figure 15 the effect of inlet choking is shown. The figure shows cumulative volume plots for $\dot{Q}_{tot} = 500$ L/min, 50 % WC_{in} test points at the respective choke settings.

It is clear that the no-choke test points have the smallest droplets, which agrees with the previous explanation. Of the two choke settings (where the inlet regimes are fully dispersed), 50 $mbar$ displays overall larger droplet sizes, which agrees with expectations (smaller droplets for larger energy input) and presented WC_r results. For the choked inlet streams, adding surfactant is seen to shift the distribution to the left, indicating smaller droplets and

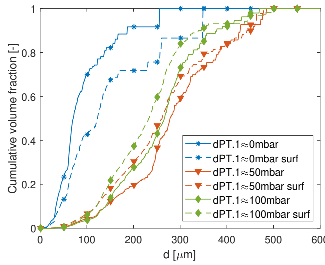

Figure 15: Cumulative volume fraction at respective droplet diameters and choke settings for $\dot{Q}_{tot} = 500\ L/min$, $WC_{in} = 50\ \%$

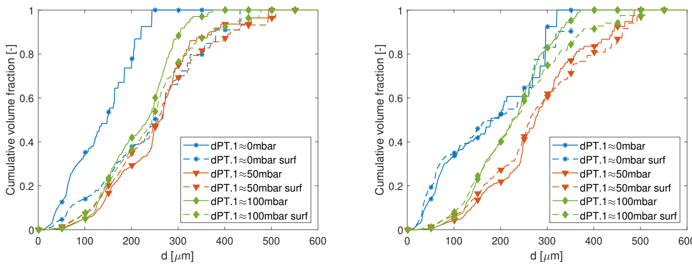

(a) bottom location (b) top location

Figure 16: Cumulative volume fraction for $\dot{Q}_{tot} = 500\ L/min$, $30\ \%\ WC_{in}$

hence slower separation. This also agrees with reported WC_r data. The distribution trends are the same for the 70 % WC_{in} test points.

The top and bottom cumulative volume fraction distributions for the $\dot{Q}_{tot} = 500\ L/min$, 30 % WC_{in} test point are given in Figure 16.

The top distribution displays a similar trend as for the 50 % WC_{in} case, however, a slight shift to the right is observed when adding surfactant. A rightward shift for the open and 50 $mbar$ choke settings is more clear for the bottom location distribution, which supports reported WC_r results for these test points.

The $d32$ data for all bottom location recordings are presented in Table 5.

For the water-continuous inlet regimes (50 and 70 % inlet water cut) a clear trend is observed. Smallest droplets are seen for the no choke test points,

Table 5: Bottom location $d32$ [μm] data for **no surfactant** and *surfactant* test points

WC_{in} [%]	$dPT.1$ [$mbar$]	Total flow rate [L/min] 300		400		500	
30	-	**90.8**	*33.7*	**99.4**	*80.3*	**89.8**	*152.9*
	50	**253.6**	*236.9*	**245.3**	*220.5*	**205.5**	*191.1*
	100	**212.4**	*212.9*	**203.1**	*207.5*	**185.2**	*186.2*
50	-	**51.7**	*45.9*	**44.8**	*59.4*	**63.1**	*86.9*
	50	**278.0**	*244.0*	**266.2**	*231.7*	**231.6**	*203.0*
	100	**243.3**	*241.3*	**234.0**	*207.8*	**216.9**	*188.6*
70	-	**37.1**	*40.2*	**48.4**	*67.3*	**61.6**	*63.6*
	50	**221.8**	*196.4*	**210.4**	*184.6*	**195.9**	*172.2*
	100	**207.2**	*197.1*	**191.7**	*168.8*	**161.0**	*154.3*

which corresponds with distribution trends and previous explanations. For choked test points, droplet sizes are seen to decrease with increasing choke level, flow rate and inlet WC. Further, a reduction in d_{32} is observed for the choked test points when surfactant is added. For the case with open inlet choke, a slight increase in d_{32} is observed for 5 out of 6 points.

For the 30 % WC_{in} test points, a slightly different trend is observed. For the choked test points, the trend is the same as for the water-continuous, with decreasing d_{32} for increased choke level, flow rate and the addition of surfactant. For the no choke test points, both an increase and reduction in d_{32} is observed for increasing flow rates and addition of surfactant. A general observation to all test points is that process parameters have an equal if not greater effect on droplet sizes compared to addition of surfactant.

The d_{v50} data display similar trends as reported for the d_{32} data, and is included in Appendix A.

3.4. Discussion

From presented results it is clear that inlet choking has a negative effect on the separator performance for the water-continuous inlet regimes. For the oil-continuous inlet regimes, with no surfactant added, choking led to similar or slightly improved separator performance. The recorded dispersion layer present at the separator outlet was observed to be water-continuous. Results thus indicate the dispersion of oil droplets into the water phase as being the largest contributor to decreased separator performance when applying inlet choking.

For water-dominated inlet regimes, separator performance is seen to decrease for increasing total flow rates, extraction rates and level of inlet choking. Higher flow rates lead to higher turbulence levels, causing increased entrainment and breakage. Inlet choking serves as an energy input to the flow, which again leads to dispersion being formed. High extraction rates cause parts of the present dispersion layer at the separator outlet to be extracted with the water phase, decreasing performance. Moreover, addition of surfactant further reduced separator performance in this regime, which again can be explained by smaller and more stable oil droplets forming when surfactant is added. This is supported by the reported cumulative volume fraction plot in Figure 12, corresponding well with the recorded performance data presented in Figures 4 and 9. From Figure 4, a decrease in WC_r is observed for increasing total flow rates at 50 % WC_{in} and $dPT.1 = 100\ mbar$. In Figure 9, it is also seen that WC_r decreases for $\dot{Q}_{tot} = 400$ and 500 L/min when adding surfactant, while no significant change is observed for $\dot{Q}_{tot} =$ 300 L/min. Reported d_{32} calculations further support these observations, decreasing with increased choking, flow rate and surfactant addition. For the no choke test points (with stratified flow at the inlet), an increase in d_{32} was observed when adding surfactant. A plausible explanation for this phenomenon is that addition of surfactant caused an increase in entrainment and dispersion. The droplets created in this process are larger than droplets recirculated in the flow loop (which are present in the respective continuous phases), hence causing an increase in d_{32}.

For the oil dominated inlet regimes, results indicate that inlet choking in certain cases can lead to better separation of water droplets dispersed in oil. The fact that only a water-continuous dispersion layer was observed at the separator outlet indicates that any oil-continuous dispersion present at the separator inlet was fully separated, and that performance for the 30 % WC_{in} test points is dictated by the amount of water-continuous dispersion formed in the choking process, or downstream in the separator inlet. The fact that the dispersion created by the inlet choke is believed to be oil-continuous, thus limiting the amount of water-continuous dispersion being formed, can explain why no significant decrease in performance was observed when applying choking. This is also supported by the thin dispersion layers observed at the separator outlet for the 30 % inlet WC test points. From reported WC_r results, an increase in separator performance was observed for the $\dot{Q}_{tot} = 500\ L/min$, 30 % WC_{in} test points when adding surfactant for the no choke or moderate choke (50 $mbar$) configurations. This observation was supported by reported cumulative plots (Figure 16). A possible explanation can be that the addition of surfactant causes an increase in the number of formed water droplets, which can lead to an increase in coalescence. This can again indicate that the added surfactant mostly increases oil droplet stability, and not water droplet stability. The drop in performance observed for the 100 $mbar$ inlet choke setting after adding surfactant can thus imply that this choke setting creates a significant higher level of water-continuous dispersion compared to the other choke settings. This is indicated by Figure 11, displaying a thicker water-continuous dispersion for the 100 $mbar$ choke setting.

The overall effect of adding surfactant to the system was negative in terms of separator performance. A decrease in performance was observed for all test points with water dominated inlet conditions, and for the 100 $mbar$ inlet choke configuration for the 30 % WC_{in} test points. The decrease in performance is supported by reported droplet size data, displaying a leftward shift in the cumulative plots when surfactant is added and overall lower d_{32} values. This indicates formation of smaller droplets, and because the inlet WC is the same for compared test points, also an increase in the total amount of droplets. This is further supported by the average number of droplets recorded for the surfactant and no-surfactant test points (3457 vs. 2402). Smaller droplets lead to slower separation and hence declined separator performance. Reported IFT for the system did not change after surfactant was added to the Exxsol^{TM} D60, however, an overall decrease in droplet sizes were observed. In addition, the water-continuous dispersion was observed to cause a decline in separator performance, and it is thus believed that the surfactant is causing dispersed Exxsol^{TM} D60 droplets to become more stable.

4. Conclusion

This paper has studied the effect of inlet choking and the addition of surfactant on separator performance. The overall trend indicates that separation efficiency is worse with increased levels of inlet choking, and further decreased by the addition of surfactant. These two factors generally lead to an increased dispersion layer thickness at the separator outlet, which was then extracted at higher extraction rates.

For select test points, moderate choking or addition of surfactant lead to a slight increase in recorded performance. This is observed for oil-dominated inlet regimes, and is believed to be caused by a greater number of dispersed water droplets being formed, which could increase coalescence rate.

While the addition of surfactant had an effect on the droplet size distributions, it also became clear that process variables has an equal if not greater effect on the distributions.

Water-continuous inlet regimes can be expected for late life oilfields. For water-continuous inlet regimes, the maximum reduction in calculated WC_r due to inlet choking was recorded at a total flow rate of 500 L/min, for an inlet WC of 50 %, being 14 *pp*. This is also the point with the largest decrease in WC_r due to the addition of surfactant, 4 *pp*. The maximum reduction in WC_r due to inlet choking and the addition of surfactant was 16 *pp* compared to the no-choke, no-surfactant case. The addition of surfactant is thus seen to enhance the degradation in performance, especially in combination with inlet choking, for the studied system. It can thus be argued that limiting inlet choking upstream oil-water separators will benefit separation, and that subsea separation is to be preferred, as the conditions for separation are improved the closer you get to the wellhead.

Acknowledgements

This work was carried out as a part of SUBPRO, a Research-based Innovation Centre within Subsea Production and Processing. The authors gratefully acknowledge the financial support from SUBPRO, which is financed by the Research Council of Norway, major industry partners and the Norwegian University of Science and Technology (NTNU), and the Department of Geoscience and Petroleum, NTNU. The authors would also like to thank the Department of Energy and Process Engineering at NTNU, especially Professor Ole Jørgen Nydal, for the loan of the PVM equipment used in this study.

Appendix A. Supplementary Data

References

[1] NOROG, 2017 Environmental Report - Environmental work by the oil and gas industry, facts and development trends, Technical Report, NOROG, 2017.

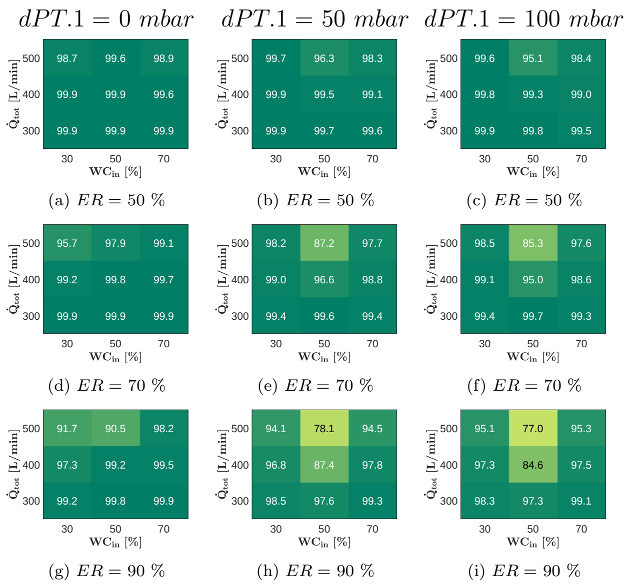

Figure A.17: WC_3 [%] results for $dPT.1 = 0,\ 50,\ 100\ mbar$ and $ER = 50,\ 70,\ 90$ % for the no surfactant tests

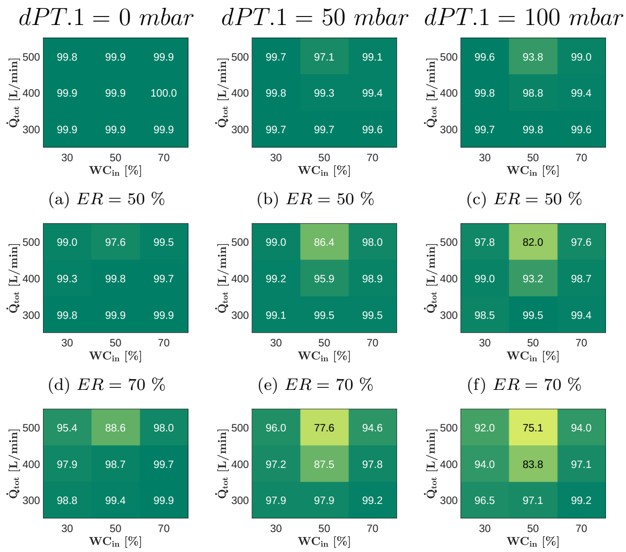

(a) $ER = 50$ % (b) $ER = 50$ % (c) $ER = 50$ %

(d) $ER = 70$ % (e) $ER = 70$ % (f) $ER = 70$ %

(g) $ER = 90$ % (h) $ER = 90$ % (i) $ER = 90$ %

Figure A.18: WC_r [%] results for $dPT.1 = 0, 50, 100\ mbar$ and $ER = 50, 70, 90$ % for the 15 ppm Span®85 surfactant tests

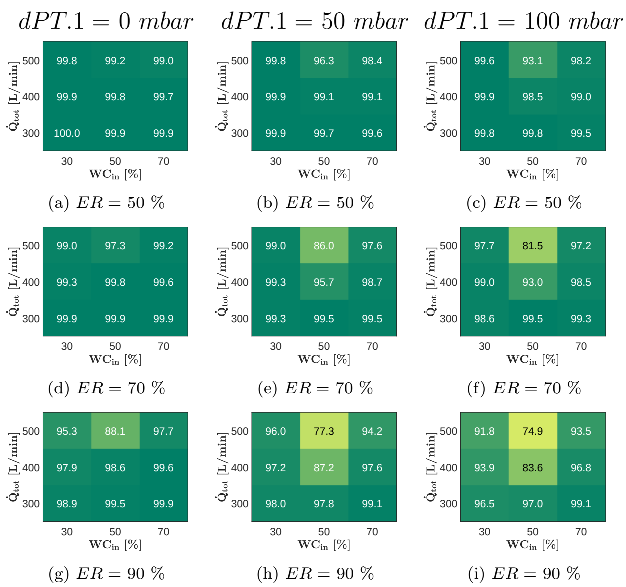

Figure A.19: WC_3 [%] results for $dPT.1 = 0$, 50, 100 $mbar$ and $ER = 50$, 70, 90 % for the 15 ppm Span®85 surfactant tests

Table A.6: Data and calculated error for fully open $VT.1$, 0 ppm Span®85 tests

Target values			Recorded values																	
$\dot{Q}_{tot}$	WC_{in}	ER	FT.1		FT.2		FT.3		DT.1		DT.2		DT.3		PT.1		dPT.1		TT.1	
[L/min]	[%]	[%]	[L/min]		[L/min]		[L/min]		[kg/m³]		[kg/m³]		[kg/m³]		[barg]		[mbar]		[°C]	
			Val	±%	Val	±%	Val	±%	Val	±%	Val	±%	Val	±%	Val	±%	Val	±%	Val	±%
		50	210,0	0,3	90,0	0,7	104,7	0,6	1020,7	0,06	795,8	0,07	1020,6	0,06	0,21	1,7	5,0	24,4	15,6	2,1
	70	70	210,0	0,3	90,0	0,7	148,6	0,4	1020,8	0,06	795,8	0,07	1020,6	0,06	0,21	1,7	5,2	23,2	15,6	2,1
		90	210,0	0,3	90,0	0,7	188,1	0,4	1020,9	0,06	795,8	0,07	1020,6	0,06	0,20	1,8	5,0	24,3	15,6	2,1
		50	150,0	0,4	150,0	0,4	76,4	0,8	1020,8	0,06	795,7	0,07	1020,7	0,06	0,22	1,7	4,9	24,5	15,5	2,1
300	50	70	150,2	0,4	150,3	0,4	103,8	0,6	1020,8	0,06	795,7	0,07	1020,7	0,06	0,23	1,7	5,0	24,0	15,5	2,1
		90	150,0	0,4	150,0	0,4	136,7	0,5	1020,9	0,06	795,8	0,07	1020,5	0,06	0,20	1,9	5,1	23,9	15,5	2,1
		50	90,0	0,7	210,0	0,3	45,0	1,4	1021,1	0,06	796,0	0,07	1020,8	0,06	0,19	1,9	5,4	22,4	15,4	2,1
	30	70	90,0	0,7	210,0	0,3	62,5	1,0	1021,1	0,06	795,9	0,07	1020,7	0,06	0,22	1,7	4,8	24,9	15,4	2,1
		90	90,0	0,7	210,0	0,3	80,9	0,8	1021,0	0,06	796,0	0,07	1019,2	0,06	0,22	1,7	4,9	24,4	15,4	2,1
		50	280,0	0,3	120,0	0,5	142,1	0,5	1020,1	0,06	795,4	0,07	1020,0	0,06	0,19	1,9	5,0	24,0	16,0	2,0
	70	70	280,0	0,3	120,0	0,5	197,1	0,3	1020,5	0,06	795,4	0,07	1020,2	0,06	0,21	1,7	5,0	24,2	16,0	2,0
		90	280,0	0,3	120,0	0,5	252,8	0,3	1020,5	0,06	795,4	0,07	1019,7	0,06	0,25	1,5	4,7	25,9	16,0	2,0
		50	200,0	0,3	200,0	0,3	100,8	0,6	1020,7	0,06	795,4	0,07	1020,5	0,06	0,25	1,5	5,5	22,0	15,9	2,0
400	50	70	200,0	0,3	200,0	0,3	140,2	0,5	1020,8	0,06	795,4	0,07	1020,5	0,06	0,22	1,6	5,1	23,4	15,9	2,0
		90	200,0	0,3	200,0	0,3	180,2	0,4	1020,7	0,06	795,4	0,07	1019,0	0,06	0,20	1,8	5,0	24,0	15,9	2,0
		50	120,0	0,5	280,0	0,3	59,8	1,0	1020,9	0,06	795,6	0,07	1020,7	0,06	0,22	1,6	5,6	21,6	15,8	2,0
	30	70	120,0	0,5	280,0	0,3	83,5	0,7	1020,8	0,06	795,6	0,07	1019,0	0,06	0,25	1,4	5,4	22,2	15,8	2,0
		90	120,0	0,5	280,0	0,3	108,4	0,6	1020,6	0,06	795,6	0,07	1014,7	0,06	0,21	1,7	5,5	21,8	15,8	2,0
		50	350,0	0,2	150,0	0,4	175,4	0,4	1018,6	0,06	795,1	0,07	1018,4	0,06	0,22	1,6	5,4	22,4	16,1	2,0
	70	70	350,0	0,2	150,0	0,4	245,9	0,3	1019,8	0,06	795,1	0,07	1018,7	0,06	0,21	1,7	5,4	22,4	16,2	2,0
		90	350,0	0,2	150,0	0,4	316,7	0,3	1020,0	0,06	795,2	0,07	1016,6	0,06	0,22	1,7	5,2	23,0	16,3	2,0
		50	250,0	0,3	250,0	0,3	124,8	0,5	1020,6	0,06	795,9	0,07	1019,9	0,06	0,27	1,3	6,1	19,8	16,0	2,0
500	50	70	250,0	0,3	250,0	0,3	174,9	0,4	1020,4	0,06	795,3	0,07	1016,2	0,06	0,20	1,8	5,4	22,5	16,0	2,0
		90	250,0	0,3	250,0	0,3	225,3	0,3	1019,4	0,06	795,3	0,07	999,3	0,06	0,21	1,8	5,2	23,4	16,1	2,0
		50	150,0	0,4	350,0	0,2	75,2	0,8	1020,7	0,06	795,5	0,07	1017,8	0,06	0,29	1,3	6,7	18,1	15,9	2,0
	30	70	150,0	0,4	350,0	0,2	106,0	0,6	1020,5	0,06	795,6	0,07	1011,0	0,06	0,24	1,5	5,8	20,7	15,9	2,0
		90	150,0	0,4	350,0	0,2	134,8	0,5	1020,3	0,06	795,6	0,07	1002,0	0,06	0,19	1,9	6,3	19,3	15,9	2,0

Table A.7: Data and calculated error for $dPT.1 = 50\ mbar$, 0 ppm Span®85 tests

Target values			Recorded values																	
$\dot{Q}_{tot}$	WC_{in}	ER	FT.1		FT.2		FT.3		DT.1		DT.2		DT.3		PT.1		dPT.1		TT.1	
[L/min]	[%]	[%]	[L/min]		[L/min]		[L/min]		[kg/m³]		[kg/m³]		[kg/m³]		[barg]		[mbar]		[°C]	
			Val	±%	Val	±%	Val	±%	Val	±%	Val	±%	Val	±%	Val	±%	Val	±%	Val	±%
		50	210,0	0,3	90,0	0,7	104,8	0,6	1020,8	0,06	796,8	0,07	1020,2	0,06	0,16	2,2	49,3	2,4	14,2	2,3
	70	70	210,0	0,3	90,0	0,7	146,1	0,4	1020,9	0,06	796,8	0,07	1020,0	0,06	0,18	2,1	48,8	2,5	14,2	2,3
		90	210,0	0,3	90,0	0,7	188,6	0,4	1020,8	0,06	796,8	0,07	1019,5	0,06	0,18	2,0	48,4	2,5	14,3	2,2
		50	150,0	0,4	150,0	0,4	74,7	0,8	1021,1	0,06	796,8	0,07	1020,6	0,06	0,18	2,0	50,3	2,4	14,0	2,3
300	50	70	150,0	0,4	150,0	0,4	103,8	0,6	1021,0	0,06	796,8	0,07	1020,3	0,06	0,13	2,9	51,1	2,4	14,1	2,3
		90	150,0	0,4	150,0	0,4	134,3	0,5	1020,7	0,06	796,9	0,07	1015,9	0,06	0,26	1,4	52,9	2,3	14,1	2,3
		50	90,0	0,7	210,0	0,3	46,0	1,3	1021,3	0,06	797,0	0,07	1021,1	0,06	0,23	1,5	51,4	2,3	14,0	2,3
	30	70	90,0	0,7	210,0	0,3	64,1	1,0	1021,3	0,06	797,0	0,07	1020,0	0,06	0,22	1,7	50,8	2,4	14,0	2,3
		90	90,0	0,7	210,0	0,3	81,8	0,8	1021,1	0,06	797,1	0,07	1017,9	0,06	0,17	2,2	50,1	2,4	14,0	2,3
		50	280,0	0,3	120,0	0,5	139,8	0,5	1020,0	0,06	796,1	0,07	1019,1	0,06	0,22	1,7	49,9	2,4	14,7	2,2
	70	70	280,0	0,3	120,0	0,5	195,1	0,3	1020,4	0,06	796,2	0,07	1018,4	0,06	0,15	2,3	50,3	2,4	14,8	2,2
		90	280,0	0,3	120,0	0,5	251,3	0,3	1020,3	0,06	796,2	0,07	1016,0	0,06	0,21	1,7	49,7	2,4	14,8	2,2
		50	200,0	0,3	200,0	0,3	100,2	0,6	1020,5	0,06	796,2	0,07	1020,0	0,06	0,21	1,7	51,5	2,3	14,6	2,2
400	50	70	200,0	0,3	200,0	0,3	140,6	0,5	1020,6	0,06	796,2	0,07	1013,4	0,06	0,23	1,6	50,8	2,4	14,6	2,2
		90	200,0	0,3	200,0	0,3	180,5	0,4	1020,3	0,06	796,4	0,07	992,7	0,07	0,21	1,8	50,6	2,4	14,6	2,2
		50	120,0	0,5	280,0	0,3	60,1	1,0	1021,2	0,06	796,6	0,07	1020,9	0,06	0,20	1,9	49,3	2,4	14,4	2,2
	30	70	120,0	0,5	280,0	0,3	84,4	0,7	1021,1	0,06	796,6	0,07	1018,9	0,06	0,18	2,0	49,3	2,4	14,4	2,2
		90	120,0	0,5	280,0	0,3	108,3	0,6	1020,9	0,06	796,6	0,07	1014,1	0,06	0,16	2,3	49,7	2,4	14,4	2,2
		50	350,0	0,2	150,0	0,4	173,8	0,4	1018,9	0,06	795,8	0,07	1017,3	0,06	0,21	1,7	51,9	2,3	15,1	2,1
	70	70	350,0	0,2	150,0	0,4	243,7	0,3	1019,8	0,06	795,8	0,07	1015,8	0,06	0,17	2,1	51,7	2,3	15,1	2,1
		90	350,0	0,2	150,0	0,4	316,6	0,2	1019,7	0,06	795,8	0,07	1008,6	0,06	0,19	2,0	52,2	2,3	15,2	2,1
		50	250,0	0,3	250,0	0,3	125,0	0,5	1019,0	0,06	795,9	0,07	1012,7	0,06	0,28	1,3	49,6	2,4	15,0	2,1
500	50	70	250,0	0,3	250,0	0,3	174,6	0,4	1019,3	0,06	795,9	0,07	992,2	0,06	0,21	1,7	50,1	2,4	15,0	2,1
		90	250,0	0,3	250,0	0,3	226,0	0,3	1019,5	0,06	795,9	0,07	971,7	0,07	0,21	1,7	49,5	2,4	15,1	2,1
		50	150,0	0,4	350,0	0,2	75,5	0,8	1020,9	0,06	796,5	0,07	1020,4	0,06	0,29	1,3	48,4	2,5	14,9	2,1
	30	70	150,0	0,4	350,0	0,2	104,6	0,6	1020,9	0,06	796,3	0,07	1016,9	0,06	0,24	1,5	48,3	2,5	14,9	2,1
		90	150,0	0,4	350,0	0,2	135,0	0,5	1020,6	0,06	796,4	0,07	1007,7	0,06	0,20	1,8	49,0	2,5	15,0	2,1

Table A.8: Data and calculated error for $dPT.1 = 100\ mbar$, 0 ppm Span®85 tests

Target values: $\dot{Q}_{tot}$ [L/min]	WC_{in} [%]	ER [%]	Recorded values: FT.1 [L/min] Val	±%	FT.2 [L/min] Val	±%	FT.3 [L/min] Val	±%	DT.1 [kg/m³] Val	±%	DT.2 [kg/m³] Val	±%	DT.3 [kg/m³] Val	±%	PT.1 [barg] Val	±%	dPT.1 [mbar] Val	±%	TT.1 [°C] Val	±%
		50	210,0	0,3	90,0	0,7	104,3	0,6	1020,6	0,06	796,4	0,07	1019,9	0,06	0,27	1,3	100,9	1,2	14,9	2,1
	70	70	210,0	0,3	90,0	0,7	148,6	0,4	1020,6	0,06	796,4	0,07	1019,6	0,06	0,27	1,3	101,1	1,2	14,9	2,1
		90	210,0	0,3	90,0	0,7	189,8	0,4	1020,6	0,06	796,4	0,07	1018,9	0,06	0,23	1,6	100,0	1,2	15,0	2,1
		50	150,0	0,4	150,0	0,4	74,8	0,8	1020,9	0,06	796,2	0,07	1020,6	0,06	0,26	1,4	99,6	1,2	14,8	2,2
300	50	70	150,1	0,4	150,1	0,4	105,5	0,6	1020,9	0,06	796,2	0,07	1020,5	0,06	0,21	1,8	99,7	1,2	14,8	2,2
		90	150,0	0,4	150,0	0,4	135,8	0,5	1020,7	0,06	796,3	0,07	1014,9	0,06	0,21	1,7	100,3	1,2	14,9	2,2
		50	90,0	0,7	210,0	0,3	45,8	1,3	1021,1	0,06	796,4	0,07	1020,9	0,06	0,20	1,9	100,3	1,2	14,7	2,2
	30	70	90,0	0,7	210,0	0,3	63,1	1,0	1021,1	0,06	796,5	0,07	1019,7	0,06	0,17	2,1	100,6	1,2	14,7	2,2
		90	90,0	0,7	210,0	0,3	81,5	0,8	1021,0	0,06	796,5	0,07	1017,4	0,06	0,23	1,6	100,3	1,2	14,8	2,2
		50	280,0	0,3	120,0	0,5	140,3	0,5	1019,8	0,06	795,7	0,07	1018,8	0,06	0,28	1,3	98,9	1,2	15,4	2,1
	70	70	280,0	0,3	120,0	0,5	195,0	0,3	1020,2	0,06	795,8	0,07	1017,8	0,06	0,18	2,0	99,8	1,2	15,4	2,1
		90	280,0	0,3	120,0	0,5	252,5	0,3	1020,1	0,06	795,8	0,07	1015,4	0,06	0,27	1,4	99,5	1,2	15,4	2,1
		50	200,0	0,3	200,0	0,3	100,0	0,6	1020,2	0,06	795,9	0,07	1019,4	0,06	0,26	1,4	98,3	1,2	15,3	2,1
400	50	70	200,0	0,3	200,0	0,3	141,1	0,5	1020,4	0,06	795,8	0,07	1009,7	0,06	0,21	1,7	99,4	1,2	15,3	2,1
		90	200,0	0,3	200,0	0,3	182,5	0,4	1020,1	0,06	795,9	0,07	986,3	0,07	0,29	1,3	98,8	1,2	15,3	2,1
		50	120,0	0,5	280,0	0,3	59,5	1,0	1021,0	0,06	796,3	0,07	1020,6	0,06	0,17	2,2	99,8	1,2	15,1	2,1
	30	70	120,0	0,5	280,0	0,3	84,7	0,7	1020,9	0,06	796,1	0,07	1018,9	0,06	0,18	2,0	99,8	1,2	15,1	2,1
		90	120,0	0,5	280,0	0,3	107,7	0,6	1020,7	0,06	796,1	0,07	1015,0	0,06	0,21	1,8	98,8	1,2	15,1	2,1
		50	350,0	0,2	150,0	0,4	175,4	0,4	1018,8	0,06	795,2	0,07	1017,1	0,06	0,27	1,3	101,7	1,2	16,0	2,0
	70	70	350,0	0,2	150,0	0,4	244,8	0,3	1019,5	0,06	795,2	0,07	1015,5	0,06	0,24	1,5	102,0	1,2	16,0	2,0
		90	350,0	0,2	150,0	0,4	314,0	0,2	1019,5	0,06	795,2	0,07	1010,3	0,06	0,25	1,5	101,9	1,2	16,0	2,0
		50	250,0	0,3	250,0	0,3	126,2	0,5	1019,0	0,06	795,4	0,07	1009,8	0,06	0,30	1,2	99,3	1,2	15,8	2,0
500	50	70	250,0	0,3	250,0	0,3	176,9	0,4	1019,4	0,06	795,4	0,07	987,8	0,06	0,22	1,7	100,3	1,2	15,8	2,0
		90	250,0	0,3	250,0	0,3	226,0	0,3	1019,7	0,06	795,4	0,07	968,9	0,07	0,22	1,7	100,2	1,2	15,8	2,0
		50	150,0	0,4	350,0	0,2	74,4	0,8	1020,8	0,06	796,1	0,07	1020,0	0,06	0,30	1,2	98,8	1,2	15,6	2,1
	30	70	150,0	0,4	350,0	0,2	104,9	0,6	1020,8	0,06	795,9	0,07	1017,6	0,06	0,24	1,5	97,7	1,2	15,6	2,1
		90	150,0	0,4	350,0	0,2	135,3	0,5	1020,5	0,06	795,8	0,07	1009,8	0,06	0,25	1,5	98,3	1,2	15,7	2,0

Table A.9: Data and calculated error for fully open $VT.1$, 15 ppm Span®85 tests

Target values: $\dot{Q}_{tot}$ [L/min]	WC_{in} [%]	ER [%]	Recorded values: FT.1 [L/min] Val	±%	FT.2 [L/min] Val	±%	FT.3 [L/min] Val	±%	DT.1 [kg/m³] Val	±%	DT.2 [kg/m³] Val	±%	DT.3 [kg/m³] Val	±%	PT.1 [barg] Val	±%	dPT.1 [mbar] Val	±%	TT.1 [°C] Val	±%
		50	210,0	0,3	90,0	0,7	105,1	0,6	1020,6	0,06	795,1	0,07	1020,4	0,06	0,24	1,5	2,6	46,3	16,7	1,9
	70	70	210,0	0,3	90,0	0,7	147,3	0,4	1020,7	0,06	795,2	0,07	1020,4	0,06	0,18	2,0	2,7	45,4	16,7	1,9
		90	210,0	0,3	90,0	0,7	190,3	0,4	1020,7	0,06	795,1	0,07	1020,4	0,06	0,25	1,5	2,9	42,1	16,7	1,9
		50	150,0	0,4	150,0	0,4	75,1	0,8	1020,8	0,06	795,0	0,07	1020,5	0,06	0,20	1,8	2,6	45,6	16,6	1,9
300	50	70	150,0	0,4	150,0	0,4	106,0	0,6	1020,7	0,06	795,0	0,07	1020,5	0,06	0,33	1,1	2,2	53,7	16,6	1,9
		90	150,0	0,4	150,0	0,4	136,1	0,5	1020,7	0,06	795,1	0,07	1019,4	0,06	0,18	2,0	2,3	52,1	16,7	1,9
		50	90,0	0,7	210,0	0,3	44,5	1,4	1020,9	0,06	795,2	0,07	1020,6	0,06	0,21	1,7	2,8	42,4	16,6	1,9
	30	70	90,0	0,7	210,0	0,3	62,8	1,0	1020,8	0,06	795,2	0,07	1020,4	0,06	0,26	1,4	2,6	46,7	16,6	1,9
		90	90,0	0,7	210,0	0,3	81,2	0,8	1020,8	0,06	795,2	0,07	1018,2	0,06	0,19	2,0	2,5	48,3	16,6	1,9
		50	280,0	0,3	120,0	0,5	141,6	0,5	1019,9	0,06	794,8	0,07	1019,8	0,06	0,24	1,5	2,7	44,0	17,0	1,9
	70	70	280,0	0,3	120,0	0,5	197,6	0,3	1020,3	0,06	794,8	0,07	1019,6	0,06	0,21	1,7	2,7	44,9	17,0	1,9
		90	280,0	0,3	120,0	0,5	253,7	0,3	1020,4	0,06	794,8	0,07	1019,7	0,06	0,21	1,7	2,0	60,3	17,0	1,9
		50	200,0	0,3	200,0	0,3	100,6	0,6	1020,4	0,06	794,8	0,07	1020,3	0,06	0,22	1,7	2,8	43,7	16,8	1,9
400	50	70	200,0	0,3	200,0	0,3	140,4	0,5	1020,6	0,06	794,8	0,07	1020,2	0,06	0,23	1,6	2,9	41,7	16,9	1,9
		90	200,0	0,3	200,0	0,3	179,9	0,4	1020,5	0,06	794,9	0,07	1017,5	0,06	0,21	1,7	2,7	44,3	16,9	1,9
		50	120,0	0,5	280,0	0,3	59,9	1,0	1020,7	0,06	795,1	0,07	1020,5	0,06	0,22	1,7	2,7	45,3	16,8	1,9
	30	70	120,0	0,5	280,0	0,3	84,2	0,7	1020,7	0,06	795,0	0,07	1019,1	0,06	0,18	2,0	2,7	44,6	16,8	1,9
		90	120,0	0,5	280,0	0,3	107,6	0,6	1020,6	0,06	794,9	0,07	1015,8	0,06	0,21	1,7	2,7	44,9	16,8	1,9
		50	350,0	0,2	150,0	0,4	175,2	0,4	1018,5	0,06	794,3	0,07	1018,3	0,06	0,25	1,5	2,0	61,1	17,3	1,8
	70	70	350,0	0,2	150,0	0,4	245,4	0,3	1019,7	0,06	794,3	0,07	1018,7	0,06	0,19	1,9	1,9	65,0	17,3	1,8
		90	350,0	0,2	150,0	0,4	315,2	0,2	1019,8	0,06	794,3	0,07	1015,2	0,06	0,22	1,7	2,2	55,7	17,3	1,8
		50	250,0	0,3	250,0	0,3	125,2	0,5	1019,0	0,06	794,3	0,07	1018,7	0,06	0,27	1,4	2,8	43,8	17,2	1,9
500	50	70	250,0	0,3	250,0	0,3	174,7	0,4	1019,9	0,06	794,5	0,07	1014,4	0,06	0,22	1,6	2,7	44,7	17,2	1,9
		90	250,0	0,3	250,1	0,3	225,1	0,3	1019,2	0,06	794,5	0,07	993,5	0,07	0,23	1,6	1,7	70,3	17,2	1,9
		50	150,0	0,4	350,0	0,2	74,9	0,8	1020,5	0,06	794,9	0,07	1020,2	0,06	0,31	1,2	3,3	36,6	17,1	1,9
	30	70	150,0	0,4	350,0	0,2	105,3	0,6	1020,5	0,06	794,8	0,07	1018,3	0,06	0,26	1,4	3,5	34,8	17,1	1,9
		90	150,0	0,4	350,0	0,2	135,0	0,5	1020,4	0,06	794,8	0,07	1009,9	0,06	0,21	1,7	2,8	42,4	17,1	1,9

Table A.10: Data and calculated error for $dPT.1 = 50\ mbar$, 15 ppm Span®85 tests

Target values			Recorded values																	
$\dot{Q}_{tot}$ [L/min]	WC_{in} [%]	ER [%]	FT.1 [L/min]		FT.2 [L/min]		FT.3 [L/min]		DT.1 [kg/m³]		DT.2 [kg/m³]		DT.3 [kg/m³]		PT.1 [barg]		dPT.1 [mbar]		TT.1 [°C]	
			Val	±%	Val	±%	Val	±%	Val	±%	Val	±%	Val	±%	Val	±%	Val	±%	Val	±%
		50	210,0	0,3	90,0	0,7	104,5	0,6	1020,5	0,06	795,3	0,07	1019,7	0,06	0,28	1,3	50,2	2,4	16,7	1,9
	70	70	210,0	0,3	90,0	0,7	146,4	0,4	1020,6	0,06	795,4	0,07	1019,4	0,06	0,19	1,9	48,4	2,5	16,7	1,9
		90	210,0	0,3	90,0	0,7	189,5	0,4	1020,5	0,06	795,3	0,07	1018,6	0,06	0,24	1,5	49,7	2,4	16,7	1,9
		50	150,0	0,4	150,0	0,4	75,0	0,8	1020,8	0,06	795,2	0,07	1020,1	0,06	0,22	1,7	49,2	2,5	16,6	1,9
300	50	70	150,0	0,4	150,0	0,4	105,8	0,6	1020,8	0,06	795,2	0,07	1019,6	0,06	0,19	2,0	49,2	2,5	16,6	1,9
		90	150,0	0,4	150,0	0,4	134,6	0,5	1020,6	0,06	795,3	0,07	1015,8	0,06	0,21	1,8	49,5	2,4	16,6	1,9
		50	90,0	0,7	210,0	0,3	45,0	1,4	1021,0	0,06	795,3	0,07	1020,3	0,06	0,22	1,7	49,9	2,4	16,6	1,9
	30	70	90,0	0,7	210,0	0,3	62,6	1,0	1021,0	0,06	795,4	0,07	1019,0	0,06	0,17	2,1	49,8	2,4	16,6	1,9
		90	90,0	0,7	210,0	0,3	81,3	0,8	1020,8	0,06	795,3	0,07	1016,0	0,06	0,27	1,4	51,0	2,4	16,6	1,9
		50	280,0	0,3	120,0	0,5	139,4	0,5	1019,8	0,06	794,8	0,07	1018,5	0,06	0,24	1,5	49,4	2,4	16,9	1,9
	70	70	280,0	0,3	120,0	0,5	197,8	0,3	1020,1	0,06	794,7	0,07	1017,7	0,06	0,27	1,4	48,1	2,5	16,9	1,9
		90	279,8	0,3	119,7	0,6	253,4	0,3	1020,1	0,06	794,9	0,07	1015,1	0,06	0,25	1,5	49,5	2,4	17,0	1,9
		50	200,0	0,3	200,0	0,3	101,1	0,6	1020,1	0,06	794,8	0,07	1018,5	0,06	0,21	1,8	51,1	2,4	16,8	1,9
400	50	70	200,0	0,3	200,0	0,3	139,9	0,5	1020,3	0,06	794,8	0,07	1011,0	0,06	0,20	1,8	52,0	2,3	16,8	1,9
		90	200,0	0,3	200,0	0,3	179,4	0,4	1020,0	0,06	794,9	0,07	991,7	0,07	0,26	1,4	50,6	2,4	16,8	1,9
		50	120,0	0,5	280,0	0,3	60,5	1,0	1020,8	0,06	795,3	0,07	1020,3	0,06	0,21	1,8	50,0	2,4	16,7	1,9
	30	70	120,0	0,5	280,0	0,3	84,9	0,7	1020,8	0,06	795,2	0,07	1019,0	0,06	0,20	1,8	50,4	2,4	16,8	1,9
		90	120,0	0,5	280,0	0,3	108,5	0,6	1020,6	0,06	795,1	0,07	1014,2	0,06	0,18	2,0	50,3	2,4	16,8	1,9
		50	350,0	0,2	150,0	0,4	174,4	0,4	1018,9	0,06	794,3	0,07	1016,9	0,06	0,22	1,6	51,5	2,3	17,3	1,9
	70	70	350,0	0,2	150,0	0,4	245,7	0,3	1019,5	0,06	794,3	0,07	1015,1	0,06	0,19	1,9	51,8	2,3	17,3	1,8
		90	350,0	0,2	150,0	0,4	314,3	0,2	1019,5	0,06	794,3	0,07	1007,4	0,06	0,18	2,0	52,4	2,3	17,3	1,8
		50	250,0	0,3	250,0	0,3	125,9	0,5	1018,6	0,06	794,5	0,07	1012,1	0,06	0,28	1,3	51,5	2,3	17,1	1,9
500	50	70	250,0	0,3	250,0	0,3	175,1	0,4	1019,4	0,06	794,4	0,07	988,8	0,06	0,23	1,6	52,3	2,3	17,2	1,9
		90	250,0	0,3	250,0	0,3	226,8	0,3	1019,8	0,06	794,5	0,07	969,2	0,07	0,20	1,8	52,2	2,3	17,2	1,9
		50	150,0	0,4	350,0	0,2	75,6	0,8	1020,6	0,06	795,1	0,07	1020,0	0,06	0,30	1,2	50,2	2,4	17,1	1,9
	30	70	150,0	0,4	350,0	0,2	104,6	0,6	1020,6	0,06	795,0	0,07	1018,3	0,06	0,25	1,5	50,0	2,4	17,1	1,9
		90	150,0	0,4	350,0	0,2	134,7	0,5	1020,4	0,06	795,0	0,07	1011,5	0,06	0,20	1,8	50,3	2,4	17,1	1,9

Table A.11: Data and calculated error for $dPT.1 = 100\ mbar$, 15 ppm Span®85 tests

Target values			Recorded values																	
$\dot{Q}_{tot}$ [L/min]	WC_{in} [%]	ER [%]	FT.1 [L/min]		FT.2 [L/min]		FT.3 [L/min]		DT.1 [kg/m³]		DT.2 [kg/m³]		DT.3 [kg/m³]		PT.1 [barg]		dPT.1 [mbar]		TT.1 [°C]	
			Val	±%	Val	±%	Val	±%	Val	±%	Val	±%	Val	±%	Val	±%	Val	±%	Val	±%
		50	210,0	0,3	90,0	0,7	106,2	0,6	1020,4	0,06	795,4	0,07	1019,6	0,06	0,23	1,6	100,4	1,2	16,6	1,9
	70	70	210,0	0,3	90,0	0,7	149,0	0,4	1020,5	0,06	795,3	0,07	1019,2	0,06	0,24	1,5	100,9	1,2	16,6	1,9
		90	210,0	0,3	90,0	0,7	188,1	0,4	1020,4	0,06	795,3	0,07	1018,5	0,06	0,17	2,1	99,7	1,2	16,6	1,9
		50	150,0	0,4	150,0	0,4	75,4	0,8	1020,7	0,06	795,2	0,07	1020,3	0,06	0,18	2,0	99,4	1,2	16,6	1,9
300	50	70	149,9	0,4	149,9	0,4	105,8	0,6	1020,7	0,06	795,2	0,07	1019,6	0,06	0,26	1,4	100,2	1,2	16,6	1,9
		90	150,0	0,4	150,0	0,4	135,5	0,5	1020,5	0,06	795,3	0,07	1014,0	0,06	0,24	1,5	99,7	1,2	16,6	1,9
		50	90,0	0,7	210,0	0,3	45,7	1,3	1020,9	0,06	795,4	0,07	1020,3	0,06	0,25	1,5	99,1	1,2	16,5	1,9
	30	70	90,0	0,7	210,0	0,3	63,3	1,0	1020,9	0,06	795,4	0,07	1017,6	0,06	0,20	1,8	99,0	1,2	16,5	1,9
		90	90,0	0,7	210,0	0,3	81,4	0,8	1020,7	0,06	795,3	0,07	1012,7	0,06	0,18	2,0	98,7	1,2	16,5	1,9
		50	280,0	0,3	120,0	0,5	139,9	0,5	1019,8	0,06	794,7	0,07	1018,4	0,06	0,17	2,1	100,9	1,2	16,8	1,9
	70	70	280,0	0,3	120,0	0,5	197,1	0,3	1020,1	0,06	794,7	0,07	1017,1	0,06	0,22	1,6	100,2	1,2	16,9	1,9
		90	280,0	0,3	120,0	0,5	253,6	0,3	1019,9	0,06	794,8	0,07	1013,3	0,06	0,18	2,0	100,6	1,2	16,9	1,9
		50	200,0	0,3	200,0	0,3	100,9	0,6	1019,9	0,06	794,8	0,07	1017,3	0,06	0,26	1,4	101,4	1,2	16,8	1,9
400	50	70	200,0	0,3	200,0	0,3	140,0	0,5	1020,2	0,06	794,8	0,07	1004,8	0,06	0,19	1,9	103,4	1,2	16,8	1,9
		90	200,0	0,3	200,0	0,3	180,1	0,4	1020,1	0,06	794,8	0,07	983,6	0,07	0,20	1,8	101,9	1,2	16,8	1,9
		50	120,0	0,5	280,0	0,3	60,3	1,0	1020,7	0,06	795,3	0,07	1020,3	0,06	0,19	1,9	99,0	1,2	16,7	1,9
	30	70	120,0	0,5	280,0	0,3	83,8	0,7	1020,7	0,06	795,2	0,07	1018,4	0,06	0,22	1,7	98,1	1,2	16,7	1,9
		90	120,0	0,5	280,0	0,3	109,1	0,6	1020,5	0,06	795,1	0,07	1006,9	0,06	0,24	1,5	98,2	1,2	16,7	1,9
		50	350,0	0,2	150,0	0,4	176,2	0,4	1018,7	0,06	794,2	0,07	1016,4	0,06	0,21	1,8	100,6	1,2	17,2	1,9
	70	70	350,0	0,2	150,0	0,4	246,1	0,3	1019,5	0,06	794,2	0,07	1014,2	0,06	0,19	1,9	99,6	1,2	17,3	1,8
		90	350,0	0,2	150,0	0,4	318,0	0,2	1019,4	0,06	794,2	0,07	1005,9	0,06	0,21	1,7	99,5	1,2	17,3	1,8
		50	250,0	0,3	250,0	0,3	126,3	0,5	1018,8	0,06	794,3	0,07	1004,9	0,06	0,27	1,3	100,2	1,2	17,1	1,9
500	50	70	250,0	0,3	250,0	0,3	176,3	0,4	1019,3	0,06	794,3	0,07	978,7	0,07	0,19	1,9	101,1	1,2	17,1	1,9
		90	250,0	0,3	250,0	0,3	226,0	0,3	1019,8	0,06	794,4	0,07	963,6	0,06	0,18	2,0	101,3	1,2	17,2	1,9
		50	150,0	0,4	350,0	0,2	75,4	0,8	1020,6	0,06	794,9	0,07	1019,7	0,06	0,30	1,2	102,1	1,2	17,1	1,9
	30	70	150,0	0,4	350,0	0,2	104,6	0,6	1020,4	0,06	794,9	0,07	1015,5	0,06	0,25	1,5	103,2	1,2	17,1	1,9
		90	150,0	0,4	350,0	0,2	134,9	0,5	1020,1	0,06	794,8	0,07	1002,0	0,06	0,20	1,8	102,4	1,2	17,1	1,9

$WC_{in} = 30$ % $WC_{in} = 50$ % $WC_{in} = 70$ %

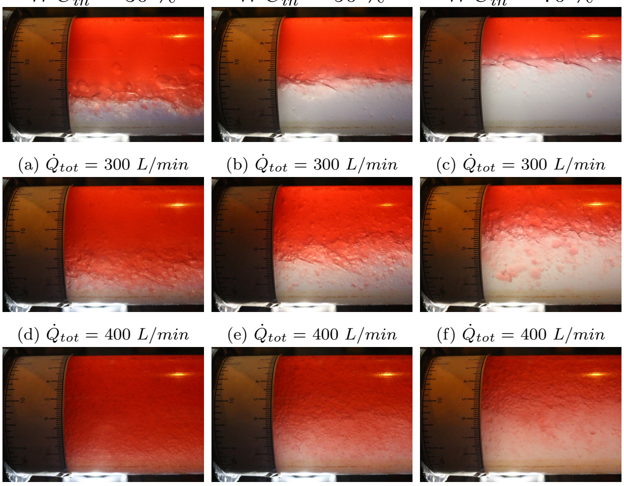

(a) $\dot{Q}_{tot} = 300\ L/min$ (b) $\dot{Q}_{tot} = 300\ L/min$ (c) $\dot{Q}_{tot} = 300\ L/min$

(d) $\dot{Q}_{tot} = 400\ L/min$ (e) $\dot{Q}_{tot} = 400\ L/min$ (f) $\dot{Q}_{tot} = 400\ L/min$

(g) $\dot{Q}_{tot} = 500\ L/min$ (h) $\dot{Q}_{tot} = 500\ L/min$ (i) $\dot{Q}_{tot} = 500\ L/min$

Figure A.20: Inlet flow regime for open choke valve with no surfactant test points

Table A.12: Bottom location d_{v50} $[\mu m]$ data for **no surfactant** and *surfactant* test points

WC_{in} [%]	$dPT.1$ $[mbar]$	Total flow rate $[L/min]$					
		300		400		500	
	-	**199.1**	*42.1*	**235.6**	*145.8*	**148.6**	*247.2*
30	50	**290.3**	*300.8*	**290.5**	*271.8*	**262.6**	*256.3*
	100	**251.5**	*259.3*	**250.7**	*258.5*	**234.9**	*244.0*
	-	**64.4**	*59.2*	**60.5**	*72.5*	**71.4**	*123.2*
50	50	**335.1**	*297.2*	**295.1**	*283.1*	**278.2**	*261.6*
	100	**282.0**	*285.6*	**268.9**	*255.4*	**266.3**	*233.2*
	-	**43.3**	*52.7*	**61.5**	*81.4*	**69.4**	*72.5*
70	50	**268.6**	*257.5*	**260.7**	*250.1*	**254.4**	*231.9*
	100	**247.7**	*244.3*	**237.0**	*204.7*	**194.4**	*185.8*

$WC_{in} = 30$ % $WC_{in} = 50$ % $WC_{in} = 70$ %

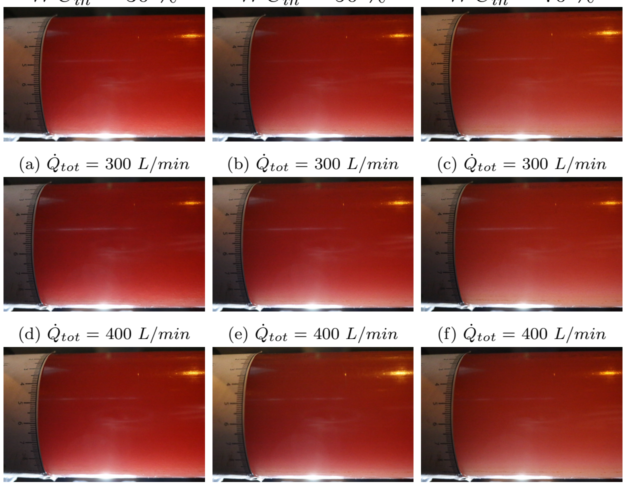

(a) $\dot{Q}_{tot} = 300\ L/min$ (b) $\dot{Q}_{tot} = 300\ L/min$ (c) $\dot{Q}_{tot} = 300\ L/min$

(d) $\dot{Q}_{tot} = 400\ L/min$ (e) $\dot{Q}_{tot} = 400\ L/min$ (f) $\dot{Q}_{tot} = 400\ L/min$

(g) $\dot{Q}_{tot} = 500\ L/min$ (h) $\dot{Q}_{tot} = 500\ L/min$ (i) $\dot{Q}_{tot} = 500\ L/min$

Figure A.21: Inlet flow regime for $dPT.1 = 100\ mbar$ with 15 ppm Span®85 test points

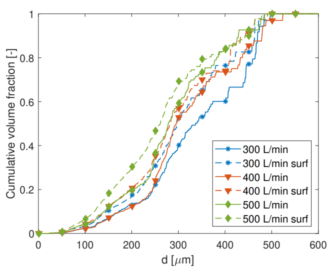

Figure A.22: Cumulative volume fraction for $WC_{in} = 50$ %, $dPT.1 = 50\ mbar$

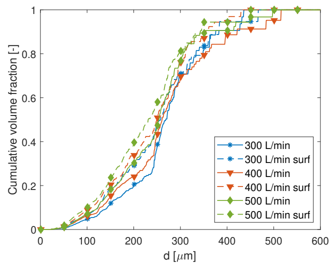

Figure A.23: Cumulative volume fraction for $WC_{in} = 70$ %, $dPT.1 = 50$ $mbar$

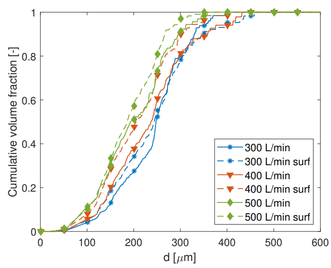

Figure A.24: Cumulative volume fraction for $WC_{in} = 70$ %, $dPT.1 = 100$ $mbar$

[2] R. Zolfaghari, A. Fakhru'l-Razi, L. C. Abdullah, S. S. Elnashaie, A. Pendashteh, Demulsification techniques of water-in-oil and oil-in-water emulsions in petroleum industry, Separation and Purification Technology 170 (2016) 377–407.

[3] S. Wong, J. Lim, S. Dol, Crude oil emulsion: A review on formation, classification and stability of water-in-oil emulsions, Journal of Petroleum Science and Engineering 135 (2015) 498–504.

[4] C. J. Backi, B. A. Grimes, S. Skogestad, A control-and estimation-oriented gravity separator model for oil and gas applications based upon first-principles, Industrial & Engineering Chemistry Research 57 (2018) 7201–7217.

[5] M. Fossen, R. Arntzen, P. V. Hemmingsen, J. Sjöblom, J. Jakobsson, A laboratory-scale vertical gravity separator for emulsion characterization, Journal of dispersion science and technology 27 (2006) 453–461.

[6] P. A. K. Andresen, R. Arntzen, J. Sjøblom, Stability of model emulsions and determination of droplet size distributions in a gravity separator with different inlet characteristics, Colloids and Surfaces A: Physicochemical and Engineering Aspects 170 (2000) 33–44.

[7] M. Dudek, A. Bertheussen, T. Dumaire, G. Øye, Microfluidic tools for studying coalescence of crude oil droplets in produced water, Chemical Engineering Science 191 (2018) 448–458.

[8] H. Schümann, M. Khatibi, M. Tutkun, B. H. Pettersen, Z. Yang, O. J. Nydal, Droplet size measurements in oil–water dispersions: A comparison study using fbrm and pvm, Journal of Dispersion Science and Technology 36 (2015) 1432–1443.

[9] M. Fossen, H. Schümann, Experimental study of the relative effect of pressure drop and flow rate on the droplet size downstream of a pipe restriction, Journal of Dispersion Science and Technology 38 (2017) 826–831.

[10] B. Bringedal, T. Ingebretsen, K. Haugen, et al., Subsea separation and reinjection of produced water, in: Offshore Technology Conference, Offshore Technology Conference.

[11] H. S. Skjefstad, M. Stanko, Subsea water separation: a state of the art review, future technologies and the development of a compact separator test facility, in: 18th International Conference on Multiphase Production Technology, BHR Group.

[12] H. S. Skjefstad, M. Stanko, An experimental study of a novel parallel pipe separator design for subsea oil-water bulk separation, in: SPE Asia Pacific Oil and Gas Conference and Exhibition, Society of Petroleum Engineers.

[13] H. S. Skjefstad, M. Stanko, Experimental performance evaluation and design optimization of a horizontal multi-pipe separator for subsea oil-water bulk separation, Journal of Petroleum Science and Engineering (2019).

[14] T. Tichelkamp, E. Teigen, M. Nourani, G. Øye, Systematic study of the effect of electrolyte composition on interfacial tensions between surfactant solutions and crude oils, Chemical Engineering Science 132 (2015) 244–249.

[15] M. Dudek, E. Kancir, G. Øye, Influence of the crude oil and water compositions on the quality of synthetic produced water, Energy & Fuels 31 (2017) 3708–3716.

[16] R. P. Panckow, L. Reinecke, M. C. Cuellar, S. Maaß, Photo-optical in-situ measurement of drop size distributions: applications in research and industry, Oil & Gas Science and Technology–Revue d'IFP Energies nouvelles 72 (2017) 14.

[17] P. Riegler, T. Chrusciel, A. Mayer, K. Doll, D. Weuster-Botz, Reversible retrofitting of a stirred-tank bioreactor for gas-lift operation to perform synthesis gas fermentation studies, Biochemical Engineering Journal 141 (2019) 89–101.

[18] C. Bliatsiou, A. Malik, L. Böhm, M. Kraume, Influence of impeller geometry on hydromechanical stress in stirred liquid/liquid dispersions, Industrial & Engineering Chemistry Research (2018).

[19] J. Trallero, C. Sarica, J. Brill, et al., A study of oil-water flow patterns in horizontal pipes, SPE Production & Facilities 12 (1997) 165–172.

Chapter 8

Modelling

This chapter presents performed work on modelling of the developed multiple parallel pipe oil-water bulk separator concept. Work is centred around model development and validation, investigating influence of varying dispersed phase droplet size specifications and the influence of respective non-drag forces. Droplet size specifications include Sauter mean diameter (d_{32}), De Brouckere mean diameter (d_{43}) and 50 % volume based median diameter (d_{v50}), all based on separator inlet droplet size measurements.

8.1 Modelling background

One of the objectives of this PhD was to study the developed separator concept numerically. A validated numerical model will allow for eased design optimization of the developed concept, and provide a basis for preliminary studies of new design features.

The goal of this modelling study is thus to develop and validate a numerical model for the developed MPPS concept. The model can serve as a baseline for future work and continued development and improvement of the MPPS.

8.2 Modelling approach

Computational Fluid Dynamics (CFD), which is the use of computational methods to solve the respective differential conservation and transport equations of a fluid system, is the basis of modelling in this study. The commercially available software Ansys CFX has been used to develop a two-phase oil-water model of the developed MPPS concept. The Ansys CFX solver is based on the Finite Volume Method (FVM), which means that the fluid domain is discretized into a finite set of control volumes, and that general phasic conservation and momentum equations are solved on this set of control volumes.

Focus has been given to develop a model that is not too computationally demanding. For this reason, breakup and coalescence effects are not included in the model setup, and any dispersions will be treated as uniform in size. Forces acting on dispersed phase droplets will be limited to drag and non-drag forces. Other droplet interaction physics will not be included, neither will interfacial tension effects.

This section will present the utilized fluid domain, the control volume discretization (meshing) and details of the model employed.

8.2.1 Fluid domain

The fluid domain is illustrated in Figure 8.1. The geometry used for domain creation is a 3D model of the developed MPPS prototype. The inlet has a normal configuration, which was one of three inlet configurations tested in Paper III.

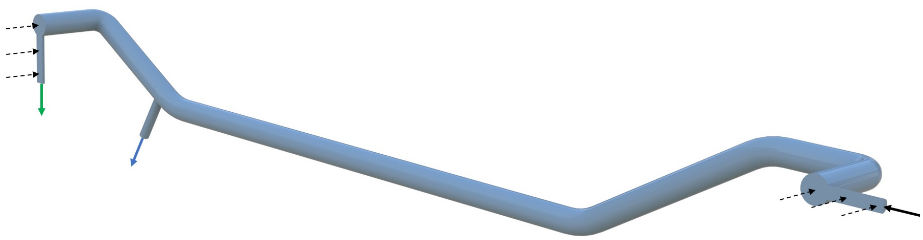

Fig. 8.1 Fluid domain of the MPPS CFD model

The inlet is indicated with a solid black arrow, the water outlet with a blue arrow, and the oil outlet with a green arrow. Only one tapping location for water is included in the geometry, which was the one used for the performance mapping study in Paper III. A symmetry plane is used in simulations, indicated with stippled arrows. The domain is thus half of the constructed MPPS prototype. As a result, the feed and oil extraction pipes are cut in half, while only one separation pipe and water extraction pipe is included. The inlet and extraction pipes have the same diameter as the ID of the rig feed and extraction pipes (67.8 *mm*), while the main separator pipe has a diameter of 150.6 *mm*. Dimensions are equal to those of the MPPS prototype, given in Chapter 3, Figure 3.7.

8.2.2 Meshing

The mesh used for simulations was a result of a mesh refinement study which will be presented in Section 8.3. The mesh consists of hexahedral elements, and a picture of the main pipe mesh cross section is given in Figure 8.2a. This mesh is extruded along the entire length of the main separator path. An equivalent mesh is used for the water extraction pipe. The mesh for the feed and oil extraction pipes are given in Figure 8.2b.

The total number of elements in the complete mesh is 1191506. This gives an average element volume of 1.12e-01 cm^3. The average length between nodes in the main pipe cross section is 3.42 *mm* , while it is 1.54 *mm* for the feed and extraction pipe cross sections. It

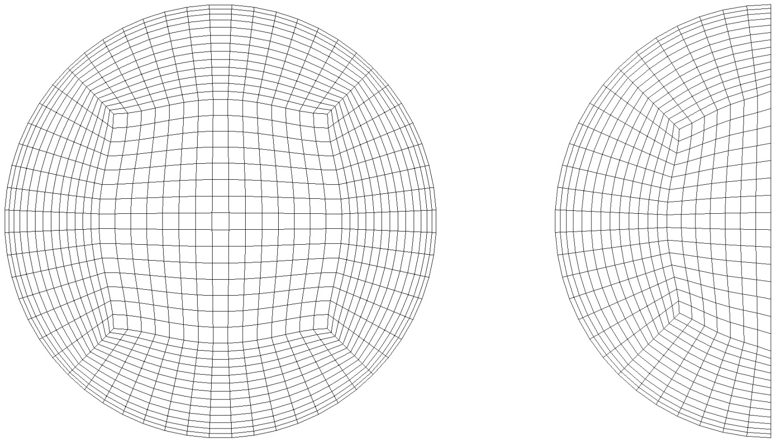

(a) Main separator pipe (b) Feed and oil extraction pipes

Fig. 8.2 Mesh cross sections

should be noted that the node spacing is decreasing towards the pipe wall, to a minimum of 1 *mm*. The node spacing in the pipe centre is thus larger than the average, approximately 5 *mm* for the main separator pipe. Lengthwise, the average node spacing is 7 *mm*.

8.2.3 Model specifications

The model is set up with a two-phase Eulerian-Eulerian solver, where one phase is fully dispersed in the other. This means that phasic momentum and continuity equations are solved for the respective phases. Model fluids are considered as Newtonian. The system is considered as isothermal, and with no mass transfer between the respective phases. Turbulence is treated as homogeneous, and is calculated with a k-Epsilon model. All simulations are steady state simulations, with specified convergence criteria. Buoyancy is specified for all simulations, with a reference density equal to that of the continuous fluid, and a specified gravity component of 9.81 m/s^2.

CFX offers several options for calculating interfaces and interfacial forces. Applied specifications will be outlined and explained in the following sections.

Interface modelling

For multiphase flows, the momentum equation will have a term governing interfacial forces between the respective phases. For an assumed two-phase domain with phases β and γ and no inerphase mass transfer, the momentum equation for phase β will take on the form [1]:

$$\frac{\partial}{\partial t}(\alpha_\beta \rho_\beta \mathbf{U}_\beta) + \nabla \cdot (\alpha_\beta(\rho_\beta \mathbf{U}_\beta \otimes \mathbf{U}_\beta)) = -\alpha_\beta \nabla P_\beta + \nabla \cdot (\alpha_\beta \mu_\beta(\nabla \mathbf{U}_\beta + (\nabla \mathbf{U}_\beta)^T) + \mathbf{S}_\beta + \mathbf{M}_\beta \tag{8.1}$$

Here, α_β represents the phase β volume fraction and $\mathbf{U}_\beta$ the phase β velocity vector. The right hand side terms $\mathbf{S}_\beta$ and $\mathbf{M}_\beta$ represents momentum forces due to external body forces and the interfacial forces acting on phase β due to the presence of other phases. For further derivation, the interfacial force term will be denoted $\mathbf{M}_{\beta\gamma}$, and represents interfacial forces acting on phase β due to phase γ. $\mathbf{M}_{\beta\gamma}$ is a sum of several independent physical effects, as illustrated in Eq. 8.2.

$$\mathbf{M}_{\beta\gamma} = \mathbf{M}_{\beta\gamma}{}^{D} + \mathbf{M}_{\beta\gamma}{}^{L} + \mathbf{M}_{\beta\gamma}{}^{VM} + \mathbf{M}_{\beta\gamma}{}^{TD} \tag{8.2}$$

Here, D symbolizes drag force, L symbolizes lift force, VM symbolizes virtual mass force and TD symbolizes turbulence dispersion force. An additional force term available in Ansys CFX is the wall lubrication force. This force captures the phenomenon of gas bubbles not fully approaching solid walls (an effect observed for bubbly upflow in vertical pipes [1]). The wall lubrication force tends to push the dispersed phase away from the wall. In the developed model, the effect of liquid-liquid separation is studied. In a real system, for appropriate flow rates, the heavier phase will settle at the bottom of the pipe, while the lighter phase will settle in the top region of the pipe. Depending on which phase is the dispersed, droplets will merge to the associated pipe region, coalesce and form a permanent liquid layer. The wall lubrication force which pushes the dispersed phase away from the wall has therefore been disabled for presented simulations.

The way the interfacial area is modelled dictates how the outlined forces are treated in CFX.

Drag force

In the present study, interfacial area is modelled as spherical droplet surfaces. In the following derivations, phase β is considered as the continuous phase, while phase γ is fully dispersed in β as spherical droplets with diameter d. The volume fraction of each phase is given as α_β and α_γ, with densities and viscosities given as ρ_β/ρ_γ and μ_β/μ_γ respectively. Spherical droplets will be denoted as particles to be consistent with the referenced terminology.

The area of a single particle projected in the flow direction, A_p, and the volume of a single particle, V_p, are derived in the following manner:

$$A_p = \frac{\pi d^2}{4} \tag{8.3}$$

$$V_p = \frac{\pi d^3}{6} \tag{8.4}$$

The number of particles in a unit (cell) volume, n_p/V_c, can be expressed as a function of the phase volume fraction, and the particle volume.

$$n_p/V_c = \frac{\alpha_\gamma}{V_p} = \frac{6\alpha_\gamma}{\pi d^3} \tag{8.5}$$

Knowing the number of particles per unit volume, the total drag per unit volume can be calculated. The drag force exerted by a single particle on the continuous phase β is given as:

$$\mathbf{D}_p = \frac{1}{2} C_D \rho_\beta A_p |\mathbf{U}_\gamma - \mathbf{U}_\beta|(\mathbf{U}_\gamma - \mathbf{U}_\beta) \tag{8.6}$$

C_D is here representing the particle drag coefficient, which is dependant on the particle Reynolds number. The total drag force on the continuous phase per unit volume can then be derived as:

$$\mathbf{D}_{\beta\gamma}/V_c = n_p \mathbf{D}_p/V_c = \frac{3}{4}\frac{C_D}{d}\alpha_\gamma \rho_\beta |\mathbf{U}_\gamma - \mathbf{U}_\beta|(\mathbf{U}_\gamma - \mathbf{U}_\beta) \tag{8.7}$$

In Ansys CFX the drag force is modelled as a function of the relative particle speed such that ${\mathbf{M}_{\beta\gamma}}^D$ in Eq. 8.2 is equal to ${c_{\beta\gamma}}^D(\mathbf{U}_\gamma - \mathbf{U}_\beta)$ [1]. Comparing this expression to Eq. 8.7, it is seen that ${c_{\beta\gamma}}^D$ takes on the form:

$${c_{\beta\gamma}}^D = \frac{3}{4}\frac{C_D}{d}\alpha_\gamma \rho_\beta |\mathbf{U}_\gamma - \mathbf{U}_\beta| \tag{8.8}$$

This formulation for interface drag is what is known as the particle model in Ansys CFX [1].

The particle drag coefficient is as mentioned dependant on the particle Reynolds number.

$$Re_p = \frac{\rho_\beta |\mathbf{U}_\gamma - \mathbf{U}_\beta| d_p}{\mu_\beta} \tag{8.9}$$

A modified Schiller-Naumann drag model has been used for calculating C_D in the presented work. The model specifies C_D as [1]:

$$C_D = max\left(\frac{24}{Re_p}(1 + 0.15{Re_p}^{0.687}), 0.44\right) \tag{8.10}$$

The model utilises the empirical correlations derived by Schiller and Naumann [27] for the Stokes and Transitional drag regimes ($0.1 < Re_p < 1000$) and a constant value of 0.44 in the Newton's drag regime ($Re_p > 1000$) where inertial effects dominate viscous effects, and the drag coefficient becomes independent of Re_p [1].

The Schiller-Naumann empirical correlations are made with spherical solid particles. The Eötvös number, Eo, indicates the ratio between gravitational and surface tension forces.

$$Eo = \frac{\Delta\rho g {d_p}^2}{\sigma} \tag{8.11}$$

For the current case, $\Delta\rho$ is the density difference between phases β and γ, g is the gravitational acceleration and σ is the interfacial tension. For cases where surface tension forces dominate ($Eo << 1$), spherical droplets are expected. The current study investigates liquid-liquid separation (low $\Delta\rho$), and as will be seen later, fairly small droplet diameters ($d \leq 250\ \mu m$). Calculated Eo for simulated test points indicate that dispersed droplets will be spherical, and the Schiller-Naumann approximation is therefore considered appropriate for the cases studied.

Non-drag forces

As outlined in Eq. 8.2, there are several forces besides drag acting on the interfaces of multicomponent systems. These forces are denoted non-drag forces, and Ansys CFX has several approaches for capturing the specific contributions. This section will give a brief overview of the non-drag forces that are included in the model setup, and which models have been used for capturing the individual contributions. Exact analytical expressions will not be provided for the non drag forces, and the reader is directed to [1] for a detailed overview.

Lift force The lift force (${\mathbf{M}_{\beta\gamma}}^L$) acts perpendicular to the direction of relative motion between the phases [1]. The model selected for lift force modelling in presented simulations is the Saffman Mei model [20]. The model is based on Saffman's correlation of the lift force for low Reynolds number flow past a spherical solid particle, which was later generalized by Mei and Klausner to include a higher range of particle Reynolds number flows [1]. The model is applicable for spherical solid particles and liquid droplets which are not significantly distorted [1]. The Saffman Mei model captures lift force arising from velocity gradients in the flow field.

Virtual Mass force The virtual mass force (${\mathbf{M}_{\beta\gamma}}^{VM}$) is important when the dispersed phase accelerates relative to the continuous. As a dispersed particle/droplet accelerates, it will also accelerate some of the surrounding fluid. This acceleration exerts an opposing force on the fluid particle, known as the virtual mass force. The virtual mass force has been included in the simulations given the nature of the fluid domain geometry. As seen in Figure 8.1, the inlet section can be a source of rapid deceleration and mixing, and there are downstream inclined sections promoting phase acceleration. A virtual mass coefficient of 0.5 is used for the simulations, which is the default value proposed by Ansys CFX [1].

Turbulent Dispersion force The turbulent dispersion force (${\mathbf{M}_{\beta\gamma}}^{TD}$) captures how a turbulent continuous phase interacts with a dispersed particulate phase. Particles will tend to be caught in continuous phase turbulent eddies, and be carried from regions of high volume fraction, to regions of low volume fraction [6]. The modelled fluid domain will have regions of higher turbulence (inlet and outlets) and regions of lower turbulence (main separator pipe). In regions of high turbulence, turbulent dispersion is expected to have an effect on the dispersed phase distribution. However, as the studied system consist of dispersed liquid droplets, regions of densely packed liquid droplets will promote coalescence, especially in low turbulent regions. Simulations will therefore be run with and without the turbulent dispersion force, to look how simulation results are affected by the inclusion. For simulations where the turbulent dispersion force is activated, a Favre averaged drag model will be used [1, 6]. The dispersion coefficient is set to 1.0, which is the default value proposed by Ansys CFX [1].

8.3 Mesh refinement

A mesh refinement study was carried out to ensure simulation results that are independent of the mesh quality. The number of elements in a mesh dictates simulation time, so finding the correct balance between accuracy and simulation speed is an important aspect of the model development.

Mesh refinement was done by running simulations with an initial coarse mesh, then gradually increasing the mesh quality until resulting deviation in results were within a specified tolerance. Parameters that will be used for model validation are the WC in the water and oil extraction lines, together with the resulting water extraction rate. The error in WC measurements that will be used for validation are all in the range of $\pm$ 0.25 pp. For the extraction rate, errors are in the range $\pm$ 0.2-0.7 pp. These values will be used as baseline maximum deviation targets for selecting a fitting mesh resolution. Test points used for model validation and associated errors are presented in Section 8.4.

8.3.1 Meshes

Five meshes were generated for the mesh refinement study. Each mesh is of increasingly finer resolution, with resolution being increased by the same factor in all three dimensions. In Table 8.1, an overview of the number of elements in the respective meshes is given.

Simulations with the same fluid property specifications and boundary conditions were run for all meshes.

Table 8.1 Number of elements in evaluated meshes

Mesh	Number of elements
1	120693
2	233096
3	575504
4	1191506
5	1946562

8.3.2 Boundary conditions and model specifications

There are in total five boundary locations that must be specified in order to close the simulation. Referring to Figure 8.1, these are the inlet, each of the two outlets, the pipe wall and the symmetry plane. For the mesh refinement process, a fictitious test point was ran. In the model validation part, details on how boundary conditions are calculated from test data will be given.

In Table 8.2, data for the fictitious test point used for the refinement process are given.

Table 8.2 Fictitious test point for mesh refinement

Variable	Unit	Value
Inlet flow rate	L/min	500.0
Inlet WC	$\%$	70.0
Water density	kg/m^3	1024.0
Oil density	kg/m^3	795.0
Water viscosity	cP	1.0
Oil viscosity	cP	1.3
Total inlet pressure	bar	1.53
Mass fraction of water extracted	$\%$	90.0

As the fluid domain in the simulations is only half of the constructed MPPS prototype, The inlet flow rate will be divided in two when calculating boundary conditions. For the five outlined boundaries, the following parameters will be specified:

- Inlet: Total pressure and phase fractions (P_{tot}, α_w, α_o)
- Water outlet: Bulk mass flow rate ($\dot{m}_{wo}$)
- Oil outlet: Bulk mass flow rate ($\dot{m}_{oo}$)
- Wall: Slip condition and pipe roughness
- Symmetry: Symmetry

In Table 8.3, resulting boundary conditions for the mesh refinement simulations are given.

Table 8.3 Mesh refinement boundary conditions

Location	Parameter	Unit	Value
Inlet total pressure	P_{tot}	bar	1.53
Inlet water fraction	α_w	$\%$	70.0
Inlet oil fraction	α_o	$\%$	30.0
Water outlet	$\dot{m}_{wo}$	kg/s	2.69
Oil outlet	$\dot{m}_{oo}$	kg/s	1.29
Wall slip	-	-	No slip
Wall roughness	-	-	Smooth

The oil phase is specified to be homogeneously dispersed in the water phase at the inlet, with a mean diameter of 250 μm. Of the discussed non-drag forces, lift, virtual mass and turbulent dispersion is included. The solver is specified with a residual root mean square (RMS) target of 1.0e-05 for the respective mass, momentum, pressure and turbulence equations.

8.3.3 Results

Results of the mesh refinement study is given in Figure 8.3. The figure displays deviation in respective parameter values for meshes 1-4 in relation to resulting parameter values for mesh 5. Results are given as deviation in percentage points (pp) and as % deviation of the corresponding mesh 5 value. Plot entries are numbered from 1-5 according to mesh statistics given in Table 8.1. A description of how reported parameters are calculated will be given in Section 8.4.

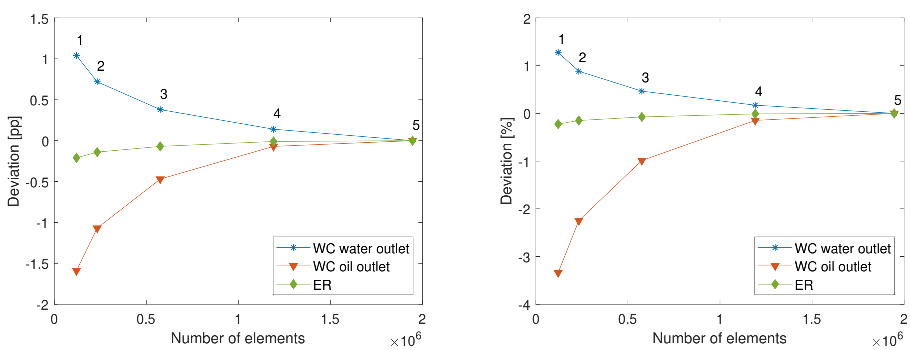

(a) Deviation in pp (b) Deviation in %

Fig. 8.3 Deviation from mesh number 5 results

From presented results it is seen that variable deviations decrease with increasing number of mesh elements, and that the deviation of mesh 4 is below 0.25 *pp* for all variables. The exact absolute deviations are 0.14 *pp*, 0.07 *pp* and 0.01 *pp* for the water outlet WC, oil outlet WC and ER respectively. Mesh number 4 is therefore used in further simulations.

8.4 Model validation

Validation of the developed model will be performed with normal inlet separation performance data gathered in Paper III, Chapter 5. In addition, droplet size measurements performed by master student Ellen Kristine Ellertsen will be used for droplet size specifications in the validation process. Three droplet diameter (d) specifications will be tested for the mono dispersed phase. These are the area weighted Sauter mean diameter (d_{32}), the volume weighted De Brouckere mean diameter (d_{43}) and the 50 % volume based median diameter (d_{v50}). The d_{v50} diameter is the largest droplet diameter below which 50 % of the accumulated sample volume exists.

8.4.1 Reference points and model input

The test points selected for model validation are the 650 L/min total flow rate, normal inlet test points from Paper III, Chapter 5. The study is limited to inlet water cuts of 30 % and 70 %. The reason for choosing these test points was that the inlet regimes are fully dispersed as either oil in water (70 % inlet WC) or as water in oil (30 % inlet WC). This can be observed from the presented flow pattern map in Paper III.

The referenced flow pattern map was developed based on test points run by master student Ellen Kristine Ellertsen. In parallel with flow pattern map development, the master student performed droplet size measurements with the same PVM equipment and experimental setup as described in Chapter 3. The mapping and droplet size measurements were performed with a normal inlet configuration, in the same time period as the normal inlet performance map was established. Experiments were run with a fully open inlet choke (VT.1), and fully open return valves (VT.2/3). The test matrix for the flow pattern mapping study is outlined in Paper III. PVM pictures were captured for the 30 % and 70 % inlet water cut test points. Pictures were captured over a 2 minute period, with a frequency of 2 Hz, resulting in a total of 240 images per test point. Measurements were taken approximately 0.15 ID from the top of the internal pipe wall. The images recorded by the master student are used for droplet size estimates in the presented modelling work.

Parameter values

Measured reference parameters used for boundary condition calculation and model validation are listed in Table 8.4.

Table 8.4 Parameter reference values

Parameter	Unit	$WC_{in} = 70$ %			$WC_{in} = 30$ %		
		90 % ER	70 % ER	50 % ER	90 % ER	70 % ER	50 % ER
$\dot{Q}_1$	L/min	455.1	455.1	455.1	195.0	195.0	195.0
$\dot{Q}_2$	L/min	195.1	195.1	195.1	455.3	455.2	455.2
$\dot{Q}_3$	L/min	412.8	319.1	229.4	176.4	136.0	98.5
ρ_1	kg/m^3	1019.1	1019.5	1018.2	1020.1	1021.5	1021.3
ρ_2	kg/m^3	794.3	794.3	794.4	795.1	795.1	797.1
ρ_3	kg/m^3	999.3	1010.8	1015.1	981.4	993.35	1006.4
P_1	bar	1.51	1.24	1.25	1.28	1.36	1.45
T_1	$°C$	16.8	16.7	16.7	17.1	17.1	17.1
ρ_w	kg/m^3	1022.4	1022.5	1022.5	1022.4	1022.4	1022.4
ρ_o	kg/m^3	794.0	794.1	794.1	793.8	793.8	793.8

Parameter notations correspond to parameters listed in Table 3.4, Chapter 3, which also indicates the location of the measurements. The procedure for calculating stream water cuts (Eq. 3.1), inlet WC (Eq. 3.2) and extraction rates (Eq. 3.3) are also included in the referenced chapter. For model validation, the WC at the water extraction point (WC_3), together with the ER will be used. In Table 8.5, calculated values for WC_3 and ER are given for all test points. In addition, resulting inlet water cuts (WC_{in}) are listed, which are used for boundary condition calculations. The reference densities for water and Exxsol^{TM} D60 (ρ_w, ρ_o) listed in Table 8.4 are used in the calculations.

Table 8.5 Validation and input parameters

Parameter	Unit	$WC_{in} = 70$ %			$WC_{in} = 30$ %		
		90 % ER	70 % ER	50 % ER	90 % ER	70 % ER	50 % ER
WC_3	%	89.9	94.9	96.8	82.1	87.3	93.0
ER	%	90.7	70.1	50.4	90.5	69.8	50.5
WC_{in}	%	69.0	69.1	68.7	30.2	30.3	30.9

Errors associated with the validation and input parameters have maximum values of $\pm$ 0.25 pp for WC_3, $\pm$ 0.40 pp for ER and $\pm$ 0.27 pp for WC_{in}.

8.4.2 Boundary conditions

The following boundary conditions are calculated and specified for the respective boundaries.

Inlet

Boundary conditions specified for the inlet are the total inlet pressure (P_{tot}) and phase volume fractions of oil and water (α_o, α_w). The total inlet pressure is calculated as a function of the recorded static pressure and estimated dynamic pressure.

$$P_{tot} = P_1 + \frac{1}{2}\rho_m(\dot{Q}_1 + \dot{Q}_2)/A \tag{8.12}$$

Here, A is the inlet pipe (67.8 mm ID) cross sectional area, and all parameters are given in SI units (m^3/s for flow, Pa for pressure, m^2 for area and kg/m^3 for density). SI units is also the basis of all further calculation. The mixture density (ρ_m) is calculated as given in Eq. 8.13.

$$\rho_m = WC_{in}\rho_w + (1 - WC_{in})\rho_o = \alpha_w\rho_w + \alpha_o\rho_o \tag{8.13}$$

Eq. 8.13 also gives the corresponding values for the inlet water and oil phase fractions (α_w, α_o) which are set according to the calculated inlet water cut, WC_{in}.

Outlets

The outlet boundary conditions are specified as bulk mass flow rates. The bulk mass flow rate for the water outlet ($\dot{m}_{wo}$) is calculated from reported values in Table 8.4.

$$\dot{m}_{wo} = 0.5\dot{Q}_3\rho_3 \tag{8.14}$$

Half the recorded flow rate is used in calculation because of the applied symmetry plane. A resulting assumption is that the measured water extraction flow rate is divided equally between the two water extraction points of the MPPS prototype.

The bulk mass flow rate for the oil outlet is calculated by assuming steady state operation and an even phase distribution over the inlet and oil outlet cross sectional areas.

$$\dot{m}_{oo} = 0.5(\dot{Q}_1\rho_1 + \dot{Q}_2\rho_2) - \dot{m}_{wo} \tag{8.15}$$

Overview

An overview of the calculated and applied boundary conditions are given in Table 8.6.

As for the mesh refinement study, walls are specified as no-slip smooth walls for all simulations, and the symmetry plane is specified as illustrated in Figure 8.1.

8.4.3 Droplet size estimation

As previously mentioned, the three mono dispersed droplet diameters to be tested in this study are the d_{32}, d_{43} and d_{v50}. PVM pictures recorded by master student Ellen Kristine Ellertsen

Table 8.6 Validation tests boundary conditions

Parameter	Unit	$WC_{in} = 70$ %			$WC_{in} = 30$ %		
		90 % ER	70 % ER	50 % ER	90 % ER	70 % ER	50 % ER
P_{tot}	bar	1.55	1.28	1.29	1.32	1.40	1.49
α_w	%	69.0	69.1	68.7	30.2	30.3	30.9
α_o	%	31.0	30.9	31.3	69.8	69.7	69.1
$\dot{m}_{wo}$	kg/s	3.44	2.69	1.94	1.44	1.13	0.83
$\dot{m}_{oo}$	kg/s	1.72	2.47	3.21	3.23	3.55	3.86

are used for droplet size estimations. Pictures were analyzed with an image analysis software (SOPAT GmbH, Germany), which automatically registers individual droplet diameters. This is the same analysis tool used in Paper V, which also includes references outlining the software functionality as well as previous applications of the software in literature.

In Table 8.7, the number of droplets recorded, and the resulting droplet size estimates for the two test points are reported.

Table 8.7 Droplet size data for the 70 % and 30 % inlet water cut, 650 L/min total flow rate test points

WC_{in} [%]	Number of droplets	d_{32} [μm]	d_{43} [μm]	d_{v50}[μm]
70	4743	121.0	177.3	192.1
30	3696	151.2	196.6	213.8

8.4.4 Validation procedure

The validation procedure is divided in three steps. The first step is evaluating the effect of the different droplet size specifications. The second step studies the effect of initial droplet distribution at the inlet and the effect of the turbulent dispersion force, while the third step validates performance against recorded data.

Initial simulations (step one) were run with input data from the 70 % WC_{in}, 90 % ER test point. Phase densities were specified as outlined in Table 8.4 (ρ_o and ρ_w), and phase viscosities were set to values given in Paper III. Drag and non-drag forces were specified as outlined in Section 8.2.3, with the turbulent dispersion force enabled. The water phase is specified as continuous and the oil phase as dispersed (according to the test point flow regime), with the oil phase being homogeneously dispersed at the inlet. Droplet sizes are varied according to values given in Table 8.7. The solver was set with a residual root mean square (RMS) target of 1.0e-05 for the respective momentum, pressure and turbulence equations, and 1.0e-04 for the mass equations. These targets are the same for further simulations, and were set to reduce simulation time. The mass imbalance will be reported for all test points.

The second step was performed on the simulation setting from step one providing the best results. In this step, a homogeneous dispersion at the inlet was compared to a variable inlet dispersion. A variable inlet dispersion is here signifying that the phase fraction over the inlet is not uniform. For the variable inlet fraction, the inlet volume fraction of oil was specified as a function of the height (h) from the centre of the inlet pipe, and the radius (R) of the same pipe.

$$\alpha_o(h) = \frac{\alpha_o}{R}(R+h) \tag{8.16}$$

This gives a shifted phase distribution at the inlet, where there is no oil dispersion at the bottom of the pipe, and the amount of dispersion gradually increases to a maximum at the top of the pipe. The overall volume fraction is the same as for the homogeneous inlet fraction case, and the droplet sizes are the same for all heights. In addition to investigating the effect of phase distribution, both cases were run with and without the turbulent dispersion force.

Finally, the simulation configuration displaying best conformance to logged separator performance was run for all test points outlined in Table 8.5 to evaluate model accuracy.

The validation parameters WC_3 and ER are compared with equivalent values calculated form completed simulations (WC_{wo}, ER_{wo}). Values are calculated in the following manner:

$$WC_{wo} = \frac{\dot{m}_{w_{wo}}/\rho_w}{\dot{m}_{w_{wo}}/\rho_w + \dot{m}_{o_{wo}}/\rho_o} \tag{8.17}$$

Here, $\dot{m}_{w_{wo}}$ and $\dot{m}_{owo}$ are the total accumulated mass flow of water and oil at the water outlet boundary. Equivalently, for calculation of ER_{wo}, $\dot{m}_{w_{in}}$ symbolizes the total accumulated mass flow rate of water at the inlet boundary.

$$ER_{wo} = \frac{\dot{m}_{w_{wo}}/\rho_w + \dot{m}_{o_{wo}}/\rho_o}{\dot{m}_{w_{in}}/\rho_w} \tag{8.18}$$

8.4.5 Results

In Table 8.8, results for the initial simulations investigating appropriate droplet size specification are given.

Reported errors are deviations in percentage from reported values in Table 8.5. The mass imbalance for the same simulations are given in Table 8.9. Negative values are out of the domain, while positive values are in to the domain.

From reported results it is seen that a d_{v50} droplet size specification provided best results of the tested values, reporting WC_3 and ER with errors of 15.6 % and 4.9 % respectively. d_{v50} is thus used for the further analysis.

Table 8.8 Simulation results for droplet size evaluation study

WC_{in} [%]	ER [%]	Turb. disp.	d	WC_{wo} [%] Val.	WC_{wo} [%] Error	ER_{wo} [%] Val.	ER_{wo} [%] Error
70	90	Yes	d_{32}	72.5	19.4	95.9	5.7
			d_{43}	75.1	16.5	95.3	5.1
			d_{v50}	75.9	15.6	95.1	4.9

Table 8.9 Mass imbalances for droplet size evaluation study

WC_{in} [%]	ER [%]	Turb. disp.	d	Mass imbalance [kg/s] Water	Exxsol^{TM} D60	Total
70	90	Yes	d_{32}	-5.85e-04	4.55e-04	-1.30e-04
			d_{43}	-9.02e-03	7.01e-03	-2.02e-03
			d_{v50}	-1.03e-02	8.03e-03	-2.31e-03

The next step looked at the effect of disabling turbulence dispersion, and specifying a non-homogeneous volume fraction for dispersed droplets at the inlet. Results are given in Table 8.10, with associated mass imbalances given in Table 8.11.

Table 8.10 Simulation results for turbulent dispersion and inlet volume fraction distribution study

WC_{in} [%]	ER [%]	Turb. disp.	Inlet dist.	d	WC_{wo} [%] Val.	WC_{wo} [%] Error	ER_{wo} [%] Val.	ER_{wo} [%] Error
70	90	Yes	Hom.	d_{v50}	75.9	15.6	95.1	4.9
			Var.		75.6	15.9	95.5	5.3
		No	Hom.		85.1	5.3	93.1	2.6
			Var.		85.2	5.2	93.3	2.9

Table 8.11 Mass imbalances for turbulent dispersion and inlet volume fraction distribution study

WC_{in} [%]	ER [%]	Turb. disp.	Inlet dist.	d	Mass imbalance [kg/s] Water	Exxsol^{TM} D60	Total
70	90	Yes	Hom.	d_{v50}	-1.03e-02	8.03e-03	-2.31e-03
			Var.		-1.35e-02	1.05e-02	-3.02e-03
		No	Hom.		-1.86e-02	1.45e-02	-4.16e-03
			Var.		-4.50e-03	3.49e-03	-1.01e-03

Presented results display minimal effect of utilizing a variable volume fraction distribution at the separator inlet. A large effect is however observed for disabling the turbulent dispersion force in the simulations. For the homogeneous inlet distribution case, a reduction in WC_{wo} error from 15.6 % to 5.3 % was achieved by disabling the turbulent dispersion. Final simulations are therefore ran with no turbulent dispersion enabled, and the distribution of the dispersed phase at the inlet is selected as homogeneous.

In Table 8.12, the final simulation results for all test points are given. The corresponding mass imbalance values are listed in Table 8.13.

Table 8.12 Final simulation results for all test points

WC_{in} [%]	ER [%]	Turb. disp.	Inlet dist.	d	WC_{wo} [%] Val.	Error	ER_{wo} [%] Val.	Error
70	90	No	Hom.	d_{v50}	85.1	5.3	93.1	2.6
	70				90.2	5.0	71.9	2.6
	50				97.6	0.8	51.3	1.8
30	90				60.1	26.8	94.6	4.5
	70				70.6	19.1	71.9	3.0
	50				79.7	14.3	50.6	0.2

Table 8.13 Mass imbalances for final simulations

WC_{in} [%]	ER [%]	Turb. disp.	Inlet dist.	d	Mass imbalance [kg/s] Water	Exxsol^{TM} D60	Total
70	90	No	Hom.	d_{v50}	-1.86e-02	1.45e-02	-4.16e-03
	70				-3.762e-02	2.92e-02	-8.40e-03
	50				-1.59e-02	1.24e-02	-3.55e-03
30	90				-2.15e-02	1.67e-02	-4.81e-03
	70				-7.42e-03	5.76e-03	-1.66e-03
	50				-1.44e-03	1.12e-03	-3.21e-04

From presented results it is seen that the developed model works well for water-continuous inlet regimes, predicting WC of extracted water with errors ranging from 5.3 % to 0.8 %. Best model performance is observed for low extraction rates.

The model is not predictive for oil-continuous inlet regimes. Predicted WC of extracted water greatly deviates from reported test results, showing deviations in the range of 20 %. Again, model predictivity is observed to increase with reducing extraction rates, but minimum deviation is still 14.3 % for an extraction rate of 50 %.

Reported mass imbalances are within acceptable levels, with a maximum water phase imbalance of -3.76e-02 kg/s, being equal to -2.2 L/min or 1.0 % of the inlet water rate.

In Figure 8.4, pictures of the experimental and simulated holdup directly upstream the ascending extraction pipe is given. The pictures are from experimental testing, at a total flow rate of 650 L/min, 70 % inlet water cut and 50 % ER, and post processing of the same modelled test point.

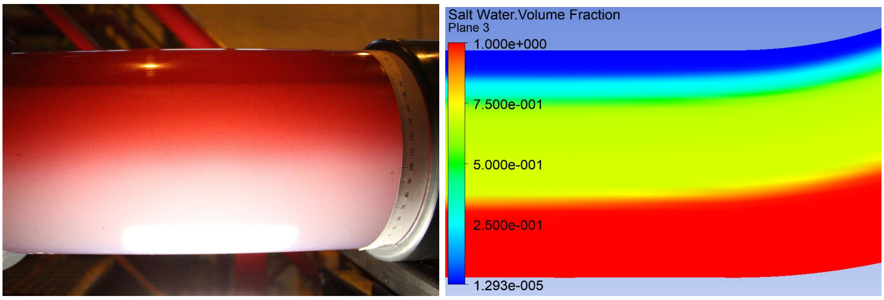

(a) Experimental (b) Simulation

Fig. 8.4 Experimental and simulates holdup at $\dot{Q}_{tot} = 650\ L/min$, $WC_{in} = 70$ % and $ER = 50$ %

From the figures, the predicted holdup appears to be close to actual, with a slight under-prediction of the established water and Exxsol^{TM} D60 layer heights. An under-predicted water layer thickness can explain why simulation results improved for low extraction rates.

8.5 Conclusion

The developed model, utilizing dispersed phase droplet diameters equal to measured d_{v50} and no turbulent dispersion is able to predict separator performance to within 5 % of experimental values for water-continuous inlet regimes. The model is well suited for further evaluation of the MPPS design, and can be used as an initial step to predict separator performance for suggested improvements.

Model performance for oil-continuous inlet regimes is not satisfactory, and further modifications and improvements should be made to the model for study of these cases.

Chapter 9

Conclusions and recommendations for future work

This chapter gives a summary of conclusions from published papers and journal articles. Conclusions from the performed modelling study are also summarized here. Additionally, recommendations for future work are presented. Recommendations are made for both the experimental part and the modelling part of performed studies.

9.1 Summary of conclusions

Conclusions will be summarized according to experimental campaigns outlined in Chapter 3. Conclusions from the modelling study are summarized in a separate section.

9.1.1 Campaign 1

Presented results indicate that there is re-entrainment of Exxsol^{TM} D60 droplets along the length of the ascending extraction pipe. Performed tests indicate that water should be extracted close to the horizontal section of the pipe, where re-entrainment is minimal.

9.1.2 Campaign 2

Of the three inlet designs evaluated, the tangential inlet with novel phase re-arranging internals resulted in best separator performance. The separator prototype exhibits a wide operational envelope, providing good separation efficiencies at flow rates ranging from 550 L/min (4982 bpd) at 30 % inlet WC, 50 % ER, to 650 L/min (5887 bpd) at 90 % inlet WC, 90 % ER. Separator performance is observed to drop with decreasing inlet water cuts and increasing water extraction rates. Drop in performance is seen in connection with formation of a dispersion layer in the 30-50 % inlet WC range, which is partly extracted through the water extraction line at high extraction rates. The thickness of the dispersion layer increases with increasing inlet flow rates.

An uneven distribution of the formed dispersion layer in the separator branches was observed, and the operational range for where it occurs was identified. The dispersion layer was originally present in both separator branches, but was observed to fully migrate into one separator branch over time. Migration of the dispersion layer was eliminated by the installation of developed internals.

9.1.3 Campaign 3

The control strategy based on proxy level monitoring of the water level in the inclined extraction pipe sections provided the best separator performance. When utilizing measured WC_r as a control variable, the controller would continuously increase the extraction rate until Exxsol$^{\text{TM}}$ D60 was carried under in the water extraction line. A sudden automatic adjustment to the valve opening was then made, brining the WC_r back to acceptable values. This behaviour would repeat in a cycle and several instances of unacceptable water quality were recorded. When controlling separator performance with the established proxy level indicator, more stable operation was observed, as a permanent buffer layer of water was maintained in the ascending extraction pipe. This eliminated the problem of repeating drops in water quality, and secured good separator performance for the inlet cycle tested.

The control strategy developed in this study utilized two decoupled controllers in parallel. As the separator is a multiple input, multiple output system, it is expected that separator performance would increase with the use of a multivariable controller or a model predictive controller.

9.1.4 Campaign 4

The study revealed an overall decrease in separator performance with increasing levels of inlet choking. A further performance decrease was observed when adding surfactant. The decrease in performance is seen in connection with an increased dispersion layer thickness at the separator outlet, which was extracted at high extraction rates. For water-continuous inlet regimes, maximum decrease in WC_r due to inlet choking was found to be 14 pp. Maximum decrease in WC_r due to the addition of surfactant was 4 pp. The addition of surfactant was seen to enhance degradation in performance, especially in combination with inlet choking. Results indicate that the operational envelope can be significantly affected by inlet choking and surfactants, especially in the 50 % inlet WC range.

For oil-continuous inlet regimes, at select test points, moderate choking or addition of surfactant lead to a slight increase in recorded performance.

9.1.5 Modelling

A two-phase Euler-Euler CFD model considering one dispersed and one continuous phase provided an accurate prediction of extracted water quality for the water-continuous inlet regimes tested.

9.1.6 Fulfilment of outlined research goal

The goal of this PhD was to develop and test a novel oil-water separator concept for subsea produced water bulk separation. The developed concept was to meet identified challenges with current subsea oil-water bulk separator technologies, and by that promote future subsea produced water separator developments. The study was to be both experimental and numerical, investigating design improvements, control strategies and fundamental oil-water flow behaviour in the separator.

It is the author's belief that the outlined research goal has been met. A novel separator concept (the MPPS) has been designed, developed and tested. The developed concept exhibits good overall performance, and entails a significant size and weight reduction compared to traditional separator designs. A flow phenomenon involving uneven distribution of forming dispersion layers has been reported, and flow behaviour within the separator has been analyzed. Better understanding of the reported phenomenon can assist development of novel technologies for targeted dispersion and emulsion breakage. Concept design improvements have been investigated, and a strategy for efficiently controlling separator performance has been outlined. The effect inlet choking and addition of surfactant has on separator performance has been evaluated. The presence of surfactant in combination with inlet choking was observed to give the largest degradation in separator performance. This illustrates a potential benefit of subsea produced water separation.

The developed separator concept provides a good foundation for further development and study. It is believed that the presented design can serve as a basis for the development and implementation of next generation subsea produced water separators, which overcomes outlined challenges with current designs. Additionally, the results of this research can be useful and relevant for the development and refinement other oil-water bulk separator concepts based on a parallel pipe design.

9.2 Future work

Proposals for future work is divided between experimental and modelling activities.

9.2.1 Experimental

Proposed future activities are related to enhancing the developed separator concept in terms of technology readiness, further study of discovered flow effects and design improvements of the current configuration.

Gas-liquid experiments

Separator performance can be greatly affected by the presence of gas. Investigating separator performance with small amounts of gas (residual gas from upstream gas-liquid separation) in the inlet stream is therefore a natural next step in the development. In addition, the inlet section should be modified for gas-liquid separation, so the gas liquid separating capability of the concept can be evaluated. Required design improvements for gas-liquid separation should be identified, tested and implemented.

Solid-liquid experiments

In real field operation, solids can accumulate in the separator pipes. Investigating how solids are transported in the separator, and identify locations for potential solids build up, are important steps for further concept development. This also includes developing strategies for solids removal if needed. Needed design improvements for solid-liquid separation should be identified, tested and implemented.

Design improvements

Completed studies of the developed separator concept have revealed several areas for potential design improvements. The current extraction and tapping design causes re-entrainment of oil droplets into the established water layer. A more gradual transition from horizontal to inclined can reduce mixing and result in better separator efficiency. The effect of inclination angle can also be studied, to evaluate if there are better configurations for promoting water layer growth and minimizing mixing and re-entrainment.

The effect descending pipe sections at the inlet has on liquid-liquid separation should be evaluated. If up-stream gas-liquid separation is installed, and no gas is present at the separator inlet, a horizontal inlet alignment with subsequent splitting might be preferred. This will reduce excessive mixing.

Effects for future study

The discovered uneven splitting phenomenon is an effect that is attractive for further study. Possible topics include cause of occurrence, how migration can be controlled, and why installed internals prohibit uneven splitting to occur. Further understanding of this phenomenon can allow development of technologies for targeted breaking of formed oil-water emulsions.

Control

The separator is subject to several constraints and control objectives. Model predictive control was therefore suggested as a more fitting controller approach, compared to the two decoupled controllers used in the reported study. Suggestions for future work includes development of a model predictive controller for the separator, and finding optimal setpoints and outputs to maximize separator performance within specified constraints.

9.2.2 Modelling

The developed model displayed good conformance to experimental results for water-continuous inlet regimes. As part of future work, the model should be used to evaluate proposals for separator design improvement. An improvement to the developed model is to use existing droplet size prediction models in literature to provide d_{v50} sizes based on input parameters and not droplet size measurements. Models should be validated against reported data in literature, for instance reported droplet size values in Paper V, Chapter 7. Further model improvement is needed for oil-continuous inlet regimes, where the current model fails to predict separator performance.

References

[1] *Ansys CFX Modeling guide, Version 17.2*, 2019.

[2] S. Abrand, S. Shaiek, S. J. Anres, R. Hallot, et al. Subsea gas-liquid and water-hydrocarbon separation: Pipe solutions for deep and ultra deepwater. In *OTC Brasil*. Offshore Technology Conference, 2013.

[3] M. Berard, K. Babour, and I. Babelli. In-line flow separation of fluids in a pipe separator, Aug. 23 2011. US Patent 8,002,121.

[4] M. Bothamley et al. Offshore processing options for oil platforms. In *SPE Annual Technical Conference and Exhibition*. Society of Petroleum Engineers, 2004.

[5] B. Bringedal, T. Ingebretsen, K. Haugen, et al. Subsea separation and reinjection of produced water. In *Offshore Technology Conference*. Offshore Technology Conference, 1999.

[6] A. D. Burns, T. Frank, I. Hamill, J.-M. Shi, et al. The favre averaged drag model for turbulent dispersion in eulerian multi-phase flows. In *5th international conference on multiphase flow, ICMF*, volume 4, pages 1–17. ICMF, 2004.

[7] C. A. Capela Moraes, F. S. da Silva, L. P. M. Marins, A. S. Monteiro, D. A. de Oliveira, R. M. Pereira, R. d. S. Pereira, A. Alves, G. M. Raposo, R. Orlowski, et al. Marlim 3 phase subsea separation system: Subsea process design and technology qualification program. In *Offshore Technology Conference*. Offshore Technology Conference, 2012.

[8] F. S. da Silva, A. S. Monteiro, D. A. de Oliveira, C. A. Capela Moraes, P. M. Marins, et al. Subsea versus topside processing-conventional and new technologies. In *OTC Brasil*. Offshore Technology Conference, 2013.

[9] S. R. Davies, W. Bakke, R. M. Ramberg, R. O. Jensen, et al. Experience to date and future opportunities for subsea processing in statoilhydro. In *Offshore Technology Conference*. Offshore Technology Conference, 2010.

[10] D. A. de Oliveira, R. d. S. Pereira, C. A. Capela Moraes, V. P. Baracho, R. d. S. A. de Souza, M. L. L. Euphemio, F. S. da Silva, A. S. Monteiro, C. C. Casanova, D. G. Duarte, et al. Comissioning and startup of subsea marlim oil and water separation system. In *OTC Brasil*. Offshore Technology Conference, 2013.

[11] M. Dudek, A. Bertheussen, T. Dumaire, and G. Øye. Microfluidic tools for studying coalescence of crude oil droplets in produced water. *Chemical Engineering Science*, 191:448–458, 2018.

[12] M. Dudek, E. Kancir, and G. Øye. Influence of the crude oil and water compositions on the quality of synthetic produced water. *Energy & Fuels*, 31(4):3708–3716, 2017.

[13] M. Euphemio, R. Oliveira, G. Nunes, C. Capela, L. Ferreira, et al. Subsea oil/water separation of heavy oil: Overview of the main challenges for the marlim field-campos basin. In *Offshore Technology Conference*. Offshore Technology Conference, 2007.

[14] A. Fakhru'l-Razi, A. Pendashteh, L. C. Abdullah, D. R. A. Biak, S. S. Madaeni, and Z. Z. Abidin. Review of technologies for oil and gas produced water treatment. *Journal of hazardous materials*, 170(2-3):530–551, 2009.

[15] P. Gramme and G. H. Lie. Pipe separator with improved separation, Feb. 17 2009. US Patent 7,490,671.

[16] P. E. Gramme and I. Haukom. Pipe separator for the separation of fluids, particularly oil, gas and water, Apr. 14 2009. US Patent 7,516,794.

[17] A. Hannisdal, R. Westra, M. R. Akdim, A. Bymaster, E. Grave, D. T. Teng, et al. Compact separation technologies and their applicability for subsea field development in deep water. In *Offshore technology conference*. Offshore Technology Conference, 2012.

[18] T. Horn, W. Bakke, G. Eriksen, et al. Experience in operating world's first subsea separation and water injection station at troll oil field in the north sea. In *Offshore Technology Conference*. Offshore Technology Conference, 2003.

[19] O. Kristiansen, Ø. Sørensen, O. Nilssen, et al. Compactsep™-compact subsea gas-liquid separator for high-pressure wellstream boosting. In *Offshore Technology Conference*. Offshore Technology Conference, 2016.

[20] R. Mei and J. Klausner. Shear lift force on spherical bubbles. *International Journal of Heat and Fluid Flow*, 15(1):62–65, 1994.

[21] R. J. Moffat. Describing the uncertainties in experimental results. *Experimental thermal and fluid science*, 1(1):3–17, 1988.

[22] G. Mogseth et al. Functional verification of the worlds first full field subsea separation system-tiora. In *Offshore technology conference*. Offshore Technology Conference, 2008.

[23] NOROG. 2018 environmental report - environmental work by the oil and gas industry, facts and development trends. Technical report, NOROG, 2018.

[24] S. J. Ohrem, H. S. Skjefstad, M. Stanko, and C. Holden. Controller design and control structure analysis for a novel oil–water multi-pipe separator. *Processes*, 7(4):190, 2019.

[25] R. Orlowski, M. L. L. Euphemio, M. L. Euphemio, C. A. Andrade, F. Guedes, L. C. Tosta da Silva, R. G. Pestana, G. de Cerqueira, I. Lourenço, A. Pivari, et al. Marlim 3 phase subsea separation system-challenges and solutions for the subsea separation station to cope with process requirements. In *Offshore Technology Conference*. Offshore Technology Conference, 2012.

[26] R. M. Rivera, M. Golan, J. D. Friedemann, B. Bourgeois, et al. Water separation from wellstream in inclined separation tube with distributed tapping. In *SPE Annual Technical Conference and Exhibition*. Society of Petroleum Engineers, 2006.

[27] L. Schiller and A. Naumann. *VDI Zeitz*, 77:318, 1933.

[28] S. Shaiek, L. Grandjean, et al. Spoolsep for subsea produced water separation-experimental results. In *Offshore Technology Conference*. Offshore Technology Conference, 2015.

[29] H. S. Skjefstad and M. Stanko. Subsea water separation: a state of the art review, future technologies and the development of a compact separator test facility. In *18th International Conference on Multiphase Production Technology*. BHR Group, 2017.

[30] H. S. Skjefstad and M. Stanko. An experimental study of a novel parallel pipe separator design for subsea oil-water bulk separation. In *SPE Asia Pacific Oil and Gas Conference and Exhibition*. Society of Petroleum Engineers, 2018.

[31] H. S. Skjefstad and M. Stanko. Experimental performance evaluation and design optimization of a horizontal multi-pipe separator for subsea oil-water bulk separation. *Journal of Petroleum Science and Engineering*, 176:203–219, 2019.

[32] S. Skogestad and C. Grimholt. The simc method for smooth pid controller tuning. In *PID Control in the Third Millennium*, pages 147–175. Springer, 2012.

[33] O. Skovholt. Inclined tubular separator for separating oil well substances, Aug. 8 2017. US Patent 9,724,623.

[34] O. Skovholt. Method for separating substances mixed in fluids from oil wells, Nov. 28 2017. US Patent 9,827,509.

[35] S. Wong, J. Lim, and S. Dol. Crude oil emulsion: A review on formation, classification and stability of water-in-oil emulsions. *Journal of Petroleum Science and Engineering*, 135:498–504, 2015.

Appendix A

Calibration certificates

Micro Motion, Inc. — **Mass Flowmeter Calibration Certificate** — **15018910**

Product Code	Serial ID	Order ID	Line	Item	Customer Tag
F200S369C2EZNZKZZ	15018910	22045314	2.1	1	
PUCK800	33369466				

Process

Process ID : 2.41668262
Process Time : 2017.06.15 11:01:58
Process Stand : SSF2A@SSCE
Stand Uncertainty : +/-0.030%
Fluid : H20
100% Rate : 725.7477 KG/MIN
Pickoff : 1
Max Rate P/T : 17.14 PSIG/19.5 C

Results

Status : PASS
D1 : 0
D2 : 1
K1 : 3375.878
K2 : 3885.176
DT : 4.5
FD : 6000
DTG : 0
DFQ1 : 0
DFQ2 : 0
FlowCal : 1518.84.56
FFQ : 0
FTG : 0
DensCal : 03376038854.50
FCF : 1518.8
FT : 4.56

Detail

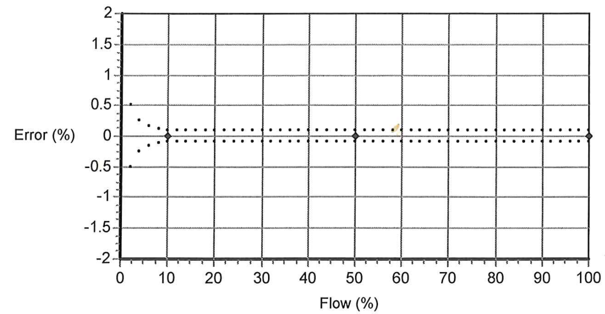

Flow (%)	Flow Rate (kg/min)	Meter Total (kg)	Reference Total (kg)	Error (%)	Specification (±%)
100.0	725.7477	751.9714	751.8981	0.010	0.100
10.0	72.57477	98.63879	98.62951	0.009	0.100
50.0	362.8739	373.6875	373.6937	-0.002	0.100
100.0	725.7477	753.7616	753.7493	0.002	0.100

STOLP T.
Technician 014 EPM-C
This certificate is produced by an electronic data system and is valid without signature.

Traceable to one or more of the following National Metrology Institutes: NIM-China, NIST-USA, and VSL-The Netherlands 15.0.0.140 2017.06.15 11:15:33 1/1

Micro Motion, Inc.

Transmitter Configuration Report — **19005565**

Product Code	Serial ID	Order ID	Line	Item	Customer Tag
F200S369C2EZNZKZZ	15018910	22045314	2.1	1	
5700R12AEFAZZZ	19005565	22045314	2.48	1	
PUCK800	33369466				

Process

Process ID : 2.41674782
Process Time : 2017.06.15 15:28:10
Process Stand : MMIV XMTR CONFIG@SSCE

Sensor

D1 : 0
D2 : 1
DFQ1 : 0
DFQ2 : 0
DT : 4.5
DTG : 0
Density Meter Factor : 1
Density Press Comp Factor : 0
FCF : 1518.8
FD : 6000
FFQ : 0
FT : 4.56
FTG : 0
Flow PCP : 19.99998
Flow PCF : 0
K1 : 3375.878
K2 : 3885.176
Mass Flow Meter Factor : 1
Temperature Cal Factor : 1.00000T.00000
Volume Flow Meter Factor : 1

Units

Density Unit : G/CUCM
GSV Flow Unit : SCFM
Mass Flow Unit : KG/MIN
Pressure Unit : PSI
Special GSV Base Time Unit : MIN
Special GSV Base Volume Unit : STANDARD_CUBIC_FEET
Special GSV Conv Factor : 1
Special GSV Flow Unit Text : NONE
Special GSV Total Text : NONE
Special Mass Base Unit : GRAM
Special Mass Conv Factor : 1

Units

Special Mass Flow Text : NONE
Special Mass Time Unit : SEC
Special Mass Total Text : NONE
Special Volume Base Unit : LITER
Special Volume Conv Factor : 1
Special Volume Flow Text : NONE
Special Volume Time Unit : SEC
Special Volume Total Text : NONE
Temperature Unit : DEGC
Velocity Unit : MTR/S
Volume Flow Unit : L/MIN

MVD Channel Assignments

Channel A Assignment : ANALOG 1
Channel B Assignment : ANALOG 2
Channel B Power : INTERNAL
Channel C Assignment : NONE
Channel C Power : INTERNAL
Channel D Assignment : NONE
Channel D Power : EXTERNAL

Assignments

Discrete Output 1 Assignment : FWD / REV
Discrete Output 2 Assignment : FWD / REV
Discrete Output 3 Assignment : FWD / REV
Event 1 Variable : DENSITY
Event 2 Variable : DENSITY
Frequency1 Scaling Method : FREQUENCY/FLOW
Frequency Variable 1 : MASS FLOW RATE
Frequency Variable 2 : MASS FLOW RATE
mA1 Variable : MASS FLOW RATE
mA2 Variable : DENSITY
mA3 Variable : TEMPERATURE

Ranges

Micro Motion, Inc. Transmitter Configuration Report **19005565**

Ranges

Event 1 Setpoint : 0
Event 1 Type : LOW ALARM
Event 2 Setpoint : 0
Event 2 Type : LOW ALARM
Frequency1 Hertz : 1000
Frequency1 Output Mode : SINGLE
Frequency1 Pulses/Unit : 82.67336
Frequency1 Rate : 725.7477
Frequency1 Units/Pulse : 0.0120958
Frequency2 Hertz : 1000
Frequency2 Pulses/Unit : 59.99999
Frequency2 Rate : 1000
Frequency2 Units/Pulse : 0.01666667
mA1 LRV : 0
mA1 URV : 725.7477
mA2 LRV : 0
mA2 URV : 5
mA3 LRV : -240
mA3 URV : 450

Faults

Frequency1 Fault Behavior : DOWNSCALE
Frequency1 Fault Value : 14500
Frequency2 Fault Behavior : DOWNSCALE
Frequency2 Fault Value : 14500
RS485 Fault Behavior : NONE
mA1 Fault Behavior : DOWNSCALE
mA1 Fault Value : 2
mA2 Fault Behavior : DOWNSCALE
mA2 Fault Value : 2
mA3 Fault Behavior : DOWNSCALE
mA3 Fault Value : 2

Other

Calibration Process ID : 2.41668262
Core Software Rev : 420
Density Cutoff : 0.2
Density Damping : 1.28
Density High Limit : 5
Density Low Limit : 0
Direction : 5700 ENABLED
Fault Dwell Time : 0
Feature Bits : 197120
Flow Damping : 0.64
HART Device ID : 3348975

Other

LD Coil : 0
LD Type : 0
Mass Flow Cutoff : 2.0736
Pressure Comp Line Pressure : 0
Pressure Compensation State : OFF
Slug Duration : 0
Tag :
Temperature Damping : 4.8
Transmitter Software Rev : 13
Volume Flow Cutoff : 2.0736

Micro Motion, Inc.

Mass Flowmeter Calibration Certificate — **15018877**

Product Code	Serial ID	Order ID	Line	Item	Customer Tag
F200S369C2EZNZKZZ	15018877	22045314	1.1	1	

Process

Process ID : 9.23670276
Process Time : 2017.05.23 12:53:01
Process Stand : TSM2G@SSCCL
Stand Uncertainty : +/-0.030%
Fluid : H2O
100% Rate : 725.7477 KG/MIN
Pickoff : 1
Max Rate P/T : 50.7 PSIG/25 C

Results

Status : PASS
D1 : 0
D2 : 1
K1 : 3390.66
K2 : 3899.263
DT : 4.5
FD : 6000
DTG : 0
DFQ1 : 0
DFQ2 : 0
FlowCal : 1530.34.56
FFQ : 0
FTG : 0
DensCal : 03391038994.50
FCF : 1530.3
FT : 4.56

Detail

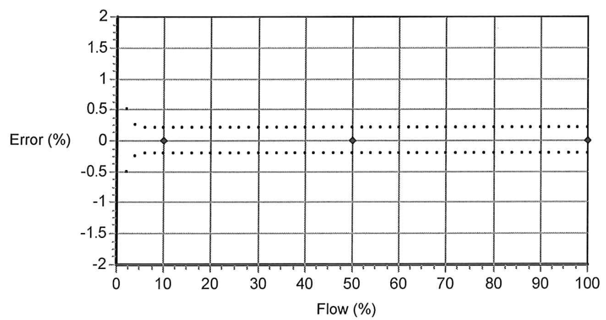

Flow (%)	Flow Rate (kg/min)	Meter Total (kg)	Reference Total (kg)	Error (%)	Specification (±%)
100.0	725.7477	712.8294	712.8368	-0.001	0.200
10.0	72.57477	70.65759	70.66615	-0.012	0.200
50.0	362.8739	369.8471	369.8633	-0.004	0.200
100.0	725.7477	714.3535	714.3505	0.000	0.200

CRISTIAN CIMPEAN
Technician
This certificate is produced by an electronic data system and is valid without signature.

Traceable to one or more of the following National Metrology Institutes: NIM-China, NIST-USA, and VSL-The Netherlands

Micro Motion, Inc. — Transmitter Configuration Report — **19005564**

Product Code	Serial ID	Order ID	Line	Item	Customer Tag
F200S369C2EZNZKZZ	15018877	22045314	1.1	1	
5700R12AEFAZZZAAZZZ	19005564	22045314	1.48	1	
PUCK800	33369436				

Process

Process ID : 2.41690863
Process Time : 2017.06.16 11:43:53
Process Stand : MMIV XMTR CONFIG@SSCE

Sensor

D1 : 0
D2 : 1
DFQ1 : 0
DFQ2 : 0
DT : 4.5
DTG : 0
Density Meter Factor : 1
Density Press Comp Factor : 0
FCF : 1530.3
FD : 6000
FFQ : 0
FT : 4.56
FTG : 0
Flow PCP : 19.99998
Flow PCF : 0
K1 : 3390.66
K2 : 3899.263
Mass Flow Meter Factor : 1
Temperature Cal Factor : 1.00000T.00000
Volume Flow Meter Factor : 1

Units

Density Unit : G/CUCM
GSV Flow Unit : SCFM
Mass Flow Unit : KG/MIN
Pressure Unit : PSI
Special GSV Base Time Unit : MIN
Special GSV Base Volume Unit : STANDARD_CUBIC_FEET
Special GSV Conv Factor : 1
Special GSV Flow Unit Text : NONE
Special GSV Total Text : NONE
Special Mass Base Unit : GRAM
Special Mass Conv Factor : 1

Units

Special Mass Flow Text : NONE
Special Mass Time Unit : SEC
Special Mass Total Text : NONE
Special Volume Base Unit : LITER
Special Volume Conv Factor : 1
Special Volume Flow Text : NONE
Special Volume Time Unit : SEC
Special Volume Total Text : NONE
Temperature Unit : DEGC
Velocity Unit : MTR/S
Volume Flow Unit : L/MIN

MVD Channel Assignments

Channel A Assignment : ANALOG 1
Channel B Assignment : ANALOG 2
Channel B Power : INTERNAL
Channel C Assignment : NONE
Channel C Power : INTERNAL
Channel D Assignment : NONE
Channel D Power : EXTERNAL

Assignments

Discrete Output 1 Assignment : FWD / REV
Discrete Output 2 Assignment : FWD / REV
Discrete Output 3 Assignment : FWD / REV
Event 1 Variable : DENSITY
Event 2 Variable : DENSITY
Frequency1 Scaling Method : FREQUENCY/FLOW
Frequency Variable 1 : MASS FLOW RATE
Frequency Variable 2 : MASS FLOW RATE
mA1 Variable : MASS FLOW RATE
mA2 Variable : DENSITY
mA3 Variable : TEMPERATURE

Ranges

15.0.0.138 2017.06.16 12:35:26 1/2

Micro Motion, Inc.	Transmitter Configuration Report	19005564

Ranges

Event 1 Setpoint : 0
Event 1 Type : LOW ALARM
Event 2 Setpoint : 0
Event 2 Type : LOW ALARM
Frequency1 Hertz : 1000
Frequency1 Output Mode : SINGLE
Frequency1 Pulses/Unit : 82.67336
Frequency1 Rate : 725.7477
Frequency1 Units/Pulse : 0.0120958
Frequency2 Hertz : 1000
Frequency2 Pulses/Unit : 59.99999
Frequency2 Rate : 1000
Frequency2 Units/Pulse : 0.01666667
mA1 LRV : 0
mA1 URV : 725.7477
mA2 LRV : 0
mA2 URV : 5
mA3 LRV : -240
mA3 URV : 450

Faults

Frequency1 Fault Behavior : DOWNSCALE
Frequency1 Fault Value : 14500
Frequency2 Fault Behavior : DOWNSCALE
Frequency2 Fault Value : 14500
RS485 Fault Behavior : NONE
mA1 Fault Behavior : DOWNSCALE
mA1 Fault Value : 2
mA2 Fault Behavior : DOWNSCALE
mA2 Fault Value : 2
mA3 Fault Behavior : DOWNSCALE
mA3 Fault Value : 2

Other

Calibration Process ID : 9.23670276
Core Software Rev : 420
Density Cutoff : 0.2
Density Damping : 1.28
Density High Limit : 5
Density Low Limit : 0
Direction : 5700 ENABLED
Fault Dwell Time : 0
Feature Bits : 197120
Flow Damping : 0.64
HART Device ID : 3348942

Other

LD Coil : 0
LD Type : 0
Mass Flow Cutoff : 2.0736
Pressure Comp Line Pressure : 0
Pressure Compensation State : OFF
Slug Duration : 0
Tag :
Temperature Damping : 4.8
Transmitter Software Rev : 13
Volume Flow Cutoff : 2.0736

SIEMENS **Industry Sector**

Factory Calibration Certificate / Werkskalibrierungszertifikat / Certificat d'étalonnage usine

Topic / Thema / Sujet: SITRANS F Flowmeter / Durchflussmessgerät / Débitmètre

Object / Betreff / Objet:

Customer order / Kundenauftrag / Commande client	:	N1740736
Siemens order / Siemensauftrag / Commande Siemens	:	0001531239/000010
Flowmeter type / Durchflussmessgerättyp / Type de débitmètre	:	SITRANS FC400
Nominal sensor diameter / Messaufnehmer-Nennweite / Diamètre nominal de capteur	:	DN 50 (2")
Product order No. / Produktbestellnummer / N° de référence d'appareil	:	7ME46134CA014DA3-Z
Options ordered / Bestellten Optionen / Options commandées	:	A02+B11+E06+F40
Sensor serial No. / Messaufnehmer Seriennummer / N° de série de capteur	:	FDKJ6190005780

Technical data / Technische Daten / Données techniques:

Calibration factor / Kalibrierungsfaktor / Facteur d'étalonnage	:	1526589000
Calibration medium / Kalibriermedium / Moyen de calibration	:	Water / Wasser / Eau
Calibrated full scale flow / Kalibrierter Messbereichsendwert / Fin de plage de mesure étalonnée	:	50000 kg/h / 110231 lb/h
Calibration rig / Kalibrierstand / Plate-forme d'étalonnage	:	CAL00130

Standards / Normen / Normes:

ISO 4185-1980

Results / Ergebnisse / Résultats:

Point #	Flowrate	Fluid temperature		Reference flow value		Flowmeter output / Duchflussmessgerätausgang / Sortie de débitmètre		
Messpunkt nr Point mesure n°	Durchfluss Débit	Flüssigkeitstemperatur Température du fluide		Referenz Durchflusswert Débit de référence		Flowrate Durchflussmenge / Débit		Error Fehler / Erreur
	[%]	[°C]	[°F]	[kg/h]	[lb/h]	[kg/h]	[lb/h]	[%]
1	90	23.2	73.8	44905.7593	99000.2527	44906.8389	99002.6329	0.00
2	90	23.3	73.9	45231.4219	99718.2158	45228.7035	99712.2228	-0.01
3	20	23.3	73.9	9756.2305	21508.8064	9760.4530	21518.1155	0.04
4	20	23.3	73.9	10144.5193	22364.8367	10147.0267	22370.3646	0.02

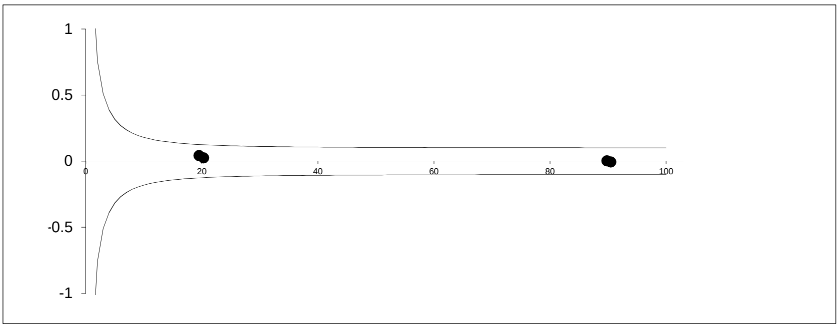

Summary of the results / Zusammenfassung der Ergebnisse: / Sommaire des résultats obtenus : :

- The measured values are within the specified limits / Die gemessenen Werte liegen innerhalb der Toleranzen / Les résultats de mesure se trouvent dans les tolérances définies

Siemens A/S, Flow Instruments	Issued by / Erstellt von / émis par	Date / Datum / Date
	MD	2017-06-22

SIEMENS Industry Sector

Factory Calibration Certificate / Werkskalibrierungszertifikat / Certificat d'étalonnage usine

Test rig characteristics

Prüfstand Merkmale / Caractéristiques de la plate-forme de test

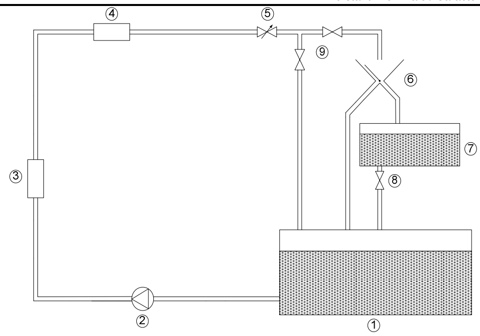

1) Reservoir / Tank / Réservoir
2) Pump / Pumpe / Pompe
3) One or more reference meters / Ein order mehrer Referenz Messgeräte / un ou plusieurs débitmètres de référence
4) Meter under test / Messgerät unter Prüfung / Débitmètre en test
5) Control valve / Kontrollventil / Vanne de régulation
6) Diverter / Kippschaltung / Bascule
7) Weighing tank / Gewichtsmessungstank / Cuve de mesure
8) Drain valve / Abflussventil / Vanne de vidange
9) Valve to switch between reference meter method and static/dynamic weighing method / Ventile zom switchen zwischen Referenz Methode und statische/dynamische Gewichtmessung Methode / Vanne de basculement entre méthode avec débitmètres de référence et méthode par pesée statique or dynamique

Test rig ID / Prüfstand ID / ID de la plate-forme de test	**CAL00130**
Fluid / Flüssigkeit / Fluide	**Water** / Wasser / Eau
Fluid temperature / Flüssigkeit Temp. / Temp. du fluide	**15-30 °C** / 59-86 °F
Test rig capacity / Prüfstand Kapazität / Capacité de la plate-forme	**DN 25...80** / 1"...3"
Max. Flowrate / Max. Durchfluss / Débit max.	**50000 kg/h** / 110231 lb/h
Min. Flowrate / Min. Durchfluss. / Débit min	**220 kg/h** / 485.02 lb/h
Max. Mass / Max.Masse / Masse max.	**600 kg** / 1322.77 lb
Uncertainty / Ungenauhigkeit / Incertitude	**< 0.05%**

Traceability / Rückverfolgbarkeit / Traçabilité

The Siemens flowmeter calibration process is ISO9001-certified, ensuring the entire calibration procedure is controlled to the highest quality standards.

All primary measuring instrumentation used by the Siemens Flow Laboratory during the performance of its calibrations, has been calibrated with international standards traceability referring directly to the physical unit of measurement according to the International System of Units (SI). Therefore the calibration certificate ensures recognition of the test results worldwide, including the US (NIST traceability).

Der Siemens Kalibrierungsprozess für Durchflussmessgeräte ist ISO9001 zertifiziert, sicherstellend, dass das ganze Kalibrierungsverfahren nach den höchsten Qualitätsstandards kontrolliert ist.

Alle Hauptmessinstrumente, die zur Durchführung der Kalibrierungen vom Siemens Durchfluss Laboratorium genutzt werden, sind kalibriert, um eine Rückverfolgbarkeit auf internationale Normen sicherzustellen. Dies bezieht sich direkt auf die Maßeinheit gemäß dem Internationalen Einheitensystem (SI). Das Kalibrierungszertifikat gewährleistet daher die Anerkennung der Prüfergebnisse weltweit, einschließlich in den USA (NIST-Rückverfolgbarkeit).

Le processus d'étalonnage des débitmètres Siemens est certifiée ISO9001 et est contrôlé périodiquement selon les normes qualités en vigueur les plus élevées.

Tous les instruments de mesure primaires utilisés dans les laboratoires Siemens Flow durant les opérations d'étalonnage ont été étalonnés en conformité avec les normes internationales relatives à l'unité de mesure physique, conformément au système international d'unités (SI). Le certificat d'étalonnage garantit ainsi que les résultats obtenus lors des essais sont conformes aux normes internationales, y compris NIST (USA).

Siemens A/S, Flow Instruments

Coriolisvej 1-3
DK-6400 Soenderborg
Denmark

Tel (+45) 29 49 32 32

SIEMENS **Industry Sector**

Factory Calibration Certificate / Werkskalibrierungszertifikat / Certificat d'étalonnage usine

Object / Betreff / Objet:

Customer order / Kundenauftrag / Commande client	:	N1740736
Siemens order / Siemensauftrag / Commande Siemens	:	0001531239/000010
Flowmeter type / Durchflussmessgerättyp / Type de débitmètre	:	SITRANS FC400
Nominal sensor diameter / Messaufnehmer-Nennweite / Diamètre nominal de capteur	:	DN 50 (2")
Product order No. / Produktbestellnummer / N° de référence d'appareil	:	7ME46134CA014DA3-Z
Options ordered / Bestellten Optionen / Options commandées	:	A02+B11+E06+F40
Sensor serial No. / Messaufnehmer Seriennummer / N° de série de capteur	:	FDKJ6190005780

Technical data / Technische Daten / Données techniques:

Calibration rig / Kalibrierstand / Plate-forme d'étalonnage	:	20001973
A Constant / Konstante A / Constante A	:	-2.399724E+03
B constant / Konstante B / Constante B	:	8.045804E+08
Density TC / Dichte TC / CT densité	:	-4.417412E-04
D Constant / Konstante D / Constante D	:	1.500000E-05

Density results / Dichte Ergebnisse / Résultats de la densité:

Point # Messpunkt nr Point mesure n°	Calibration medium Kalibriermedium Moyen de calibration	True density Wahre Dichte Densité réelle		Flowmeter output / Duchflussmessgerätausgang / Sortie de débitmètre			
				Density Dichte / Densité		Error Fehler / Erreur	
		[kg/m3]	[lb/ft^3]	[kg/m3]	[lb/ft^3]	[kg/m3]	[lb/ft^3]
1	Warm water	981.45	61.270	981.47	61.271	0.0	0.00
2	Cold water	997.55	62.275	997.69	62.284	0.1	0.01

Temperature results / Temperatur Ergebnisse / Résultats de la température:

Point # Messpunkt nr Point mesure n°	Calibration medium Kalibriermedium Moyen de calibration	True Temperature Wahre Temperatur Température réelle		Flowmeter output / Duchflussmessgerätausgang / Sortie de débitmètre			
				Temperature Temperatur / Température		Error Fehler / Erreur	
		[°C]	[°F]	[°C]	[°F]	[°C]	[°F]
1	Warm water	63.3	145.9	63.4	146.1	0.06	0.11
2	Cold water	22.7	72.9	22.8	73.0	0.11	0.20

Summary of the results / Zusammenfassung der Ergebnisse: / Sommaire des résultats obtenus : :

- The measured values are within the specified limits / Die gemessenen Werte liegen innerhalb der Toleranzen / Les résultats de mesure se trouvent dans les tolérances définies

	Issued by / Erstellt von / émis par	Date / Datum / Date
Siemens A/S, Flow Instruments	MD	2017-06-22

SIEMENS **Industry Sector**

Factory Calibration Certificate / Werkskalibrierungszertifikat / Certificat d'étalonnage usine

<table>
<tr><td colspan="3">Test rig characteristics
Prüfstand Merkmale / Caractéristiques de la plate-forme de test</td></tr>
<tr><td rowspan="4">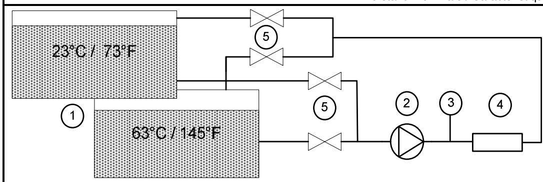

1) Reservoir / Tank / Réservoir
2) Pump / Pumpe / Pompe
3) Temperature sensor / Temperatursensor / Capteur de la température
4) Meter under test / Messgerät unter Prüfung / Débitmètre en test
5) Control valve / Kontrollventil / Vanne de régulation</td><td>Test rig ID /
Prüfstand ID /
ID de la plate-forme de test</td><td>20001973</td></tr>
<tr><td>Fluid /
Flüssigkeit /
Fluide</td><td>Water / Wasser / Eau
Air / Luft / l'air</td></tr>
<tr><td>Fluid temperature /
Flüssigkeit Temp. /
Temp. du fluide</td><td>23 & 63 °C / 73 & 145 °F</td></tr>
<tr><td>Test rig capacity /
Prüfstand Kapazität /
Capacité de la plate-forme</td><td>DN 15...150 / 1/2"…6"</td></tr>
</table>

Density calibration / Dichtekalibrierung / Etalonnage densité

Density measurements on Siemens massflow meters are calculated on the basis of media temperature and period of the sensor.
Density = A + B(1 + at)T2
A,B = Calibration constants, a = Density TC, t = Fluid temperature, T = period time of sensor

Dichtemessungen bei Siemens Massedurchflussmessgeräten werden anhand der Medientemperatur und des Messaufnehmer-Zeitraums berechnet.
Dichte = A + B(1 + at)T2
A,B = Kalibrierungskonstanten, a = Dichte TC, t = Temperatur der Flüssigkeit, T = Zeitraum des Messaufnehmer

Les débitmètres massiques de Siemens mesurent la densité par rapport à la température du milieu et à la période du capteur.
Densité = A + B (1 + à)T2.
A,B = constantes d'étalonnage, a = CT densité, t = température fluide, T = période temps du capteur

Siemens A/S, Flow Instruments

Coriolisvej 1-3
DK-6400 Soenderborg
Denmark

Tel (+45) 29 49 32 32

Appendix B

Validation of water cut measurements

Validation of Coriolis water cut estimates were performed by comparing recorded data with ultraviolet (UV) analysis of collected samples.

The water feed line Coriolis meter (FT.1/DT.1) was used for validation experiments. The rig was operated to induce contamination of the water feed line (trace amounts of dispersed Exxsol^{TM} D60 in the water). For a stable contamination level, a 5 Hz, 60 s recording was made. Directly after the end of the recording, a sample of the feed water was collected through a flush mounted sampling point on the water feed line upstream the Coriolis meter. This was done for three contamination levels. Recorded data was corrected with established calibration curves, and the water cut in the water feed line (WC_1) was calculated according to the procedure outlined in Chapter 3. The collected samples were analyzed with a UV-vis spectrophotometer, where prepared calibration curves were used to calculate oil concentrations of respective samples from absorbance measurements. Sample analysis was performed by Postdoctoral fellow Marcin Dudek, who also provided error estimates for the resulting concentration values. A more thorough description of the measurement technique can be found in [12].

In Figure B.1, the resulting WC from Coriolis measurements (Experimental) and sample analysis (Sample value) are plotted for the three contamination levels tested.

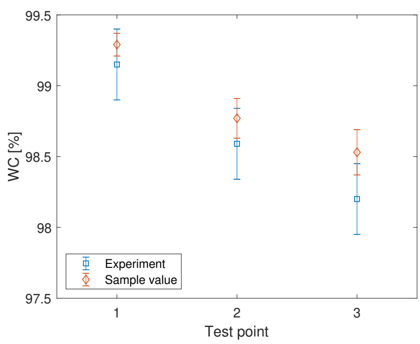

Fig. B.1 Validation of WC measurements

Error bars are seen to overlap for all test points, and a good match between recordings and sample analysis is displayed. An error not captured in performed experiments is the potential influence the tapping procedure has on sample composition. However, the feed stream contamination is observed to be homogeneous, and the tapping is not expected to alter fluid composition.

Appendix C

Pump controller specifications

The controllers developed for automatic test point adjustment were PI controllers. The controllers utilized corrected volume flow measurements to control the respective pump frequency inputs, adjusting flow rates to desired values. With reference to Table 3.1, the developed controllers are for the two Pedrollo F40/200 A pumps. These were the two pumps used for all experiments in this dissertation. Each pump is controlled by one PI controller, so the complete control system consist of two PI controllers working in parallel.

Values for desired total flow rate and WC at the separator inlet are specified in the LabVIEW VI. From these values, the set points (SP) for the two controllers are calculated. For further denotation, controller values for the water pump will be subscripted with 1, while controller values for the Exxsol^{TM} D60 pump will be subscripted with 2.

$$SP_1 = \dot{Q}_{tot} WC \tag{C.1}$$

$$SP_2 = \dot{Q}_{tot}(1 - WC) \tag{C.2}$$

The respective set points are compared with measured and corrected flow rates in the respective feed lines ($\dot{Q}_1$, $\dot{Q}_2$, from Table 3.4), from which an error (ω) is calculated. The feed line flow rates are denoted as process variables (PV), which vary with time.

$$\omega_1(t) = SP_1 - PV_1(t) \tag{C.3}$$

$$\omega_2(t) = SP_2 - PV_2(t) \tag{C.4}$$

These errors are the inputs for the two controllers, which calculate appropriate responses ($u(t)$) that are sent to the corresponding pump frequency converters. The control loop is illustrated in Figure C.1.

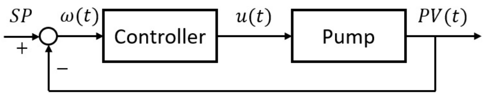

Fig. C.1 Illustration of control loop

The respective controller responses are functions of tunable controller variables. The variables used for a PI controller are the controller gain (K), and the derivative time constant (τ). The controller response is calculated according to Eq. C.5.

$$u(t) = K\left(\omega(t) + \frac{1}{\tau}\int_0^t \omega(t)dt\right) \tag{C.5}$$

Controller tuning was performed with the well established SIMC tuning rules, outlined in [32]. The resulting tuning parameters are the same for both controllers ($K = 0.035\ min/L$, $\tau = 1.2\ s$).